



MAX PLANCK INSTITUTE
FOR DYNAMICS OF COMPLEX
TECHNICAL SYSTEMS
MAGDEBURG



**Experimental investigations and modeling of extracting natural products
from plants: from batch to continuous processes**

Dissertation

Zur Erlangung des akademischen Grades

**Doktoringenieur
(Dr.-Ing.)**

von M.Sc. Truong Giang Vu

geb. am 28.06.1980 in Hanoi, Vietnam

genehmigt durch die Fakultät für Verfahrens- und Systemtechnik
der Otto-von-Guericke Universität Magdeburg

Promotionskommission: Prof. Dr.-Ing. Andreas Seidel-Morgenstern (Vorsitz)
Prof. Dr.-Ing. Malte Kaspereit (Gutachter)
Assoc. Prof. Dr.-Ing. Nguyen Minh Tan (Gutachter)
Apl. Prof. Dr. rer. Nat. Heike Lorenz (Mitglied)

eingereicht am: 04.07.2023

Promotionskolloquium am: 10.11.2023

Declaration

I hereby declare that I personally prepared the present academic work, carried out myself the activities and submitted without inadmissible assistance. Fact or ideas taken from other sources, either directly or indirectly have been marked as given and I confirm that I have used no resources other than those declared. The support provided during the work, including significant assistance from my supervisor has been indicated in full.

This academic work has not so far been submitted to any other examination office authority either in Germany or abroad.

Magdeburg, 28.06.2023

Place, Date

Signature

Abstract

In 2020, 241 million infection cases of malaria were reported worldwide causing approximately 627000 deaths mainly in African countries. The number of infections increased by 6 % and the fatalities by 12 % compared to the previous year 2019 [World malaria report 2021]. World Health Organization (WHO) recommended Artemisinin (ARTE) as the first-line treatment of malaria. ARTE is produced by chemical synthesis, semi-synthetically or by extraction from plants and subsequent purification. Due to the complexity and expenses related to the synthetic processes, the isolation of ARTE from sweet wormwood (*Artemisia annua L.*) is recommended to provide the increasing quantities required on the international market. In pharmaceutical industry, batch-wise extraction of valuable target components from plants is the state of the art. Less activities have been devoted to develop continuous extraction techniques.

The research described in this thesis focused on studying continuous counter-current extraction of ARTE from *Artemisia annua L.* with joint isolation of dihydroartemisinic acid (DHAA), which is known to be a precursor for the biosynthesis of ARTE. It was shown that DHAA could be oxidized photocatalytically to ARTE, which allows increasing the overall ARTE yield of the extraction process. For the mentioned photoreaction, the additional co-extraction of chlorophyll is desirable since it acts as an efficient green photosensitizer.

This thesis will present results regarding the determining distribution equilibria and extraction rates. Exploiting analogies to chemical reaction engineering this information is incorporated into a model which describes steady state counter-current solid liquid extraction processes. The model allows identifying suitable operating conditions, which maximize the production of ARTE. Finally, results of continuous extraction experiments carried out with a self-developed pilot plant will be presented to demonstrate the general applicability of the concept and the efficiency of the process.

Kurzzusammenfassung

Im Jahr 2020 wurden weltweit 241 Millionen Malaria-Infektionen dokumentiert, die zu etwa 627000 Todesfällen führten. Die meisten Erkrankungen traten auf dem afrikanischen Kontinent auf. Die Zahl der Infektionen stieg um 6 % und die Zahl der Todesfälle um 12 % im Vergleich zum Vorjahr 2019 [Weltmalariabericht 2021]. Die Weltgesundheitsorganisation (WHO) empfiehlt Artemisinin (ARTE) als präferiertes Mittel zur Behandlung von Malaria. ARTE wird über chemische Synthese, semisynthetisch oder durch Extraktion aus Pflanzenmaterial mit anschließender Aufreinigung produziert. Aufgrund der Komplexität der Synthese und der dadurch entstehenden hohen Kosten ist es empfehlenswert ARTE aus dem Einjährigen Beifuß (*Artemisia annua L.*) zu isolieren, um die steigende Nachfrage an ARTE auf dem internationalen Markt decken zu können. Derzeit ist in der pharmazeutischen Industrie die chargenweise Extraktion von wertvollen Zielsubstanzen aus Pflanzen der Stand der Technik. Bisher wurde vergleichsweise wenig Aufwand betrieben, kontinuierliche Extraktionstechniken zu entwickeln.

Diese Arbeit widmet sich der systematischen Erforschung der kontinuierlichen gleichzeitigen Gegenstromextraktion aus *Artemisia annua L.* von ARTE und Dihydroartemisininsäure (DHAA), welche eine Vorstufe in der Biosynthese von ARTE darstellt. DHAA kann photokatalytisch zu ARTE oxidiert werden, was eine Steigerung der Gesamtausbeute an ARTE in extraktionsbasierten Produktionsprozessen ermöglicht. Für die Photoreaktion ist auch die zusätzliche Koextraktion von Chlorophyll von Bedeutung, da dieses als effizienter Photosensibilisator wirkt.

In dieser Arbeit werden Ergebnisse zu den ermittelten Verteilungsgleichgewichten und Extraktionsgeschwindigkeiten vorgestellt. Unter Verwendung von Analogiebetrachtungen zur Quantifizierung reversibler chemischer Reaktion werden diese Informationen in ein entwickeltes stationäres Modell eingebunden, welches den Gegenstromextraktionsprozess beschreibt. Das Modell erlaubt die Identifizierung geeigneter Betriebsbedingungen zur Maximierung der Produktion von ARTE. Schließlich werden an einer eigens entwickelten Pilotenanlage ermittelte

experimentelle Versuchsergebnisse zur kontinuierlichen extraktion präsentiert, um die Umsetzbarkeit des Konzeptes und die Effizienz des Prozesses zu demonstrieren.

Preface

The following research papers related to this thesis are already published.

[1] S. Triemer, K. Gilmore, G.T. Vu, P.H. Seeberger, A. Seidel-Morgenstern. Literally Green Chemical Synthesis of Artemisinin from Plant Extracts. *Angew. Chem. Int. Ed.*, vol 57 (19), p. 5525-5528, 2018. (Results are described in the thesis chapters 2, 4 and 5)

Own contribution: Preparing the crude extract. Analyzing the extract, providing extraction techniques, determining kinetics and equilibrium data, optimizing extraction conditions.

[2] S. Münzberg, G.T. Vu; A. Seidel-Morgenstern. Generalizing countercurrent processes: Distillation and beyond. *Chem. Ing. Tech.*, vol. 90 (11), p. 1769-1781, 2018. (Results are described in the thesis chapters 2, 3)

Own contribution: Theory of distillation and extraction parts, in particular the multi-stage counter-current equilibrium model and the solutions based on Kremser method.

[3] A. Lehr, G.T. Vu, G. Janiga, A. Seidel-Morgenstern, D. Thévenin. Experimental investigation of the residence time distribution in a screw-type apparatus designated to extract artemisinin. *Chem. Eng. Process.*, vol. 187, 109337, 2023. (Results are described in the thesis chapters 2, 5 and 6)

Own contribution: Conceptualization of the RTD analysis, counter-current extractor design, RTD analysis and interpretation of experimental data.

Two master theses were supervised:

(1) Sandra Gruner analyzed different variants of counter-current separation processes (Chapters 2, 5).

(2) Christoph Krieger focused on simulation and experiments of residence time distribution for the newly developed counter-current extractor (Chapters 5, 6).

Contents

1	Introduction	1
1.1	Aim of the research.....	2
1.2	Structure of this thesis	6
2	Solid liquid extraction.....	8
2.1	Phytoextraction	9
2.2	Fundamentals.....	11
2.2.1	Phases involved in natural product extraction	11
2.2.2	Equilibrium.....	16
2.2.3	Operation modes and corresponding mass balances.....	17
2.2.4	Kinetics and extraction rate constants	22
2.2.5	Residence time analysis.....	23
2.3	Parameters influencing the extraction process	27
2.3.1	Solvent.....	27
2.3.2	Solid-to-liquid ratio.....	27
2.3.3	Particle size of solid starting material	28
2.4	Extraction concepts	28
2.5	Operation modes and equipment for solid liquid extraction processes 31	
2.5.1	Continuous processes and types of equipment	32
2.6	Options for extraction and chemical engineering processes	34
3	Modeling solid liquid extraction processes.....	36
3.1	Basics of chemical reaction engineering (CRE).....	37
3.2	Modeling extraction processes.....	43
3.3	Evaluation of counter-current extraction: Simulation results	57
3.3.1	The influences of important parameters on the counter-current extraction performance (Scenario 1: fixed phase ratio).....	59
3.3.2	Alternative option of counter-current operation (Scenario 2)	62
3.4	Objectives of extraction processes.....	63
3.4.1	Productivity	64
3.4.2	Recovery	64
4	Materials, analytical methods and procedures.....	65
4.1	Primary investigations.....	65
4.1.1	Solvent selection	65
4.1.2	Analytical methods and materials	67
4.2	Results: Important parameters from batch extraction runs	80
4.2.1	Batch process.....	80
4.2.2	Equilibrium constants for ARTE and DHAA	81
4.2.3	Kinetics of extraction	83
5	Experimental study and evaluation of process variants	85

5.1	Evaluation of a simple batch extraction process.....	85
5.2	Counter-current sequential batch operation (equilibrium conditions)	88
5.2.1	Model-based prediction for ARTE extraction from <i>Artemisia annua</i> L. dried leaves.....	88
5.2.2	Experimental setup of sequential counter-current operation	90
6	Continuous counter-current steady state extraction.....	94
6.1	Design of a continuous counter-current extractor.....	95
6.1.1	Idea and conceptual design.....	95
6.1.2	Engineering design and dimension estimation	97
6.2	Preliminary investigations of continuous extraction process	103
6.2.1	Residence time of leaves	103
6.2.2	Residence time of solvent	108
6.3	Continuous counter-current extraction experiments	112
6.3.1	Overall mass balance to verify steady state conditions	114
6.3.2	Continuous steady state experiments.....	115
7	Summary and outlook	121

Appendices

List of Figures

Figure 1.1. <i>Artemisia annua</i> L. Left: plant, Right: molecular structure of the active substance Artemisinin.	2
Figure 1.2. Chinese scientist Youyou Tu – Nobel Prize 2015 in Physiology or Medicine.....	3
Figure 1.3. Scheme of producing ARTE-based anti-malaria API [28].....	4
Figure 1.4. Scheme of combination between extraction and semi-synthesis to provide ARTE.....	5
Figure 2.1. Illustration of the steps related to solid liquid extraction processes. <i>The extract is typically the target outlet stream which contains a desired component. The raffinate which contains amounts of remaining target solutes is sometimes considered as “waste”.</i>	8
Figure 2.2. Typical steps of producing API based on phytoextraction.	9
Figure 2.3. Scheme of solute transfer during a phytoextraction process according to [47]. <i>The solvent dissolves solutes in interstitials and pores of the solid start material and these solutes diffused then back into the liquid body.</i>	10
Figure 2.4. Illustration of phases involved in phytoextraction. <i>Left: the two initial phases involved before contacting them. Right: mass transfer directions of a solute i and the solvent along with the designation of extract (liquid without solid) and raffinate (solid with adherent liquid).</i>	12
Figure 2.5. Illustration of involved volumes described in eq. (2.19). <i>The volumes of additional devices are the volumes of screw; housing volume is the occupied space of extractor housing; the suspension volume is the total volume of liquid and solid phases introduced in eq. (2.18).</i>	15
Figure 2.6. Illustration of initial and final masses and mass fractions for a batch process. <i>The initial compositions of component i of solid and liquid phases are defined by eqs. (2.14) and (2.15) respectively. The final amounts of component i in extract (external liquid without solid) and raffinate (internal liquid and solid) are derived from eqs. (2.23) and (2.25). The dashed arrows represent the filling and emptying of the extraction vessel. If all masses m are replaced by mass fluxes \dot{m}, this scheme also describes continuous extraction processes to be discussed later.</i>	18

Figure 2.7. Development of fractions of component i with corresponding masses of the phases over time in a typical batch extraction process.	18
Figure 2.8. Concentration profile of component i in a tubular continuous counter-current extractor process at steady state. <i>The solid material and fresh liquid phase are supplied in opposite directions with corresponding compositions of component i (eqs.(2.14) and (2.15), the obtained extract (E) and raffinate (R) compositions are based on eqs.(2.23) and (2.25).</i>	21
Figure 2.9. Plotting the two distribution functions $E(t)$ and $F(t)$ for selected ideal and non-ideal RTD according to [71].....	26
Figure 2.10. Soxhlet extraction. <i>1-Heating plate, 2-Boiling flask, 3-Soxhlet device, 4-Extraction thimble, 5-Condenser.</i> [79].....	30
Figure 2.11. Rotocel extractor [82].	32
Figure 2.12. Desmet LM belt extractor [83]. <i>1-Material, 2-Solvent, 3- Extract, 4-Raffinate.</i>	33
Figure 2.13. Screw-based extractor of GEA [84]. <i>Left: CONTEX screw extractor; Right: Principle of extraction equipment.</i>	33
Figure 3.1. Comparison of BR (and PFTR), CSTR and a cascade of CSTR for performing a simple first order reversible chemical reaction. <i>The upper and lower curves are represented for compositions in the solid and liquid phases respectively. The black curves present the concentration development for BR; the other curves show the different numbers of CSTR. Input parameters for Code1: $c_A^0 = 1, c_B^0 = 0, k_R = K_R^{eq} = 1, \tau = 5.$</i>	42
Figure 3.2. Illustration of two CSTR in co-current operation for extraction. <i>The liquid phase and solid phase are fed at the same side to the first stage ($N = I$) and taken out at the second stage ($N = II$). The residence time in the two identical sized CSTR τ_I and τ_{II} are a half of the overall residence time τ (eq. (3.22)).</i>	48
Figure 3.3. Illustration of two CSTR counter-current operation for extraction. <i>The liquid phase and solid phase are provided at two opposite ends of the cascade. The outgoing concentrations of component i in the liquid phase c_i^{II} and in the solid phase q_i^I decide the productivity and recovery of the extraction process respectively.</i>	49
Figure 3.4. The composition in the liquid and solid phases of two stage co- and counter-current ($N = 2$) and the enhancement factor (eq. (3.70)). <i>Left: The modified</i>	

concentration development in the liquid and solid phases of two operations; *Right*: the enhancement factor between co- and counter-current operations calculated based on real concentrations. *The input parameters selected for illustration are given as: $q_i^{in} = 1, c_i^{in} = 0, \varepsilon = 0.5, k_{i,E} = 10, K_{i,E}^{eq} = 1, \tau = 1$. The red-square points show the maximal value when the number of stage N goes to infinity and the asterisk points are resulted based on the Kremser method which is going to be shown below.* 51

Figure 3.5. Description of N -stage counter-current operation for extraction. *The unknowns are the concentrations of component i at every stages, in which the most interested unknowns are the outgoing concentrations of component i in the liquid phase $c_{i,N}$ at stage N and that in the solid phase $q_{i,1}$ at stage 1.....* 52

Figure 3.6. The coefficient matrix of the system of equations describes the kinetically controlled operation for N CSTR counter-current extraction process. *The four non-zero elements of the right-hand side (r.h.s) vector are also depicted.....* 53

Figure 3.7. The influence of number of stages N on the kinetically controlled concentrations of component i in the counter-current extraction processes. *The red-square points correspond to plug counter-current regimes and are constant. The asterisk points correspond to concentrations based on equilibrated stage model and can be calculated by the Kremser method (eqs.(3.75),(3.77)). Given parameters: $q_i^{in} = 0.5, c_i^{in} = 0, \varepsilon = 0.5, k_{i,E} = 10, K_{i,E}^{eq} = 1, \tau = 1$* 54

Figure 3.8. The tridiagonal coefficient matrix of the counter-current equilibrium stage model and the 2 non-zero r.h.s elements. 55

Figure 3.9. The concentration development of component i in the liquid and solid phase of counter-current operation. *Left*: The pseudo-homogeneous modified concentration as treated in eq. (3.72); *Right*: The real concentration arising ε dependent after splitting into two individual phases. *Given parameters: $\tilde{q}_i^{in} = 0.5, q_i^{in} = 1$ (eq. (3.38)), $\tilde{c}_i^{in} = c_i^{in} = 0, \varepsilon = 0.5, k_{i,E} = 10, K_{i,E}^{eq} = 1, \tau = 5$. The asterisk points are derived from Kremser solutions (eqs. (3.75), (3.77)).* 58

Figure 3.10. Sensitivity in case of equilibrium distribution coefficient $K_{i,E}^{eq}$ adjustment. *Each diagram corresponds to a specific value of $K_{i,E}^{eq}$ and other parameters are kept at reference values (Table 3.1). The blue and green curve represent the compositions in the liquid and solid phase respectively. The red curve*

is for obtained amount of component i which is direct related to productivity.
Reference case parameters: $q_i^{in} = 1, c_i^{in} = 0, \varepsilon = 0.5, k_{i,E} = 1, K_{i,E}^{eq} = 1, \tau = 5$ 59

Figure 3.11. Sensitivity in case of equilibrium distribution coefficient $k_{i,E}$ adjustment.
The variation range is from Table 3.1. Reference case parameters: $q_i^{in} = 1, c_i^{in} = 0, \varepsilon = 0.5, k_{i,E} = 1, K_{i,E}^{eq} = 1, \tau = 5$ 60

Figure 3.12. Influence of number of stages N on concentrations of the liquid and solid phases. Reference case parameters: $q_i^{in} = 1, c_i^{in} = 0, \varepsilon = 0.5, k_{i,E} = 1, K_{i,E}^{eq} = 1, \tau = 5$ 60

Figure 3.13. Illustration of the influence of number of stages N and equilibrium coefficient $K_{i,E}^{eq}$ on gain parameter G in counter-current operation. Given parameters: $q_i^{in} = 1, c_i^{in} = 0, N = 1 \div 20, K_{i,E}^{eq} = 0.5 \div 1.5$. Each curve corresponds to a fixed equilibrium distribution coefficient $K_{i,E}^{eq}$ 61

Figure 3.14. Illustration of the influence of the residence time τ on the outgoing concentrations and nL . Reference case parameters: $q_i^{in} = 1, c_i^{in} = 0, \varepsilon = 0.5, k_{i,E} = 1, K_{i,E}^{eq} = 1, \tau = 5$ 61

Figure 3.15. Illustration of determination of corresponding concentrations of the two phases related to liquid flowrate. Left: Reference case with corresponding lines of specific values of τ^* and ε . Right: The concentrations and obtained amount in different liquid flowrate \dot{V}_L 63

Figure 4.1. Solubility of ARTE in different solvent as a function of temperature [105]. 66

Figure 4.2. Travelled distance identification on developed plate. Left: distance travelled in standard and sample; Right: distance travelled in developing chamber for real analysis of different samples. The plate containing samples and standards are developed inside a closed chamber. 68

Figure 4.3. High performance thin layer chromatography (HPTLC) procedures. ... 69

Figure 4.4. Developed high performance thin layer chromatography plate. The samples and standards are applied on the plate. The standards show only one retention factor of a specific solute at different concentrations and the samples perform relating components. 69

Figure 4.5. Principle of high performance liquid chromatography (HPLC)..... 70

Figure 4.6. The principle of evaporative light scattering detector (ELSD).....	71
Figure 4.7. Identification of LOD and LOQ for HPLC based on signal and noise. .	72
Figure 4.8. Vibration sieve machine (AS200) and ultra centrifugal milling machine (ZM200 from Retsch).	74
Figure 4.9. The size distribution of originally imported <i>Artemisia annua L.</i> leaves.	74
Figure 4.10. The size distribution of ground <i>Artemisia annua L.</i> leaves. <i>Left:</i> ground leaves by mill machine ZM200 at 12000rpm; <i>Right:</i> ground leaves size distribution of three portions.	75
Figure 4.11. Scheme of the exhaustive extraction technique. <i>The dried leaves are filled into the extractor, each color corresponds to an input and an output of one batch extraction run. Each cycle corresponds to one complete single batch extraction designated as stage j ($j = 1 \dots M$). When the first cycle is finished by providing and withdrawing process, the second cycle starts. The process stops when the final extract contains no more ARTE ($x_{ARTE,M} = 0$).</i>	76
Figure 4.12. Wetting parameter measurement data. <i>The ratio of internal extract mass and initial leaves mass represents wetting factor ($W_{Toluene} = 2.25$; $W_{n_Hexane} = 1.7$; $W_{Ethanol} = 2.4$).</i>	79
Figure 4.13. Experimental illustration of a single batch extraction with a defined dosage in eq. (2.8). <i>The mixture of leaves and solvent is settled and extract (E) contains no solid particles, the dried leaves contain a defined amount of solvent and establishes raffinate (R).</i>	80
Figure 4.14. Equilibrium concentration of ARTE extraction in Toluene as the solvent. <i>The effective distribution coefficient β_i^{eff} is estimated based on eq. (2.28) and thermodynamic distribution coefficient β_i is derived from eq. (2.29).</i>	82
Figure 4.15. Kinetics of ARTE extraction in Toluene. <i>The experiments are carried out by a series of batch extraction processes. The masses of initial solvent are constant in all cases, only the initial masses of leaves are changed.</i>	83
Figure 5.1. The relations of relevant parameters of single batch ARTE extraction in Toluene at different dosages. <i>Experimental conditions, analyzed concentration and productivity (eq. (5.2)), recovery (eq. (5.3)) data are summarized in Appendix A10.</i>	88

Figure 5.2. Concentration development of a sequential counter-current equilibrium stage cascade. <i>Fresh solvent and dried leaves are fed in two opposite directions. Points present the equilibrated concentration of each stage and are calculated based on eqs. (3.80), (3.81). Two red-circled points $x_{ARTE,R,1}, x_{ARTE,E,N}$ presenting the outgoing ARTE concentrations are the most interested.</i>	90
Figure 5.3. Experimental setup of sequential 3-stage counter-current extraction operation. <i>The three pre-extractors are filled by dried leaves. The green dotted arrows present the transported steps, in which the raffinate is remained in the extractor. The blue dotted arrows show the shifting of extract phase.</i>	91
Figure 5.4. Productivity and recovery of ARTE in batch and multi-stage counter-current extraction operations. <i>Input parameters of each stage: $m_S = 3\text{ g}$; $m_L = 30\text{ g}$; $m_E = 23\text{ g}$; $\beta_{ARTE}^{eff} = 0.4$. The productivity and recovery are calculated based on corresponding volume $V_{suspension} = 0.04\text{ L}$ and cycle time $t_{cycle} = 0.5\text{ h}$. The outcomes of the batch extraction at identical working conditions are also presented.</i>	93
Figure 6.1. Outline of the conceptual design process of continuous extractor. <i>The review 1 is basically carried out in-house and the review 2 is assessed by external experts.</i>	95
Figure 6.2. Conceptual design of continuous counter-current extractor using a screw type of apparatus. <i>The conceptual development is relied on the observation, feasibility and manipulation of prototype devices. The compressed segment established by a perforated disk forces the solvent to flow in one direction.</i>	96
Figure 6.3. Typical geometrical parameters of a screw.	98
Figure 6.4. The prototype and the main extractor. <i>Left: the prototype extractor with manual feeding; Right: the main extractor. The free volume of extractor V_{free} is 0.4 Liter and the extractor volume $V_{Extractor}$ is 0.45 Liter.</i>	100
Figure 6.5. The flowsheet of continuous counter-current extraction plant.	102
Figure 6.6. Glass beads as tracers in residence time investigation. <i>Left: Mixture of glass beads and leaves; Right: Glass beads after sieving.</i>	104
Figure 6.7. The distributions in empty extractor of different leaves amounts (1÷4 g) at speed $n = 1.8\text{ rpm}$. <i>The masses are weighed at the outlet in 30-second time interval. Each point on the curves corresponds to a leaves mass in one fraction.</i>	105

Figure 6.8. Illustration of leaves distribution in empty and fulfilled operation mode.	106
Figure 6.9. The distributions in filled extractor of different leaves amounts (1÷4 g) at speed $n=1.8$ rpm. <i>Mass fractions of glass beads measured at the outlet in 30-second time intervals.</i>	107
Figure 6.10. Experimental setup of solvent residence time investigation.	108
Figure 6.11. The collection of fractions in solvent residence time investigation...	109
Figure 6.12. The dependence of solvent mean residence time on solvent flowrate and speed. <i>The plotted data are extracted from Table 6.4.</i>	110
Figure 6.13. Bodenstein (Bo) number of solvent phase in dependence on solvent flowrate and speed.	110
Figure 6.14. The transparent extractor. <i>Photo of a second transparent extractor to investigate the influence of residence time, phase distribution and pressure (provided by PhD student Annemarie Lehr, Institute of Fluid Dynamics and Thermodynamics, Otto von Guericke University Magdeburg, who constructed it for her detailed RTD studies).</i>	111
Figure 6.15. The illustration of input and output of the main counter-current extractor. <i>The extractor is horizontal assembled and the flow of leaves and solvent are not depended on the inclination of the device. At steady state, the size of compressed segment is constant.</i>	112
Figure 6.16. The theoretical ARTE concentration development in extract phase. <i>The composition develops sharply at the beginning and is slowly decreased.</i>	113
Figure 6.17. The continuous counter-current extraction plant. <i>Left: Description of flow and relevant instruments, devices; Right: Switch cabinet. 1-Dried leaves storage tank; 2- Motor M2; 3- Screw feeder; 4- Motor M1; 5- Main extractor; 6- Solvent pump; 7- Raffinate container; 8- Weighing scale for raffinate; 9- Extract container; 10- Weighing scale for extract.</i>	113
Figure 6.18. The ARTE concentration development of a continuous counter-current steady state extraction. <i>Left: Run 1 (input parameters: $n = 1.8$ rpm, $\dot{m}_S = 0.98$ g/min, $\dot{m}_L = 11.7$ g/min); Right: Run 2 (input parameters: $n = 2.2$ rpm, $\dot{m}_S = 1.2$ g/min, $\dot{m}_L = 11.7$ g/min) corresponding to higher screw speed and leaves flowrate \dot{m}_S.</i>	117

List of Tables

Table 2.1. Summary of various alternative possible definitions for extraction and chemical reaction engineering processes.	35
Table 3.1. The relevant important parameters and parameter space.	59
Table 4.1. HPLC gradient method of quantifying ARTE concentrations.	72
Table 4.2. LOD and LOQ values of two desired components ARTE and DHAA for HPLC.	73
Table 4.3. The ARTE, DHAA content of the homogenized dried leaves. The extraction is carried out in 30 minutes for each contact.	77
Table 4.4. Measuring data of dried leaves density. <i>The experiments are carried out in two different masses of leaves and the results confirm the density of dried leaves.</i>	78
Table 4.5. Measuring data of mixture density. <i>The experiments are tested in three different dosages. The results are later applied in geometrical calculation of continuous extractor in chapter 6.</i>	78
Table 4.6. Effective distribution coefficients β_i^{eff} derived from eq. (2.28) of ARTE and DHAA in three solvents.	83
Table 5.1. Single batch extractions of ARTE in Toluene at equilibrium for different dosages. <i>The batch processes are validated if the extraction is long enough to reach equilibrium. All batch extraction processes are carried out at the identical total solvent masses (30 grams). The theoretical extract mass m_E^{Theo} is based on wetting parameter W (eq. (2.3) to determine the extract raffinate phase ratio χ_{ER}^{Theo}, thus, the extract composition $x_{ARTE,E}^{Theo}$ in eq. (2.41) is calculated.</i>	86
Table 5.2. Input data for sequential counter-current equilibrium model in case of ARTE extraction from <i>Artemisia annua L.</i> in Toluene. <i>A fixed dosage (3g leaves / 30g Toluene) was applied for all stages. (*) initial ARTE amount in dried leaves is determined via eq.(3.38) and Table 4.3, (**) distribution coefficient of ARTE, β_{ARTE}^{eff} in Toluene from experimental data (Figure 4.14). N number of stages Figure 3.13...</i>	89
Table 5.3. Experimental conditions of sequential counter-current equilibrium stage extraction. <i>Each extractor is considered as a single batch extractor and has the identical dosage $D = 0.1$ (as discussed in batch extraction (Figure 5.1)).</i>	91

Table 5.4. The simulated and experimental data of outgoing ARTE concentrations in sequential counter-current equilibrium extraction. <i>The 5-stage counter-current cascade is chosen and only outgoing concentrations are interested.</i>	92
Table 5.5. Experimental results of counter-current sequential batch extraction.....	92
Table 6.1. Parameter space of investigation.....	103
Table 6.2. Mean residence time of leaves in empty extractor at different speed. <i>The parameters as mean residence time \bar{t}_S, dimensionless variance σ_n^2 and number of stages are calculated by the introduced eqs.(2.51), (2.54) and (2.57) respectively.</i>	105
Table 6.3. Mean residence time of leaves \bar{t}_S in filled extractor at different speeds.	107
Table 6.4. The dependence of solvent mean residence time \bar{t}_L on speed and solvent flowrate. <i>The setup values of \dot{V}_L and n are taken from calibration data.</i>	109
Table 6.5. Run 1: The steady state working condition of continuous ARTE extraction from <i>Artemisia annua L.</i> based on verified steady state conditions (section 6.3.1). <i>Given parameters: m_S is estimated via eq. (6.15), m_L from pump calibration data (Appendix A18), $x_{ARTE,S,0}$ from Table 4.3, $n_{Feeder}, n_{Extractor}$ from calibration data in Appendix A17. Nitrogen pressure is 3.6 bar.</i>	116
Table 6.6. Run 2: The input parameters for optimized steady state run. <i>The experiment can be implemented at higher input leaves flowrate m_S than previous steady state.</i>	117
Table 6.7. Summary of two steady state continuous extraction combining simulation results. <i>The extract and raffinate flowrates \dot{m}_E, \dot{m}_R are calculated from recorded data (Appendix A28). $x_{ARTE,E}$ is mean value of outlet concentration analyzed by HPLC. $x_{ARTE,E}^{Sim}$ is the simulated results.</i>	118
Table 6.8. Input and output parameters of three experimental extraction operations for ARTE extraction from <i>Artemisia annua L.</i> in Toluene. <i>The dosages of each operation are identical ($D = 0.1$). The parameters in continuous operation are presented in fluxes. The objective functions of batch, sequential multi-stage and continuous operations are taken from Appendix A10 and Table 5.5 respectively. The productivity and recovery of continuous counter-current steady state operation are provided by eqs. (6.16), (6.17).</i>	119

List of Symbols

Latin symbols

Symbol	Designation	Unit
A	dimensionless factor	[-]
D	dosage	[-]
d_{trough}	inner diameter of the trough/casing	[m]
d_{outer}	outer diameter of the screw	[m]
d_{inner}	inner diameter of the screw	[m]
$E(t)$	probability time distribution function	[s ⁻¹]
$F(t)$	cumulative distribution function	[-]
H	moisture	[%]
i	component	[-]
j	stage	[-]
k	extraction rate constant	[kgs ⁻¹ m ⁻²]
k^{eff}	effective mass transfer coefficient	[s ⁻¹]
$\tilde{k}_{i,E}$	modified mass transfer rate	[kgs ⁻¹ m ⁻²]
$\tilde{K}_{i,E}^{eq}$	Modified equilibrium distribution coefficient	[-]
L	liquid phase	[-]
L_{ext}	external liquid/extract phase	[-]
L_{int}	internal liquid/extract phase	[-]
m	mass	[g]
\dot{m}	mass flowrate	[gs ⁻¹]
N	number of stages	[-]
n	rotational speed	[rpm]
$Prod$	productivity	[gh ⁻¹ L ⁻¹]
R_f	retention factor	[-]
Rec	recovery	[%]
S	solid phase	[-]
T	temperature	[°C]
t	residence time	[s]

\bar{t}	mean residence time	[s]
u	velocity	[ms ⁻¹]
V	volume	[m ³]
\dot{V}	volumetric flow rate	[m ³ s ⁻¹]
W	wetting parameter	[-]
x	mass fraction	[-]

Greek symbols

Symbol	Designation	Unit
β	distribution coefficient	[-]
ε	volume fraction	[-]
θ	fraction	[-]
γ	dimensionless factor	[-]
η	dimensionless factor	[-]
κ	conductivity	[Sm ⁻¹]
ρ	density	[kgm ⁻³]
σ	standard deviation	[s]
σ^2	variance	[s ²]
σ_n^2	dimensionless variance	[-]
τ	residence time	[s]

Dimensionless numbers

Symbol	Name	Describes
Bo	Bodenstein number, eq. (2.56)	convection and diffusion effects
Da	Damköhler number, eqs. (3.8), (3.49)	extraction rate and residence time

List of Abbreviations

Abbreviation	Subscription
ACTs	Artemisinin-based combination therapies
ARTE	Artemisinin
DHAA	Dihydroartemisinic acid
WHO	World health organization
APIs	Active pharmaceutical ingredients
A.A	<i>Artemisia annua L.</i>
SLE	Solid liquid extraction
LEL	Lower explosive limit
UEL	Upper explosive limit
RTD	Residence time distribution
CSTR	Continuous stirred-tank reactor
PFTR	Plug-flow tubular reactor
PFE	Pressurized fluid extraction
MAE	Microwave-assisted extraction
SFE	Supercritical fluid extraction
LEDs	Light-emitting diodes
PDE	Permitted daily exposure
TLC	Thin layer chromatography
HPLC	High performance liquid chromatography
ELSD	Evaporative light scattering detector
ECD	Electrochemical detection
UV	Ultra violet
LOD	Limit of detection
LOQ	Limit of quantification
E	Extract
R	Raffinate

1 Introduction

Many synthesized or semi-synthesized pharmaceutical drugs have been developed and exploited in the last decades. Nevertheless, many people still rely on the traditional medicines to deal with psychological and physical health problems since they are not able to afford the expensive medicines from pharmaceutical industries and afraid of side effects of the drugs. Furthermore, there is still a lack of distribution systems and health facilities [1, 2]. Additionally, counterfeiting and illicit drugs cause drug shortages globally [3-5]. Therefore, medicinal products from plants with the advantages of availability, safety and cost still continue to play an essential role in our healthcare systems. Over decades, batch-wise operation is the state of the art in extracting ingredients of interest from plants. There is a lack of activities devoted to develop continuous extraction techniques. As a consequence, the pharmaceutical production capacity for essential medicines is still far away from fulfilling global demands.

Even less activities have been performed with the particular goal of simultaneously co-extracting in addition valuable precursors which are also present in the plants.

The research described in this thesis focused on studying continuous counter-current extraction of a well-known anti-malarial substance, called Artemisinin (designated below also as ARTE) [6-11] from *Artemisia annua L.* or sweet wormwood. More recently the isolation and exploitation of the ARTE precursor dihydroartemisinic acid (DHAA) was reported. Promising results of conversion processes of DHAA to ARTE based on photocatalytical reaction techniques have been achieved by Professor Seeberger and his group at Max Planck Institute of Colloids and Interfaces in Potsdam-Golm [12-14]. Later, besides isolating also DHAA the value of simultaneously co-extracting chlorophyll as a potential photocatalyst was reported [15].

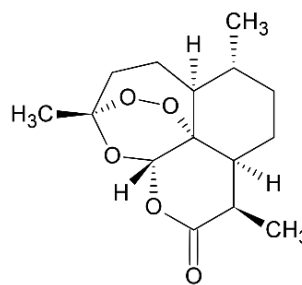


Figure 1.1. *Artemisia annua* L. *Left:* plant, *Right:* molecular structure of the active substance Artemisinin.

In this thesis project an efficient continuous extraction process was realized in a self-designed counter-current screw-based extractor characterized by high extract concentration, good recovery and low solvent consumption.

1.1 Aim of the research

The motivation of the project was to contribute to a better provision of artemisinin-based anti-malaria drugs.

Malaria is a disease caused by *Plasmodium* parasites and transmitted by female *Anopheles* mosquitoes. There are four different *Plasmodium* species, *P.falciparum*, *P.vivax*, *P.malariae* and *P.ovale*. *Plasmodium falciparum* is the most prevalent and most dangerous. In 2020, globally 241 million infection cases and were reported (increasing from 227 million in 2019), most of the cases occurred in Africa countries and an estimation of more than 627 000 deaths increased by 12 % compared by 2019 [16].

In spite of the fact that malaria is a preventable and treatable disease, it continues having a devastating impact on people's lives and health.

Although there are several projects with remarkable progress to fight against malaria, the disease still affects poor countries where people have limited access to health facilities and can barely afford recommended treatments. In the 21st century, malaria gained renewed attention and is of prior global health concern, since morbidity and mortality rates again increase.

The first effective malaria treatment originated from the bark of cinchona tree which contains quinine. This compound remained an important anti-malaria drug over almost 400 years until more effective synthetic anti-malaria drugs became available. In the 1940s, chloroquine was discovered by German scientists and quickly became the most important anti-malaria remedy. With its intensive use, chloroquine resistance significantly emerged [17] and a large mortality escalation occurred only 19 years after introduction. Nevertheless, quinine based treatments possess still a key role [18].

In the 1960s during the Vietnam-US War malaria caused by chloroquine-resistant *Plasmodium falciparum* was a major problem. Because of research infrastructure scarcity, North Vietnam asked China for help. An extensive research was carried out under the name “Project 523” starting in 1967. In the course of this project *Artemisinin* (ARTE), also named *Qinghaosu*, was rediscovered as an effective treatment against malaria. In 1977 the structure of the molecule was identified and reported [19-21]. ARTE is a sesquiterpene lactone with a peroxide function, which is highly effective against malaria [22, 23]. It was discovered by a Chinese scientist named Youyou Tu who achieved Nobel Prize in 2015 [24-26].



Figure 1.2. Chinese scientist Youyou Tu – Nobel Prize 2015 in Physiology or Medicine.

From that milestone on, medication based on ARTE and its derivatives artemether and artesunate has brought the global anti-malaria treatment to a new era. Millions of people could be saved over the past years. In 2002, World Health Organization (WHO) recommended ARTE-based combination therapies (ACTs) as the first-line treatment of malaria. Nevertheless, currently there is the global risk of new rises in malaria morbidity and mortality. Several projects estimate that the global demand for

anti-malaria drugs was around 1.6 billion anti-malaria treatments from 2010 - 2017. It is predicted that there will be an increase to over 1.7 billion treatments by 2021 [3, 5, 27].

A summary of selected recent research activities devoted to improve the production of ARTE-derived API is given below.

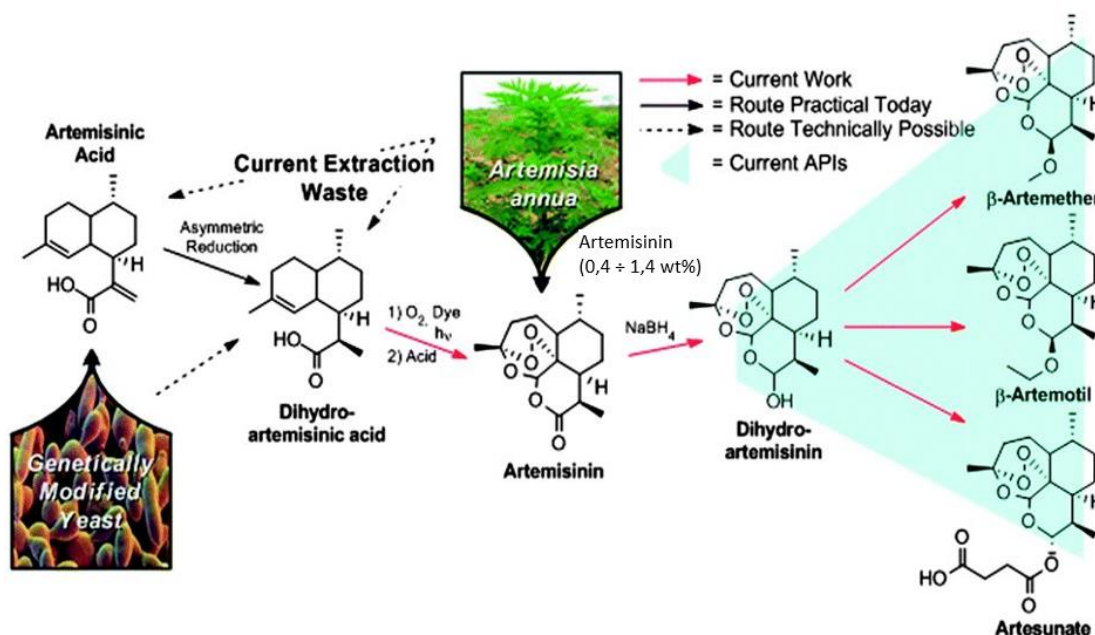


Figure 1.3. Scheme of producing ARTE-based anti-malaria API [28].

It was reported that a precursor for ARTE, namely artemisinic acid can be produced by genetically engineered yeast. This process step has been successfully scaled up. Based on this a further conversion to ARTE has been realized requiring a rather expensive photo-reaction [15, 29, 30]. Several other biotechnological approaches have been developed for heterogeneous production of ARTE [31, 32], but the corresponding processes were not very efficient because of complexities and costs [33].

Furthermore, progress of ARTE extraction from *Artemisia annua* L. has been achieved exploiting supercritical fluid extraction using carbon dioxide [34-41].

All processes suggested are characterized by relatively high investment and operating costs and by limited reproducibility [30, 42-44]. Thus, the development of efficient and preferably continuous concepts for extracting ARTE from *Artemisia*

annua L. is still an open and essential task to better meet the anti-malarial drug global demand. In particular, the development of efficient continuous extraction processes remains a challenging task. This is due to the following specific problems: the content of the valuable target component is very low (the ARTE amount in *Artemisia annua L.* leaves is around 0.4-1.4% based on dried weight) and the effective solid-liquid contact and phase transportation are difficult.

The joint isolation of dihydroartemisinic acid (DHAA), an important precursor for the biosynthesis of ARTE, was essential part of our research. Significant amounts of DHAA were reported to be present in different extracts of *Artemisia annua L.* leaves. It was shown in an independent preliminary work that DHAA could be oxidized photocatalytically to ARTE [12-14, 28], which allows increasing the overall ARTE productivity of the extraction process. For the mentioned photoreaction, the simultaneous co-extraction of chlorophyll A is also highly desirable, since chlorophyll acts as an efficient green photosensitizer [15]. Figure 1.4 illustrates the combination of extraction and photocatalytical synthesis process, in which co-extracted DHAA is photocatalytically converted to ARTE using chlorophyll as photocatalyst.

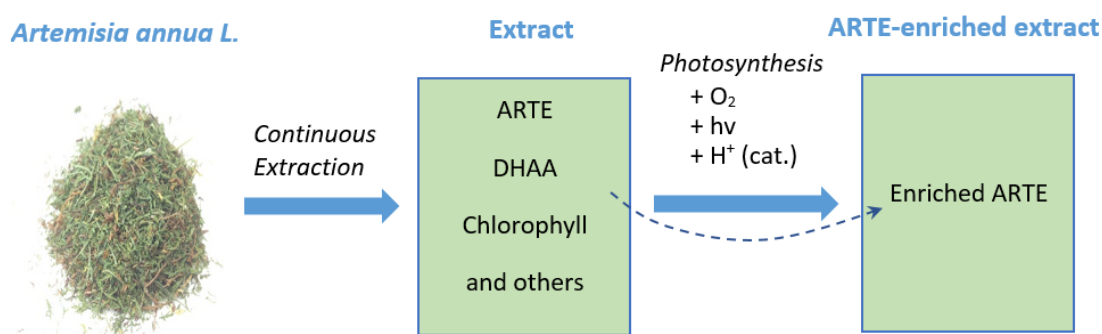


Figure 1.4. Scheme of combination between extraction and semi-synthesis to provide ARTE.

In the frame of the research project, systematic investigations of batch and continuous extraction mode were carried out.

A self-developed continuous counter-current extractor was designed, built and tested. One of the features of this extractor is the realization of suitable residence times of the relevant two phases. In a cooperating PhD project, Annemarie Lehr from the Institute of Fluid Dynamics and Thermodynamics of Otto von Guericke University Magdeburg applied numerical CFD techniques to study phase distributions in the

counter-current extractor. Information regarding this parallel project will be briefly described in Chapter 6.

The research to be described in this thesis focused on the following three directions:

- Analyzing extraction processes including single stage batch, multi-stage counter-current batch and continuous operation.
- Designing, implementing, characterizing and applying a novel screw-type extractor.
- Comparing the new type of extractor with well-established conventional configurations.

1.2 Structure of this thesis

This research is constructed by following structure: *Chapter 1* addresses the essential role of high valuable component extraction from plants, called phytoextraction, the anti-malarial substance ARTE, and its precursor DHAA. The investigation is motivated by the ARTE global demand and technology improvement in phytoextraction. Additionally, the challenges and problems of recent extraction in the pharmaceutical industry are addressed and the development of continuous counter-current extraction is the aim of the research. The relevant research projects have been taken out to improve the total efficiency. *Chapter 2* presents basics of describing solid liquid extraction with a focus on extraction of natural products. The crucial parameters as kinetics, equilibrium, distribution coefficients in different solvents and other relevant parameters are shown. Also, the residence time distribution strongly related to the continuous extractor is introduced. The extraction concepts and close related equipment are presented. *Chapter 3* focuses on the simulation model. It is divided into two main parts: the first part shows the analogy of Chemical Reaction Engineering (CRE) to solid liquid extraction process and the second part is the adaption to the extraction processes. Many different scenarios and configurations are given and discussed. Also the influence of important parameters as mass transfer rate, distribution coefficient, residence time, phase fraction on the efficiency is included. The advantage of counter-current operation is pointed out, the analogy of CRE and extraction exploits more possibilities to advance the process.

The quantifying objective functions are introduced and later applied in the experimental chapters. *Chapter 4* explains the details of experimental successive procedures from analytical methods to preliminary investigations of the material. The important parameters as thermodynamics and kinetics for a specific study case of ARTE extraction from *Artemisia annua L.* are determined experimentally. These important parameters will be later applied in three main extraction operations: batch, multi-stage and continuous extraction. *Chapter 5* focuses on the evaluation of batch and sequential multi-stage counter-current extraction. An experimental setup of multi-stage counter-current extraction is introduced. The simulated and experimental results are compared. *Chapter 6* shows the systematical investigation of continuous counter-current extraction. The dimension of the self-developed extractor for the specific case of ARTE extraction is estimated based on experimental data of the previous section. All the relevant design steps are also briefly explained. The experiments are divided into two main sections: (1) residence time distribution investigation and (2) continuous extraction implementation. The estimation of residence time is very important to decide on the working condition of the runs. For the continuous extraction, the calibration of relevant devices and equipment is the first task, then, the verification of steady state conditions is a must. The evaluation is carried out based on continuous experimental data. A comparison of all three operation modes is given as conclusion of this chapter. *Chapter 7* summarizes the results and presents an outlook.

2 Solid liquid extraction

Solid liquid extraction (SLE), i.e. the dissolution of soluble components (solutes) out of a solid material applying an appropriate solvent, has a very long tradition and is widely used in metallurgical, food, pharmaceutical and chemical industries. Examples are the extraction of rare earth elements (for example scandium and yttrium) for civil and military applications and the extraction of natural products from plant materials. For the sugar industry the exploitation of sugar beets applying extraction techniques is most essential.

A common solid liquid extraction process is embedded in a sequence of several other steps as illustrated in the following scheme:

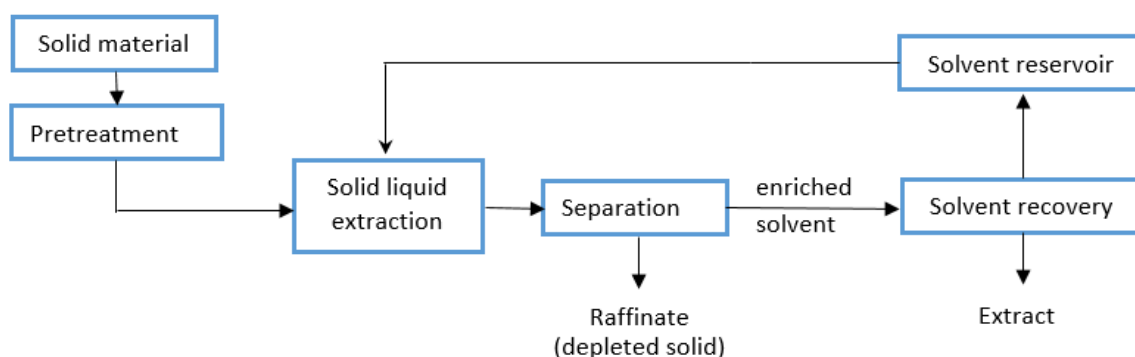


Figure 2.1. Illustration of the steps related to solid liquid extraction processes. *The extract is typically the target outlet stream which contains a desired component. The raffinate which contains amounts of remaining target solutes is sometimes considered as “waste”.*

Typically, fresh (unloaded) solvent is used. It is desirable to recover this solvent from the extract phase and to recycle it after isolating the target component. Pretreatment steps such as drying and grinding might be required for preliminary feed storage but also to decrease the size of solid particles. Grinding helps shortening the penetration time of the solvent and accelerates the extraction kinetics. The intrinsic extraction step depends on many different parameters as temperature, pressure, the liquid-to-solid ratio, the mean solid particle size and the size distributions. The specific characteristics of the solid feed material and the objectives of the process need to be evaluated case by case in order to select and develop an appropriate extraction

method. The intrinsic extraction process is terminated by separating the raffinate and extract phases from each other. To get the final product, the extract will be subsequently further treated in subsequent downstream processes like evaporation, crystallization and eventually formulation.

2.1 Phytoextraction

The potential of using natural products to fight against illnesses was recognized when man first used plants as food and discovered parallel occurring therapeutic effects. Healing methods were developed exploiting seeds, bark, leaves and other parts of the plants. For millennia, a diversity of naturally medical products was exploited and specific extraction methods have been developed and applied [45-53].

There is a large amount of different compounds in plants classified into primary and secondary metabolites. Primary metabolites are directly related to the growth, development, reproduction of the cells and do not show any pharmacological effects. Meanwhile, secondary metabolites, known as natural products, are produced not only as a result of the organism adapting to the surroundings. They possess an ecological role, are pollinators or offer defense against predators. These secondary metabolites are frequently found in plants in smaller quantities than the preliminary metabolites [54]. They have multiple functional groups classified into three main groups: alkaloids, terpenoids and phenols characterized by different functioning mechanism as antimoral, antibacterial, anti-insecticidal and other. These bioactive compounds are located in a complicate microstructure (capillaries, pores, and cells). They can be dissolved by solvents applying various types of extraction processes.

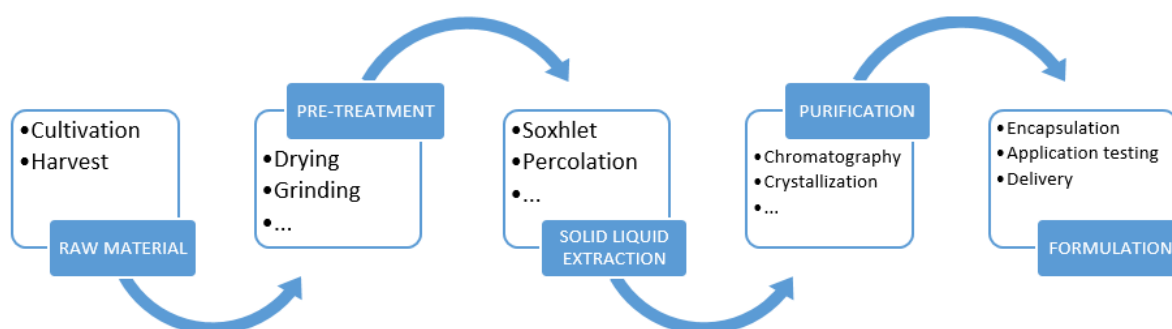


Figure 2.2. Typical steps of producing API based on phytoextraction.

Above is the principle of a general extraction process devoted to the isolated and exploited natural products. Generally, the target content in the plant material strongly depends on the climate condition, the nutrient of the soil, the harvest time and so on. After harvesting, the plants are dried to a specific moisture level to allow longer storage. Then, they can be cut into pieces or ground to enhance the contacting surface area aiding the solvent penetration into interstitials and pores of material. This size reduction should be limited since pressure drop, flow instability and slow drainage rate might happen. The contacting of the solvent and plant material causes a penetration of the solvent into the solid matrix. The solvent will dissolve soluble components, which subsequently diffuse back to the outer liquid bulk phase (Figure 2.3).

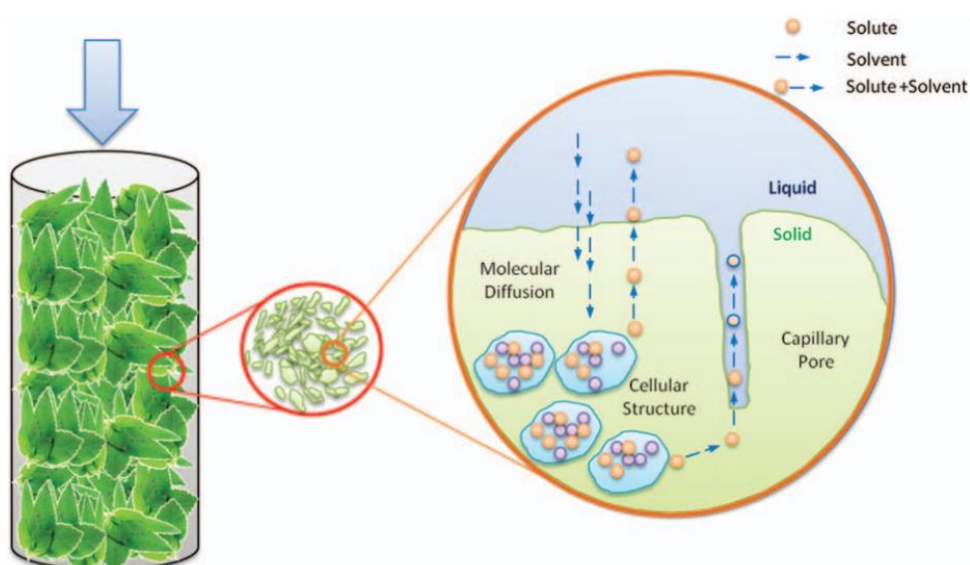


Figure 2.3. Scheme of solute transfer during a phytoextraction process according to [47]. *The solvent dissolves solutes in interstitials and pores of the solid start material and these solutes diffused then back into the liquid body.*

The selection of a suitable solvent with high solubility with respect to the desired component is essential. The choice of a suitable extraction operation method is also crucial. Sometimes, a combination of different extraction methods is necessary to maximize the efficiency of the production. Subsequently, dedicated purification processes might be required, since the enriched solvent contains both desired target but also unwanted other components [55]. The design of all of these process steps depends on the specific character of the starting material and the properties of the solvent.

2.2 Fundamentals

2.2.1 Phases involved in natural product extraction

Total mass balances

Not all extractable substances present in the solid phase are transferred to the liquid phase. Definite specific amounts of extract are retained in solid phase.

In this thesis, the initial amounts of the unloaded solvent and the dry solid material are designated by $m_{L,0}$ and $m_{S,0}$. Furthermore, it is assumed that the total amount of the solid matrix is preserved during the extraction operations. Thus:

$$m_S = \text{constant} = m_{S,0} \quad (2.1)$$

A specific problem of quantifying solid-liquid extraction processes is the unavoidable occurrence of liquid adherent to the solid after separating the two product phases from each other. A mass balance of the liquid phase needs to respect this split. We split $m_{L,0}$ in $m_{L,ext}$ (quantifying the liquid phase not bound to the solid material) and $m_{L,int}$ (representing the liquid adherent to the solid matrix). Both the solid and the internal liquid phase form the raffinate R. With these assumptions, the following two liquid phase mass fractions can be defined:

$$x_{L,ext} = \frac{m_{L,ext}}{m_{L,0}} \quad \text{and} \quad x_{L,int} = \frac{m_{L,int}}{m_{L,0}} \quad (2.2)$$

In the beginning of the extraction process the solid material is wetted by contacting it with the unloaded solvent. This leads to a new (“soaked”) solid phase with adherent liquid. To characterize this lumped phase we introduce a characteristic wetting parameter W as follows:

$$W = \frac{m_{L,int}}{m_S} \quad (2.3)$$

This parameter W is assumed to be specific and constant for a given solid/solvent. W is zero if no adherent liquid is incorporated into the solid after an initial contact of solid and liquid.

With the parameters introduced above, the following overall liquid phase mass balances can be formulated for a closed batch system:

$$m_{L,0} = m_{L_{ext}} + m_{L_{int}} = x_{L_{ext}} * m_{L,0} + x_{L_{int}} * m_{L,0} \quad (2.4)$$

$$m_E = m_{L_{ext}} = m_{L,0} - m_{L_{int}} \quad (2.5)$$

$$m_R = m_S + x_{L_{int}} m_{L,0} = m_S + m_{L_{int}} \quad (2.6)$$

An overall mass balance quantifying the total mass considering both phases can be formulated in the following way:

$$m_{total} = m_{L,0} + m_S = x_{L_{ext}} m_{L,0} + x_{L_{int}} m_{L,0} + m_S = m_E + m_R \quad (2.7)$$

The depiction of the phase situation defined above is illustrated in the following sketch:

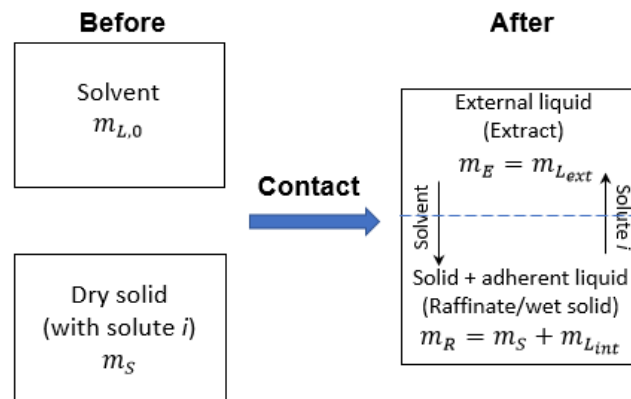


Figure 2.4. Illustration of phases involved in phytoextraction. *Left:* the two initial phases involved before contacting them. *Right:* mass transfer directions of a solute i and the solvent along with the designation of extract (liquid without solid) and raffinate (solid with adherent liquid).

An important information required to quantify the course of an extraction process is the specification of the amounts of the two main phases to be contacted. For this it is expedient to introduce a dimensionless parameter representing the ratio of the phases, namely the dosage, D , which is defined for a conventional batch process as:

$$D_{Batch} = \frac{m_S}{m_{L,0}} \quad (2.8)$$

Analogously holds for the dosage later in this thesis discussed continuous processes using the mass fluxes of the solid and liquid phases, \dot{m}_S and $\dot{m}_{L,0}$:

$$D_{Continuous} = \frac{\dot{m}_S}{\dot{m}_{L,0}} \quad (2.9)$$

Characteristic mass fractions of the three phases arising after splitting the liquid phase can be described using both the wetting parameter W and the dosage D as:

$$x_{L_{ext}} = \frac{m_{L_{ext}}}{m_{L,0}} = 1 - W * D \quad (2.10)$$

$$x_{L_{int}} = \frac{m_{L_{int}}}{m_{L,0}} = W * D \quad (2.11)$$

$$x_{S,0} = \frac{m_S}{m_{total}} = \frac{D}{1+D} \quad (2.12)$$

Of interest for the quantification of extraction processes is to evaluate also another mass ratio, namely the ratio between the total masses of the extract and raffinate phases χ_{ER} . This can be expressed by combining eqs.(2.8), (2.10), (2.11) as:

$$\chi_{ER} = \frac{m_E}{m_R} = \frac{m_{L,0} - m_{L_{int}}}{m_S + m_{L_{int}}} = \frac{1 - D * W}{D + D * W} \quad (2.13)$$

The ratio χ_{ER} plays an important role for estimating the extraction efficiency and will be used below.

To conclude this section which introduced essential definitions, it should be mentioned that an equivalent alternative option would have been possible with respect to the definition of the phases and their ratios. This option would exclude the adherent (internal) liquid phase from the raffinate and balance it together with the extract, which comprises then the total liquid phase. This alternative and equally applicable option is not followed in this work. However, related to the definition of thermodynamic distribution coefficients it will be shortly addressed in sections 2.2.2 and 4.2.

Solid phase component mass balances

After quantifying the overall masses of the phases involved, we consider now the mass balances of specific solutes i which are introduced into the extraction process with the feed material. They are present in specific amounts in the entering solid phase. An initial solid phase mass fraction of component i in the dried solid material can be formulated as follows:

$$x_{i,S,0} = \frac{m_{i,S,0}}{m_S} \quad i = 1, N_C \quad (2.14)$$

This equation is valid for any of N_C extractable components. The masses and fractions of a specific component i need to be determined typically by preliminary exhaustive extraction experiments as introduced in section 5.2.

Since before the initial contact with the solvent there is no external liquid phase present it holds:

$$x_{i,L_{ext},0} = x_{i,L,0} = \frac{m_{i,L,0}}{m_{L,0}} = 0 \quad i = 1, N_C \quad (2.15)$$

This is complimented by the fact that in a single stage batch extraction process, there is initially no internal liquid phase present, i.e.

$$m_{L_{int},0} = 0 \quad \text{and} \quad m_{i,L_{int},0} = 0 \quad i = 1, N_C \quad (2.16)$$

For a closed system, the overall mass of component i is preserved. This means that a component specific mass transfer from the solid to the external liquid phase, $\dot{m}_{i,S \rightarrow L}$, can be expressed by:

$$\frac{dm_{i,S}(t)}{dt} = -\frac{dm_{i,L}(t)}{dt} = -\dot{m}_{i,S \rightarrow L}(t) \quad i = 1, N_C \quad (2.17)$$

Besides considering the masses involved, it is also important to keep track of characteristic volumes and to quantify them. This is due to the fact that each extraction apparatus provides a specific internal volume for accommodating the two phase during operation. Thus, the densities of the phases become also relevant. For a simplified quantitative discussion, it is helpful to introduce a suspension density, $\rho_{suspension}$. This suspension density allows estimating the volume of the suspension, $V_{suspension}$, from the related masses of the two phases as follows:

$$V_{suspension} = \frac{m_S + m_{L,0}}{\rho_{suspension}} = \frac{m_{suspension}}{\rho_{suspension}} \quad (2.18)$$

The suspension density can be experimentally estimated as described in section 5.2.

Extraction processes are carried out in a defined space, which we describe below by the volume $V_{extractor}$. This volume consists also of additional elements (e.g. stirrers,

screws, ...), housing requirements and eventually an overhead gas space (typically air present in the apparatus). The following equation keeps track of these specific volumes:

$$V_{extractor} = V_{suspension} + V_{additional\ devices} + V_{housing} + V_{gas} \quad (2.19)$$

A depiction of the volumes mentioned is shown in Figure 2.5.

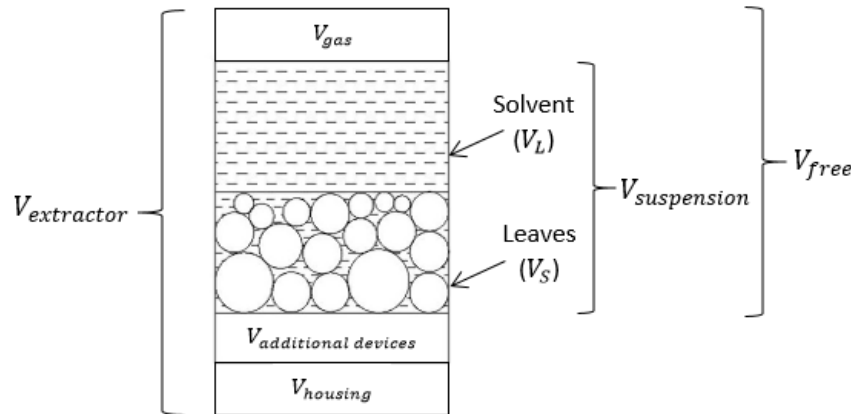


Figure 2.5. Illustration of involved volumes described in eq. (2.19). *The volumes of additional devices are the volumes of screw; housing volume is the occupied space of extractor housing; the suspension volume is the total volume of liquid and solid phases introduced in eq. (2.18).*

The housing volume $V_{housing}$ is the thickness of extractor housing. The combined volume of suspension and gas can be designated as a free volume, V_{free} :

$$V_{free} = V_{suspension} + V_{gas} = V_{suspension} + \theta V_{suspension} = (1 + \theta)V_{suspension} \quad (2.20)$$

In eq. (2.20) the gas volume is expressed as a fraction θ of the suspension volume, which will be used in efficiency evaluations presented later in chapters 5 and 6.

Finally, the extractor can be in addition characterized by two instructive specific volume fractions considering also the gaseous void phase and solid phase:

$$\text{Void fraction:} \quad \varepsilon_L^* = \frac{V_L}{V_{free}} \quad (2.21)$$

$$\text{Solid fraction:} \quad \varepsilon_S^* = \frac{V_S}{V_{free}} \quad (2.22)$$

The application of the above introduced definitions is of help for specifying suitable geometrical dimensions of an extractor. This will be demonstrated for the specific case of extracting ARTE in chapters 5 and 6.

2.2.2 Equilibrium

If the solid and liquid phases are contacted in a closed system for a sufficiently long time ($t \rightarrow \infty$) constant compositions will be established in both phases. These compositions characterize the extraction equilibrium [56-61], which will be designated using the superscript "eq".

For a component i , the external liquid phase composition in equilibrium can be designated as:

$$x_{i,L_{ext}}^{eq} = \frac{m_{i,L_{ext}}^{eq}}{m_{L_{ext}}} \quad i = 1, N_C \quad (2.23)$$

Since in equilibrium the compositions are the same in the external and internal liquid phases, it further holds:

$$x_{i,L_{ext}}^{eq} = x_{i,L_{int}}^{eq} = x_{i,L}^{eq} = x_{i,E}^{eq} \quad i = 1, N_C \quad (2.24)$$

Similarly, equilibrium fractions of components i characterizing the equilibrium compositions in the raffinate phase of mass $m_{i,R}^{eq}$ can be introduced. These fractions are designated below as the raffinate mass fractions, which can be expressed by:

$$x_{i,R}^{eq} = \frac{m_{i,L_{int}}^{eq} + m_{i,S}^{eq}}{m_{L_{int}} + m_S} = \frac{m_{i,R}^{eq}}{m_{L_{int}} + m_S} \quad i = 1, N_C \quad (2.25)$$

The corresponding equilibrium amounts stored in the extract (external liquid phase) and raffinate (internal liquid and solid phases) (eqs.(2.23) and (2.25)) need to respect for a constant temperature a thermodynamic function, which is specific for the system solid phase/solvent/solute i . This equilibrium function can be expressed in a general form for a mixture of N_C solutes as follows:

$$x_{i,E}^{eq} = x_{i,E}^{eq}(x_{1,R}^{eq}, \dots, x_{N_C,R}^{eq}) \quad i = 1, N_C \quad (2.26)$$

If there are no competition effects of other components on the equilibrium of a specific component i the following simplification holds:

$$x_{i,E}^{eq} = x_{i,E}^{eq}(x_{i,R}^{eq}) \quad i = 1, N_C \quad (2.27)$$

A very simple equilibrium function, which is valid for diluted extracts, is the following linear equilibrium function introducing an effective distribution coefficient, designated as β_i^{eff} :

$$x_{i,E}^{eq} = \beta_i^{eff} x_{i,R}^{eq} \quad i = 1, N_C \quad (2.28)$$

Referring to the final paragraph of section 2.2.1 it should be mentioned that instead of eq. (2.26), another split of the two phases can be made, which then needs to respect accordingly adjusted equilibrium functions and distribution coefficients β_i defined by the ratio of the amounts of component i in the external liquid phase (extract phase) and in the solid phase:

$$\beta_i = \frac{x_{i,E}^{eq}}{x_{i,S}^{eq}} \quad i = 1, N_C \quad (2.29)$$

As mentioned above, at equilibrium, the composition of component i in the external liquid phase is identical to that in the internal liquid phase. Therefore, a conversion between the different thermodynamic coefficients is possible, provided the wetting parameter W is known. Alternative phase definitions just need to be applied consistently. This is exemplified in *Appendix A1*.

2.2.3 Operation modes and corresponding mass balances

As introduced, we focus in this thesis on developing a continuous extraction process. Before introducing corresponding concepts, it is instructive to describe first conventional batch operation in a single stage and then discuss possible extensions exploiting multiple consecutive batchwise operated stages.

In a batch extraction process, the plant material and the solvent are supplied into the extractor jointly. The extract and raffinate phases are also collected jointly after a certain operation time.

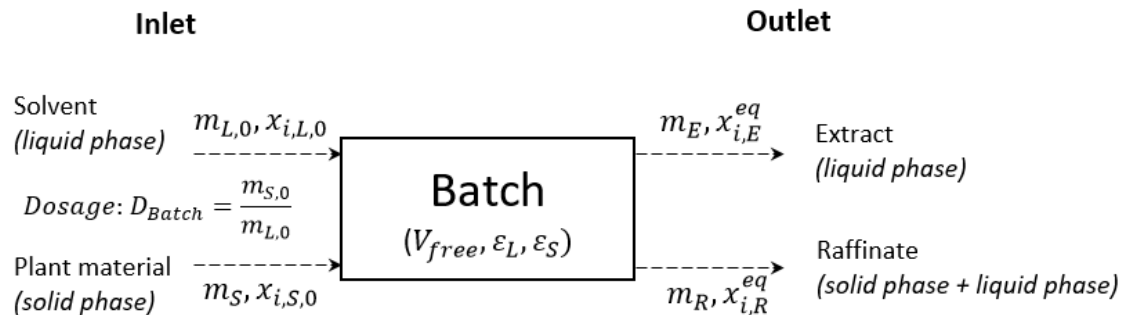


Figure 2.6. Illustration of initial and final masses and mass fractions for a batch process. The initial compositions of component i of solid and liquid phases are defined by eqs.(2.14) and (2.15) respectively. The final amounts of component i in extract (external liquid without solid) and raffinate (internal liquid and solid) are derived from eqs.(2.23) and (2.25). The dashed arrows represent the filling and emptying of the extraction vessel. If all masses m are replaced by mass fluxes \dot{m} , this scheme also describes continuous extraction processes to be discussed later.

The development of characteristic masses and fractions of a component i over time evolving in a batch process are illustrated schematically in Figure 2.7.

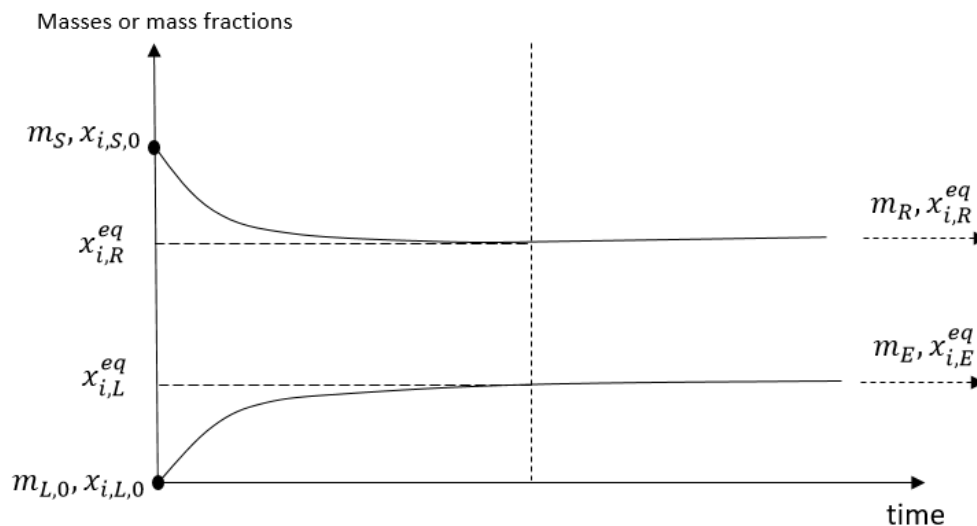


Figure 2.7. Development of fractions of component i with corresponding masses of the phases over time in a typical batch extraction process.

In batch processes the mass fraction of a component i in liquid phase converges for progressing time to a certain final value, at which the mass transfer rates between

the two phases becomes zero and the fraction does not change anymore. The opposite (mirror like) behavior is observed for the solid phase fraction of component i , which changes from the initial fraction to the equilibrium raffinate fraction. The equilibrium liquid phase mass fractions $x_{i,Lext}^{eq}$, $x_{i,Lint}^{eq}$, $x_{i,L}^{eq}$ and $x_{i,E}^{eq}$ are identical. The fraction $x_{i,R}^{eq}$ introduced in eq. (2.25) is accessible via the overall mass balance given by eq.(2.17):

$$\frac{dm_{i,R}}{dt} + \frac{dm_{i,E}}{dt} = 0 \quad i = 1, N_C \quad (2.30)$$

Integration of this equation requires initial conditions. If we assume that the solvent is not preloaded ($m_{i,E,0} = 0$), only the material brought with the solid raffinate phase ($m_{i,R,0} \neq 0$) is available for distribution.

Then, the integrated form of eq. (2.30) is:

$$m_{i,R}(t) + m_{i,E}(t) = m_{i,R,0} \quad i = 1, N_C \quad (2.31)$$

Assuming a simple first order rate law for the kinetics of extraction, the transportation of a component i from the solid phase to the extract can be described as:

$$\frac{dm_{i,E}}{dt} = k_i * A(m_{i,E}^{eq}(m_{i,R}) - m_{i,E}) \quad i = 1, N_C \quad (2.32)$$

Lumping the rate coefficient k_i and the interface area A into an effective rate constant k_i^{eff} gives:

$$\frac{dm_{i,E}}{dt} = k_i^{eff} (m_{i,E}^{eq}(m_{i,R}) - m_{i,E}) \quad i = 1, N_C \quad (2.33)$$

Combining with eqs. (2.13) and (2.28) we can rewrite eq. (2.33) as:

$$\frac{dm_{i,E}}{dt} = k_i^{eff} (\beta_i^{eff} * \chi_{ER} * m_{i,R} - m_{i,E}) \quad i = 1, N_C \quad (2.34)$$

Substituting eq. (2.31) into eq. (2.34) provides:

$$\frac{dm_{i,E}}{dt} = k_i^{eff} (\beta_i^{eff} * \chi_{ER} (m_{i,R,0} - m_{i,E}) - m_{i,E}) \quad i = 1, N_C \quad (2.35)$$

Rearrangement provides:

$$\frac{dm_{i,E}(t)}{dt} = (-k_i^{eff}(\beta_i^{eff} * \chi_{ER} + 1)m_{i,E} + \beta_i^{eff} * k_i^{eff} * \chi_{ER} * m_{i,R,0})$$

$$i = 1, N_C \quad (2.36)$$

This is a linear differential equation of the general form:

$$\frac{dx}{dt} = (-Ax + B) \quad (2.37)$$

For $x(t = 0) = 0$ the following solution holds:

$$x(t) = \frac{B}{A}(1 - e^{-At}) \quad (2.38)$$

Thus, the solution of eq. (2.36) is:

$$m_{i,E}(t) = \frac{\beta_i^{eff} * \chi_{ER} * m_{i,R,0}}{(\beta_i^{eff} * \chi_{ER} + 1)} \left(1 - e^{-k_i^{eff}(\beta_i^{eff} * \chi_{ER} + 1)t} \right) \quad i = 1, N_C \quad (2.39)$$

According to the overall mass balance eq. (2.31), $m_{i,R}(t)$ is:

$$m_{i,R}(t) = m_{i,R,0} - m_{i,E}(t) = \frac{m_{i,R,0}}{(\beta_i^{eff} * \chi_{ER} + 1)} \left(1 + \beta_i^{eff} * \chi_{ER} * e^{-k_i^{eff}(\beta_i^{eff} * \chi_{ER} + 1)t} \right)$$

$$i = 1, N_C \quad (2.40)$$

When time goes to infinity, the obtained equilibrium amount of component i in the liquid phase is:

$$m_{i,E}^{eq} = \frac{\beta_i^{eff} * \chi_{ER} * m_{i,R,0}}{(\beta_i^{eff} * \chi_{ER} + 1)} \quad i = 1, N_C \quad (2.41)$$

The corresponding raffinate phase mass at equilibrium is characterized by:

$$m_{i,R}^{eq} = \frac{m_{i,R,0}}{(\beta_i^{eff} * \chi_{ER} + 1)} \quad i = 1, N_C \quad (2.42)$$

The ratios of the two values $m_{i,E}^{eq}$ and $m_{i,R}^{eq}$ together with χ_{ER} and β_i^{eff} confirms eq.(2.28).

Eqs. (2.41) and (2.46) allow estimating masses of component i in both phases at any time and at equilibrium. This knowledge will be used below in evaluating the efficiency of the extraction process.

One of the most important tasks required to evaluate and design batch extraction processes is the identification of suitable extraction times which as going to be discussed below in section 2.2.4.

Analogously to batch operation, the mass balances of continuous extraction at steady state can be expressed by quantifying fluxes of phases.

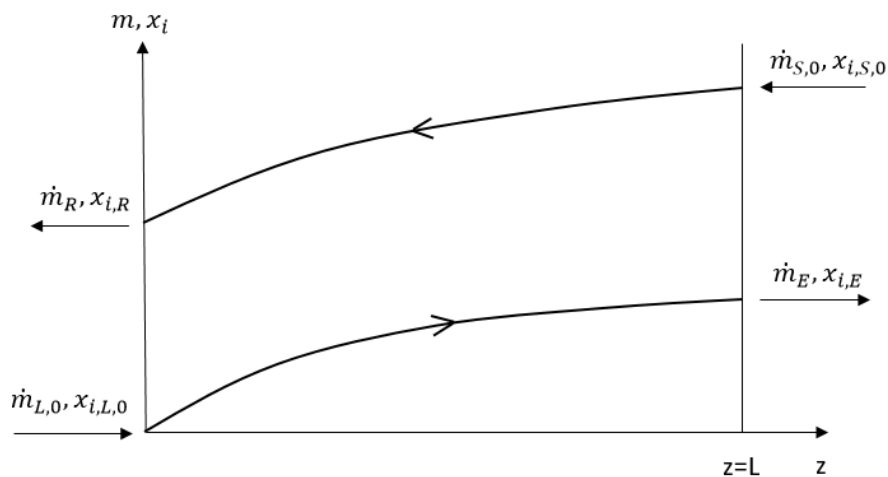


Figure 2.8. Concentration profile of component i in a tubular continuous counter-current extractor process at steady state. The solid material and fresh liquid phase are supplied in opposite directions with corresponding compositions of component i (eqs.(2.14) and (2.15), the obtained extract (E) and raffinate (R) compositions are based on eqs.(2.23) and (2.25).

However, in contrast to batch operation, the continuous steady state mode is characterized by constant process parameters at the inlet and outlet as well as at all positions within the extractor. In Figure 2.8, the fractions of component i in the two phases develop over the length of the equipment in the counter-current mode, while in batch process the progress is over time. It is obvious the longer the equipment, the higher the concentration of the extract. One of the advantages of this counter-current arrangement is the fact that there is contact of enriched liquid phases and fully loaded materials. This leads to efficient driving forces and highly concentrated extracts at the outlet (Figure 2.8).

Further discussion and specific calculations based on mass balances for continuous operation will be given in chapters 5 and 6.

2.2.4 Kinetics and extraction rate constants

Quantitative understanding of kinetics is important to estimate the productivity of the extraction process, to design the size of the unit and to adjust the operating conditions. In phytoextraction, the solvent penetrates into the plant matrices and dissolve the soluble components. The dissolution process can be divided into two main steps: a first fast “washing” step and a second slower diffusion step. The solvent dissolves in the first step the solutes from accessible layers with relatively high mass transfer rate. Then the rate decreases significantly in a subsequent diffusion step [62-64]. After a sufficiently large extraction time, the solute concentration in liquid phase does not change anymore and equilibrium is achieved (Figure 2.7). The concentration transients are controlled by specific kinetics. Knowing them allows defining the necessary time to achieve a desired extraction success. Typical concentration profiles illustrating the rate of the solute mass transfer were presented in Figure 2.7. The overall mass transfer rate of component i from the solid to the liquid phase was introduced in eq. (2.17). Simple first order kinetics for the rate of this transport were introduced in eq. (2.32). The solution given with eq. (2.39) allows calculating the mass of a component i in the extract. It is useful to define a normalized uptake of the liquid phase as:

$$\gamma_i(t) = \frac{m_{i,E}(t) - m_{i,E,0}}{m_{i,E}(t \rightarrow \infty) - m_{i,E,0}} \quad [0,1] \quad i = 1, N_C \quad (2.43)$$

The values of $m_{i,E}(t)$ and $m_{i,E}(t \rightarrow \infty)$ can be taken from eqs.(2.39) and (2.41), thus:

$$\gamma_i(t) = 1 - e^{-k_i^{eff}(\chi_{ER} * \beta_i^{eff} + 1)t} \quad i = 1, N_C \quad (2.44)$$

A characteristic time \bar{t} renders the absolute value of the exponent to be unity, i.e.:

$$k_i^{eff} (\chi_{ER} * \beta_i^{eff} + 1) \bar{t} = 1$$

Assuming the correctness of the exponential behavior at time \bar{t} the uptake γ_i is $1 - e^{-1} = 0.63$. Estimating this characteristic time from experimental data allows a simple and quick estimation of the effective rate constant k_i^{eff} provided the thermodynamic coefficient β_i^{eff} and the mass ratio χ_{ER} are available:

$$k_i^{eff} = \frac{1}{\bar{t}(\chi_{ER} * \beta_i^{eff} + 1)} \quad i = 1, N_C \quad (2.45)$$

It should be mentioned that \bar{t} corresponds to the first moment μ_1 of the first derivative of the uptake curve, γ_i' . For this derivative holds:

$$\gamma_i'(t) = k_i^{eff} (\beta_i^{eff} * \chi_{ER} + 1) * e^{-k_i^{eff} (\beta_i^{eff} * \chi_{ER} + 1)t} \quad i = 1, N_C \quad (2.46)$$

The first moment μ_1 can be also estimated more rigorously analyzing the whole course of the derivative of the uptake measurements $\gamma_i'(t)$ using the following expression:

$$\bar{t} = \mu_1 = \frac{\int_0^{\infty} t * \gamma_i'(t) dt}{\int_0^{\infty} \gamma_i'(t) dt} \quad i = 1, N_C \quad (2.47)$$

The specific application of the above theory to estimate suitable extraction times will be presented in chapter 5.

2.2.5 Residence time analysis

In continuous processes as studied in this work, there will be specific residence distributions for the solid and liquid phases. These distributions can differ from each other. When the solid material stays for short in the extracting environment, the plant material is released too early and both extraction productivity and recovery are relatively low. In contrast, when the material stays too long, the process is not efficient. Similar behavior holds for the liquid phase. Below we will shortly introduce basic concepts of quantifying residence time distributions (RTD) exploiting the first two moments of these distributions.

The quantification of RTD plays in numerous processes an essential role to achieve the best performance. For example, during the development of polymerization processes, many researches have investigated different types of extruders and investigated carefully the character of flow field using RTD analysis [65-70]. However, there is lack of research devoted to evaluate continuous extraction of ingredients stored in plants, in particular for designing new concepts for performing the extraction in counter-current operation.

Generally, when feed material (solid or liquid) is supplied at one side of the extractor, it is distributed in different form during its propagation through the apparatus. The developing distributions also depend on the input characteristics. The study of RTD typically experiments with a marker i are carried out using well defined pulse or step inputs characterized by a fraction of a marker substance i , $x_{i,o}(t)$. Measured are the corresponding output concentration profiles of the marker substance i , $x_{i,out}(t)$.

For pulse inputs, a normalized residence time distribution function $E(t)$ is defined as [71]:

$$E(t) = \frac{x_{i,out}(t)}{\int_0^{\infty} x_{i,out}(t) dt} \quad (2.48)$$

For step inputs, a corresponding cumulative distribution function $F(t)$ quantifies the RTD.

$$F(t) = \frac{x_{i,out}(t)}{x_{i,0}} = \int_0^t E(t) dt \quad (2.49)$$

Eq. (2.49) shows the connection between $E(t)$ and $F(t)$. Because the experimental data are collected typically as discrete instants of time, integrals need to be approximated via summations. Using the typically constant time intervals used for data acquisition, Δt :

$$\int_0^{\infty} x_{i,out}(t) dt \approx \sum_{k=1}^{n_k} x_{i,out}(t_k) \Delta t \quad (2.50)$$

To condense the information provided by the RTD it is expedient to introduce and evaluate moments of these distributions. Hereby, the first moment designates the mean value of the distribution. It is calculated as (see also eq. (2.47)):

$$\bar{t} = \frac{\int_0^{\infty} tE(t) dt}{\int_0^{\infty} E(t) dt} = \int_0^{\infty} tE(t) dt \approx \sum_{k=1}^{n_k} t_k E(t_k) \Delta t_k = \frac{\sum_{k=1}^{n_k} t_k x_{i,k} \Delta t_k}{\sum_{k=1}^{n_k} x_{i,k} \Delta t_k} \quad (2.51)$$

When the volumetric flow \dot{V} of the carrier stream is constant, the mean residence time \bar{t} can be simply estimated based on the system volume V_{total} .

$$\bar{t} = \frac{V_{total}}{\dot{V}} \quad (2.52)$$

The second central moment μ'_2 , also called variance σ^2 , considers the mean residence time \bar{t} and is defined as:

$$\mu'_2 = \sigma^2 = \int_0^{\infty} (t - \bar{t})^2 E(t) dt \quad (2.53)$$

Eq. (2.53) can be given in discretized form as:

$$\sigma^2 = \frac{\sum_{k=1}^{n_k} t_k^2 x_{i,k} \Delta t_k}{\sum_{k=1}^{n_k} x_{i,k} \Delta t_k} - \bar{t}^2 \quad (2.54)$$

Evaluation of the second central moment provides an indication on the degree of backmixing. Of special interest and widely used in characterizing RTD in chromatography columns is in particular the ratio $\left(\frac{\bar{t}}{\sigma}\right)^2$, which is interpreted as a number of theoretical separation stages N [72]:

$$N = \frac{\bar{t}^2}{\sigma^2} \quad (2.55)$$

This stage number can be used in mixed-cell in series (cascade) models or also in dispersion models, where the number of stages is also frequently related to an equivalent Bodenstein number, Bo , which represents the ratio of the amount of tracer transported by convection to that transported by diffusion. It holds:

$$Bo = \frac{uL}{D_{ax}} = \frac{N}{2} \quad (2.56)$$

In eq. (2.56), u is the flow velocity; L is the length of the extractor and D_{ax} represents an axial dispersion coefficient.

If Bo tends to infinity, the flow approaches plug flow behavior. If Bo is closed to zero, the behavior approaches the RTD of a continuous stirred-tank reactor (CSTR) (Figure 2.9).

It should be finally mentioned that for symmetrical RTDs following the Gaussian distribution the number of stages N can be quickly estimated from the peak widths at half-heights $\omega_{1/2}$ as follow [72]:

$$N = 5.54 \left(\frac{\bar{t}}{\omega_{1/2}} \right)^2 \quad (2.57)$$

The value of 5.54 results from the width of a Gaussian distribution which is 2.35σ at half height.

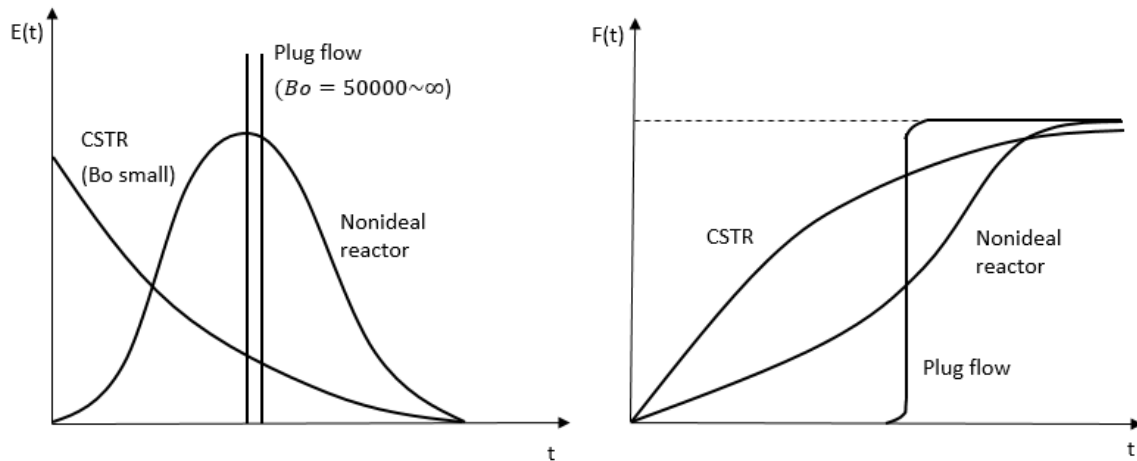


Figure 2.9. Plotting the two distribution functions $E(t)$ and $F(t)$ for selected ideal and non-ideal RTD according to [71].

In conclusion, the understanding and simplified quantification of distribution function enables to experimentally estimate the mean residence time of the phases by using proper tracers. The continuous transportation of leaves driven by rotating screws to be discussed later is influenced by many parameters leading to asymmetrical distributions. The RTD analysis for the newly developed counter-current extractor (to be discussed in section 6.2) was carried out together with Annemarie Lehr (Ph.D. student in the Institute of Fluid Dynamics and Thermodynamics of Otto von Guericke University Magdeburg). In the parallel Ph.D. project Annemarie Lehr developed a transparent extractor, which was manufactured and systematically tested. The author of the thesis presented here contributed to the engineering design, the identification of suitable steady state working conditions and the analysis of the RTD data. The results of this joint work are described in [59].

Details regarding the RTD examination in the real extractor will be given in the experimental section in chapter 6.

2.3 Parameters influencing the extraction process

Essential parameters that are of key of plant material for the course of the extraction process are the solvent used, the cellular structure, the mass transfer rate, length of the extraction time, the solid-to-liquid ratio, temperature, the extraction techniques used and more. Specific aspects related to selected parameters are discussed below.

2.3.1 Solvent

The identification of a suitable solvent is of ample relevance. Such a solvent should easily dissolve the desired components present in the plant material. Of large interest is in addition to have a good selectivity with respect to other solvable components. Further desired criteria are the possibility to achieve high yields, low costs and short operation times. The selection process is based on solubility measurements, which can be determined by one of two main approaches: a) based on empirical and semi-empirical equations which consider functional groups, molecular structure and so on, or b) based on experimental-based data with the rule “like” dissolves “like”, meaning, polar solutes are dissolved by polar solvents and vice versa. The solvent must be optimized not only in isolation but also in conjunction with the other extraction variables.

Relating to this study, ARTE is considered as a key component and the research focuses on the solubility of ARTE in different single solvent to avoid the complexity of solvent separation in downstream process. The solubility of ARTE in many solvents has been carried out in several researches [73-79]. The solvent selection procedure is further in chapter 4.

2.3.2 Solid-to-liquid ratio

The dosage D , introduced in eq. (2.8) as the solid-to-liquid ratio or phase ratio χ_{ER} in eq. (2.13), play a crucial role to optimum the productivity of the extraction process. For a defined volume of solvent, increasing the mass of leaves results higher extract

concentration but lower extract amount since the material absorbs more solvent into solid matrices. Then, the total obtained desired components are considerably influenced. The influence of the dosages on efficiency of ARTE extraction from *Artemisia annua L.* will be further discussed in chapter 5.

2.3.3 Particle size of solid starting material

The rate of extraction connected to the mass transfer from the plant material depends on the location of the solute inside the solid matrices. The transfer rate is also influenced by the solid superficial area. Thus, reducing the particle size by rupturing its organ, tissue, and cell structure results in higher superficial area and decreases intra-particle diffusion paths, this leads to enhance the extraction rates. However, if the particles are too fine, there will be a lower process efficiency because of bed compression. Hence, the particle size should be in an appropriate range to assure adequate balance of mass transfer area, flow channeling and pressure drop.

Additionally, the quality of plant material depends on many parameters as: climate, soil nutrients, cultivate condition. Therefore, a homogeneity of plant material process is one of the most essential procedures to minimize the errors during the research.

The feed composition needs to be determined with HPLC analytical methods. Details of these procedures will be further explained in chapter 4.

2.4 Extraction concepts

There is a large variety of extraction equipment and a complete classification is difficult. Some references divide the equipment according to the volatility of the solvent or whether it is desired to obtain the solvent again or not. Extraction techniques can be implemented by different general methods: maceration, immersion, percolation, pressurized fluid extraction (PFE), microwave-assisted extraction (MAE), supercritical fluid extraction (SFE), Soxhlet extraction and more. Most of these techniques are carried out at batch processes and can be classified as follows [61].

Immersion

The solid material is completely dipped into the solvent, in which intense contact among phases under agitation happens. The advantage of this technique is that the mechanical stress on the particle is relatively high and the equilibrium of solute concentration between plant material and enriched solvent can be achieved. However, the weak point is that the separation of material and extract is separately taken place.

Percolation

The solid material is loaded and stacked as a fixed bed with reasonable free volume which allows solvent pouring in and passing through by gravity. However, the particle size distribution of packed plant material needs to be considered, if the particles are too coarse, the speed of solvent flow is too high, it does not have sufficient time to penetrate into the capillaries and cellular structures leading to low efficiency. If the particles are too fine, it leads to difficult in separation them from the extract creating a cloudy solution. On another hand, the fixed bed acts as a filter which minimizes the solid content in extract, as a result, it reduces the effort of solid removing in downstream processes. To prolong the extraction time, the solvent can be repeatedly recycled in several times. This method can be used to take the target out of the material exhaustively but it also requires high solvent consumption.

Microwave-assisted extraction (MAE)

A combination of microwave and conventional solvent extraction accelerates the extraction rate due to microwave energy, thus, the extraction time is reduced and the yield is improved [80, 81]. But this technique consists of several drawbacks as: the efficacy is quite poor in case of extraction with nonpolar solvents, it is not suitable for the thermo-labile compounds because of high temperature. However, MAE is still applied in the extraction of pesticides, bioactive compounds from plants, vegetables, pigments and so on.

Supercritical fluid extraction (SFE)

Solubilization is much improved by using a fluid phase which has unique properties between gas and liquid with low viscosity and high diffusivity. The most commonly used supercritical fluid is carbon dioxide with a low critical temperature at 31.2°C and 72.8 bar pressure. Carbon dioxide is inexpensive, nontoxic, nonflammable, inert and a good solvent for nonpolar compounds. Generally, this technique has been applied in a very wide fields as in cosmetics, food, pharmaceutical, environmental industry to extract pesticides, fats and lipids, flavors, natural products.

Soxhlet extraction

This technique is basically based on the circulation of the evaporated solvent by a heating plate and set up as follows.

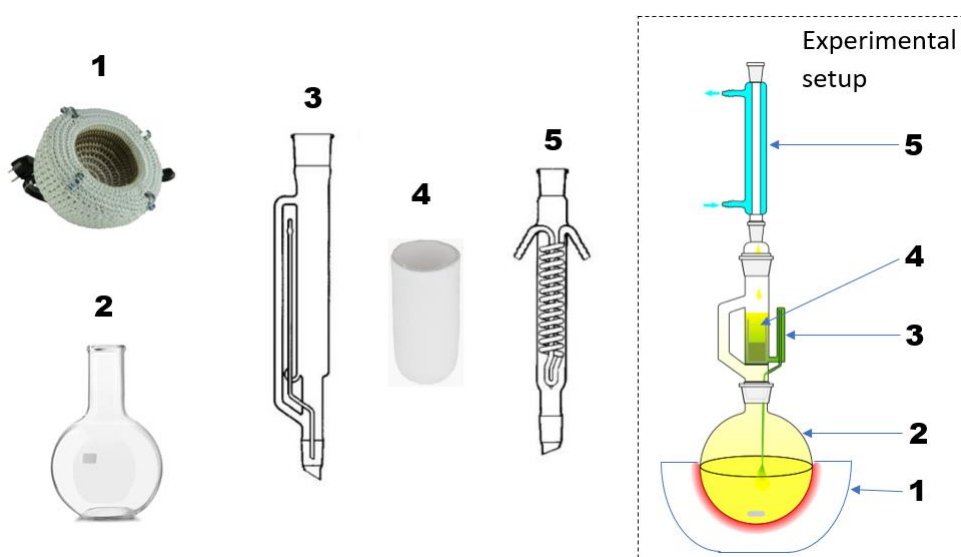


Figure 2.10. Soxhlet extraction. 1-Heating plate, 2-Boiling flask, 3-Soxhlet device, 4-Extraction thimble, 5-Condenser. [79]

The solid material is packed inside an extraction thimble, the solvent is pre-prepared in boiling flask. The solvent is heated by a heater plate, then, the vapor goes through the extraction thimble to the condenser where it is condensed and dropped back to the thimble. This solvent is contacted to solid material and the solute is diluted and diffused back to the liquid phase. The level of liquid phase is gained over time, then, it is emptied at a certain level by a special siphon structure on Soxhlet device. This liquid phase is oriented back to the boiling flask. The process is automatically

implemented by circulation of introduced procedure until no more heat is applied. Each circulation of solvent will increase the concentration of extract in the containing flask. This extraction method allows us to extract the solute exhaustively, therefore, it is very suitable to determine the maximal solute content in plant material. But it is also enclosed to drawbacks that it has limited scalability and the thermo-labile components are possibly damaged due to high temperature.

2.5 Operation modes and equipment for solid liquid extraction processes

In principle, a phytoextraction process can be carried out in batch as sequential multi-stage batches and in continuous mode. In all mentioned case the solid and solvent contacting methods, e.g. immersion, percolation, can be applied. In industrial equipment, when immersion is used, multi-stage, counter-current operation is common, while percolation is suitable for stage-wise or differential contacting devices.

The single batch extraction can be performed by immersion or percolation contacting methods. The advantage of batch extraction is the simplicity in operating and the robustness of construction. However, there are some disadvantages are limited capacity, discontinuous product output, high manpower requirement and high solvent consumption. Also, each batch requires a certain time to prepare, purge, clean before starting a new run, this leads to productivity reduction. In some cases, the combination of several single batch equipment in a multi-stage arrangement is highly recommended.

A series of extractors assembled in different arrangements results in substantial reduction of the solvent requirement, hence, energy consumption is lower for the solvent recovery downstream processes. The cascade can be setup in co-current or counter-current manner and the arrangement can be also modified in order to reduce the solvent usage and extraction time, e.g. recirculation of solvent, carousel extractors, ... However, this mode still has some drawbacks since each stage is actually a batch process including the time for preparing for the next stage, hence, the productivity is decreased. The continuous extraction will fulfill this handicap.

2.5.1 Continuous processes and types of equipment

The counter-current continuous extraction is highly recommended since it has many advantages as: robustness, consistent product quality, less solvent and energy consumption, high productivity and recovery. The selection of the appropriate counter-current equipment types is depended on the physical properties, the quantity of the plant material. Many different counter-current types described in literature become out of dates because of various limitations from ineffective contacting mode, bypassing, such as: Hildebrand, Betrex, Anderson, Bonotto extractors [69,70]. Therefore, in the following paragraphs selected equipment for continuous extraction processes is introduced and described.

Rotocel extractor [82] (Figure 2.11) is an assembling of a series of walled cells on a horizontal plane in a circular shape rotated clock-wise by a motor. Each perforated cell is fulfilled by solid material from inlet, the solvent is supplied from above by a series of spray nozzles and passes through the solid material. The enriched solvent is collected at the bottom of each cell and is pumped to the preceding cell until drainage cell reaches solvent discharge position.

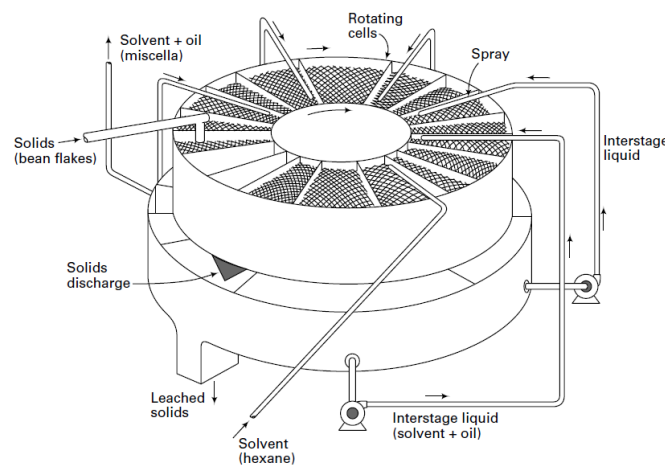


Figure 2.11. Rotocel extractor [82].

Belt extractor integrates a continuous, perforated slow-moving belt which is driven by sprockets at two ends. The material is fed by a hopper, then, it is respectively contacted to enriched solvent pumped from preceding stage. The obtained solvent at each compartment is recycled and driven through the perforated belt. The depleted

material is finally extracted by fresh solvent at the end of the belt and is discharged by a scraper (Figure 2.12). Meanwhile, the extract is withdrawn at another end of the extractor. This arrangement establishes a counter-current continuous mode.

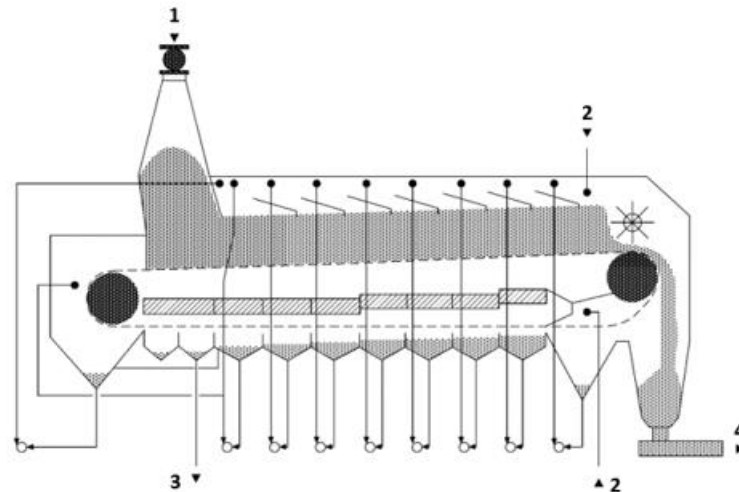


Figure 2.12. Desmet LM belt extractor [83]. 1-Material, 2-Solvent, 3- Extract, 4-Raffinate.

This type of equipment is normally used to process sugar beets, sugar cane, oil seeds, fruits and so on. Two types of equipment above are based on the percolation principle, another equipment based on immersion, named *screw extractor*, is introduced in Figure 2.13. An example of a typical screw extractor developed by GEA is shown below.

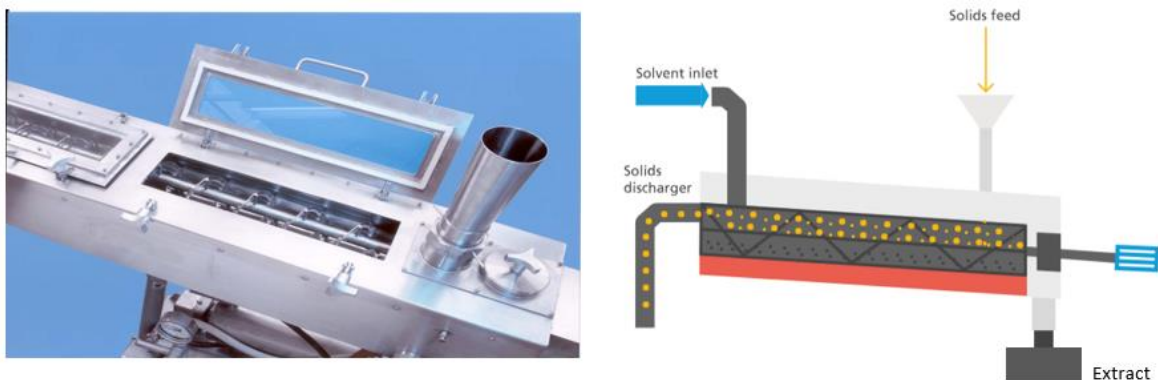


Figure 2.13. Screw-based extractor of GEA [84]. *Left:* CONTEX screw extractor; *Right:* Principle of extraction equipment.

The solvent, which is provided at the high end of extractor and is in contact with depleted material, performs as downward flow. From another side of extractor, the material is brought into contact with highly concentrated solvent. The depleted

material is further upward transported by the rotation of the screw to another end, by this manner, the counter-current flow is established. In comparison to other equipment types, the screw extractor does not integrate solvent pumps, perforated objects, it is robust, simple to construct, leading to investment and operation cost reduction. This type of extractor is successfully applied and is often seen in food industry like: sugar beets, sugar canes, flaked seeds, beans, ginger, licorice extraction and many more, however, it is rarely seen in specific fields, e.g. pharmaceutical production.

Several types of counter-current extraction equipment are ready on the market, however most of them are depended on the inclination of the equipment which is not easy to control the flow of solvent. Furthermore, they are mostly applied for food industry, rarely seen in pharmaceutical product production and in laboratory scale. Thus, the aim of this research is to design a suitable equipment which allows us to control the flow of the phases and to minimize the solvent in the depleted materials. Due to the simplicity, simple operation, mobility of this screw-based equipment, this thesis project focuses on improving and developing an efficient equipment for continuous extraction based on counter-current principle. As a result, the self-designed extractor with several specific adjustments of screw-based equipment shows very high productivity and recovery. The detail of the design steps, in particular application on ARTE extraction from *Artemisia annua L.* leaves will be given in chapter 6.

2.6 Options for extraction and chemical engineering processes

The conventional concentration consideration from Chemical Reaction Engineering (CRE) is based on mass of solute in a volume of solution or mole fractions. In solid liquid extraction, it is more useful and practical to use mass percentage (or mass fraction) in quantifying the amount of a substance in relation to the total mass of mixture. This research is going to use in addition to the properties in chapter 2 also alternatively possible other definitions which are already shortly mentioned here and in the subsequent chapter 3 devoted to model development and comparison of

process options. To prepare this chapter and to illustrate alternative definitions Table 2.1 provides an overview.

Nr.	Phenomena/ Parameters	Chapter 2,4,5,6 (extraction)	Chapter 3 (CRE inspired)
1	Compositions	$x_{i,p} = \frac{m_{i,p}}{m_p}$ - mass fraction of component i in phase p (eq.(2.14)) $x_{i,S,0}, x_{i,L,0}$ - initial mass fraction of component i in material and solvent (eq.(2.14), (2.15))	$c_i = \frac{m_{i,L}}{V_L}$ and $q_i = \frac{m_{i,S}}{V_S}$ - volume based concentration and loadings c_i^{in}, q_i^{in} - inlet concentration in the liquid and solid phases
2	Thermodynamic	$\beta_i^{eff} = \frac{x_{i,E}^{eq}}{x_{i,R}^{eq}}$ - thermodynamic distribution coefficient (eq.(2.28))	$K_R^{eq} = \frac{c_i}{q_i}$ - reaction distribution coefficient $K_E^{eq} = \frac{c_i^{hom}}{q_i^{hom}}$ - extraction distribution coefficient
3	Kinetic	k_i and k_i^{eff} - mass transfer coefficient and effective mass transfer coefficient (eq. (2.32), (2.33))	$k_{i,E}$ - coefficient for extraction including area
4	Phase ratio/ Fractions of phases	$\chi_{ER} = \frac{m_E}{m_R}$ - phase ratio (eq.(2.13)) $D = \frac{m_S}{m_L} = \frac{m_S}{m_L}$ - dosage (eqs.(2.8), (2.9)) $\varepsilon_L^*, \varepsilon_S^*$ - volume fractions of phases (including gas)	$\varepsilon_L = \varepsilon = \frac{V_L}{V_{tot}} = \frac{\dot{V}_L}{\dot{V}_{tot}}$ - volume fraction of liquid phase $\varepsilon_S = (1 - \varepsilon)$ - volume fraction of solid phase (excluding gas)
5	Capacity factors	$\chi_{ER}\beta_i^{eff} = \frac{m_E x_{i,E}^{eq}}{m_R x_{i,R}^{eq}}$	$\bar{K}_{i,E}^{eq} = \frac{\varepsilon}{1 - \varepsilon} K_{i,E}^{eq}$
6	Dispersion- (backmixing)	N - number of stages as estimated from RTD analysis	N - number of stages in CSTR cascade model

Table 2.1. Summary of various alternative possible definitions for extraction and chemical reaction engineering processes.

3 Modeling solid liquid extraction processes

Since decades, many research investigated the solid liquid extraction processes with a variety of mass transfer-based approaches, such as: internal diffusion in a spherical solid particle [85], diffusion model [86, 87], kinetics models with different influencing parameters as solvent composition, temperature, particle size, porosity, solid-to-liquid ration [63, 64, 88-94]. These models revealed all relevant parameters as effective diffusion coefficient, extraction rates, thermodynamics. A considerable effort was put on multi-stage counter-current extraction development to calculate the required number of extraction stages and to predict the extract concentration [95-98], however, they were not associated with fundamental properties of solid structure such as in-solid diffusivity or absorbability of solid matrix and so on. Some recent investigations focused on evaluating the extract retained in solid matrix [62, 99, 100]. Furthermore, the state-of-the-art counter-current operation has been modeled considering liquid-liquid extraction and rarely for solid-liquid extraction.

This chapter exploits the connection of CRE and extraction processes to design the continuous extractor (chapter 6) more efficient. It includes of two main parts: (1) introducing an instructive analogy of chemical reactor models as the batch reactor (BR), the continuously stirred tank reactor (CSTR) and the plug flow tubular reactor (PFTR) to extraction processes; (2) focusing on extraction processes, especially for steady state operation and equilibrium situations.

Related results for the linear distribution case were already published together with Stephan Münzberg [101] who worked in a parallel project on counter-current crystallization processes. The aim of [101] was to generalize counter-current manners by comparing different separation processes as distillation, extraction, chromatography and crystallization. The derived model is finally simplified to solve equilibrium stage model, which will be further used in chapters 5 and 6 for quantifying the extraction of ARTE from *Artemisia annua L.* leaves.

3.1 Basics of chemical reaction engineering (CRE)

In order to develop and understand different models capable to describe main features of extraction processes, it is expedient to refer to the classical reactor models used in Chemical Reaction Engineering (CRE) and their solutions.

Due to the fact that there exists a certain analogy between the process of extracting a substance from a solid matrix and transporting it into a solvent it is helpful to consider as an example a reversible reaction which takes place in a homogeneous phase.

In CRE typically three ideal reactors are evaluated and compared, namely the batch reactor (BR), the continuously stirred tank reactor (CSTR) and the plug flow tubular reactor (PFTR). The latter two continuously operated reactors are assumed to operate in the steady state regime.

The rate of a reversible homogeneous reaction of a component A to a product B:



can be described with the following equation exploiting volume-based concentrations c_A and c_B :

$$r = k_R \left(c_A - \frac{c_B}{K_R^{eq}} \right) \quad (3.2)$$

In the above k_R stands for the reaction rate constant and K_R^{eq} for the thermodynamic equilibrium constant of this reaction.

Batch reactor

The following mass balance equation describes the isothermal batch reactor:

$$\frac{dc_i}{dt} = \nu_i r \quad i = A, B \quad (3.3)$$

The overall balance allows to connect the concentrations of the two species by:

$$c_A(t) + c_B(t) = c_A^0 + c_B^0 \quad (3.4)$$

Using this balance, the concentration of component A can be inserted in the rate law (eq. (3.2)) to give:

$$r = k_R(c_A^0 + c_B^0 - c_B(t) - \frac{c_B}{K_R^{eq}}) \quad (3.5)$$

The solution of the mass balance equation (eq. (3.3)) for component B using (3.4) is:

$$c_B(t) = \frac{K_R^{eq}}{1+K_R^{eq}}(c_A^0 + c_B^0) - \left(\frac{K_R^{eq}}{1+K_R^{eq}}c_A^0 - \frac{1}{1+K_R^{eq}}c_B^0 \right) * e^{-\left(1+\frac{1}{K_R^{eq}}\right)k_R t} \quad (3.6)$$

This result can be inserted back into the total mass balance (eq. (3.4)) to provide the concentration course of component A.

$$c_A(t) = \frac{1}{1+K_R^{eq}}(c_A^0 + c_B^0) + \left(\frac{K_R^{eq}}{1+K_R^{eq}}c_A^0 - \frac{1}{1+K_R^{eq}}c_B^0 \right) * e^{-\left(1+\frac{1}{K_R^{eq}}\right)k_R t} \quad (3.7)$$

Instead of using the time dependence, this result can be also conveniently expressed as function of the following Damköhler number Da_R as:

$$Da_R(t) = k_R t \quad (3.8)$$

A special case arises if there is no component B initially provided. Then for $K_R^{eq} \rightarrow$ infinity the classical rate law for an irreversible first order reaction results:

$$c_A(t) = c_A^0 e^{-Da_R(t)} \quad \text{and} \quad c_B(t) = c_A^0(1 - e^{-Da_R(t)}) \quad (3.9)$$

This result can be also expressed a function of the conversion of A defined as:

$$X_A(t) = \frac{c_A^0 - c_A(t)}{c_A^0} = 1 - \frac{c_A(t)}{c_A^0} \quad (3.10)$$

This leads to:

$$X_A(t) = 1 - e^{-Da_R(t)} \quad (3.11)$$

Single CSTR

For an isothermal well-mixed stirred tank reactor operated under steady state conditions holds the following mass balance:

$$0 = \frac{c_i^{in} - c_i}{\tau} + v_i r \quad i = A, B \quad (3.12)$$

In the above τ stands for the mean residence time, which depends on the reactor volume V and flowrate \dot{V} :

$$\tau = \frac{V}{\dot{V}} \quad (3.13)$$

With eq. (3.1) and the overall balance for the open system:

$$c_A(\tau) + c_B(\tau) = c_A^{\text{in}} + c_B^{\text{in}} \quad (3.14)$$

and holds for the mass balance of component A:

$$0 = \frac{c_A^{\text{in}} - c_A}{\tau} - k_R * (c_A(\tau) - \frac{c_A^{\text{in}} + c_B^{\text{in}} - c_A(\tau)}{K_R^{\text{eq}}}) \quad (3.15)$$

The solution for the concentration of component A is:

$$c_A(\tau) = \frac{c_A^{\text{in}} + (c_A^{\text{in}} + c_B^{\text{in}}) \frac{k_R \tau}{K_R^{\text{eq}}}}{1 + \left(1 + \frac{1}{K_R^{\text{eq}}}\right) k_R \tau} \quad (3.16)$$

With eq. (3.14) the corresponding concentration of component B is:

$$c_B(\tau) = \frac{c_B^{\text{in}} + (c_A^{\text{in}} + c_B^{\text{in}}) \frac{k_R \tau}{K_R^{\text{eq}}}}{1 + \left(1 + \frac{1}{K_R^{\text{eq}}}\right) k_R \tau} \quad (3.17)$$

Again a limiting case arises for having only A in the feed and an irreversible reaction:

$$c_A(\tau) = \frac{c_A^{\text{in}}}{1 + k_R \tau} \quad (3.18)$$

Using again the Da_R number (eq. (3.8)) holds:

$$c_A(\tau) = \frac{c_A^{\text{in}}}{1 + Da_R(\tau)} \quad \text{and} \quad c_B(\tau) = c_A^{\text{in}} \frac{Da_R(\tau)}{1 + Da_R(\tau)} \quad (3.19)$$

These results can be again expressed a function of the conversion of A (eq. (3.10)):

$$X_A(\tau) = \frac{Da_R(\tau)}{1 + Da_R(\tau)} \quad (3.20)$$

PFTR

The mass balance of an ideal isothermal plug flow reactor operated under steady state conditions can be expressed using again the residence time τ (eq. (3.13)) as follows:

$$\frac{dc_i}{d\tau} = v_i r \quad i = A, B \quad (3.21)$$

Comparing this balance with the balance for the batch reactor (eq. (3.3)) it becomes obvious that these two reactors can be described in an identical way provided $\tau = t$. Thus, the development of the concentration profiles over the space and time coordinates are identical [71].

The range between PFTR and CSTR can be described using for example a model for a cascade of N sequentially connected and equally sized stages that each behave as a CSTR.

Cascade of N sequentially connected CSTR

In the beginning we look at 2 identically sized CSTR which is designated by I and II to differ from the subsequent case of counter-current operation ($j = I, II; N = 2$). In this case, the residence time in each CSTR is half of the overall residence time τ :

$$\tau_{II} = \frac{V_I}{\dot{V}} = \frac{V_{II}}{\dot{V}} = \frac{1}{2} \frac{V_{tot}}{\dot{V}} = \frac{\tau}{2} \quad (3.22)$$

The balance for component A in the second CSTR is formulated using again the overall mass balance:

$$0 = \frac{c_{A,I}(\tau) - c_{A,II}(\tau)}{\tau/2} - k_R * \left(c_{A,II}(\tau) - \frac{c_A^{in} + c_B^{in} - c_{A,II}(\tau)}{K_R^{eq}} \right) \quad (3.23)$$

Without providing the derivation in detail, the finally resulting steady state solution for the concentration of A at the outlet of the second CSTR is:

$$c_{A,II}(\tau) = \frac{c_{A,I}(\tau) + (c_A^{in} + c_B^{in}) \frac{k_R \tau}{K_R^{eq} 2}}{1 + \left(1 + \frac{1}{K_R^{eq}} \right) \frac{k_R \tau}{2}} \quad (3.24)$$

With the known solution for the first CSTR $c_{A,I}(\tau)$ (eq. (3.16)) follows:

$$c_{A,II}(\tau) = \frac{(c_A^{in} + c_B^{in}) \frac{k_R \tau}{K_R^{eq} 2}}{1 + k_{R2} \tau + \frac{k_R \tau}{K_R^{eq} 2}} + \frac{c_A^{in} + (c_A^{in} + c_B^{in}) \frac{k_R \tau}{K_R^{eq} 2}}{\left(1 + k_{R2} \tau + \frac{k_R \tau}{K_R^{eq} 2} \right)^2} \quad (3.25)$$

The outlet concentration of component B can be calculated via the total mass balance.

For $c_B^{in} = 0$ and an irreversible reaction results as a limiting case the well-known expression [71]:

$$c_{A,II}(\tau) = \frac{\frac{c_A^{in}}{1 + \frac{k_R \tau}{2}}}{1 + \frac{k_R \tau}{2}} = \frac{c_A^{in}}{\left(1 + \frac{k_R \tau}{2}\right)^2} \quad (3.26)$$

If we now consider $N = 3$ holds for component A in the third stage:

$$0 = \frac{c_{A,II}(\tau) - c_{A,III}(\tau)}{\tau/3} - k_R * (c_{A,III}(\tau) - \frac{c_A^{in} + c_B^{in} - c_{A,III}(\tau)}{K_R^{eq}}) \quad (3.27)$$

With the known outlet of the second CSTR $c_{A,II}(\tau)$ (eq. (3.16)) follows:

$$c_{A,III}(\tau) = \frac{\left(c_A^{in} + c_B^{in}\right) \frac{k_R \tau}{K_R^{eq} 3}}{1 + k_{R3} \frac{\tau}{K_R^{eq} 3}} + \frac{\left(c_A^{in} + c_B^{in}\right) \frac{k_R \tau}{K_R^{eq} 3}}{\left(1 + k_{R3} \frac{\tau}{K_R^{eq} 3}\right)^2} + \frac{c_A^{in} + \left(c_A^{in} + c_B^{in}\right) \frac{k_R \tau}{K_R^{eq} 3}}{\left(1 + k_{R3} \frac{\tau}{K_R^{eq} 3}\right)^3} \quad (3.28)$$

Here the limiting for $c_B^{in} = 0$ and irreversible reaction is:

$$c_{A,III}(\tau) = \frac{c_A^{in}}{\left(1 + \frac{k_R \tau}{3}\right)^3} \quad (3.29)$$

Exploiting the recursive character of the solution development the concept can be extended easily to describe a cascade of N stages. The resulting solution for the final outlet concentration of component A is:

$$c_{A,N}(\tau) = \frac{\left(c_A^{in} + c_B^{in}\right) \frac{k_R \tau}{K_R^{eq} N}}{\left(1 + k_{RN} \frac{\tau}{K_R^{eq} N}\right)^1} + \dots + \frac{\left(c_A^{in} + c_B^{in}\right) \frac{k_R \tau}{K_R^{eq} N}}{\left(1 + k_{RN} \frac{\tau}{K_R^{eq} N}\right)^{N-1}} + \frac{c_A^{in} + \left(c_A^{in} + c_B^{in}\right) \frac{k_R \tau}{K_R^{eq} N}}{\left(1 + k_{RN} \frac{\tau}{K_R^{eq} N}\right)^N} \quad (3.30)$$

The solution for B is again easily available using the overall mass balance.

For the special case, that no B is supplied at the inlet of the first CSTR and considering an irreversible reaction result:

$$c_{A,N}(\tau) = \frac{c_A^{in}}{\left(1 + \frac{k_R \tau}{N}\right)^N} \quad (3.31)$$

Using instead of the concentration of A its conversion (eq. (3.11), introducing the Damköhler number and applying the following mathematical rule:

$$\lim_{N \rightarrow \infty} \left(1 + \frac{Da_R}{N}\right)^N = e^{Da_R} \quad (3.32)$$

provides for an infinite number of stages:

$$X_A(\tau) = 1 - e^{-Da_R(\tau)} \quad (3.33)$$

This limiting solution shows that a CSTR cascade for an infinite number of stages approaches the PFTR behavior (which in turn resembles the BR case substituting τ by t). This is a general rule. However, we do not prove here the convergence of eq.(3.30) for N towards infinity into eq. (3.7).

Figure 3.1 shows a comparison between BR (and PFTR) with the CSTR and a cascade of CSTR showing the classical result that for positive order reactions (like the one considered here) the former reactor achieve higher conversion.

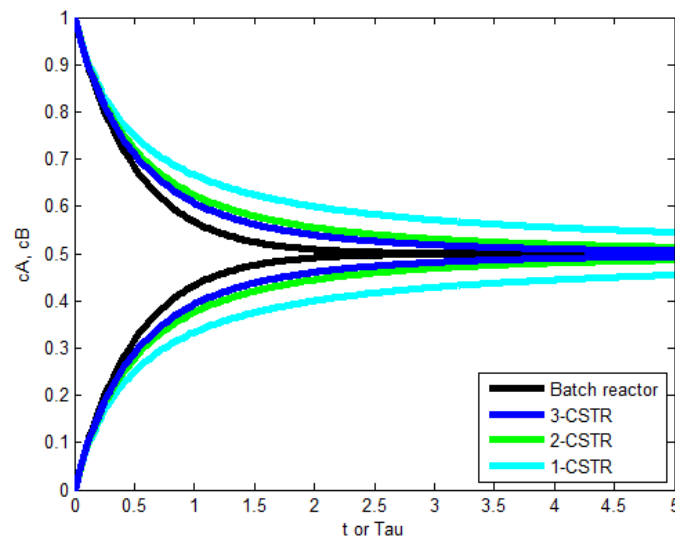


Figure 3.1. Comparison of BR (and PFTR), CSTR and a cascade of CSTR for performing a simple first order reversible chemical reaction. *The upper and lower curves are represented for compositions in the solid and liquid phases respectively. The black curves present the concentration development for BR; the other curves show the different numbers of CSTR. Input parameters for Code1: $c_A^0 = 1, c_B^0 = 0, k_R = K_R^{eq} = 1, \tau = 5$.*

The curves are plotted based on the simulated data from Matlab code (*Code 1*).

It should be mentioned that instead of plotting the courses of the concentrations over t or τ similar trends can be generated plotting over the Damköhler number Da_R (eq. (3.8)).

Also for the extraction processes studied in this work the well-known trends in CRE can be applied to describe the performance of batch and continuous extraction systems. This will be demonstrated below.

In transferring the above given CRE equations, which are based on considering only one single homogeneous phase and the continuous reactors (PFTR, CSTR and CSTR cascade), a few modifications need to be done to quantify solid-liquid extraction processes. These modifications introduced in the next section will capture the two-phase behavior and offer the opportunity to operate in counter-current mode.

3.2 Modeling extraction processes

As in CRE we will describe below the process for operation in batch and continuous mode. Since there are two phases immiscible involved and a possible counter-current operation is of large interest, several modifications have to be made.

The extraction of a component i in a mixture N_C components can be considered to be similar to a reversible reaction given by eq. (3.1). Thus, our starting view on the process is:

amount of a component i in solid phase \leftrightarrow *amount of component i in solvent*

The amounts will be quantified below by the concentration in the solid phase, q_i and the concentration in the liquid phase, c_i . The latter, representing the main target of the extraction process, corresponds to the product concentration in the reaction system above, c_B . Thus, start of the model development is (as above eq. 4.1):

$$q_i \leftrightarrow c_i \quad i = 1, N_C \quad (3.34)$$

The exchange process is driven by a rate expression similar to eq. (3.2) just substituting k_R by $k_{i,E}$ and K_R^{eq} by $K_{i,E}^{eq}$, already formulated as in section 2 as:

$$r_{i,E} = k_{i,E} \left(q_i^{hom} - \frac{c_i^{hom}}{K_{i,E}^{eq}} \right) \quad i = 1, N_C \quad (3.35)$$

It should be mentioned that this approach assumes the reversibility of the extraction process. Obviously, it is doubtful whether the refilling of the plant material from a supersaturated solution can be described this simple.

Adaptation to a two phase situation

Of importance is now to capture the fact that q_i and c_i are concentrations assuming a pseudo-homogeneous phase in a volume (V_{tot}) or in a pseudo-homogeneous flow (\dot{V}_{tot}). Thus, there is need in distinguishing between two concentration definitions. The second definition considers the amount of i in the segregated single solid or liquid phases. To express the relation between these two sets of concentrations we need to provide liquid solid volume fractions ε_L and ε_S , with:

$$\varepsilon_S = 1 - \varepsilon_L \quad (3.36)$$

Below we will use exclusively the liquid fraction and designate it as $\varepsilon = \varepsilon_L$.

Furthermore, we will designate the modified concentrations in the pseudo-homogeneous phase by \tilde{c}_i and \tilde{q}_i and the concentrations in the segregated individual single phases by c_i and q_i . Then the following connections hold for these concentrations both in batch and continuous operation mode:

$$\tilde{c}_i = c_i \varepsilon = c_i \frac{V_L}{V_{tot}} = c_i \frac{\dot{V}_L}{\dot{V}_{tot}} \quad i = 1, N_C \quad (3.37)$$

$$\tilde{q}_i = q_i (1 - \varepsilon) = q_i \frac{V_S}{V_{tot}} = q_i \frac{\dot{V}_S}{\dot{V}_{tot}} \quad i = 1, N_C \quad (3.38)$$

In these equations the fact is used that in the continuous mode also the flowrate fractions can be expressed via the liquid phase fraction ε . From now on we will not refer anymore to the fact that i runs from 1 to N_C .

Furthermore, for the concentration in the initial state (needed for batch operation) or the inlet state (needed for steady state continuous operation) holds:

$$\tilde{c}_i^0 = c_i^0 \varepsilon = c_i^0 \frac{V_L}{V_{tot}} \quad (3.39a)$$

$$\tilde{q}_i^0 = q_i^0 (1 - \varepsilon) = q_i^0 \frac{V_S}{V_{tot}} \quad (b)$$

$$\tilde{c}_i^{in} = c_i^{in} \varepsilon = c_i^{in} \frac{\dot{V}_L}{\dot{V}_{tot}} \quad (c)$$

$$\tilde{q}_i^{in} = q_i^{in} (1 - \varepsilon) = q_i^{in} \frac{\dot{V}_S}{\dot{V}_{tot}} \quad (d)$$

We start our analysis of the extraction process again with the batch process. With the (pseudo-homogeneous) modified concentrations the following two mass balance equations hold:

$$\frac{d\tilde{c}_i}{dt} = \tilde{k}_{i,E} \left(\tilde{q}_i - \frac{\tilde{c}_i}{\tilde{K}_{i,E}^{eq}} \right) \quad (3.40)$$

$$\frac{d\tilde{q}_i}{dt} = -\tilde{k}_{i,E} \left(\tilde{q}_i - \frac{\tilde{c}_i}{\tilde{K}_{i,E}^{eq}} \right) \quad (3.41)$$

These equations contain the modified rate constant $\tilde{k}_{i,E}$ and the equilibrium coefficient $\tilde{K}_{i,E}^{eq}$ for which holds:

$$\tilde{k}_{i,E} = \frac{k_{i,E}}{1 - \varepsilon} \quad (3.42)$$

and

$$\tilde{K}_{i,E}^{eq} = \frac{\varepsilon}{1 - \varepsilon} K_{i,E}^{eq} \quad (3.43)$$

Thus, in accordance with eq. (3.6) holds:

$$\tilde{c}_i(t) = \frac{\tilde{K}_{i,E}^{eq}}{1 + \tilde{K}_{i,E}^{eq}} (\tilde{q}_i^0 + \tilde{c}_i^0) - \left(\frac{\tilde{K}_{i,E}^{eq}}{1 + \tilde{K}_{i,E}^{eq}} \tilde{q}_i^0 - \frac{1}{1 + \tilde{K}_{i,E}^{eq}} \tilde{c}_i^0 \right) * e^{-\left(1 + \frac{1}{\tilde{K}_{i,E}^{eq}}\right) \tilde{k}_{i,E} t} \quad (3.44)$$

If there is no component i initially provided for a special case, then eq. (3.44) has similar form as introduced extraction concentration in eq. (2.39). The second concentration in the solid phase, which decides about the recovery of the extraction process, is accessible via the total balance:

$$\tilde{q}_i(t) = \tilde{q}_i^0 + \tilde{c}_i^0 - \tilde{c}_i(t) \quad (3.45)$$

These equations allow to determine subsequently the corresponding concentration courses after a possible phase splitting exploiting eqs. (3.37) and (3.38).

Single stage CSTR type of operation for extraction

Similar to eq. (3.15) the mass balance using the concentrations of the pseudo-homogeneous phase the balance for component i in the liquid phase with modified concentration of phases (eqs. (3.37)-(3.39a)) is:

$$0 = \frac{(\tilde{c}_i^{in} - \tilde{c}_i)}{\bar{\tau}} + \tilde{k}_{i,E}(\tilde{c}_i^{in} + \tilde{q}_i^{in} - \tilde{c}_i - \frac{\tilde{c}_i}{\tilde{K}_{i,E}^{eq}}) \quad (3.46)$$

In CRE part, we introduced residence time τ (eq. (3.13)). This residence time is identical to the mean residence time $\bar{\tau}$ introduced in eq. (2.52) for the extraction process. It includes the flows of the two phases as:

$$\bar{\tau} = \tau = \frac{V_{tot}}{\dot{V}_{tot}} = \frac{V_{tot}}{\dot{V}_L + \dot{V}_S} \quad (3.47)$$

which is from now on used as τ . Then, the solution is (as above eq. (3.16)):

$$\tilde{c}_i(\tau) = \frac{\tilde{c}_i^{in} + (\tilde{c}_i^{in} + \tilde{q}_i^{in})\tilde{k}_{i,E}\tau}{1 + \left(1 + \frac{1}{\tilde{K}_{i,E}^{eq}}\right)\tilde{k}_{i,E}\tau} \quad (3.48)$$

The Damköhler number for extraction operation can be derived from Da_R (eq. (3.8)) with substituting k_R by $\tilde{k}_{i,E}$ as:

$$Da_E(\tau) = \tilde{k}_{i,E}\tau \quad (3.49)$$

Therefore, the solution of $\tilde{c}_i(\tau)$ in eq. (3.48) can be described as:

$$\tilde{c}_i(\tau) = \frac{\tilde{c}_i^{in} + (\tilde{c}_i^{in} + \tilde{q}_i^{in})Da_E}{1 + \left(1 + \frac{1}{\tilde{K}_{i,E}^{eq}}\right)Da_E} \quad (3.50)$$

The corresponding concentration in solid phase can be calculated based on eq. (3.17) as:

$$\tilde{q}_i(\tau) = \frac{\tilde{q}_i^{in} + (c_i^{in} + \tilde{q}_i^{in}) \frac{\tilde{k}_{i,E}\tau}{\tilde{K}_{i,E}^{eq}}}{1 + \left(1 + \frac{1}{\tilde{K}_{i,E}^{eq}}\right) \tilde{k}_{i,E}\tau} \quad (3.51)$$

We can now return to the concentrations in the individual two phases. This leads for the liquid phase to:

$$c_i(\tau) = \frac{(1 + \tilde{k}_{i,E}\tau)}{1 + \frac{\tilde{k}_{i,E}\tau}{\tilde{K}_{i,E}^{eq}} + \tilde{k}_{i,E}\tau} c_i^{in} + \frac{\tilde{k}_{i,E}\tau}{1 + \frac{\tilde{k}_{i,E}\tau}{\tilde{K}_{i,E}^{eq}} + \tilde{k}_{i,E}\tau} \frac{1-\varepsilon}{\varepsilon} q_i^{in} \quad (3.52)$$

The integrated overall mass balance provides:

$$0 = (1 - \varepsilon) (q_i^{in} - q_i(\tau)) + \varepsilon (c_i^{in} - c_i(\tau)) \quad (3.53)$$

This leads to:

$$q_i(\tau) = \frac{\frac{\varepsilon}{1-\varepsilon} \frac{\tilde{k}_{i,E}\tau}{\tilde{K}_{i,E}^{eq}}}{1 + \frac{\tilde{k}_{i,E}\tau}{\tilde{K}_{i,E}^{eq}} + \tilde{k}_{i,E}\tau} c_i^{in} + \frac{1 + \frac{\tilde{k}_{i,E}\tau}{\tilde{K}_{i,E}^{eq}}}{1 + \frac{\tilde{k}_{i,E}\tau}{\tilde{K}_{i,E}^{eq}} + \tilde{k}_{i,E}\tau} q_i^{in} \quad (3.54)$$

Cascade of two CSTR applied for extraction (N=2)

In 2-phase systems the availability of two stages offers the option to operate in co-current or in counter-current. Below we will show that the two outgoing streams will differ and that counter-operations allows to exceed equilibrium limitations.

Co-current operation

Let us first look again at co-current operation as studied for the CRE case above.

With the known solution of the first CSTR (eq. (3.17)) follows for the modified concentrations of the pseudo-homogeneous liquid phase in the second CSTR:

$$\tilde{c}_{i,II}(\tau) = \frac{(\tilde{q}_i^{in} + c_i^{in}) \frac{\tilde{k}_{i,E}\tau}{2}}{1 + \frac{\tilde{k}_{i,E}\tau}{\tilde{K}_{i,E}^{eq}} + \tilde{k}_{i,E}\tau} + \frac{c_i^{in} + (\tilde{q}_i^{in} + c_i^{in}) \frac{\tilde{k}_{i,E}\tau}{2}}{\left(1 + \frac{\tilde{k}_{i,E}\tau}{\tilde{K}_{i,E}^{eq}} + \tilde{k}_{i,E}\tau\right)^2} \quad (3.55)$$

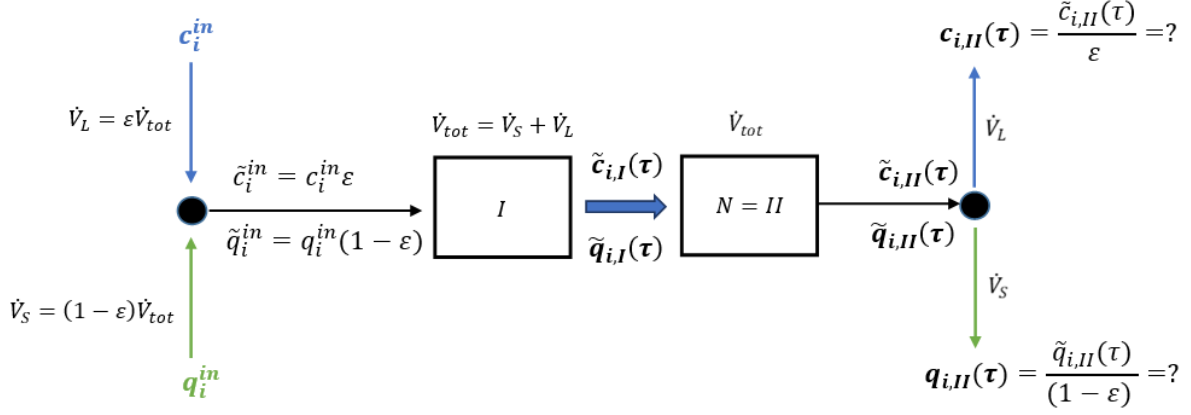


Figure 3.2. Illustration of two CSTR in co-current operation for extraction. The liquid phase and solid phase are fed at the same side to the first stage ($N = I$) and taken out at the second stage ($N = II$). The residence time in the two identical sized CSTR τ_I and τ_{II} are a half of the overall residence time τ (eq. (3.22)).

In order to simplify the formulas, we introduce two following factors:

$$A_1 = \frac{\left(1 + \frac{N}{\tilde{k}_{i,E}\tau}\right)}{1 + \frac{1}{\tilde{K}_{i,E}^{eq}} + \frac{N}{\tilde{k}_{i,E}\tau}} \quad \text{and} \quad A_2 = \frac{1}{1 + \frac{1}{\tilde{K}_{i,E}^{eq}} + \frac{N}{\tilde{k}_{i,E}\tau}} \quad (3.56)$$

Then, eq. (3.55) can be rearranged as:

$$\tilde{c}_{i,II}(\tau) = (A_2(1 + A_1 - A_2) + (A_1 - A_2)^2)\tilde{c}_i^{in} + A_2(1 + A_1 - A_2)\tilde{q}_i^{in} \quad (3.57)$$

The corresponding pseudo-homogeneous solid phase concentration $\tilde{q}_{i,II}$ is available via the overall mass balance for the second CSTR:

$$\tilde{q}_{i,II}(\tau) = (1 - \varepsilon)q_i^{in} - \tilde{c}_{i,II}(\tau) + \varepsilon c_i^{in} \quad (3.58)$$

Then,

$$\tilde{q}_{i,II}(\tau) = [1 - A_2(1 + A_1 - A_2) - (A_1 - A_2)^2]\tilde{c}_i^{in} + [1 - A_2(1 + A_1 - A_2)]\tilde{q}_i^{in} \quad (3.59)$$

Finally, the concentration of component i in the liquid phase at initial state is:

$$c_{i,II}(\tau) = \frac{\tilde{c}_{i,II}(\tau)}{\varepsilon} = (A_2(1 + A_1 - A_2) + (A_1 - A_2)^2)c_i^{in} + A_2(1 + A_1 - A_2)\frac{1 - \varepsilon}{\varepsilon}q_i^{in} \quad (3.60)$$

The concentration of component i in solid phase can also expressed as:

$$q_{i,II}(\tau) = [1 - A_2(1 + A_1 - A_2) - (A_1 - A_2)^2]\frac{\varepsilon}{1 - \varepsilon}c_i^{in} + [1 - A_2(1 + A_1 - A_2)]q_i^{in} \quad (3.61)$$

Counter-current operation

Now we will consider 2 stages operated in counter-current. Based on established chemical engineering knowledge, this allows exceeding equilibrium concentrations (Perry handbook), which limit the co-current operation. The principle is illustrated in Figure 3.3.

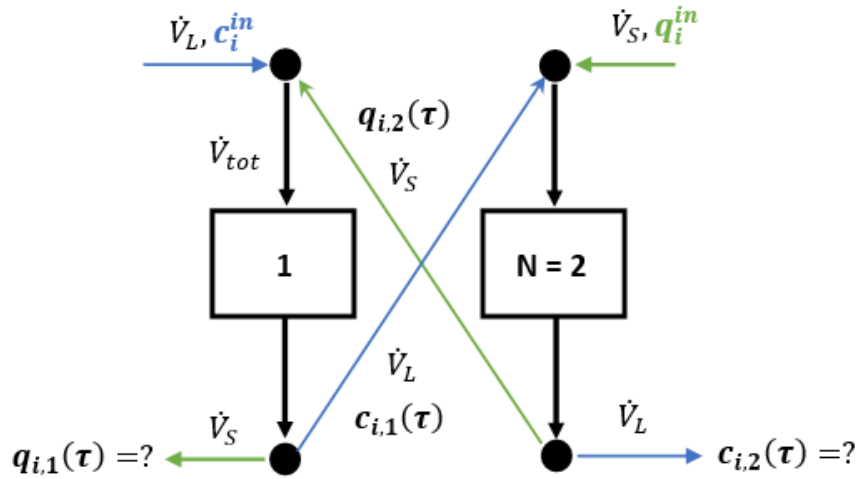


Figure 3.3. Illustration of two CSTR counter-current operation for extraction. The liquid phase and solid phase are provided at two opposite ends of the cascade. The outgoing concentrations of component i in the liquid phase c_i^l and in the solid phase q_i^l decide the productivity and recovery of the extraction process respectively.

The two-stage counter-current extraction process is characterized by four equations with four unknowns.

Therefore, the following four mass balances can be used to describe the modified concentrations of phases for the two stages:

$j=1$:

$$\tilde{c}_{i,1}(\tau) = A_1 \tilde{c}_i^{in} + A_2 \tilde{q}_{i,2}(\tau) \quad (3.62)$$

$$\tilde{q}_{i,1}(\tau) = (1 - A_1) \tilde{c}_i^{in} + (1 - A_2) \tilde{q}_{i,2}(\tau) \quad (3.63)$$

$j=2$:

$$\tilde{c}_{i,2}(\tau) = A_1 \tilde{c}_{i,1}(\tau) + A_2 \tilde{q}_i^{in} \quad (3.64)$$

$$\tilde{q}_{i,2}(\tau) = (1 - A_1) \tilde{c}_{i,1}(\tau) + (1 - A_2) \tilde{q}_i^{in} \quad (3.65)$$

The four unknown concentrations can be isolated from these four linear equations.

The two results are:

$$\tilde{c}_{i,1}(\tau) = \frac{A_1}{1-A_2+A_1A_2} \tilde{c}_i^{in} + \frac{(1-A_2)A_2}{1-A_2+A_1A_2} \tilde{q}_i^{in} \quad (3.66)$$

$$\tilde{q}_{i,2}(\tau) = \frac{A_1(1-A_1)}{1-A_2+A_1A_2} \tilde{c}_i^{in} + \frac{1-A_2}{1-A_2+A_1A_2} \tilde{q}_i^{in} \quad (3.67)$$

The values of $\tilde{c}_{i,1}$ and $\tilde{q}_{i,2}$ allow to calculate the two other concentrations $\tilde{c}_{i,2}$ and $\tilde{q}_{i,1}$ (from eqs. (3.63) and (3.64)) as:

$$\tilde{c}_{i,2}(\tau) = \frac{A_1^2}{1-A_2+A_1A_2} \tilde{c}_i^{in} + \left(1 - \frac{(A_2-1)^2}{1-A_2+A_1A_2}\right) \tilde{q}_i^{in} \quad (3.68)$$

$$\tilde{q}_{i,1}(\tau) = \left(1 - \frac{A_1^2}{1-A_2+A_1A_2}\right) \tilde{c}_i^{in} + \frac{(1-A_2)^2}{1-A_2+A_1A_2} \tilde{q}_i^{in} \quad (3.69)$$

It should be noticed that the interest concentrations of liquid and solid phase in counter-current operation are from two opposite sides of cascade.

Of key interest are the two last outlets concentrations $\tilde{c}_{i,2}$ and $\tilde{q}_{i,1}$ (eqs. (3.68) and (3.69)) which can be compared to the two outlets of co-current operation $\tilde{q}_{i,II}(\tau)$ and $\tilde{c}_{i,II}(\tau)$ (eqs. (3.55) and (3.59)).

Comparison between co-current and counter-current operation

For a case of two stages, the liquid phase concentrations of component i at the outlet of two operations are determined based on eqs. (3.57) and (3.68) respectively.

A dimensionless *enhancement factor* E , can be used to evaluate the difference between the liquid phase concentrations of two operations and is calculated as:

$$E = \frac{\tilde{c}_{i,2}(\tau)}{\tilde{c}_{i,II}(\tau)} = \frac{\alpha_1 \tilde{c}_i^{in} + \alpha_2 \tilde{q}_i^{in}}{\alpha_3 \tilde{c}_i^{in} + \alpha_4 \tilde{q}_i^{in}} \quad (3.70)$$

within,

$$\begin{aligned} \alpha_1 &= \frac{A_1^2}{[(A_2-1)^2 + A_2(1+A_1-A_2)]} & \alpha_2 &= \frac{A_2(1+A_1-A_2)}{[(A_2-1)^2 + A_2(1+A_1-A_2)]} \\ \alpha_3 &= (A_1 - A_2)^2 + A_2(1 + A_1 - A_2) & \alpha_4 &= A_2(1 + A_1 - A_2) \end{aligned} \quad (3.71)$$

The solutions for equations of two stage co- and counter-current operation above are achieved by using a Matlab code (Code2). Below is an example illustrating the results:

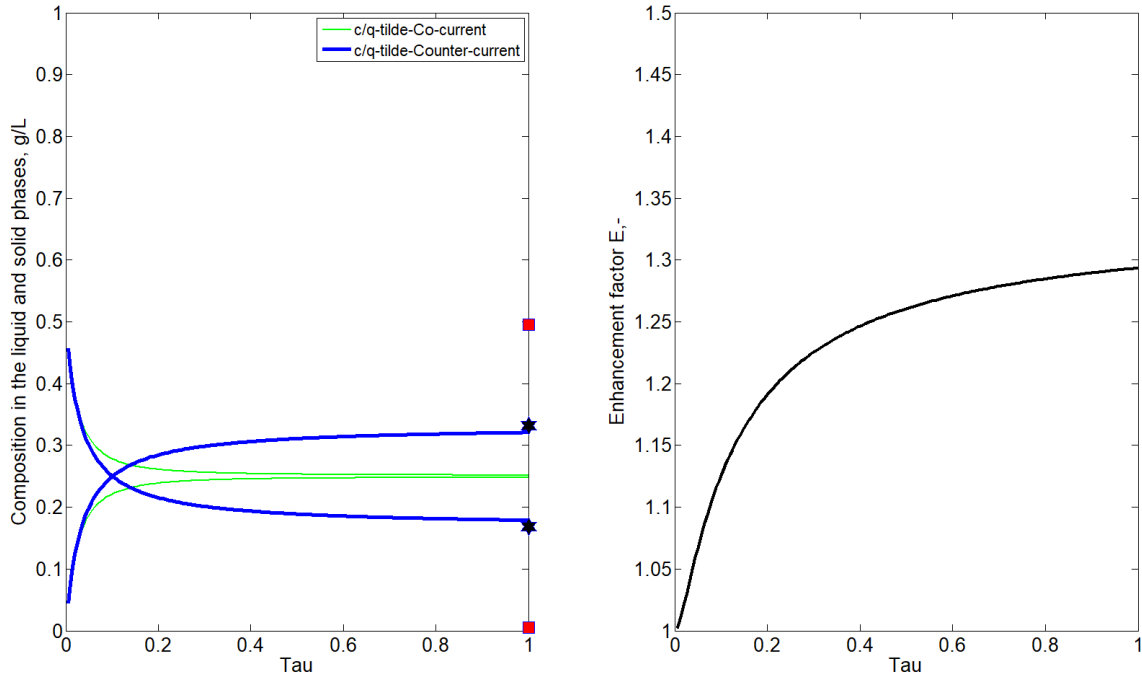


Figure 3.4. The composition in the liquid and solid phases of two stage co- and counter-current ($N = 2$) and the enhancement factor (eq. (3.70)). *Left:* The modified concentration development in the liquid and solid phases of two operations; *Right:* the enhancement factor between co- and counter-current operations calculated based on real concentrations. The input parameters selected for illustration are given as: $\tilde{q}_i^{in} = 1$, $\tilde{c}_i^{in} = 0$, $\varepsilon = 0.5$, $\tilde{k}_{i,E} = 10$, $\tilde{K}_{i,E}^{eq} = 1$, $\tau = 1$. The red-square points show the maximal value when the number of stage N goes to infinity and the asterisk points are resulted based on the Kremser method which is going to be shown below.

The results of 2-stage co- and counter-current operations show the advantage of counter-current operation based on enhancement factor (Figure 3.4). The enhancement factor E can be improved when the residence time is large enough or the number of stage is high which is going to be given in the next part.

It is shown that the counter-current is always better than the batch and co-current operation. Thus, we focus only on counter-current operation from now on.

Now a counter-current cascade of N -CSTR which can exceed the equilibrium limitation is considered.

Kinetically controlled counter-current operation for N CSTR

The advantage of counter-current operation was proven for $N = 2$. Below we will extent this analysis for a cascade of counter-current extraction operation of N stages.

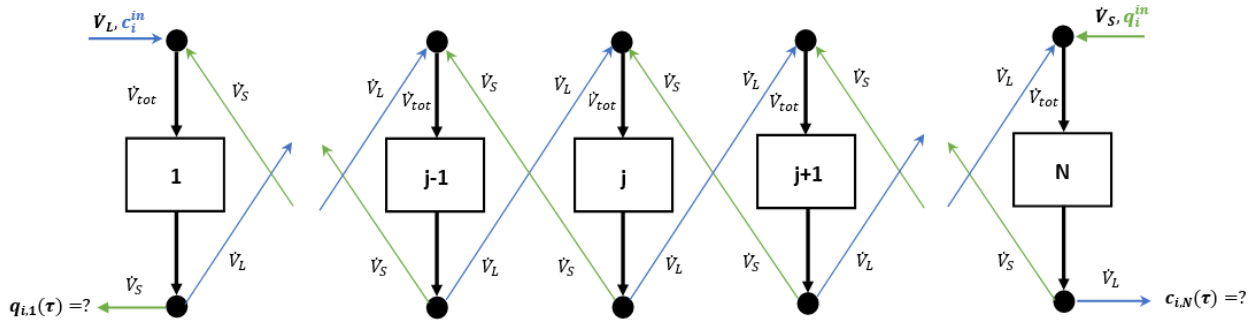


Figure 3.5. Description of N -stage counter-current operation for extraction. The unknowns are the concentrations of component i at every stages, in which the most interested unknowns are the outgoing concentrations of component i in the liquid phase $c_{i,N}$ at stage N and that in the solid phase $q_{i,1}$ at stage 1.

The system of N equations for N stage counter-current operation is very similar to the system in eqs.(3.62)-(3.65) with a notation of two specific stages connected to two inlets (stage 1 and stage N).

$$j = 1: \quad 0 = -A_1 \tilde{c}_i^{in} + \tilde{c}_{i,1}(\tau) - A_2 \tilde{q}_{i,2}(\tau) \quad (3.72)$$

$$0 = -(1 - A_1) \tilde{c}_i^{in} + \tilde{q}_{i,1}(\tau) - (1 - A_2) \tilde{q}_{i,2}(\tau)$$

$$j = 2, N-1: \quad 0 = -A_1 \tilde{c}_{i,j-1}(\tau) + \tilde{c}_{i,j}(\tau) - A_2 \tilde{q}_{i,j+1}(\tau)$$

$$0 = -(1 - A_1) \tilde{c}_{i,j-1}(\tau) + \tilde{q}_{i,j}(\tau) - (1 - A_2) \tilde{q}_{i,j+1}(\tau)$$

$$j = N: \quad 0 = -A_1 \tilde{c}_{i,N-1}(\tau) + \tilde{c}_{i,N}(\tau) - A_2 \tilde{q}_i^{in}$$

$$0 = -(1 - A_1) \tilde{c}_{i,N-1}(\tau) + \tilde{q}_{i,N}(\tau) - (1 - A_2) \tilde{q}_i^{in}$$

The above system of $2N$ equations can be presented in matrix form (Figure 3.6).

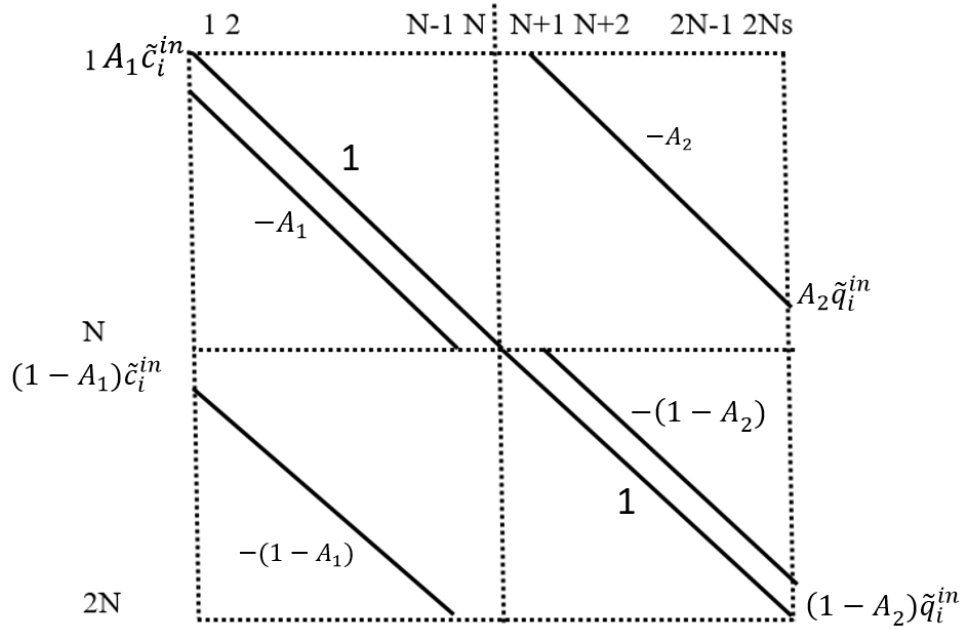


Figure 3.6. The coefficient matrix of the system of equations describes the kinetically controlled operation for N CSTR counter-current extraction process. The four non-zero elements of the right-hand side (r.h.s) vector are also depicted.

This system of $2N$ equations has a form of: $0 = \bar{A}\bar{y} + \bar{A}_0$ with a vector of unknown variables: $\bar{y}(t) = [\bar{c}_{i,1}, \dots, \bar{c}_{i,N}, \bar{q}_{i,1}, \dots, \bar{q}_{i,N}]$, a vector of given parameters: $\bar{A}_0 = [A_1\tilde{c}_i^{in}, (2N - 2) * 0, (1 - A_2)\tilde{q}_i^{in}]$ can be solved numerically.

Below is an example of concentration development in counter-current operation at different number of stages N (Figure 3.7). The results are gained by a Matlab code (*Code3*). The equilibrated concentrations (asterisk points) are calculated by Kremser method (eqs. (3.78), (3.79)) and the concentrations of plug counter-current regime (eq. (3.83)) (square points) are also included. The outgoing concentrations of component i , $\tilde{c}_{i,N}$, $\tilde{q}_{i,1}$ are depended on input parameters \tilde{c}_i^{in} , \tilde{q}_i^{in} , number of stages N and equilibrium distribution coefficient $\tilde{K}_{i,E}^{eq}$ (eqs. (3.75), (3.77)). Thus, the outgoing equilibrated concentration $\tilde{c}_{i,N}$ is changed parallel to N variation (asterisk points in Figure 3.7).

The modification of important parameters as $\tilde{k}_{i,E}$, $\tilde{K}_{i,E}^{eq}$, N , τ allows to improve the efficiency and these trends are shown in section 3.3.

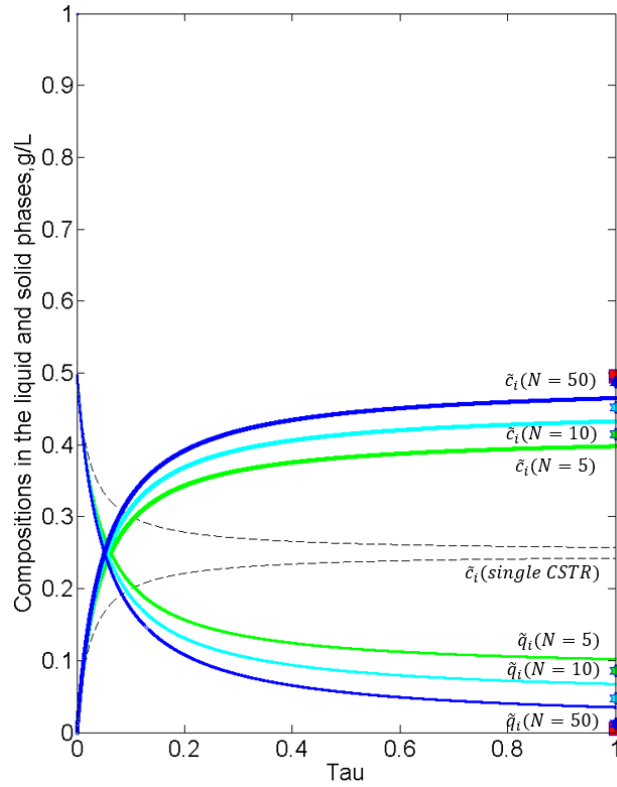


Figure 3.7. The influence of number of stages N on the kinetically controlled concentrations of component i in the counter-current extraction processes. The red-square points correspond to plug counter-current regimes and are constant. The asterisk points correspond to concentrations based on equilibrated stage model and can be calculated by the Kremser method (eqs. (3.75), (3.77)). Given parameters: $\tilde{q}_i^{in} = 0.5$, $\tilde{c}_i^{in} = 0$, $\varepsilon = 0.5$, $\tilde{k}_{i,E} = 10$, $\tilde{K}_{i,E}^{eq} = 1$, $\tau = 1$.

Furthermore, the rate model can be also simplified to equilibrium model where all stages are assumed at equilibrium.

Equilibrium controlled counter-current operation for N CSTR

The cascade can be simplified by just considering the steady state and assumed in addition a permanently established equilibrium. The latter assumption it is acceptable if sufficiently long residence times are given to the extraction process or Da_E is very big. In that case, the introduced parameters A_1 and A_2 (eq. (3.56)) can be simplified compared to kinetically controlled operation:

$$A_1 = A_2 = A = \frac{\tilde{K}_{i,E}^{eq}}{\tilde{K}_{i,E}^{eq} + 1} \quad (3.73)$$

Then, the system of $2N$ equations (eq. (3.72)) can be reduced to simpler N equations. After substitution A_1, A_2 by A (eq. (3.73)) and multiplication to $\tilde{K}_{i,E}^{eq} + 1$, eq. (3.72) takes the following tridiagonal matrix form:

$$\begin{aligned}
 j = 1: \quad & -(\tilde{K}_{i,E}^{eq} + 1)\tilde{c}_{i,1} + \tilde{c}_{i,2} = -\tilde{K}_{i,E}^{eq}\tilde{c}_i^{in} \\
 j = 2, N-1: \quad & \tilde{K}_{i,E}^{eq}\tilde{c}_{i,j-1} - (\tilde{K}_{i,E}^{eq} + 1)\tilde{c}_{i,j} + \tilde{c}_{i,j+1} = 0 \\
 j = N: \quad & \tilde{K}_{i,E}^{eq}\tilde{c}_{i,N-1} - (\tilde{K}_{i,E}^{eq} + 1)\tilde{c}_{i,N} = -\tilde{K}_{i,E}^{eq}\tilde{q}_i^{in}
 \end{aligned} \tag{3.74}$$

This can be illustrated as:

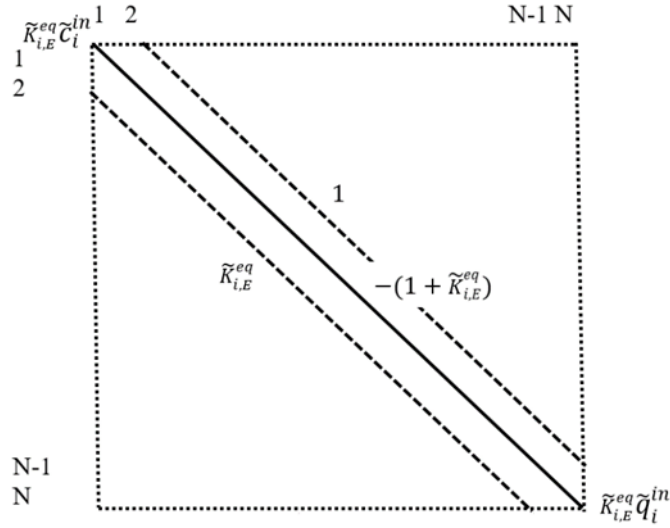


Figure 3.8. The tridiagonal coefficient matrix of the counter-current equilibrium stage model and the 2 non-zero r.h.s elements.

The system of N equations (eq. (3.74)) can be solved analytically by different methods (e.g.: Gaussian elimination, Thomas algorithm [102]). In the frame of this research, the alternative Kremser method [103, 104] was applied as explained in the *Appendix A2*). It provides the complete internal concentration profiles for both phases in all stages. Of key interest are again essentially the two outlet concentrations. A direct calculation of these concentrations as a function of the equilibrium constant $\tilde{K}_{i,E}^{eq}$ and the number of stages N is possible with the following equations:

$$\tilde{c}_{i,N} = \left(\frac{\tilde{K}_{i,E}^{eq-1} - 1}{\tilde{K}_{i,E}^{eq-(N+1)} - 1} \right) \tilde{c}_i^{in} + \left(\frac{\tilde{K}_{i,E}^{eq-N} - 1}{\tilde{K}_{i,E}^{eq-(N+1)} - 1} \right) \tilde{q}_i^{in} \tag{3.75}$$

and:

$$\tilde{c}_{i,1} = \left(\frac{\tilde{K}_{i,E}^{eqN+1} - \tilde{K}_{i,E}^{eq}}{\tilde{K}_{i,E}^{eqN+1} - 1} \right) \tilde{c}_i^{in} + \left(\frac{\tilde{K}_{i,E}^{eq} - 1}{\tilde{K}_{i,E}^{eqN+1} - 1} \right) \tilde{K}_{i,E}^{eq} \tilde{q}_i^{in} \quad (3.76)$$

Thus, the interest solid concentration at outlet $\tilde{q}_{i,1}$ can be calculated based on mass balance (eq. (3.45)) or from solution of the Kremser solution above as:

$$\tilde{q}_{i,1} = \frac{\tilde{c}_{i,1}}{\tilde{K}_{i,E}^{eq}} = \left(\frac{\tilde{K}_{i,E}^{eqN} - 1}{\tilde{K}_{i,E}^{eqN+1} - 1} \right) \tilde{c}_i^{in} + \left(\frac{\tilde{K}_{i,E}^{eq} - 1}{\tilde{K}_{i,E}^{eqN+1} - 1} \right) \tilde{q}_i^{in} \quad (3.77)$$

Furthermore, for the standard case that fresh solvent is entering the process ($\tilde{c}_i^{in} = 0$), then eqs. (3.75) and (3.77) can be simplified as:

$$\tilde{c}_{i,N} = \left(\frac{\tilde{K}_{i,E}^{eq-N} - 1}{\tilde{K}_{i,E}^{eq-(N+1)} - 1} \right) \tilde{q}_i^{in} = \left(\frac{\tilde{K}_{i,E}^{eqN+1} - \tilde{K}_{i,E}^{eq}}{\tilde{K}_{i,E}^{eqN+1} - 1} \right) \tilde{q}_i^{in} \quad (3.78)$$

and:

$$\tilde{q}_{i,1} = \left(\frac{\tilde{K}_{i,E}^{eq} - 1}{\tilde{K}_{i,E}^{eqN+1} - 1} \right) \tilde{q}_i^{in} \quad (3.79)$$

or in the real concentrations as:

$$c_{i,N} = \left(\frac{\tilde{K}_{i,E}^{eqN+1} - \tilde{K}_{i,E}^{eq}}{\tilde{K}_{i,E}^{eqN+1} - 1} \right) \frac{1-\varepsilon}{\varepsilon} q_i^{in} \quad (3.80)$$

and:

$$q_{i,1} = \left(\frac{\tilde{K}_{i,E}^{eq} - 1}{\tilde{K}_{i,E}^{eqN+1} - 1} \right) q_i^{in} \quad (3.81)$$

A Matlab code (*Code4*) based on eqs. (3.75), (3.76) is used to estimate the compositions in every stage. After dividing the outgoing liquid concentration $c_{i,N}$ (eq.(3.80)) by q_i^{in} is a percentage-wise measure for the "Gain" (G) which holds:

$$G = \frac{c_{i,N}}{q_i^{in}} \times 100 = \left(\frac{\tilde{K}_{i,E}^{eqN+1} - \tilde{K}_{i,E}^{eq}}{\tilde{K}_{i,E}^{eqN+1} - 1} \right) \frac{1-\varepsilon}{\varepsilon} \times 100 \quad (3.82)$$

The gained amount in the liquid phase is of interest because it is direct related to the productivity of the extraction process. The influence of G on the number of stages N and equilibrium coefficient $\tilde{K}_{i,E}^{eq}$ will be further expressed below (Figure 3.13).

There arises an interesting final simplification of the solution given above (eqs. (3.78), (3.79)) for $\tilde{c}_i^{in} = 0$ and for N approaching infinity. Then, gain G will be 100% and no more component i in the solid phase and the liquid phase concentration of component i at the outlet (eq. (3.78)) can be simplified as:

$$\tilde{c}_{i,N}^{max} = \tilde{q}_i^{in} \quad (3.83)$$

This represents the most optimistic “ideal” case, that everything provided with the incoming solid phase is transferred into the leaving liquid phase. This hypothetical case requires $N \rightarrow \infty$ and $\tilde{k}_{i,E} \times \tau \rightarrow \infty$.

3.3 Evaluation of counter-current extraction: Simulation results

The most flexible equation presented above which can quantify the attractive counter-current operation (eqs. (3.72)) includes the thermodynamic parameter ($\tilde{K}_{i,E}^{eq}$), the kinetic ($\tilde{k}_{i,E}$), a hydrodynamic parameter (characterizing deviation from plug flow via N) and available operating parameters (τ, ε). Regarding τ we will consider two alternative applicable residence time scenarios:

Scenario 1: the flowrates of liquid and solid phase are in a constant ε dependent ration in the whole cascade.

Scenario 2: the flowrate of the liquid phase is varied keeping the solid phase constant.

The solutions of eq. (3.72) are achieved by a Matlab code (*Code5*) and plotted below. The steady state counter-current cascade model will be used in this section for selected reference parameter to illustrate characteristic effects and parametric sensitivities. Before observing the influence of parameters and comparing the different case to reference operation, an example of diagrams is given and explained as below.

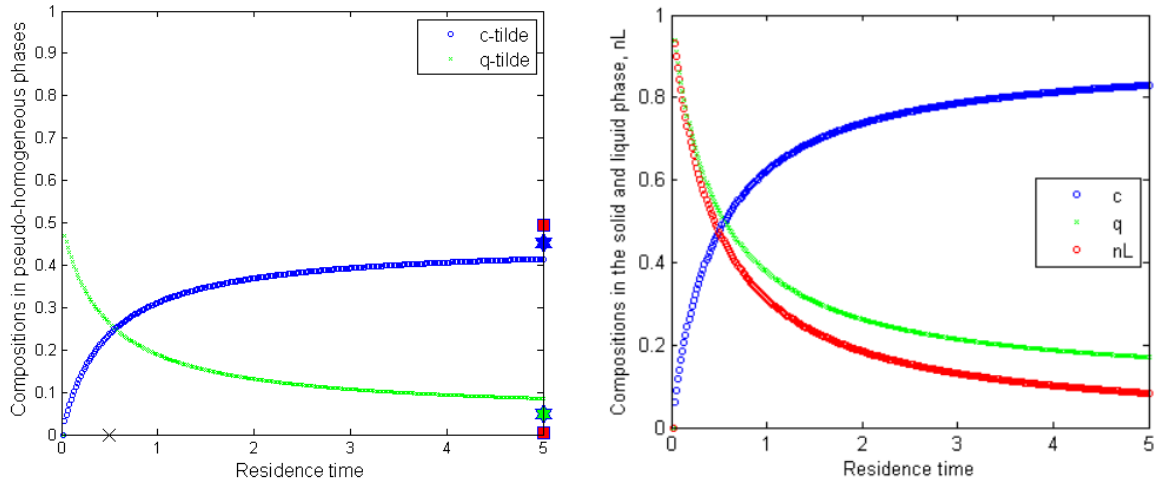


Figure 3.9. The concentration development of component i in the liquid and solid phase of counter-current operation. *Left:* The pseudo-homogeneous modified concentration as treated in eq. (3.72); *Right:* The real concentration arising ε dependent after splitting into two individual phases. *Given parameters:* $\tilde{q}_i^{in} = 0.5$, $q_i^{in} = 1$ (eq. (3.38)), $\tilde{c}_i^{in} = c_i^{in} = 0$, $\varepsilon = 0.5$, $\tilde{k}_{i,E} = 10$, $\tilde{K}_{i,E}^{eq} = 1$, $\tau = 5$. The asterisk points are derived from Kremser solutions (eqs. (3.75), (3.77)).

The concentration development of two phases is plotted via the entire length of the cascade characterized via residence time τ (eq. (3.47)). The star points represent for a finite number of equilibrated stages N in liquid and solid phase and are calculated based on eqs. (3.75), (3.77). The squared points show the infinite number of stages N in two phases calculated by eq. (3.83).

It should be noticed that the diagram can be plotted with the modified concentrations \tilde{c}_i and \tilde{q}_i or in c_i and q_i which are introduced and can be converted via eqs. (3.37), (3.38). The productivity, one of the most interesting parameters, is introduced in section 3.4 (eq. (3.87)) and also plotted in the right diagram as the red curve (\dot{n}_L).

Upcoming diagrams are going to illustrate the real concentrations c_i and q_i . Now, the important parameters as $\tilde{K}_{i,E}^{eq}$, $\tilde{k}_{i,E}$, N , τ , ε are brought into consideration, these parameters can be separately adjusted as in Table 3.1.

Table 3.1. The relevant important parameters and parameter space.

Important parameters	Units	Reference value	Varied range	Figure
$\tilde{K}_{i,E}^{eq}$	-	1	[0.5 ÷ 2]	Figure 3.10
$\tilde{k}_{i,E}$	m/min	1	[0.5 ÷ 2]	Figure 3.11
N	-	10	[5 ÷ 20]	Figure 3.12
τ	min	5	[1 ÷ 20]	Figure 3.14
ε	-	0.5	[0.25 ÷ 0.75]	Figure 3.15

In fact, the residence time τ is direct related to flowrate of the liquid phase (eq. (3.13)), thus, phase proportion ε is also changed. A separate consideration of concentration development in this specific case is given in Figure 3.15.

3.3.1 The influences of important parameters on the counter-current extraction performance (Scenario 1: fixed phase ratio)

In this part, the diagrams of reference values (Table 3.1) are presented in the middle of all 3-diagram sets below. It should be noticed that other given parameters are fixed at: $q_i^{in} = 1, c_i^{in} = 0$.

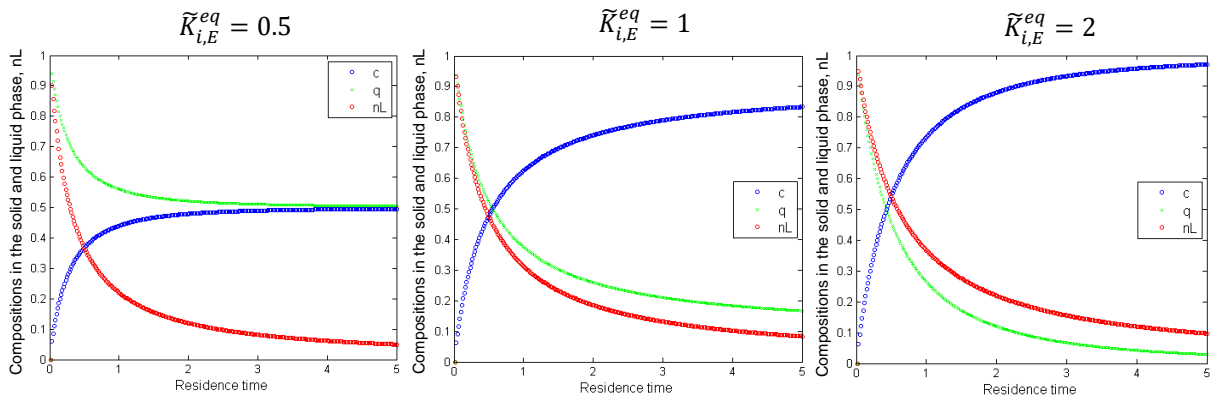


Figure 3.10. Sensitivity in case of equilibrium distribution coefficient $\tilde{K}_{i,E}^{eq}$ adjustment. Each diagram corresponds to a specific value of $\tilde{K}_{i,E}^{eq}$ and other parameters are kept at reference values (Table 3.1). The blue and green curve represent the compositions in the liquid and solid phase respectively. The red curve is for obtained amount of component i which is direct related to productivity. Reference case parameters: $q_i^{in} = 1, c_i^{in} = 0, \varepsilon = 0.5, \tilde{k}_{i,E} = 1, \tilde{K}_{i,E}^{eq} = 1, \tau = 5$.

Both the concentration in the liquid phase, $c_{i,N}$ and the obtained amount of component i , $\dot{n}L$ at the outlet are increased at higher equilibrium distribution coefficient $\tilde{K}_{i,E}^{eq}$. And of course, the solid material q_i is more depleted.

Now, we adjust the mass transfer coefficient $\tilde{k}_{i,E}$ based on reference case (Figure 3.11). When the $\tilde{k}_{i,E}$ is increased, the slopes of compositions in the liquid phase, $c_{i,N}$ and the obtained amount $\dot{n}L$ are steeper at the beginning and are slightly increased at the outlet.

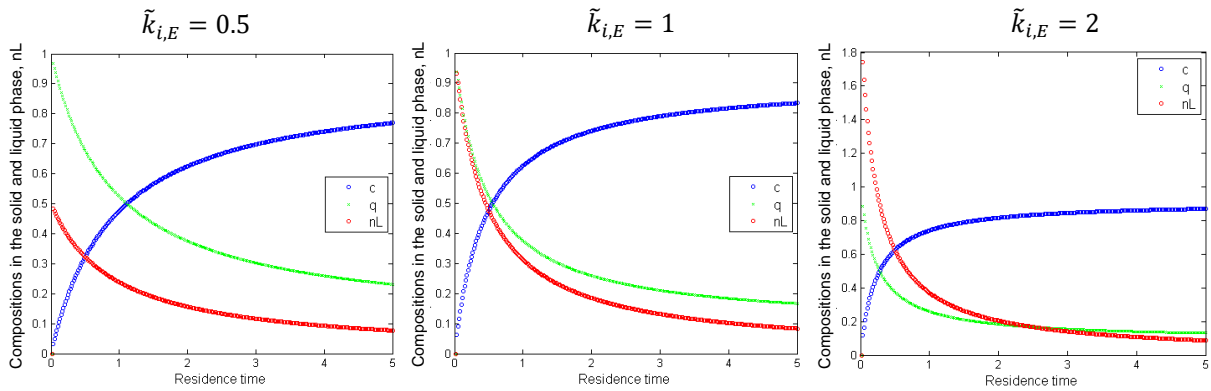


Figure 3.11. Sensitivity in case of equilibrium distribution coefficient $\tilde{k}_{i,E}$ adjustment. The variation range is from Table 3.1. Reference case parameters: $q_i^{in} = 1, c_i^{in} = 0, \varepsilon = 0.5, \tilde{k}_{i,E} = 1, \tilde{K}_{i,E}^{eq} = 1, \tau = 5$.

Now, observation of concentration development in case of number of stages N is put into consideration.

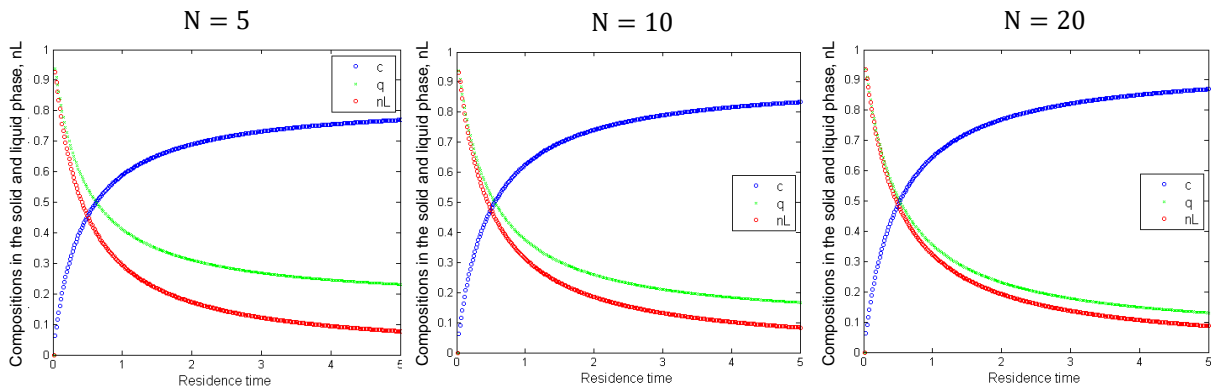


Figure 3.12. Influence of number of stages N on concentrations of the liquid and solid phases. Reference case parameters: $q_i^{in} = 1, c_i^{in} = 0, \varepsilon = 0.5, \tilde{k}_{i,E} = 1, \tilde{K}_{i,E}^{eq} = 1, \tau = 5$.

It should be noticed that the entire cascade is divided into N stages and the residence time of each stage is $\tau_N = \tau/N$. Both composition in the liquid phase, $c_{i,N}$ and the obtained amount of component i , \dot{n}_L are slightly increased. This observation can be seen clearer based on gain parameter G (eq. (3.82)) and described as below.

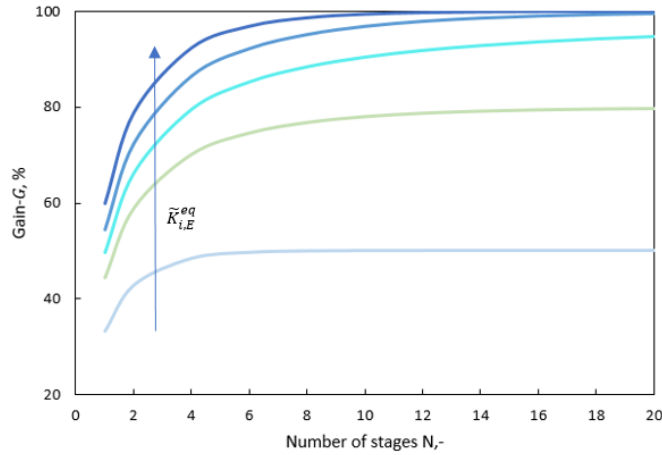


Figure 3.13. Illustration of the influence of number of stages N and equilibrium coefficient $\tilde{K}_{i,E}^{eq}$ on gain parameter G in counter-current operation. Given parameters: $q_i^{in} = 1, c_i^{in} = 0, N = 1 \div 20, \tilde{K}_{i,E}^{eq} = 0.5 \div 1.5$. Each curve corresponds to a fixed equilibrium distribution coefficient $\tilde{K}_{i,E}^{eq}$.

The gain parameter G shows the difference concentration at the outlet $c_{i,N}$ and that at the inlet q_i^{in} . When the equilibrium distribution coefficient $\tilde{K}_{i,E}^{eq}$ increases, the gain parameter G is enhanced. An influence of the number of stages N is visible only for low N smaller than 5 for the reference parameters used.

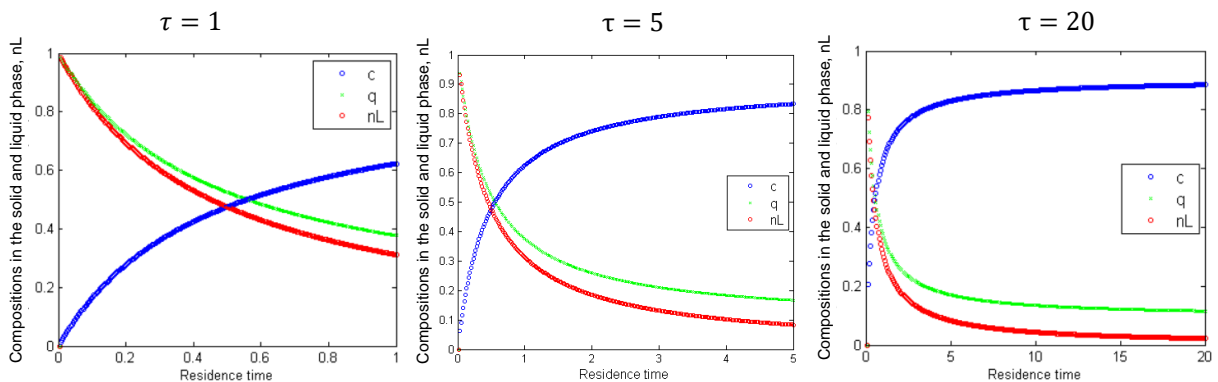


Figure 3.14. Illustration of the influence of the residence time τ on the outgoing concentrations and \dot{n}_L . Reference case parameters: $q_i^{in} = 1, c_i^{in} = 0, \varepsilon = 0.5, \tilde{K}_{i,E} = 1, \tilde{K}_{i,E}^{eq} = 1, \tau = 5$.

Furthermore, the influence of residence time τ on the concentration development is in interest. It shows whether the solid phase stays long enough or the amount of component i in waste. This behavior is presented in Figure 3.14.

The results show for the reference conditions used the longer residence times have less influence on the outgoing concentrations than shorter residence times.

All operations above are assumed that the phase ration among stages and flowrates of the liquid and solid phase are constant for the entire cascade (scenario 1). Now we consider a specific case when we keep the solid phase constant at every stage and change the liquid flowrate \dot{V}_L . In fact, the adjustment of \dot{V}_L leads to the alternation of phase ratio ε as below.

3.3.2 Alternative option of counter-current operation (Scenario 2)

As mentions at the beginning of this section, there are two interested options of operation when both flowrates are constant or liquid flowrate is varied. The first scenario considering a fixed phase ratio was given above. A possible alternative second scenario based fixing just one flowrate is considered below.

The residence time τ was introduced in eq. (3.47) and can be rewritten based on phase fraction ε in eq. (3.37) as:

$$\tau = \frac{V_{tot}}{\dot{V}_L + \dot{V}_S} = \frac{\varepsilon V_{tot}}{\dot{V}_L} \quad (3.84)$$

In fact, the liquid flowrate \dot{V}_L decides the residence time τ of both phase in the cascade and also impacts on the phase fraction ε inside the cascade. In order to implement, this scenario assumes a constant flowrate of the solid phase at $\dot{V}_S = 1 \text{ m}^3/\text{min}$, then, the corresponding specific flowrate of the liquid phase can be calculated via eq. (3.37) based on a given ε as:

$$\dot{V}_L = \frac{\varepsilon}{1-\varepsilon} \dot{V}_S \quad (3.85)$$

At this flowrate, a characterized residence time τ^* for a specific flowrate \dot{V}_L is calculated by eq. (3.84). This characteristic residence time allows us to estimate the

corresponding concentrations of two phases which can be further described the concentration profiles in different liquid flowrates as below.

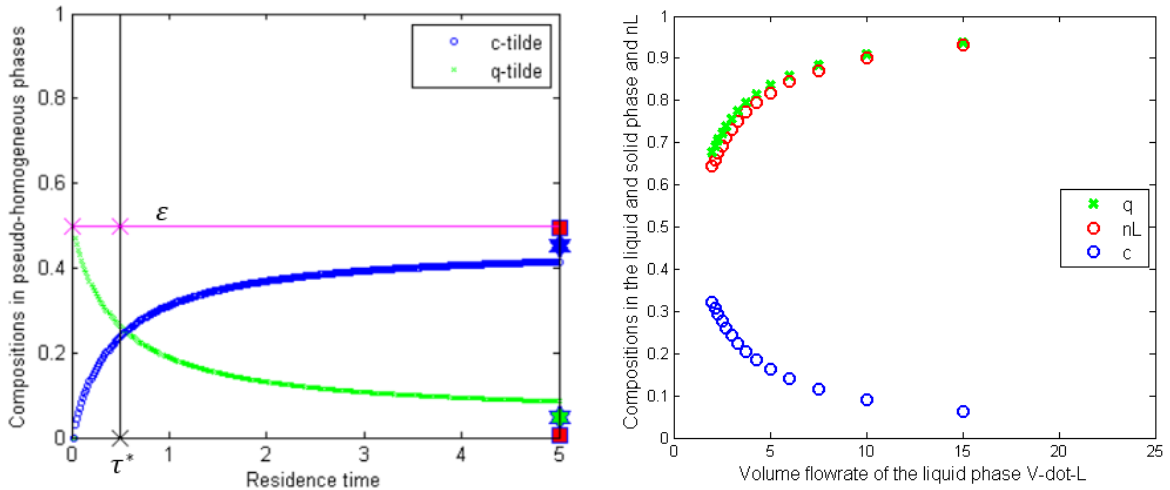


Figure 3.15. Illustration of determination of corresponding concentrations of the two phases related to liquid flowrate. *Left:* Reference case with corresponding lines of specific values of τ^* and ϵ . *Right:* The concentrations and obtained amount in different liquid flowrate \dot{V}_L .

These concentrations present for one liquid flowrate. The liquid flowrates \dot{V}_L are again adjusted by giving other ϵ values with a fixed \dot{V}_S . The corresponding concentrations in two phases are plotted over \dot{V}_L as in Figure 3.15.

The concentration of component i in the liquid phase c_i is decreased when the liquid flowrate is increased but the obtained amount \dot{n}_L behaves vice versa at high liquid flowrates. This trend is trivial because the low concentration is compensated by the higher amount of outgoing liquid amounts at higher flowrates.

Now, the quantification of objective functions (e.g. productivity, recovery) is of interest and evaluated below.

3.4 Objectives of extraction processes

To evaluate and compare the batch and continuous extraction processes, the objectives need to be specified. The most important objective functions will be introduced below.

3.4.1 Productivity

Generally, the productivity of a component i quantifies the extracted amount of component i in a certain volume, designated as $Scale$, in a unit of time t as:

$$Prod_i^{norm} = \frac{\dot{m}_{i,L}}{Scale} = \frac{c_{i,N} \times \dot{V}_L}{Scale} \quad [g/h/L] \quad (3.86)$$

or in the simplified explicit form of ignoring a $Scale$ factor as:

$$Prod_i = \dot{n}_L = c_{i,N} \times \dot{V}_L \quad [g/h] \quad (3.87)$$

The investigation and quantification of outgoing concentration $c_{i,N}$ and the liquid flowrate \dot{V}_L was discussed above. One option is to use as the $Scale$ relevant quantity the extractor volume $V_{extractor}$ (introduced in eq. (2.19)). The geometrical characteristics of extractor in different extraction modes and additional devices (e.g. stirrers, screw occupancy) might effect on the final results. Therefore, the $Scale$ factor can be considered as the free volume V_{free} (eq. (2.20)).

An example of productivity evaluation is going to be given for a specific case of ARTE extraction from *Artemisia annua L.* leaves in chapters 5 and 6.

3.4.2 Recovery

Aside from productivity, the recovery, is of interest. The evaluation is based on the difference of a desired component in the solid phase after traveling from one side to another side. The outgoing concentration of a component i $q_{i,1}$ was quantified above (eq. (3.81)) and that initially present in the solid phase q_i^{in} . Thus, recovery of a component i , Rec_i can be expressed as:

$$Rec_i = \frac{(q_i^{in} - q_{i,1}) \times \dot{V}_S}{q_i^{in} \times \dot{V}_S} \times 100 = \frac{(q_i^{in} - q_{i,1})}{q_i^{in}} \times 100 \quad (3.88)$$

The quantification of productivity and recovery for the specific case of extraction ARTE from *Artemisia annua L.* in batch and continuous operation will be given in chapters 5 and 6.

4 Materials, analytical methods and procedures

This thesis project uses the ARTE extraction process from *Artemisia annua L.* leaves as a relevant study case. The leaves were supplied in dried state by Mediplant (Switzerland) in different bags containing leaves, a small amount of stems and no roots. This chapter tends to perform the experimental processes including two main parts: (1) investigating the characteristics, properties of material, material pre-treatment procedures, homogeneity of material process and the relevant analytical methods; (2) aiming to identify the important parameters as the equilibrium distribution coefficients and the extraction mass transfer coefficient.

For this, most batch extraction experiments are performed. The determined parameters are the core for the evaluation and comparison of different extraction configurations later in chapter 5 and 6.

4.1 Primary investigations

When an appropriate solvent is chosen (e.g. high solubility to target), then the extraction time is shorter, means, the process is more efficient. Furthermore, the course of phytoextraction efficiency strongly depends on the quality of the material and is influenced by many parameters as: growing condition, climate, harvest time, pre-treatment processes and so on. Defining the characteristic of plant material as: size distribution examination, testing of maximal amount of targets in plant material, wetting effects, density... are the aims of this section and the relevant basic implementations are performed below. It should be noticed that all measured parameters below are present by the mass fractions introduced in section 2.2.

4.1.1 Solvent selection

In case of ARTE extraction, the solvent screening [75] for ARTE was carried out in different single solvents as acetonitrile, ethyl acetate and ethanol, toluene or in mixtures of these solvents [76, 78, 79]. Additionally, thanks to Prof. Seeberger in Max

Planck Institute of Colloids and Interfaces, Potsdam-Golm, he and his group successfully developed photochemical reaction technique, in which an important precursor dihydroartemisinic acid (DHAA) is photocatalytically oxidized to ARTE by singlet oxygen. In this technique, light-emitting diodes (LEDs) which are monochromatic, available in various wavelengths, highly efficient, long lasting, are in used. A recent intensive cooperated work of this conversion process was published in [15], in which a successful conversion of DHAA to ARTE was performed in very high efficiency. In that publish, own contribution of this research is the providing of crude extract, the exhaustive extraction method to define target maximal content in dried leaves, the optimized solid-to-liquid ratio and kinetics data of ARTE, DHAA extraction from dried leaves in Toluene. Furthermore, photochemical reaction has been intensively developed, chlorophyll is found in Toluene extract of ARTE and can be used as an efficient green photosensitizer [15]. Coupling to the partial synthesis downstream process, Toluene has been chosen as extraction solvent showing a higher selectivity, lower price and drastically by-product reduction. The recommended acceptable amounts for residual Toluene in pharmaceuticals distributed by the European Medicines Agency is PDE (permitted daily exposure) 8.9 mg/day (class 2). Below is the solubility of ARTE in different solvent [105].

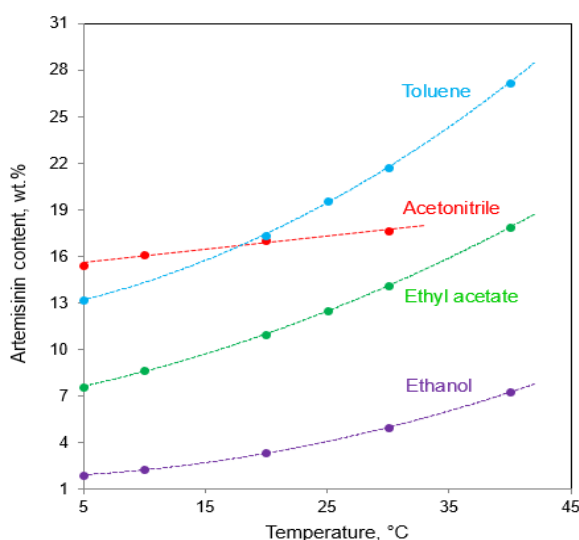


Figure 4.1. Solubility of ARTE in different solvent as a function of temperature [105].

The solubility data shows the good solubility of ARTE in Toluene and it increases from about 18 % at room temperature to 27 % at 40°C. Means, working at high temperature is definitely more productive, but it is faced up to higher energy consumption in entire production, thus, all experiments in this study are carried out at room temperature only.

4.1.2 Analytical methods and materials

4.1.2.1 Analytical methods

In phytoextraction, the analysis of the extract phase meets a lot of challenges and difficulties because the contents of active ingredients in the plants are relatively small and the extract contains not only targets, but also other unwanted components. In this thesis project, two secondary metabolites ARTE and DHAA of *Artemisia annua L.* leaves are interested, in which ARTE has been isolated since last three decades. A number of analytical procedures to quantify amount of ARTE has been reported in the previous literatures, however, there is lack of attention on DHAA in plant extract.

Regarding to ARTE analysis, the amount of ARTE in *Artemisia annua L.* is reported at around 0.01 to 1.4 wt.% which is relatively small. Recent researches have performed and developed various analytical methods from the simplest thin layer chromatography (TLC) [106-109] to other techniques as: high-performance liquid chromatography with ultra violet detector (HPLC-UV) [110-112], with evaporative light scattering detector (HPLC-ELSD) [113-119], with electrochemical detection (HPLC-ECD) [120-122], or with mass spectrometric detection (LC-MS) [123-126] and so on. HPLC-UV is robust, widely accepted but show the poor result to compound lacking of strong chromophore (e.g. ARTE), thus, it must be derivatized to a UV absorbing compound, called Q260 [127]. The major disadvantage of the derivatization process is time consuming and it introduces considerable experimental errors. Some other techniques require investment, expertise and also intensive sample preparation, thus, are not always suitable for routine and a great number of samples analysis in pharmaceutical fields.

Among ARTE developed analytical techniques, HPLC-ELSD remains as an alternative to the aforementioned detectors. Since decades, HPLC-ELSD has steadily developed, this quantification method is found as a rapid, reliable, versatile, inexpensive and reproducible detection technique in pharmaceutical analysis. It is also reported that ELSD can be applied with most solvents and is capable of detecting all analyte types regardless of its molecular structures [113, 114]. Additionally, a recent report by Lapkin et al. [111] concluded that UV detection was sufficient for quantitation of isolated ARTE but not for extracts. Therefore, in this research, the HPLC method with relatively inexpensive ELSD is chosen to quantify the desired components in extract. Besides, the development of TLC method is carried out to compare and confirm the accuracy of the analytical method.

Thin layer chromatography

The application of thin layer chromatography (TLC) is still a strong argument because of its economic advantages for many pharmaceutical labs. However, TLC advantages are rapid, relatively simple and samples need not to be very pure in comparison to HPLC, thus, it is still in large interest in quality control and stability testing of pharmaceutical active compounds and formulations in pharmaceutical field. The TLC technique, in principle, is understood that different compounds in a mixture travel at different rates due to the differences in their attraction to the stationary phase.

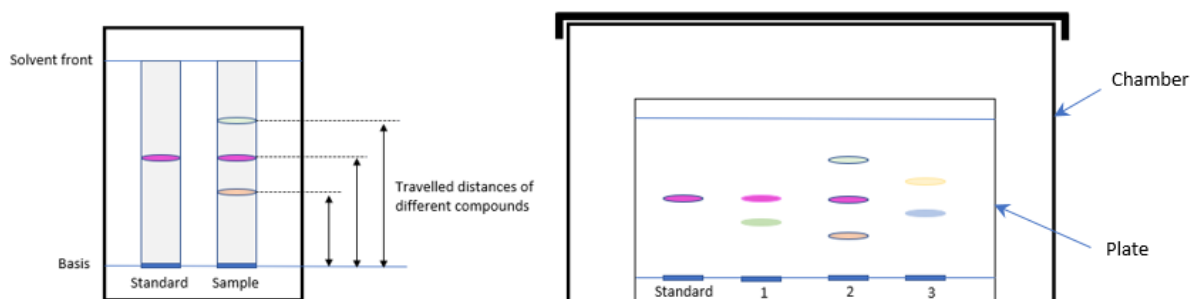


Figure 4.2. Travelled distance identification on developed plate. *Left:* distance travelled in standard and sample; *Right:* distance travelled in developing chamber for real analysis of different samples. *The plate containing samples and standards are developed inside a closed chamber.*

The travelled distances of compounds are characterized by a dimensionless factor, called retention factor, calculated as:

$$R_f = \frac{\text{distance travelled by compound}}{\text{distance travelled by solvent}} \quad (4.1)$$

In this research project, a high-performance thin layer chromatography (HPTLC) integrated with a semi-automatic sampler Linomat 5, densitometer Scanner 4 from CAMAG controlled by winCATs Planar chromatography manager, is in use. A typical procedure of an analysis can be described as below.

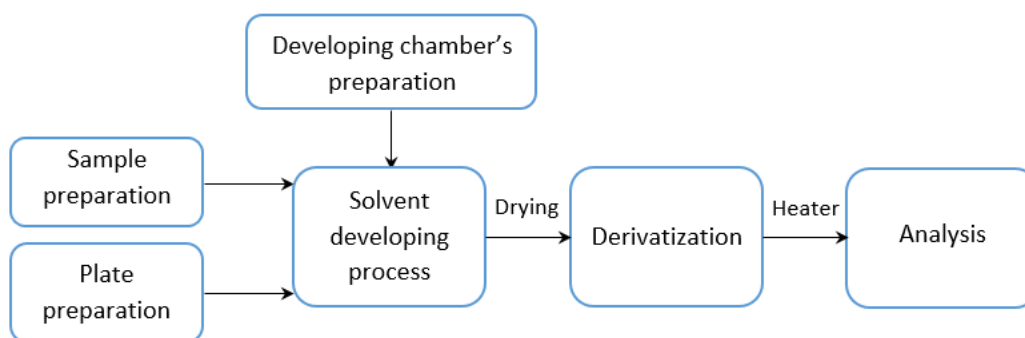


Figure 4.3. High performance thin layer chromatography (HPTLC) procedures.

The details of analytical procedures can be found in *Appendix A3* for ARTE detection. Below shows an ARTE analysis example of the developed plate with standards and extract samples.

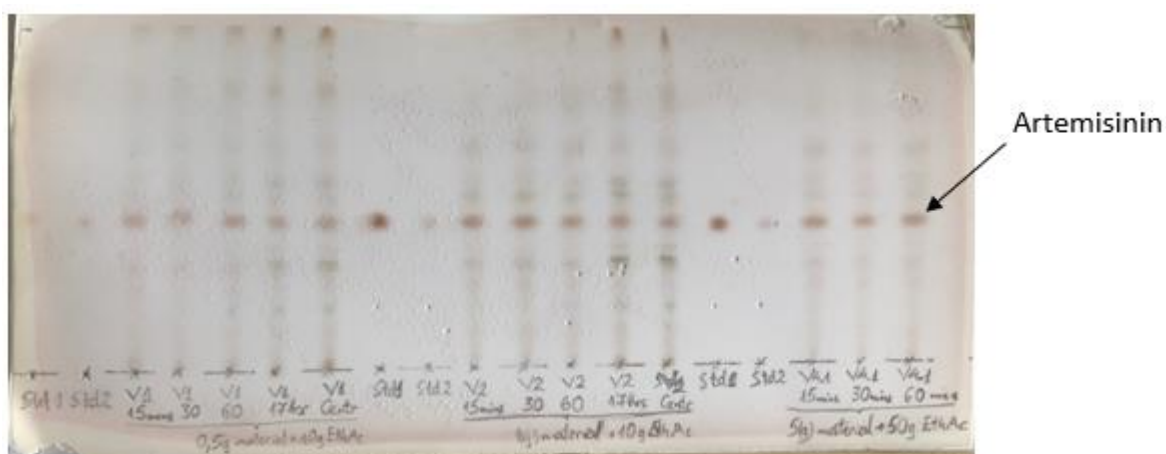


Figure 4.4. Developed high performance thin layer chromatography plate. The samples and standards are applied on the plate. The standards show only one retention factor of a specific solute at different concentrations and the samples perform relating components.

Nevertheless, the quantification process by TLC technique gets several difficulties as: the need of derivatization mixture fresh preparation, the saturated condition maintaining, the quality of the plate and so on. Therefore, it needs to develop another stable method, high performance liquid chromatography (HPLC) with an appropriate detector is chosen and is intensively developed to qualify and quantify the desired compounds presented in crude extracts.

High performance liquid chromatography

The analysis of a sample is implemented by a fully automated instrumental system controlled by a computer program recording chromatographic profiles of all individual peaks: retention time, surface areas, peak width and so on (Figure 4.5). The mobile phase is normally moderated in gradient mode for analyzing of complex herbal extracts and acid acetic is added to improve the separation and resolution of the bioactive compounds.

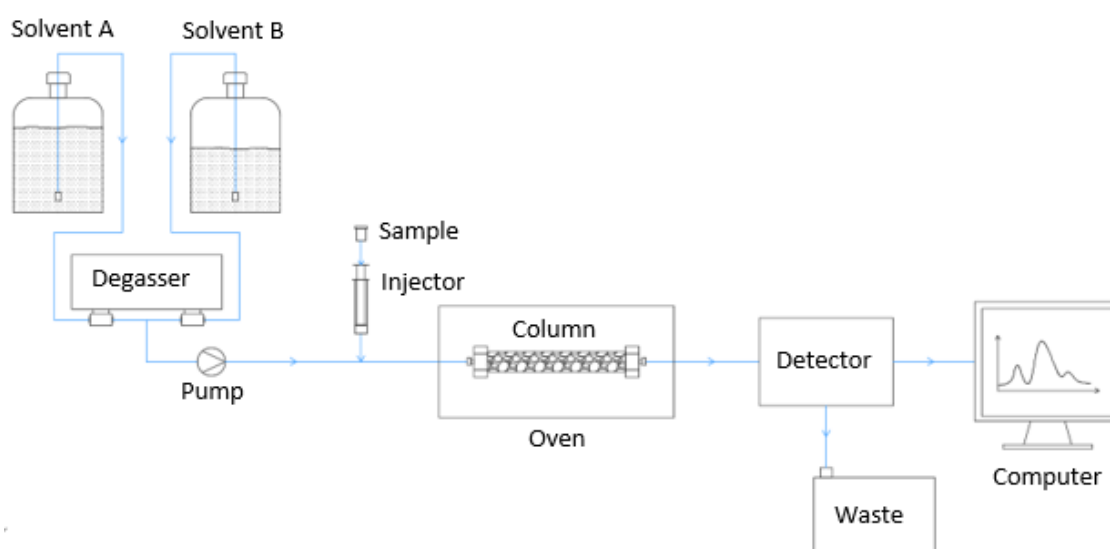


Figure 4.5. Principle of high performance liquid chromatography (HPLC).

As mentioned above, the ELSD is chosen because of its advantages, special for quantification purpose of ARTE in extract. The principle of ELSD detector is depicted in Figure 4.6. The effluent from the chromatography column is firstly nebulized into fine droplets, then, these droplets are carried to a heated tube where the solvent is evaporated and formed the aerosol. In nebulizer, the larger droplets are condensed on the wall side and are discharged to an outside siphon system (Figure 4.6), the

smaller droplets containing solute particles pass through the drift tube and reach an optical cell integrated by polychromatic light beam.

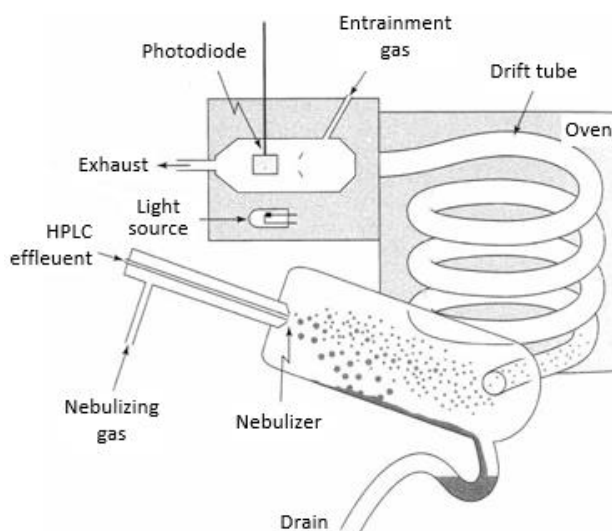


Figure 4.6. The principle of evaporative light scattering detector (ELSD).

The amount of scattered light is measured by a photomultiplier tube, in which the amount of scattered light is proportional to that of solute in the cell. It is necessary to figure out the relation of concentration and outgoing signals, however, the conversion process is lack of investigation since many decades but it has been recently improved and intensively discussed [128, 129]. The conversion between the signal and real concentration of samples is implemented via area method showed in *Appendix A4.1*.

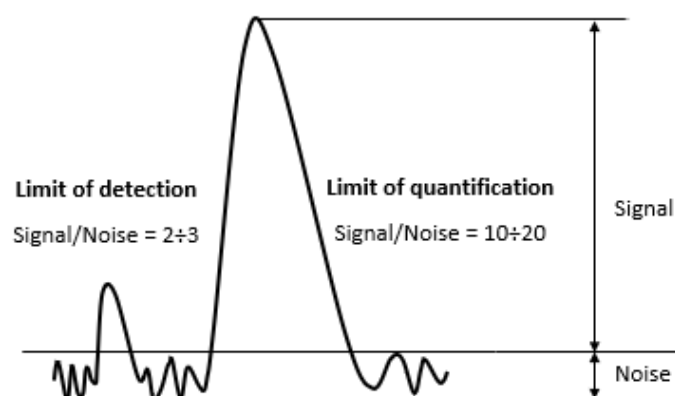
The extract samples are analyzed by HPLC Agilent 1100 system equipped and setup by following elements: a high quality Kinetex C18 column (250x4.6 mm; 2.6 μm) controlled at 25 degree Celsius; the mobile phase is supplied by quaternary pump G1311A at 1 mL/min flowrate and is performed in a gradient mode (Table 4.1) by mixing two channel A: acetonitrile and channel B: 0.1 % acetic acid in water. An evaporative light scattering detector (ELSD) is set up at 40 degree Celsius evaporative and nebulizer temperature at nitrogen flow 1.6 L/min; the injection volume of sample is 5 μL . The details of HPLC analytical procedures for ARTE analysis is given in *Appendix A4.2*. Furthermore, a calibration procedure showing the relation between instrument response and the amount of solute in standards is a must. The standard concentrations for ARTE analysis are prepared in three different ranges (*Appendix A5*).

Table 4.1. HPLC gradient method of quantifying ARTE concentrations.

Time [min]	Channel A - Acetonitrile	Channel B – 0.1 % acetic acid in water
0 - 5	68 %	32 %
5 - 10	100 %	0
10 - 15	100 %	0
15 - 20	68 %	32 %
20 - 25	68 %	32 %

Limit of detection (LOD) and limit of quantification (LOQ) for HPLC

The determination of LOD and LOQ is an essential step of the measurements, it allows us to produce reliable analytical data. In which, LOD sets the lowest concentration for assessing the qualitative presence of solute that is reliably distinguished from zero, while LOQ sets the lower limit for quantifying, it obviously equals or exceeds the LOD. Several approaches for determining LOD & LOQ are possible, in this mostly-used HPLC-ELSD, the determination of both based on signal-to-noise is performed by comparing measured signals of standards and it is limited at 2:1 and 10:1 ratio for LOD and LOQ respectively (Figure 4.7).

**Figure 4.7.** Identification of LOD and LOQ for HPLC based on signal and noise.

The measurement procedures of LOD & LOQ (*Appendix A6*) are carried out for both isocratic and gradient method of ARTE and DHAA. The results are summarized in Table 4.2.

Table 4.2. LOD and LOQ values of two desired components ARTE and DHAA for HPLC.

	Isocratic		Gradient (Table 4.1)	
	LOD	LOQ	LOD	LOQ
ARTE [wt.%]	$3.9 * 10^{-3}$	$9.9 * 10^{-3}$	$3.1 * 10^{-4}$	$1.9 * 10^{-3}$
DHAA [wt.%]	$8.1 * 10^{-3}$	$1.4 * 10^{-2}$	$7 * 10^{-3}$	-

The relevant information of used solvents, equipment, elements and substances are listed in *Appendix A7*.

4.1.2.2 Plant material characteristics

100 kilograms *Artemisia annua L.* dried leaves were provided by Mediplant (Switzerland) stored in different bags. The content of the desired target ARTE in *Artemisia annua L.* leaves is strongly depended on the growing conditions, geographical characteristics, also on genotype [130], harvesting time and plant tissue [131, 132]. ARTE locates mostly in the glandular trichomes of *Artemisia annua L.* leaves [133], in which the highest content of ARTE is in the upper, younger leaves of the plants. The typical content of ARTE is reported in the range from 0.01 to 1.4 % based on dried weight. Additionally, as introduced above, *Artemisia annua L.* leaves contain not only ARTE but also other valuable components, among DHAA is known as an important precursor [134] to synthesize ARTE. DHAA can be present in about the same amount of ARTE.

In this section, the size distributions of original leaves and of ground material are examined. Then, the homogeneity process is assured to have a unified quality of the inlet source. The maximal amounts of desired targets are determined by exhaustive extraction as well as the corresponding densities in dried and mixed states. The wetting effect related to solvent absorbability of leaves is also quantified.

Size distribution

The smaller the particle sizes, the shorter the diffusion times. Thus, reduction of material size makes the process more efficient. The size reduction is implemented in

an ultra-centrifugal mill machine and the ground portions are later mixed by hands to assure the homogeneity of sources. The size distribution analysis is carried out by a vibration sieve machine (Figure 4.8).



Figure 4.8. Vibration sieve machine (AS200) and ultra centrifugal milling machine (ZM200 from Retsch).

By using vibration sieve machine, the original imported dried leaves are separated in the different sieve size range (0.18-2) mm. The masses in separate sieve are weighed and recorded. The results are given below.

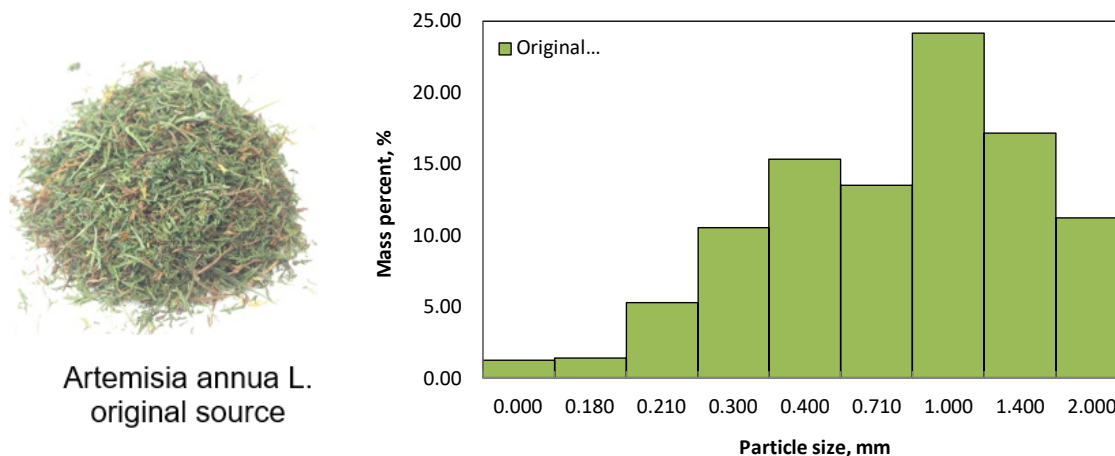


Figure 4.9. The size distribution of originally imported *Artemisia annua L.* leaves. *Left:* Original dried leaves from Mediplant; *Right:* Size distribution of original leaves.

Analytical results show that 98 % of original leaves size is in the range (0.21-2) mm (Figure 4.9). The original leaves are ground and the reduction process is implemented by milling machine as follows:

- The milling machine Ultra Centrifugal Mill ZM200-Retsch is operated at 12000 rpm speed. After milling, all portions are stored in a container and are mixed by hands which is described in homogeneity process below.
- Three portions of ground leaves at different positions in the container are collected and sieved by sieve machine at varied sizes from 0.06 to 0.4 mm.

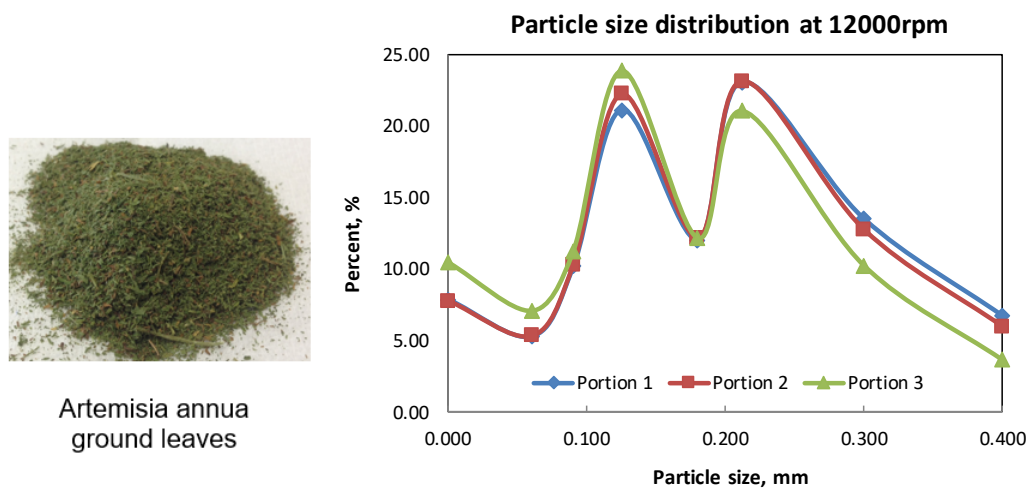


Figure 4.10. The size distribution of ground *Artemisia annua* L. leaves. *Left:* ground leaves by mill machine ZM200 at 12000 rpm; *Right:* ground leaves size distribution of three portions.

The results show that the size distributions of ground leaves at different positions are identical and are about 96 % in the range of (0.09-0.4) mm (Figure 4.10).

Homogeneity of feed

The size reduction and distribution analysis allow us to control the penetration speed of solvent into solid matrices. Nevertheless, the contents of desire components in leaves are varied by various factors like growing condition, harvest time or drying condition, thus, the consolidation of leaves quality of different stored bags is a need for a scientific study to assure a homogeneity of feed quality. This process is carried out by taking the samples of well-mixed leaves in container from different positions (upper, middle, bottom and at corners), these leaves samples are tested by relevant exhaustive extraction technic below.

Content of ARTE and DHAA in dried leaves

In principle, if the described mixing process above is well done, the target contents in homogenized portions should be identical at every position in container. This inspection is feasible by a specific technique, called exhaustive extraction, in which the desired components are completely taken out of the leaves. This technique has been applied by many previous researches and literatures [74,83-86], it can be implemented in many different ways as: maceration, immersion, percolation, Soxhlet and so on. This research uses a simple approach with a series of batch extraction of a fixed material mass (Figure 4.11). An exhaustive extraction process can be illustrated as:

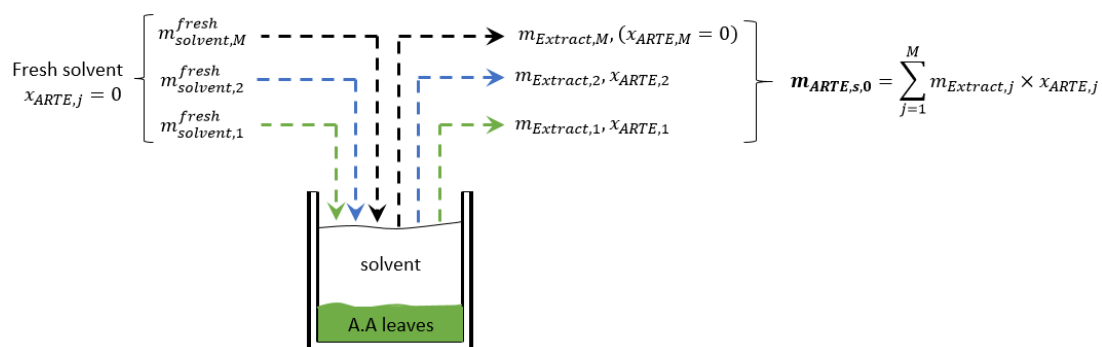


Figure 4.11. Scheme of the exhaustive extraction technique. *The dried leaves are filled into the extractor, each color corresponds to an input and an output of one batch extraction run. Each cycle corresponds to one complete single batch extraction designated as stage j ($j = 1 \dots M$). When the first cycle is finished by providing and withdrawing process, the second cycle starts. The process stops when the final extract contains no more ARTE ($x_{ARTE,M} = 0$).*

The leaves are immersed in a defined amount of fresh solvent at room temperature, the mixture is agitated. The first run is finished by collecting the first extract portion $m_{Extract,1}$ and the raffinate is still kept inside. A new fresh solvent portion is added into retained raffinate and the second run starts. The process is repeated until no more solute is found in extract ($x_{ARTE,M} = 0$). The extract samples are analyzed by HPLC (section 4.1.2.1) and the sum of obtained ARTE masses in every portion indicating the ARTE amount in initial dried leaves $m_{ARTE,S,0}$ holds:

$$m_{ARTE,S,0} = \sum_{j=1}^M m_{Extract,j} \times x_{ARTE,j} \quad j = 1, M \quad (4.2)$$

within, M is the number of measurements. The above process is applied for ARTE and DHAA quantification in *Artemisia annua L.* dried leaves (Table 4.3). To assure the accuracy of the measurement, the experiment is repeated twice by two different amounts of dried leaves collected at different positions in the container. The summary data is given below.

Table 4.3. The ARTE, DHAA content of the homogenized dried leaves. The extraction is carried out in 30 minutes for each contact.

Exp. condition	m_s (g)	Extract mass, m_j [g]	$m_{ARTE,j}$ [mg]	$x_{ARTE,S,0}$ [wt. %]	$m_{DHAA,j}$ [mg]	$x_{DHAA,S,0}$ [wt. %]	Sum [wt. %]
1.5 g leaves in Toluene	1.5	25.18	15.76		6.56		
		24.98	3.72		-		
		25.57	0.34		-		
		28.92	0		-		
Total amount			19.83	1.32	6.56	0.43	1.76
3 g leaves in Toluene	3	21.8	22.45		13.82		
		23.34	11.82		-		
		24.25	3.83		-		
		28.13	0.2		-		
Total amount			38,3	1.27	13.62	0.45	1.73

The concentrations of component i in the extract phase are analyzed by HPLC method presented in section 4.1.2.1. The data shows that the mass fractions of solute in two different masses of leaves are not much different (1.32 wt.% and 1.27 wt.%), thus, the averaged ARTE and DHAA amounts in provided dried leaves are assigned respectively at $x_{ARTE,S,0} = 1.3$ wt.% and $x_{DHAA,S,0} = 0.44$ wt.% based on dried weight.

Density of dried leaves and mixtures

As introduced, the evaluation of productivity is strongly depended on the *Scale* factor or relevant volumes (eq.(3.86)). The determination of the suspension volume or dried leaves can be experimentally defined by following processes. The measurement is carried out by using a graduated cylinder and scales. For the dried leaves density, different weighed amounts of leaves are added into cylinder, the corresponding volumes are recorded, the division of masses to relevant volumes results the density (Table 4.4).

Table 4.4. Measuring data of dried leaves density. *The experiments are carried out in two different masses of leaves and the results confirm the density of dried leaves.*

Mass of dried leaves [g]	Granulated cylinder [mL]	Density of leaves, ρ_{leaves} [g/L]
2.6	10	260
5.23	20	261

Similarly, the density of leaves and solvent mixture is strongly depended on the solid-to-liquid ratio introduced as dosage D in eq. (2.8). The measurement method is identical as above, the defined leaves and solvent masses are filled into graduated cylinder, the corresponding volumes are recorded. The outcomes are listed below.

Table 4.5. Measuring data of mixture density. *The experiments are tested in three different dosages. The results are later applied in geometrical calculation of continuous extractor in chapter 6.*

Mass of dried leaves [g]	Mass of solvent [g]	Dosage D [-]	Granulated cylinder [mL]	Density of mixture, $\rho_{suspension}$ [g/mL]
1.493	30	0.05	38	0.83
2.993	30	0.1	39.5	0.835
5.998	30	0.2	41.5	0.867

The measurement of this density parameters will be later used in evaluating of productivity introduced in section 3.4 by applying to the *Scale* factor involved to suspension volume $V_{suspension}$ in eq. (2.18). The detail of evaluation process is going to be exhibited in relevant extraction operations in chapters 5 and 6.

Wetting parameter

As introduced in section 2.1, wetting effect is represented by a parameter W (eq.(2.3)) which directly affects to the efficient distribution coefficient and overall efficiency of the extraction. When the W value is large, the solid matrix of leaves is able to absorb more solvent. Then, the obtained extract in a certain volume of initial solvent is reduced. This leads to the reduction of both productivity and recovery. Each

solvent/solid pair will give an individual W value. The W value can be determined experimentally as follows:

- A portion of leaves is mixed with an amount of weighed solvent, the mixture is stirred to equilibrated state. After settling the solid, the extract phase (without solid particles) is sucked out to the interface by a syringe.
- Weighing the extract amount allows us to calculate the solvent retained in the solid matrix based on the initial amount of solvent.
- Repeating the procedure in different masses of leaves allows estimating average W factor (Figure 4.12).

The method of collecting the extract phase by syringe aims to keep the free-flow state of extract and raffinate phases which is very close to the transportation characteristic inside continuous extractor.

Based on the experimental data, the wetting parameters of Toluene, n-Hexane, Ethanol are 2.25; 1.7 and 2.4 respectively.

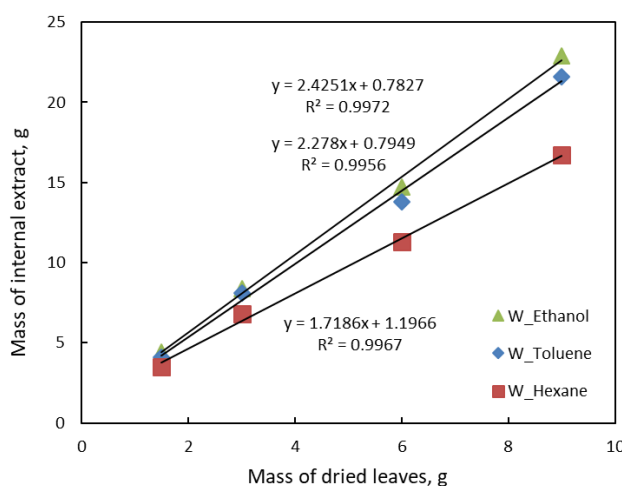


Figure 4.12. Wetting parameter measurement data. *The ratio of internal extract mass and initial leaves mass represents wetting factor ($W_{Toluene} = 2.25$; $W_{n-Hexane} = 1.7$; $W_{Ethanol} = 2.4$).*

The values of wetting parameters W allow us to calculate the phase ratio χ_{ER} (eq.(2.13)). It can also be used in the conversion between the effective and thermodynamic distribution coefficient mentioned in section 2.2.2 (*Appendix A 1*).

4.2 Results: Important parameters from batch extraction runs

As introduced in the first chapter, the pharmaceutical products are mostly batch-wise produced and the implementation of extraction in batch mode is necessary to understand the characteristics, properties and also the behavior of the target components in different extraction systems like solubility, wetting parameter, residence time, effective and thermodynamic distribution coefficients. These important parameters can be achieved by batch operation as below.

4.2.1 Batch process

In batch extraction process, a certain amount of dried leaves $m_{S,0}$ is in contact to a defined amount of solvent $m_{L,0}$ in an extractor, the mixture is agitated until equilibrium by stirrer. When the extraction process finishes, the mixture is left in few minutes to settle down the solid particles. It results two separated phases: a transparent liquid phase (extract) and a mixed dark phase (raffinate in eq. (2.6)) (Figure 4.13). Then, the extract is gently sucked out by a syringe to the interface of two phases. The rest amount of extract, introduced as internal extract, stays in depleted leaves. These experimental procedures can be described as:

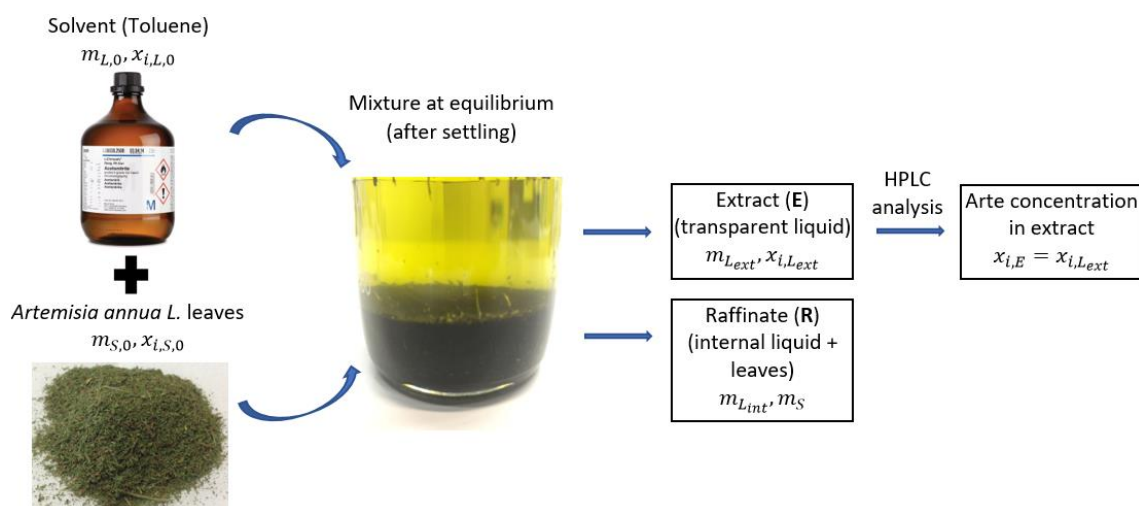


Figure 4.13. Experimental illustration of a single batch extraction with a defined dosage in eq. (2.8). The mixture of leaves and solvent is settled and extract (E) contains no solid particles, the dried leaves contain a defined amount of solvent and establishes raffinate (R).

After collecting the extract and raffinate phases, the mass of external or extract phase $m_{L_{ext}} (= m_E)$ is weighed and recorded. The relevant concentration of a specific component i , $x_{i,E}$ is analyzed by introduced HPLC method (section 4.1.2). Thus, the mass of a component i in extract as the product can be calculated.

However, the obtained mass of a specific component i at equilibrium, $m_{i,E}^{eq}$ can also be calculated based on parameters as effective distribution coefficient, phase ratio and initial mass material (eq. (2.41)). These essential parameters were mathematical introduced in eqs. (2.13) and (2.28), in which the distribution coefficients can be experimentally defined as below.

4.2.2 Equilibrium constants for ARTE and DHAA

In reality, the internal liquid is often kept by solid matrix, therefore, we use effective distribution coefficient β_i^{eff} than the thermodynamic one. However, this section is going to introduce the experimental method, calculation and expression of both parameters. As explained above in section 2.2.2, thermodynamic distribution coefficient β_i (eq. (2.29)) presents the relation between ARTE concentration in extract and that in solid phase. The effective distribution β_i^{eff} (eq. (2.28)) shows the distribution of ARTE in extract and in raffinate phase. The conversion between coefficients based on wetting parameter W is already shown in *Appendix A1*.

The dried leaves are brought into contact to solvent, then, the mixture is agitated until equilibrium reached. These experiments are implemented as single batch extractions at different dosages. It should be noticed that, the fresh solvent with the initial mass $m_{L,0}$ contains no ARTE, means, $x_{ARTE,L,0} = 0$, the mass fraction of ARTE in leaves corresponds to the maximal amount defined by exhaustive extraction technique in section 4.1 and $x_{ARTE,S,0} = 0.013$ (Table 4.3), the extract mass m_{L_e} is weighed after phase separation and the ARTE concentration in extract phase $x_{ARTE,E}$ is analyzed by introduced HPLC technique in section 4.1.2.1. The repeat of these experimental steps at different dosages D (eq. (2.8)) shows the equilibrium curve (Figure 4.14).

Furthermore, the known ARTE amount in dried leaves at inlet is distributed into external, internal and solid phases. At equilibrium, the ARTE concentration in external liquid phase equals to that in internal phase, therefore, the ARTE amount in solid phase is determined when the wetting parameter W in section 4.1.2.1 is known. Below is the distribution coefficient data of ARTE extraction in Toluene.

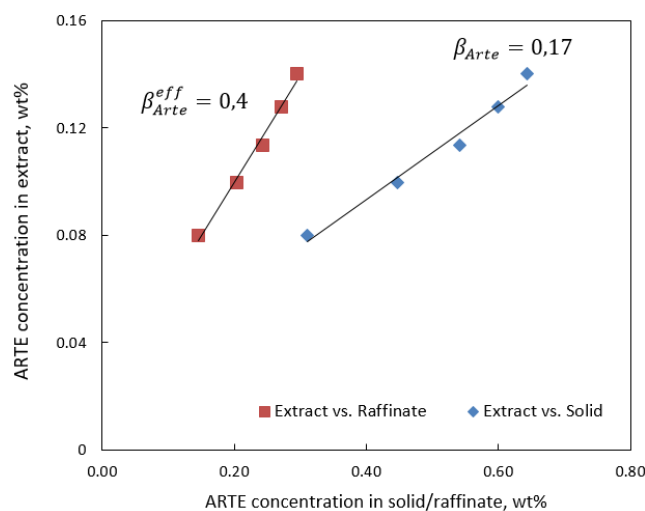


Figure 4.14. Equilibrium concentration of ARTE extraction in Toluene as the solvent. The effective distribution coefficient β_i^{eff} is estimated based on eq. (2.28) and thermodynamic distribution coefficient β_i is derived from eq. (2.29).

The red-colored points present the equilibrated concentration of ARTE between the extract and raffinate phases. The blue-colored points show the equilibrated concentration of ARTE in the extract and solid phases. The lowest points on each line corresponds to the smallest dosage ($D = 0.05$), it is hardly to go lower than this value because the extract is very diluted. In vice versa, the highest points are related to the highest dosage ($D = 0.3$) and the leaves will immediately absorb almost the whole solvent into its solid matrix and it is impossible to obtain extract. In this range, the curves can be fit by a linear and the slopes of the lines reveal the relevant efficient and thermodynamics distribution coefficients (Figure 4.14).

The distribution coefficients of ARTE are also determined for Ethanol and n-Hexane. Table 4.6 below presents the effective distribution coefficients of two desired components ARTE and DHAA in three different solvents. The measured data are given in *Appendix A8*.

Table 4.6. Effective distribution coefficients β_i^{eff} derived from eq.(2.28) of ARTE and DHAA in three solvents.

Distribution coefficients	Notation	Toluene	Ethanol	n-Hexane
ARTE effective distribution coefficient	β_{ARTE}^{eff}	0.4	0.36	0.34
DHAA effective distribution coefficient	β_{DHAA}^{eff}	0.36	0.64	0.72

Based on the measured data, both ARTE and DHAA tend to settle in the raffinate phase. The important parameters as kinetics, distribution coefficients play the key role in simulation which was shown in chapter 3. These important parameters will be again used in the design and evaluation process in the upcoming chapters.

4.2.3 Kinetics of extraction

Phytoextraction processes are mostly based on diffusion due to gradient of target content in the leaves, in which diffusion mass flow is difficult to determine. Thus, understanding of kinetics is very important to estimate the industrial applicability of the system and to adjust the plant operations which result the economic efficiency. In order to know the sufficient extraction time to reach equilibrium, a series of single extraction processes is carried out by altering the leaves amounts in a certain mass of solvent (different dosages D).

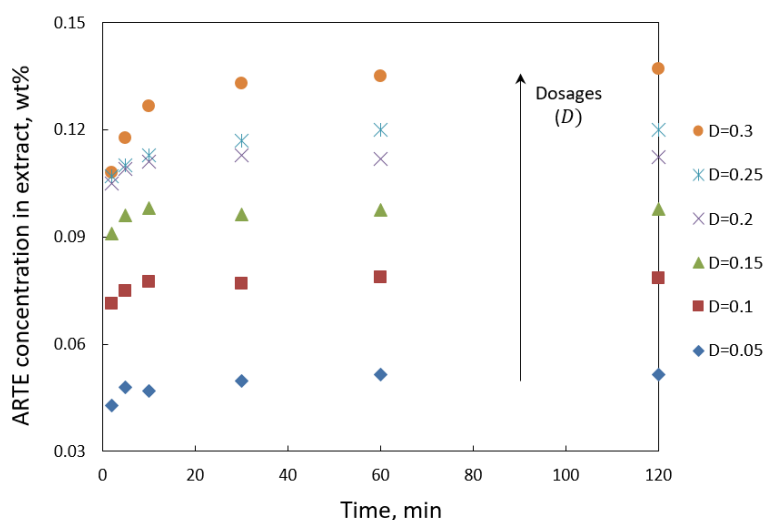


Figure 4.15. Kinetics of ARTE extraction in Toluene. *The experiments are carried out by a series of batch extraction processes. The masses of initial solvent are constant in all cases, only the initial masses of leaves are changed.*

In each single batch extraction, the samples are collected at varied interval time (2, 5, 10, 30, 60, 120, 180 minutes) and are analyzed by HPLC (section 4.1.2). The relation between ARTE concentration and the extraction time is shown in Figure 4.15.

In these experiments, the withdrawn masses of samples will definitely effect on the concentration of the entire extract amount, however, these sample amounts are relatively small and can be negligible.

The experimental data of ARTE extraction in Toluene shows that the ARTE concentration in extract increases when more leaves is supplied in a certain volume of solvent. Without analyzing the measured courses in depth it can be estimated from the results shown in Figure 4.15 that a time of 10 minutes is for all dosages a very conservative estimate for \bar{t} . It should be noticed that the increasing amount of ARTE in the extraction phase equals to the loss in the solid phase (Figure 3.1). Using eq. (2.45) from this estimated time a lower bound for the effective rate constant k_{ARTE}^{eff} can be calculated. A value of $k_{ARTE}^{eff} = 0.05 \text{ min}^{-1}$ results, which is instructive for designing processes using lower residence times than approximated 10 minutes.

By similar calculation, the equilibrium of ARTE extraction in Ethanol and n-Hexane solvent is reached after *30 minutes* and *60 minutes* respectively (*Appendix A10*). Additionally, the extraction of precursor DHAA is also investigated and it shows the identical kinetics data to ARTE (*Appendix A8*) in all three solvents, therefore, the upcoming experiments are simplified by targeting only ARTE.

5 Experimental study and evaluation of process variants

As mentioned, the production processes from plant materials are mostly based on the batch extraction. The drawbacks of single batch extraction (unsteady product quality, manpower requirements, high operating cost, low productivity) can be overcome by continuous operation. However, the existing continuous processes meet several difficulties and challenges as: the long extraction time of counter-current supercritical extraction, the counter-wise phase transportation, the scale up of production processes and so on. Therefore, development of a simple, easy-to-handle device is the priority task in this research project. The equipment design of continuous counter-current extraction is centralized in chapter 6 and the important parameters from batch experiments are needed.

Now, this chapter is going to present two main contents: (1) evaluation of batch extraction based on experimental results in chapter 5 and (2) a counter-current cascade of sequential equilibrated stages to validate the simulation results in chapter 3.

5.1 Evaluation of a simple batch extraction process

The experimental implementation of a single batch process based on ARTE extraction from *Artemisia annua L.* is taken out by following procedures:

- A defined amount of initial dried leaves m_s is in contact to a defined amount of solvent $m_{L,0}$.
- The mixture is agitated until equilibrium.
- The no solid containing extract is collected to the interfaces by a syringe and weighted.

The summarized depiction and phase separation of these procedures can be referred in Figure 2.6. A sample of the extract phase is analyzed by introduced HPLC method (section 4.1.2.1). The experimental procedures are repeated at different

solid-to-liquid ratios (dosage D in eq. (2.8)) and each separated batch process is carried out at identical cycle time t_{cycle} (eq. (5.1)) including extraction time and unavoidable dead time. For specific ARTE extraction, the extraction time $t_{extraction}$ and dead time t_{dead} are 15 minutes for each to ensure the efficient extraction.

On another hand, the extract composition at equilibrium can also be theoretically calculated based on eq. (2.41). The parameters of distribution coefficient β_{ARTE}^{eff} , initial ARTE amount in dried leaves, $m_{ARTE,R,0}$ and phase ratio χ_{ER} were experimentally determined in chapter 4. Therefore, a parallel data set of ARTE extraction in batch mode can be also described as below.

Table 5.1. Single batch extractions of ARTE in Toluene at equilibrium for different dosages. *The batch processes are validated if the extraction is long enough to reach equilibrium. All batch extraction processes are carried out at the identical total solvent masses (30 grams). The theoretical extract mass m_E^{Theo} is based on wetting parameter W (eq.(2.3) to determine the extract raffinate phase ratio χ_{ER}^{Theo} , thus, the extract composition $\chi_{ARTE,E}^{Theo}$ in eq. (2.41) is calculated.*

m_S [g]	$D^{(1)}$ [-]	$\chi_{ER}^{Theo(2)}$ [-]	Theory estimation		Experimental data	
			$m_E^{Theo(3)}$ [g]	$\chi_{ARTE,E}^{Theo(4)}$ [wt. %]	m_E^{exp} [g]	$\chi_{ARTE,E}^{exp}$ [wt. %]
1.5	0.05	5.46	26.6	0.050	26.1	0.053
3	0.1	2.38	23.3	0.082	22.5	0.08
4.5	0.15	1.36	19.9	0.104	19.4	0.099
6	0.2	0.85	16.5	0.120	16.1	0.113
7.5	0.25	0.54	13.1	0.132	12.8	0.128
9	0.3	0.33	9.8	0.141	9.8	0.14

(1) dosage from eq.(2.8); (2) phase ratio (eq.(2.13)); (3) extract mass; (4) ARTE concentration from eq. (2.41).

The experimental data of extract compositions $\chi_{ARTE,E}^{exp}$ and the extract masses m_E^{exp} are slightly smaller than the theory. The increasing of ARTE composition, when the dried leaves is increased in a certain volume of solvent, is trivial (Figure 5.1).

Furthermore, the batch extraction process is carried out in a defined volume which plays a role in estimating the productivity (eq. (3.86)). A determination of the relevant volume is necessary. It can be based on the treated amount of joint phases

corresponding to suspension volume $V_{suspension}$, free volume V_{free} or the real volumes of extractors $V_{extractor}$ (eq. (2.19)). However, the different structures of extractor types are complicated by varieties of geometrical characteristics, therefore, the characteristic volume to estimate the productivity is chosen as free volume V_{free} (eq. (2.20)) including the suspension and gas volumes with the assumed value of fraction θ is 0.1.

Additionally, every batch process requires time for preparing, product collecting and cleaning. This extra time can be called dead time t_{dead} and it can be neglected in continuous operation. The sum of the productive and unproductive periods is the cycle time:

$$t_{cycle} = t_{extraction} + t_{dead} \quad (5.1)$$

Therefore, the productivity of a single batch extraction for a specific study case of ARTE extraction based on eq. (3.86) holds:

$$Prod_{ARTE}^{Batch} = \frac{m_E * x_{ARTE,E}}{(t_{extraction} + t_{dead}) * (1 + \theta) V_{suspension}^{Batch}} \quad (5.2)$$

Within, the suspension volume $V_{suspension}^{Batch}$ is determined by total mass of phases and mixture densities (Table 4.5). It should be mentioned that the more leaves are added to a fixed solvent mass, the more solvent will be kept by solid matrices, then, the obtained amount of extract is reduced. Means, the total amount of ARTE in extract as product is declined. The trend can be observed in Figure 5.1.

Additionally, the recovery of ARTE comparing the obtained amount of ARTE in extract and that in initial dried leaves can be expressed for the batch extraction as:

$$Rec_{ARTE}^{Batch} = \frac{m_S * x_{ARTE,S,0} - m_R * x_{ARTE,R}}{m_S * x_{ARTE,S,0}} = \frac{m_E * x_{ARTE,E}}{m_S * x_{ARTE,S,0}} \times 100 \quad (5.3)$$

The initial amount of ARTE in leaves $m_{ARTE,S,0}$ is relied on the amount and quality of provided leaves at inlet and was determined by exhaustive technique in Table 4.3 ($x_{ARTE,S,0} = 1.3 \text{ wt. } \%$). The relation of obtained extract masses and ARTE composition, also productivity and recovery at different dosages are shown below.

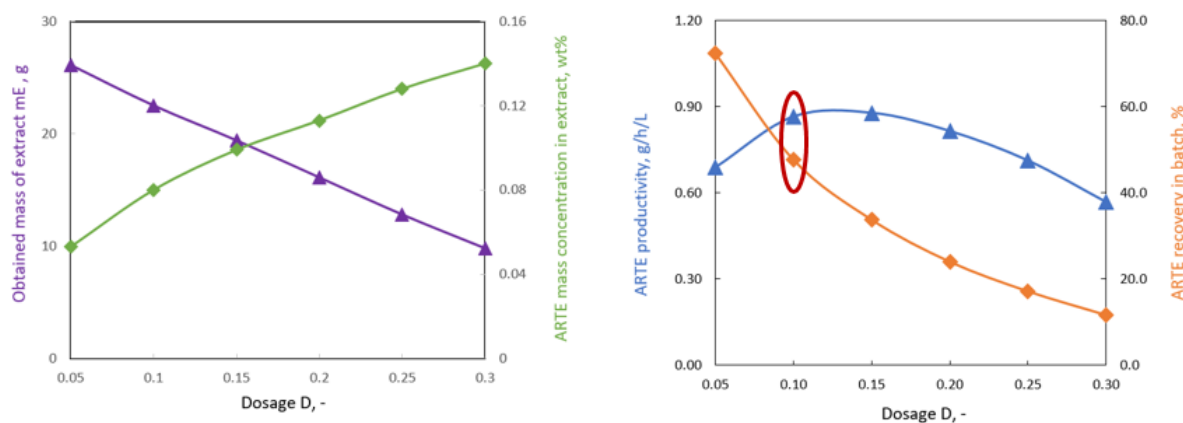


Figure 5.1. The relations of relevant parameters of single batch ARTE extraction in Toluene at different dosages. *Experimental conditions, analyzed concentration and productivity (eq.(5.2)), recovery (eq. (5.3)) data are summarized in Appendix A10.*

The productivity increases to a certain point and starts decreasing, meanwhile, the recovery keeps declining when the dosage increases. Therefore, the dosage D ($D = 0.1$) is chosen for the other extraction operations.

5.2 Counter-current sequential batch operation (equilibrium conditions)

In chapter 3, a counter-current model was introduced and mathematically explained to estimate the outgoing concentrations of extract and raffinate. This section is going to focus on validation of the model by a counter-current cascade of sequential equilibrated stage experimental setup. With the time larger than 15 minutes the extraction is long enough to reach equilibrium. The important parameters are taken from previous experimental investigations of ARTE extraction from *Artemisia annua* L. dried leaves (section 4.2).

5.2.1 Model-based prediction for ARTE extraction from *Artemisia annua* L. dried leaves

The introduced model in chapter 3 was successfully developed in dynamic and steady state/equilibrium aspects. The counter-current sequential equilibrium stage model assumes that every stage has identical dosages D ($D = 0.1$) (eq. (2.8)), each

stage is considered as a batch extractor and the extraction is carried out until equilibrium. The phase shifting processes are implemented in constant extract masses. The cascade is characterized by a system of N equations (eq. (3.74)) and it can be solved based on two important equations (eqs. (3.78), (3.79)) of Kremser method (detailed in *Appendix A2*) (*Code4*).

For the specific case of ARTE extraction from *Artemisia annua L.* dried leaves, the important parameters (kinetics, distribution coefficient, phase ratio) were provided based on the experimental results described in section 4.2 and summarized in Table 5.2 as input for simulation model.

Table 5.2. Input data for sequential counter-current equilibrium model in case of ARTE extraction from *Artemisia annua L.* in Toluene. A fixed dosage (3g leaves / 30g Toluene) was applied for all stages. (*) initial ARTE amount in dried leaves is determined via eq.(3.38) and Table 4.3, (**) distribution coefficient of ARTE, β_{ARTE}^{eff} in Toluene from experimental data (Figure 4.14). N number of stages Figure 3.13.

Input parameters	Notation	Value	Units
Mass of extract	m_E	23	g
Mass of raffinate	m_R	10	g
ARTE concentration in initial material *	q_{ARTE}^{in}	0.39	wt. %
ARTE concentration in fresh Toluene	c_{ARTE}^{in}	0	wt. %
Effective distribution coefficient **	β_{ARTE}^{eff}	0.4	-
Number of stages	N	5	-

An example of concentration development for the sequential counter-current equilibrium cascade with the given data in Table 5.2 is given below.

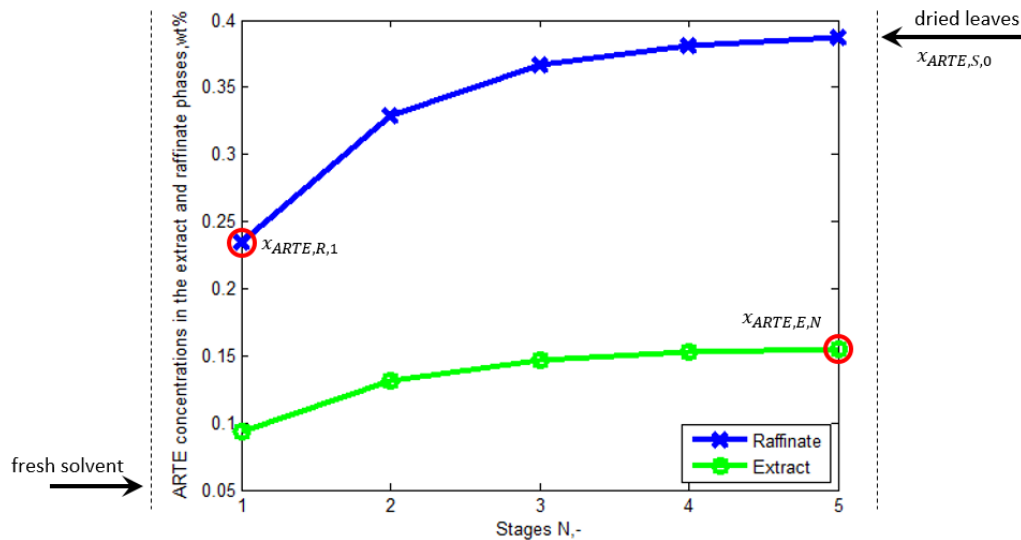


Figure 5.2. Concentration development of a sequential counter-current equilibrium stage cascade. Fresh solvent and dried leaves are fed in two opposite directions. Points present the equilibrated concentration of each stage and are calculated based on eqs. (3.80), (3.81). Two red-circled points $x_{ARTE,R,1}$, $x_{ARTE,E,N}$ presenting the outgoing ARTE concentrations are the most interested.

To validate the simulated results, an experimental setup is needed. However, the establishment of sequential counter-current experiment meets many difficulties as the counter-wise transportation of solid and liquid phases, specially, the preparation of the partly depleted raffinate for the first stage (stage 1) and the enriched extract for the last stage (stage N) (Figure 3.5).

An appropriate experimental setup to overcome these problems is given and described as below.

5.2.2 Experimental setup of sequential counter-current operation

The experiment is based on two main configurations:

- Using extra fresh solvent, called “make up” solvent, to compensate the absorbed solvent amount by material matrices.
- Using the preparation steps to establish the partly depleted leaves.

Each stage is considered as a single batch extractor, means, the material is in contact to the solvent and stirred until equilibrium before shifting the phases. The

solid-to-liquid ratio (dosage D (eq. (2.8)) and the transported masses of the extract and raffinate phase among stages are identical.

An example of 3-stage counter-current extraction is depicted below.

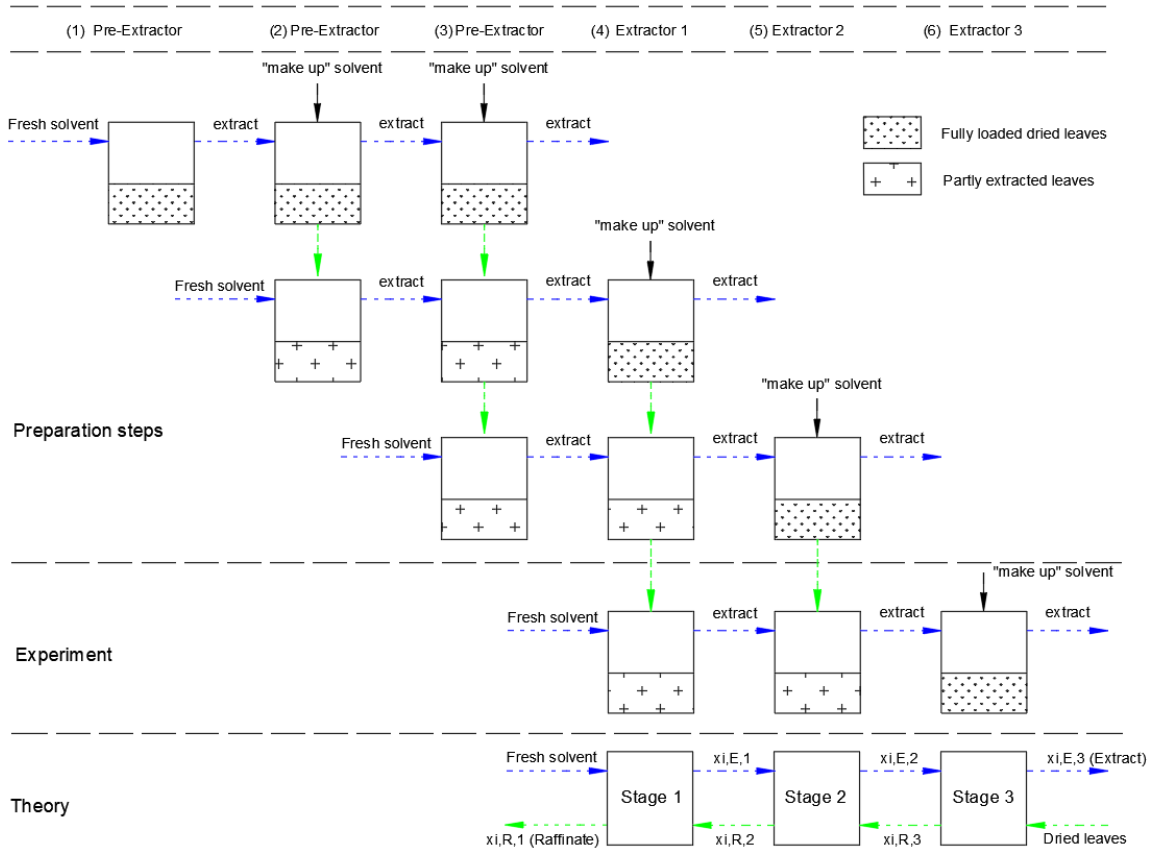


Figure 5.3. Experimental setup of sequential 3-stage counter-current extraction operation. The three pre-extractors are filled by dried leaves. The green dotted arrows present the transported steps, in which the raffinate is remained in the extractor. The blue dotted arrows show the shifting of extract phase.

The details and experimental procedures are given in *Appendix A11* and the working conditions are given in Table 5.3.

Table 5.3. Experimental conditions of sequential counter-current equilibrium stage extraction. Each extractor is considered as a single batch extractor and has the identical dosage $D = 0.1$ (as discussed in batch extraction (Figure 5.1)).

Mass of dried leaves, g	3	Residence time, min	15
Mass of Toluene, g	30	Preparation time, min	5
Agitation speed, rpm	300	Collecting and cleaning time, min	10
Temperature, $^{\circ}C$	25	Suspension volume, mL	40

The optimized dosage ($D = 0.1$) from single batch process (Figure 5.1) is applied for all stages. The wetting parameter W is 2.25 for Toluene (Figure 4.12), means, the transferred extract and raffinate phase are 23 grams and 10 grams respectively. Then, the “make-up” solvent amount is 7 grams.

The extract compositions are analyzed by introduced HPLC method (section 4.1.2.1).

This experimental setup is applied for 2, 3 and 5-stage counter-current operation. The compositions at two ends of 5-stage counter-current cascade are compared to the simulated results (Figure 1.3).

Table 5.4. The simulated and experimental data of outgoing ARTE concentrations in sequential counter-current equilibrium extraction. *The 5-stage counter-current cascade is chosen and only outgoing concentrations are interested.*

	Simulated results	Experimental results
Extract $x_{ARTE,E,5}$ (wt. %)	0.155	0.14
Raffinate $x_{ARTE,R,1}$ (wt. %)	0.235	0.0225

The using of “make up” fresh solvent causes the dilution of the extract liquid. The interested extract concentrations at the outlet $x_{ARTE,E,5}$ show an acceptable agreement between simulation and experiment.

Table 5.5. Experimental results of multi-stage counter-current sequential batch extraction.

Number of stages N	Outlet concentration $x_{ARTE,E,N}$ [wt. %]	t_{cycle} [h]	Volume [L]	$Prod_{ARTE,real}^{Multi}$ [g/h/L]	Rec_{ARTE}^{Multi} [%]
2-stage	0.115	0.5	0.04	1.32	67
3-stage	0.124	0.5	0.04	1.43	73
5-stage	0.14	0.5	0.04	1.61	82

The productivity and recovery are estimated based on experimental data of extract concentration at the outlet via eqs. (3.86), (3.88) as:

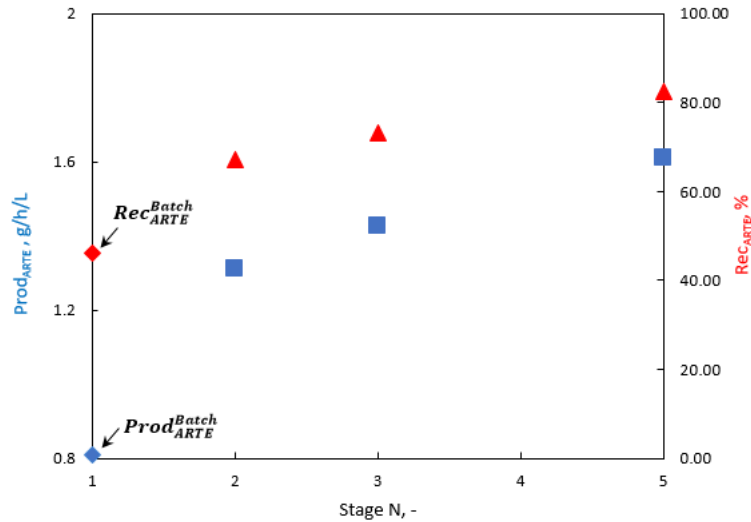


Figure 5.4. Productivity and recovery of ARTE in batch and multi-stage counter-current extraction operations. *Input parameters of each stage: $m_S = 3 \text{ g}$; $m_L = 30 \text{ g}$; $m_E = 23 \text{ g}$; $\beta_{ARTE}^{eff} = 0.4$. The productivity and recovery are calculated based on corresponding volume $V_{suspension} = 0.04 \text{ L}$ and cycle time $t_{cycle} = 0.5 \text{ h}$. The outcomes of the batch extraction at identical working conditions are also presented.*

The blue and red-colored points show the productivities and recoveries respectively. It is obvious that when the number of stages N is increased, the ARTE concentration at the final stage $x_{ARTE,E,N}$ is higher (*Appendix A11*). Both productivity and recovery are much improved compared to the batch operation.

Nevertheless, the sequential counter-current stage cascade cannot avoid the dead time because each stage is implemented as a single batch extractor. Chapter 6 will present a continuous extraction process with a self-developed counter-current extractor to illustrate the advantage of the continuous counter-current operation.

6 Continuous counter-current steady state extraction

Since last decades, the continuous solid liquid extraction (SLE) has been applied in producing a variety of products, e.g. the extraction of vegetable oil, oil extraction from soybeans, sugar from beet/cane or high-valuable metals from minerals and so on, however, there are still many mechanical problems. Besides, comparing with other unit operations such as liquid-liquid extraction, limited attention has been given in the literature to the design of solid liquid extractors. Recently, the counter-current supercritical fluid extraction has drawn the attention to extract high-valued components used in pharmaceutical productions. This technique shows a big advantage of avoiding the separation of extract and solid material but it still came up with some drawbacks, e.g. CO₂ behaves as a non-polar solvent, therefore, the polar components will be hardly extracted; the high operating and investing costs. In the near future, with rising energy prices and an increasing scale of operation based on market demand, it can be expected that a more accurate design of the extractors will be necessary [135].

Based on the predominance of less solvent consumption, consistent product quality, highly concentrated extract, the counter-current continuous extraction is in focus tending to improve the overall efficiency of the entire extraction processes. Additionally, the typical screw-based equipment shows the advantages of its operating, simplicity, mobility, therefore, this research focuses on a screw-based structure to develop and improve the efficiency of natural product extraction.

This chapter consists of three main sections: (1) design process: from idea, conceptual design, engineering design, safety concern; (2) preliminary experiment for instrument calibration and residence time investigation and (3) continuous laboratory-scale experiments at steady state condition. The evaluation is also concerned.

6.1 Design of a continuous counter-current extractor

6.1.1 Idea and conceptual design

Generally, the procedure of design process initially proposes a conceptual design which is derived from an idea and will lead, if thermodynamically feasible, to experimental verification by operation of a mini plant. Obviously, statistical design of experiments combined with model parameter determination for rigorous (physical-chemical) models are the efficient way [136, 137]. The improvement of the conceptual design is contributed by interactive processes of different parameters with repeated steps to finalize the plant.

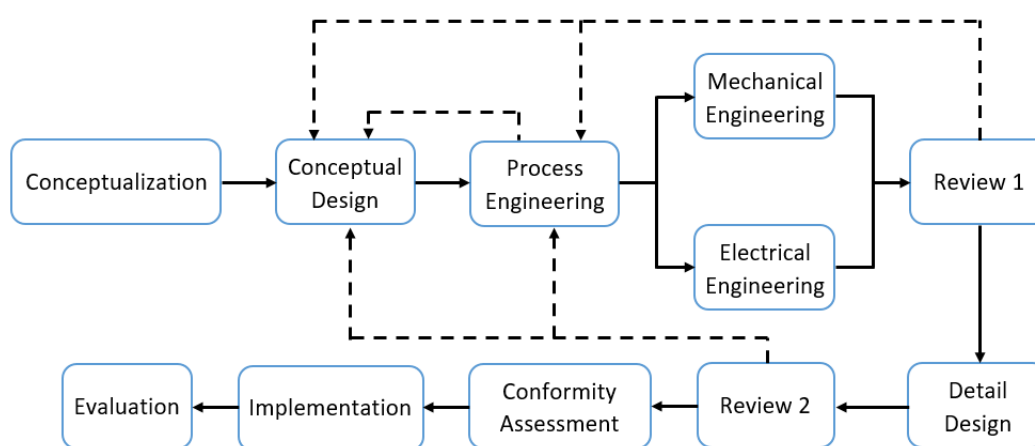


Figure 6.1. Outline of the conceptual design process of continuous extractor. *The review 1 is basically carried out in-house and the review 2 is assessed by external experts.*

As mentioned above, the principle of screw-based extractor is extensively used in SLE for chemical, biological and wood species valorization because of their simple mechanical configuration and reliable exploitation availability. But there are still some shortcomings of current screw extractor on market as: inclination dependence of flow speed of phases, the contacting time control difficulties or a high demand of energy for downstream process to recover the solvent and so on. Therefore, the brainstorm started with the understanding that the counter-current operation requires less solvent consumption and gives high-concentrated extract. Additionally, the mechanical screw-based structure enables solid and liquid phase to intensively contact. Besides, if it is possible, the probabilities of reduction of the waste to

environment and the phase separation of equipment are highly attractive for maximizing the performance. The combination of mechanical and electrical works enables to find the proper solutions for associated parts, e. g: flexible connects between product and waste container, the proper angle of feeding funnel to avoid the channeling, funnel flow; flange joints; the positions of sensors; the production control via electrical devices and so on (Review 1-Figure 6.1). Additionally, the extraction is performed with chemical solvents, therefore, the explosion protection strategies and solution ensure the safety production. Final assessments of in-house and outside experts (Review 2-Figure 6.1) are required to evaluate the risks and to finalize the regulation and procedure for production feasibility.

As a consequence, a typical screw-based structure is chosen based on the advantages of flexible installation, ability of contacting time control, robustness, availability of double jacket housing to work at high temperature. However, the normal screw conveyor works in an inclination base which makes the contacting time control of two phases difficult. Thus, a perforated disk at one end overcomes this problem by establishing a compressed segment to orient the solvent flow. (Figure 6.2).

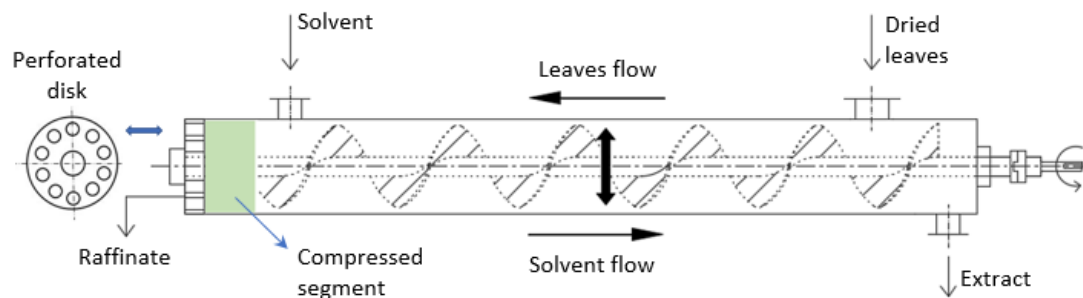


Figure 6.2. Conceptual design of continuous counter-current extractor using a screw type of apparatus. *The conceptual development is relied on the observation, feasibility and manipulation of prototype devices. The compressed segment established by a perforated disk forces the solvent to flow in one direction.*

The material as dried leaves are fed from one side of the extractor, then, are transported through the extractor by the screw. The friction between the wet leaves and the disk surface establishes a compressed segment which blocks the solvent stream and forces the solvent to flow in opposite direction, thus, the counter-current

concept is formed. It is noticed that the size of compressed segment remains constant to avoid blockage the solvent inlet during the steady state run.

6.1.2 Engineering design and dimension estimation

This process is based on material availability and specific identification, in which the improvement of process is assisted by a computer program (AutoCAD). The important parameters achieved by the batch extraction investigations are provided for calculation as follows.

- Solvent in use: Toluene
- The estimated dried leaves: $\dot{m}_S = 1.6 \text{ g/min}$ (availability of leaves source)
- Effective distribution coefficient: $\beta_{ARTE}^{eff} = 0.4$ (Figure 4.14)
- Wetting parameter for Toluene: $W = 2.25$ (Figure 4.12)
- Mass fraction of ARTE in initial dried leaves: $x_{ARTE,S,0} = 0.013$ (Table 4.3)

6.1.2.1 Screw and extractor dimension calculation

The calculation of counter-current screw-based extractor dimension is similar to a conveyor design procedure including these steps: establishing conveying requirements, identifying material, determining conveying capacity, conveyor size and speed [138, 139]. For the specific calculation of counter-current extractor, the residence time is chosen to estimate the dimension of the equipment. It is helpful to assume that the residence time of leaves and solvent inside the extractor are identical: $\bar{t}_L = \bar{t}_S = \bar{t}$. The following calculation procedures below allows estimating the geometrical dimension of the extractor.

Liquid flowrate

The fresh solvent at the inlet is assumed ($x_{ARTE,L,0} = 0$), thus, the component mass balance for continuous extraction holds:

$$\dot{m}_S * x_{ARTE,S,0} = \left(\dot{m}_E + \frac{x_{ARTE,R}}{x_{ARTE,E}} * \dot{m}_R \right) * x_{ARTE,E} \quad (6.1)$$

Substituting the distribution coefficient at equilibrium β_{ARTE}^{eff} in eq. (2.28) and mass balance in eq. (2.7) into eq. (6.1) gives:

$$\dot{m}_S * x_{ARTE,S,0} = \left[\dot{m}_{L,0} + \dot{m}_{S,0} - \left(1 - \frac{1}{\beta_{ARTE}^{eff}} \right) * \dot{m}_R \right] * x_{ARTE,E} \quad (6.2)$$

and \dot{m}_R can be obtained via wetting parameter W (eq. (2.3)) as:

$$\dot{m}_R = \dot{m}_S + \dot{m}_{L_{int}} = (1 + W) * \dot{m}_S \quad (6.3)$$

Substituting eq. (6.3) into eq. (6.2) holds:

$$\dot{m}_S * x_{ARTE,S,0} = \left[\dot{m}_{L,0} + \left[1 - \left(1 - \frac{1}{\beta_{ARTE}^{eff}} \right) * (1 + W) \right] * \dot{m}_S \right] * x_{ARTE,E} \quad (6.4)$$

or:

$$\dot{m}_{L,0} = \frac{\dot{m}_S * x_{ARTE,S,0}}{x_{ARTE,E}} - \left[1 - \left(1 - \frac{1}{\beta_{ARTE}^{eff}} \right) * (1 + W) \right] * \dot{m}_S \quad (6.5)$$

Now, the mass fraction of ARTE in the extract phase at the outlet $x_{ARTE,E}$ can be assumed at 0.001 (corresponding dosage $D = 0.1$). Then, mass flowrate of solvent phase $\dot{m}_{L,0}$ at the inlet is 11.4 g/min.

Screw and extractor dimension

The typical specifications of a screw can be described below.

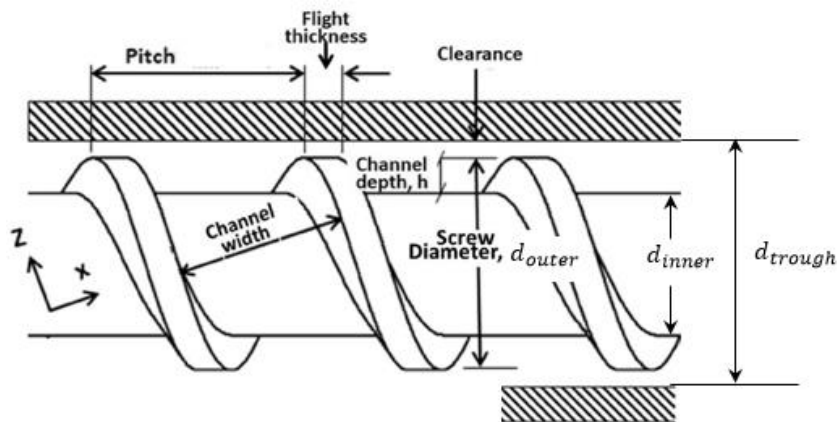


Figure 6.3. Typical geometrical parameters of a screw.

For the specific case of ARTE extraction from *Artemisia annua L.* leaves, several selections and assumptions for screw [140, 141] are given:

- Equipment contains three phases, extract, raffinate and gas, thus, the state of transportation is *very free flowing* with very less abrasion.
- Dried leaves are mixed with solvents and the mixture creates a state like “suspension”, the ribbon or cut types are not the choice because of decreasing conveying efficiency, therefore, the appropriate *screw flight* is *standard type*.
- *Screw pitch S [m]* is selected as *standard* equaling to diameter of screw d_{outer} [m].
- The assumed rotational speed n is 1 [rpm].
- The device is horizontal setup, thus, inclination $K[-]$ is 1.
- The trough is fully filled, means, trough loading $\psi[-]$ is 1.

The capacity of a screw conveyor \dot{Q} holds:

$$\dot{Q} = \frac{\pi}{4} d_{outer}^2 * S * n * 60 * \rho_{mixture} * \psi * K \quad [kg/h] \quad (6.6)$$

Applying given parameters above ($\dot{m}_S = 0.096 \frac{kg}{h}$, $\rho_{mixture} = 830 \frac{kg}{m^3}$ (Table 5.5), $\dot{m}_{L,0} = 0.684 kg/h$) into eq. (6.6), the outer diameter of screw is: $d_{outer} = 27 mm$.

Additionally, the clearance of 1 millimeter was provided to support the flow of solvent, therefore, the inner diameter of the trough is: $d_{trough} = 30 mm$.

The ratio of screw and shaft diameter can be briefly estimated based on the catalog and standards [139, 142] and it can be assumed at 0.4 to ensure the constant clearance for the entire screw length. Then, the shaft diameter is: $d_{inner} = 14 mm$.

On another hand, the solvent residence time \bar{t}_L in a certain volume of extractor can be calculated via free volume V_{free} (eq. (2.20)) and void fraction ε_L^* (eq. (2.21)) as:

$$\bar{t}_L = \bar{t} = \frac{V_L}{\dot{V}_L} = \frac{V_{free} * \varepsilon_L^*}{\dot{V}_L} \quad (6.7)$$

and residence time of leaves \bar{t}_S is determined as:

$$\bar{t}_S = \bar{t} = \frac{V_S}{\dot{V}_S} = \frac{V_{free} * (1 - \varepsilon_L^*)}{\dot{V}_S} \quad (6.8)$$

Then,

$$V_{free} = (\dot{V}_S + \dot{V}_L) * \bar{t} = \left(\frac{\dot{m}_S}{\rho_S} + \frac{\dot{m}_L}{\rho_L} \right) * \bar{t} \quad (6.9)$$

We can assume the residence time of both phases \bar{t} is 10 minutes, the densities are from Table 4.3 and Table 4.4, the solvent and leaves flowrates $\dot{m}_{L,0}$, \dot{m}_S are assumed and calculated above. Then, the free volume V_{free} of the extractor holds:

$$V_{free} = \left(\frac{\dot{m}_S}{\rho_{leaves}} + \frac{\dot{m}_{L,0}}{\rho_{solvent}} \right) * t = 0.198 [L] \quad (6.10)$$

This free volume can also be geometrically calculated by neglecting the volume of screw flights as:

$$V_{free} = \frac{\pi}{4} (d_{trough}^2 - d_{inner}^2) * L \quad (6.11)$$

Then,

$$L = \frac{0.198 * 10^{-3} * 4}{\pi * (d_{trough}^2 - d_{inner}^2)} = 0.36 m \quad (6.12)$$

The estimated dimensions are applied to manufacture a prototype extractor, however, it shows a limitation of residence time, therefore, the extractor is double-length manufactured to work in a broader range (Figure 6.4). The detail of technical drawings is attached in *Appendix A12*.

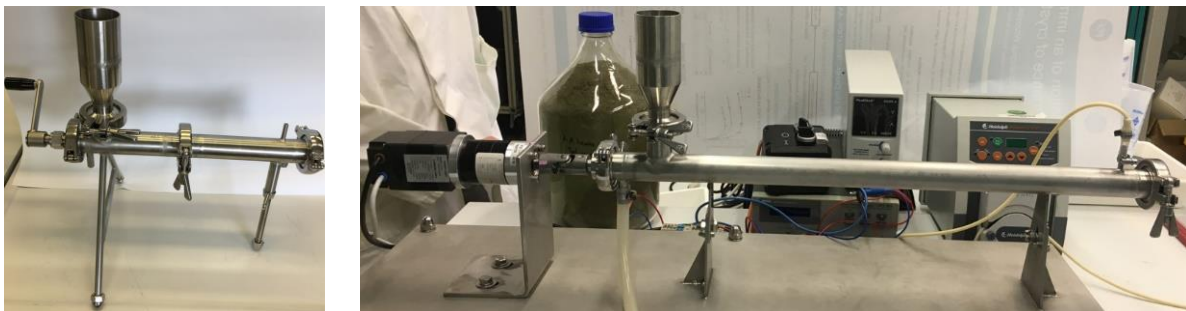


Figure 6.4. The prototype and the main extractor. *Left:* the prototype extractor with manual feeding; *Right:* the main extractor. The free volume of extractor V_{free} is 0.4 Liter and the extractor volume $V_{Extractor}$ is 0.45 Liter.

6.1.2.2 Instrument selection

Motor selection

In this extraction plant setup, there are two motors which are applied for the main extractor and feeding screw. Choosing the motor is often a complicated process. The working environment, required rotational speed, the torque, are depended on the power source, specification, performance and environment of motors. There are many different types of motor as: universal (UM), permanent magnet DC (PMDC), AC induction and brushless DC motor. The process requires that the speed is adjustable and the rotating direction can be reversed, thus, a brushless DC motor is chosen (*Appendix A13*).

Pump

A P4.1S HPLC pump integrated a 50 mL pump head from Knauer is used to supply the solvent for the extractor. The calibration procedures of pump are present in (*Appendix A18*).

Scales

Two scales (Mettler Toledo ML6002T with $d=0.01$ g and max 6200 g) are in use to quantify the extract and raffinate masses.

Furthermore, when we work in high danger environment with chemical substances, the entire system should be prevented from explosive dangers. Therefore, safety solutions for explosion protection are compulsory.

6.1.2.3 Explosion protection

This is a time-consuming process, special for a new installation plant. Risk assessment is carried out based on the technical drawings of entire plant. The high-risk positions and many danger possibilities, e.g: the break of container, the leaking of solvent, the appearance of ignition source, are often in focus. The solutions are finalized by the experts from in-house and outside before the releasing the official certification. The entire process is described in *Appendix A14*.

6.1.2.4 Assembling and electrical installation

The nitrogen is applied to avoid explosion. A system of pipelines is built up and a switch cabinet is constructed to control relevant devices and equipment automatically (Appendix A15). The complete flowsheet of the production pilot plant with all relevant devices, pipeline, valve system, detectors is sketched in Figure 6.5.

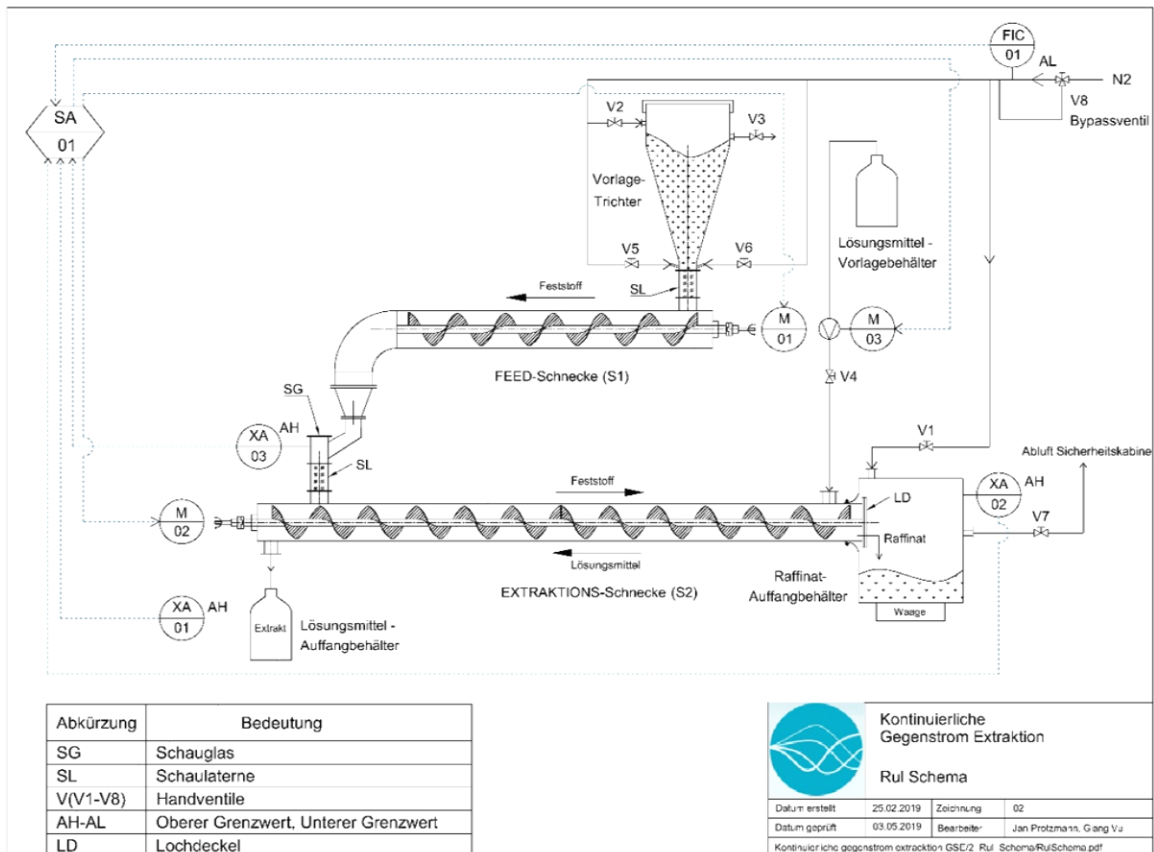


Figure 6.5. The flowsheet of continuous counter-current extraction plant.

The detail of suppliers and manufacturing company are listed in *Appendix A16*.

A 123-page operating manual technical documentation cooperated with engineering office Jürgen Bialek (Halsbrücker Str.34; 09599 Freiberg) is finalized and released.

After assembling the pilot plant, the experiments are implemented as following procedures: (1) calibrating the equipment and devices (screw feeder, screw of the extractor, pump); (2) analyzing the residence time distribution and (3) verifying of steady state conditions and operating the continuous steady state runs.

6.2 Preliminary investigations of continuous extraction process

For the constructed continuous extractor, it is necessary to control the working parameters (e.g. solvent flowrate, dried leaves flowrate, rotational speed of screws). The measurements of these procedures are summarized as below.

- The leaves flowrate is controlled by the screw speed, however, the screw speed is related to the electrical power (voltage). Thus, two successive measurement procedures are carried out. The experimental procedures and results are given (*Appendix A17*).
- The solvent flowrate \dot{m}_L is controlled by the pump speed and can be measured by weighting the solvent masses over time (*Appendix A18*).

After calibration processes, the main investigations are divided into two main parts: (1) the residence time distributions (RTD) investigation and (2) the steady state inspection for continuous operation. The evaluation of continuous production is also concerned.

Furthermore, due to the plant material availability, geometrical dimensions of extractor, the following parameter space is considered.

Table 6.1. Parameter space of investigation.

Parameters	Symbol	Units	From	To
Leaves flowrate	$\dot{m}_{S,0}$	<i>g/h</i>	0	150
Solvent flowrate	$\dot{m}_{L,0}$	<i>L/h</i>	0	1.5
Rotational speed	n	<i>rpm</i>	0	3

6.2.1 Residence time of leaves

The residence time distributions of solvent and leaves are very important. A part of the RTD investigation was reported and published in master thesis [143] of master student Christoph Krieger. My contribution was on consulting, experimental method, simulation model of process. The theoretical calculations of residence time were

introduced in section 2.2.5 and these calculations are going to be further applied in this section.

The selection of a suitable tracer was carried out by testing glass beads in different size ranges from 0.75 to 3.45 mm. The results showed that the glass beads (certificate in *Appendix A19*) in the range (0.75-1) mm are the most suitable tracer because it shows the identical residence time of the leaves [143].

The main investigations of leaves residence time are divided into two cases: (1) only leaves in empty trough; (2) the mixture of leaves and glass beads in filled trough. The measuring method is based on weighing the mass of tracer fractions in fixed time intervals which are sieved after collecting (Figure 6.6).

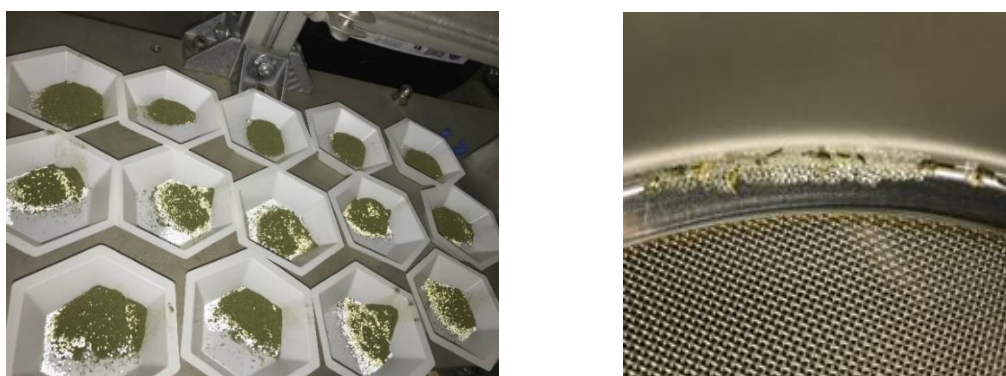


Figure 6.6. Glass beads as tracers in residence time investigation. *Left:* Mixture of glass beads and leaves; *Right:* Glass beads after sieving.

The experimental procedures are described in *Appendix A20*.

➤ **RTD analysis for leaves in unfilled extractor**

The measurement is taken out at different speed (1.8-2.2 rpm) and data are given in *Appendix A20*. Below shows a sample of a data set at speed 1.8 rpm.

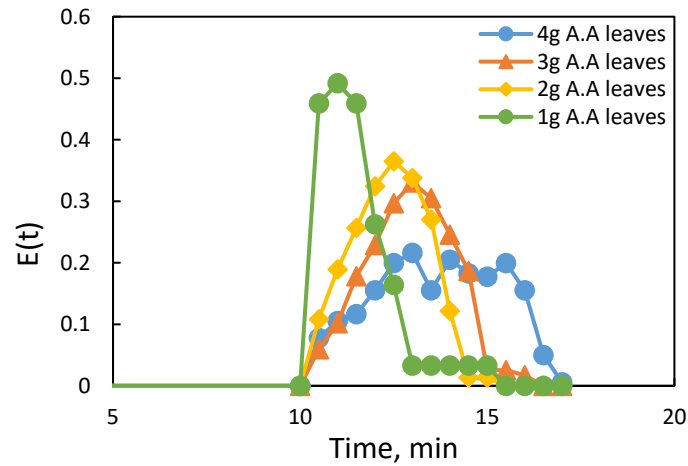


Figure 6.7. The distributions in empty extractor of different leaves amounts (1-4 g) at speed $n = 1.8 \text{ rpm}$. The masses are weighed at the outlet in 30-second time interval. Each point on the curves corresponds to a leaves mass in one fraction.

The clearance change along the extractor might cause the tails of the peaks. The mean residence time for the empty extractor is calculated and summarized below.

Table 6.2. Mean residence time of leaves in empty extractor at different speed. The parameters as mean residence time \bar{t}_S , dimensionless variance σ_n^2 and number of stages are calculated by the introduced eqs. (2.51), (2.54) and (2.57) respectively.

$n_{\text{Extractor}}$ [rpm]	m_S [g]	\bar{t}_S [min] \pm σ [min]	σ_n^2 (-)	$\omega_{1/2}$	N_{leaves}
1	2.1	21.1 \pm 2.36	0.012	5.54	81
1	3.08	22.07 \pm 2.7	0.015	6.33	68
1	4.17	23.8 \pm 3.06	0.017	7.18	61
1	5.42	24.3 \pm 3.26	0.018	7.65	56
1.8	1	11.5 \pm 0.98	0.0072	2.11	181
1.8	2	12.38 \pm 0.98	0.0063	2.31	159
1.8	3	12.92 \pm 1.14	0.0078	2.69	128
1.8	4	13.62 \pm 1.63	0.014	3.83	70
2.2	1	10.4 \pm 0.76	0.0054	1.8	184
2.2	2	10.88 \pm 0.88	0.0066	2.08	152
2.2	3	11.55 \pm 1.05	0.0083	2.47	121
2.2	4	11.99 \pm 1.25	0.011	2.95	92

The residence time \bar{t}_S is strongly depended on the speed (e.g. it takes 22 minutes to transport the leaves from inlet to outlet at 1 rpm, around 12 minutes at speed 1.8 rpm and 10 minutes at 2.2 rpm). Additionally, the higher amount of leaves is provided in one chamber, the mean residence time \bar{t}_S is slightly increased. This phenomenon comes from the fill grade of the leaves, when the leaves amount in one chamber is higher, the particles closed to the sharp are pushed forward slower than those near the trough [143]. As a consequence, it broadens the distribution and leads to a decreasing of the number of stages N_{leaves} (Table 6.2). The inspection of leaves residence time in empty extruder is necessary, however, the residence time of leaves in continuous operation is in interest.

➤ **RTD of leaves in filled extractor**

The difference between empty and filled extractor lies in the fact that, the leaves in one chamber are also interacted and blocked by those in the rear and front chamber in fulfilled operation, thus, they are not able to flow easily as those in empty operation.

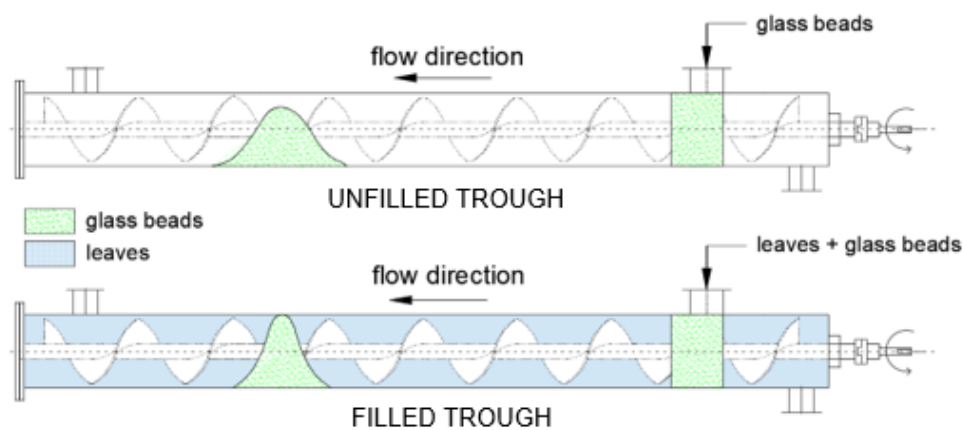


Figure 6.8. Illustration of leaves distribution in empty and fulfilled operation mode.

The experimental setup is similar to previous empty extractor, only several operating conditions are regulated as: the leaves are continuously provided for the entire run, the glass beads with identical volume of leaves in one chamber are added in a transient time and the fractions are sieved to obtain glass beads.

The data analysis is repeated as above with relevant calculation steps. Figure 6.9 presents an example of recorded data at speed 1.8 rpm for four different leaves mass flowrates in the fulfilled extruder.

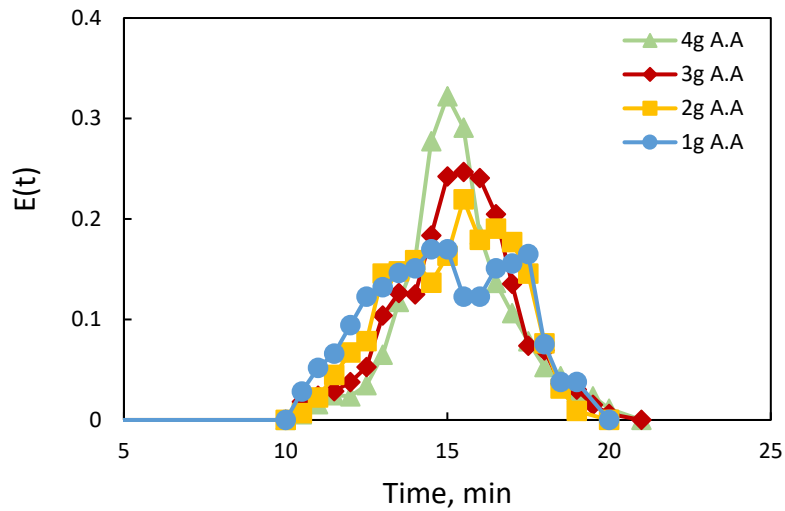


Figure 6.9. The distributions in filled extractor of different leaves amounts (1-4 g) at speed $n = 1.8$ rpm. Mass fractions of glass beads measured at the outlet in 30-second time intervals.

The measured data are in *Appendix A20.3*. And the Table 6.3 summarizes the results.

Table 6.3. Mean residence time of leaves \bar{t}_s in filled extractor at different speeds.

$n_{\text{Extractor}}$ [rpm]	\dot{m}_s [g/min]	m_{tracer} [g]	\bar{t}_s [min] \pm σ [min]	σ_n^2 [-]	$\omega_{1/2}$	N_{leaves} [-]
1	2.1	5.63	28 \pm 4.1	0.021	9.63	47
1	3	12.1	28.1 \pm 1.81	0.0041	4.27	240
1.8	1	5	14.88 \pm 2.1	0.0197	4.91	51
1.8	2	10	15.12 \pm 1.83	0.014	4.3	69
1.8	3	15	15.27 \pm 1.77	0.0134	4.1	75
1.8	4	20	15.3 \pm 1.63	0.0114	3.85	88
2.2	1	5.1	12.26 \pm 1.65	0.0182	3.9	55
2.2	2	9.7	12.83 \pm 1.52	0.0141	3.58	71
2.2	3	15	13.53 \pm 1.48	0.0121	3.5	83
2.2	4	19.7	13.97 \pm 1.47	0.0111	3.47	90

The identical behavior of the residence time \bar{t}_s in filled trough is realized when the leaves amount in one chamber is increased. However, the leaves in filled trough stay longer than those in empty one (e.g. at 1 rpm, leaves stay 6 minutes longer in filled trough than in empty one) (Table 6.2 and Table 6.3). Additionally, the width at half-height of the peak in filled trough is smaller than that in empty one, thus, the number of stages N_{leaves} is smaller than that in unfilled trough.

6.2.2 Residence time of solvent

In this experiment, water is used as solvent because of safety reason and the sodium chloride solution (*Appendix A21*) is chosen as the tracer. The conductivity is detected by a FiveEasy conductivity meter (*Appendix A22*). The conductivity is denoted by Greek symbol κ (kappa) and has the unit Siemens per centimeter (S/cm). The conductivity is used to estimate the residence time based on probability and cumulative functions (section 2.2.5). A calibration process is carried out and given in *Appendix A23*. The experimental setup is carried out as below.

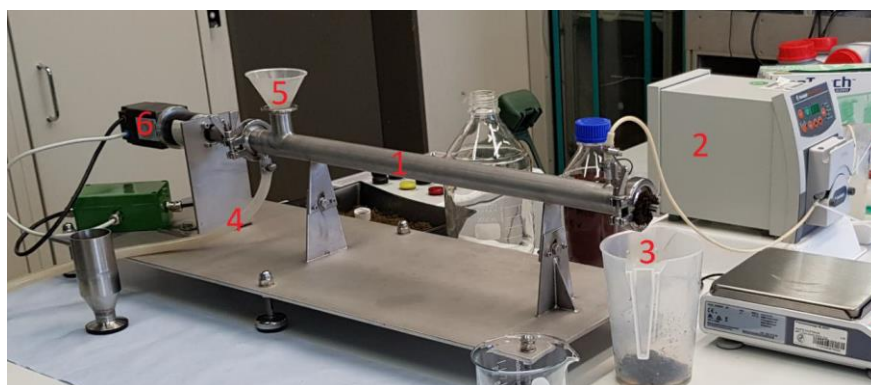


Figure 6.10. Experimental setup of solvent residence time investigation.
1- Extractor; 2- Solvent pump; 3- Outlet of wet leaves/perforated disk; 4- Outlet of extract;
5- Inlet of leaves; 6- Motor.

For all experiments, mass flowrate of leaves is kept at 1 g/min and diameter of perforated disk is fixed at 5.5 mm, the solvent flowrate is adjusted with four different flowrates in the range (0.43-1.21) L/h and three different speeds n in the range from (1-1.5) rpm. The water is used as solvent and a 1 Liter of 10% NaCl solution as tracer is prepared.

The leaves are transported from inlet **5** to the perforated disk **3**. When all the holes on disk are filled, the water is pumped in by pump **2**, the compressed segment is established. At steady state condition, the water source is changed to NaCl solution. The samples at outlet are collected in a time interval (Figure 6.11) and they are analyzed by FiveEasy conductivity meter and the NaCl content of each fraction is revealed based on the calibration curve (*Appendix A23*). The extractor is carefully rinsed several times to avoid corrosion of later runs.

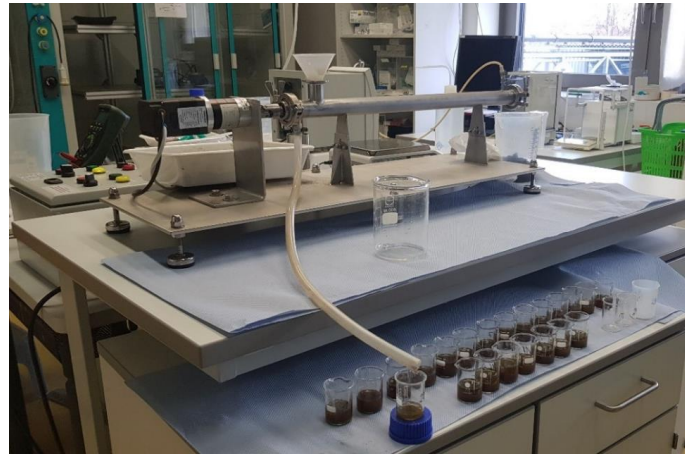


Figure 6.11. The collection of fractions in solvent residence time investigation.

The relevant parameters as mean values, standard deviation for each measure are calculated based on equations in section 2.2.5. An example of recorded data and calculated factors is given in *Appendix A24*. The mean residence time in different rotational speed and solvent flowrate is summarized below.

Table 6.4. The dependence of solvent mean residence time \bar{t}_L on speed and solvent flowrate. *The setup values of \dot{V}_L and n are taken from calibration data in Appendix A17, A18.*

\dot{V}_L [L/h]	n [rpm]		
	1	1.25	1.5
0.43	26.16	27.6	28.4
0.83	13.08	14.08	13.72
1.05	10.69	11.75	12.49
1.21	9.91	10.3	10.56

The data above show that the mean residence time of solvent \bar{t}_L is slightly influenced by the screw rotational speed and is significantly influenced by the solvent flowrates. It can be described as below.

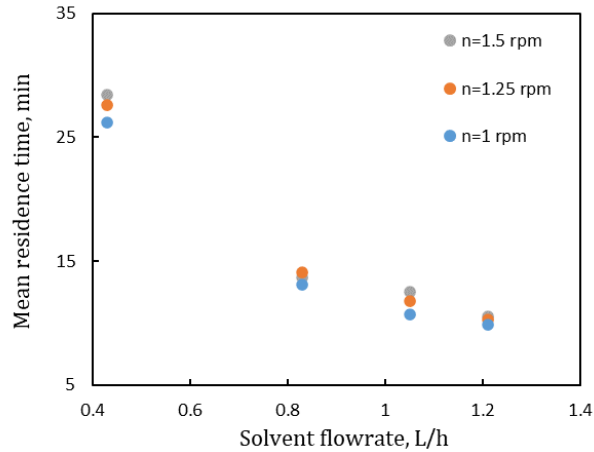


Figure 6.12. The dependence of solvent mean residence time on solvent flowrate and speed. *The plotted data are extracted from Table 6.4.*

The residence time is significantly enhanced when the solvent flowrate is lower than 0.8 L/h. The alternation of screw speed does not show much effect on the residence time of solvent. This phenomenon can be explained by the appearance of the clearance between the screw and trough which helps the solvent flows freely.

To characterize the mixing effect, the introduced Bodenstein number (eq. (2.56)) is taken into account and resulted as:

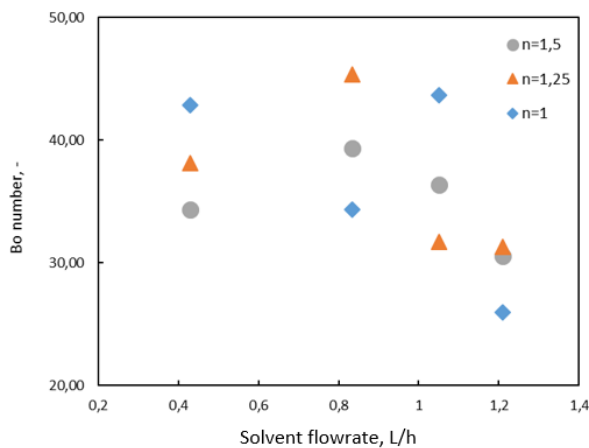


Figure 6.13. Bodenstein (Bo) number of solvent phase in dependence on solvent flowrate and speed.

The Bo number is scattered in the range from 25 to 46. The Bo number tends to decrease when the solvent flowrate increases. A significant effect of the speed on the variance or Bodenstein number is not able to be seen. Besides, Pippel [127] also describes the residence time on the helical reactor, it shows that increasing speed always causes greater axial mixing. In this study, the relatively small speed variation might be the reason for recognizing the effects, thus, the influence of the screw speed on the dispersion of the liquid phase in the extractor is negligible.

Furthermore, the study case of mixture of leaves and solvent is very difficult to operate in the real extractor because the extractor is working with explosive solvent (Toluene). This drawback is overcome by another research project which is being parallel implemented by a doctoral student, Mrs. Lehr at Institute of Fluid Dynamics and Thermodynamics, Otto von Guericke University Magdeburg. In this parallel research project, the extractor is duplicated with a transparent material, this research intensively focuses on the simulation of phase distribution inside the extractor. The influence of residence time, phase distribution, pressure on the efficiency of the extraction process can be more exploited. A part of results was recently published [59]. Below is the transparent extractor in investigation.

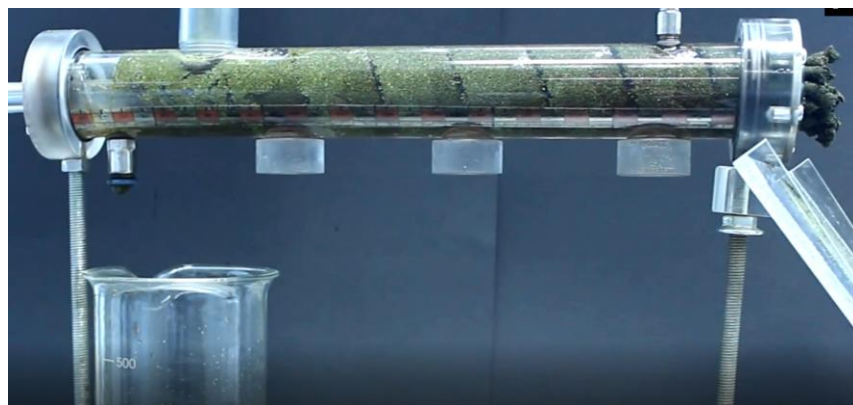


Figure 6.14. The transparent extractor. *Photo of a second transparent extractor to investigate the influence of residence time, phase distribution and pressure (provided by PhD student Annemarie Lehr, Institute of Fluid Dynamics and Thermodynamics, Otto von Guericke University Magdeburg, who constructed it for her detailed RTD studies).*

6.3 Continuous counter-current extraction experiments

The previous experiments of multi-stage counter-current sequential batch extraction showed the improvement of both productivity and recovery compared to the batch operation. However, the outgoing extract concentration still cannot exceed the equilibrium limitation (Figure 3.1), this drawback can be overcome by continuous counter-current operation (Figure 3.4). The design and construction work of the extractor were presented in section 6.1.

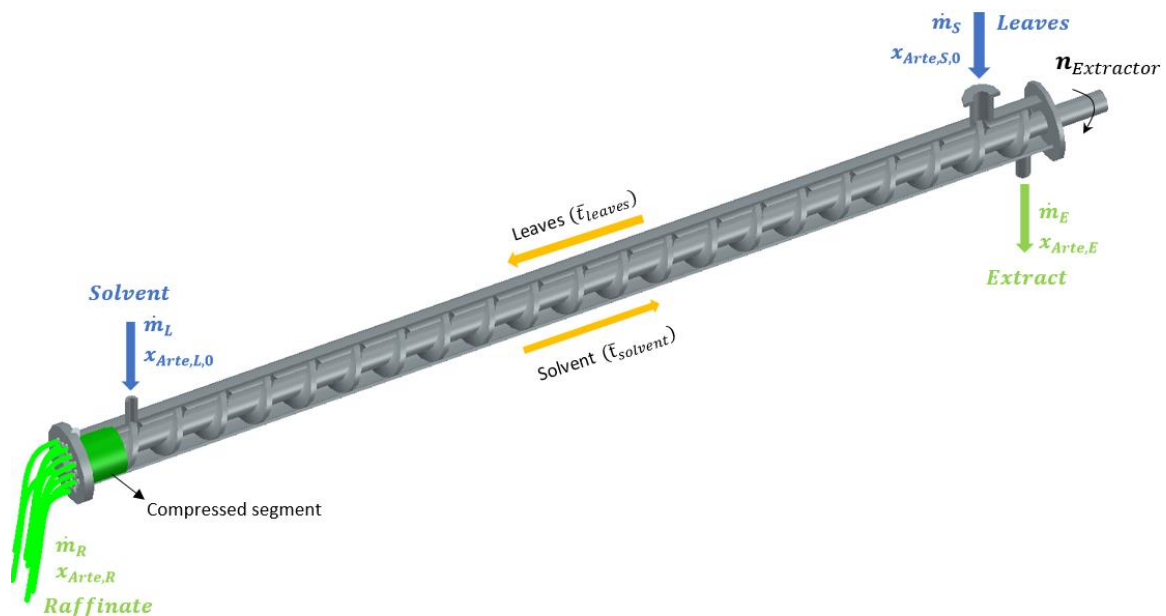


Figure 6.15. The illustration of input and output of the main counter-current extractor. The extractor is horizontal assembled and the flow of leaves and solvent are not depended on the inclination of the device. At steady state, the size of compressed segment is constant.

The concentration development of this specific constructed extractor can be explained as follows.

The entire length of extractor is filled by dried leaves at the beginning, the solvent is continuous provided only after the compressed segment is established (*Appendix A27*). Therefore, the fresh solvent is contacted to the fully loaded leaves of ARTE in the whole length of extractor, as a consequence, the extract composition is significantly high at the first moments. When the entire leaves inside the extractor are wet and ARTE is partly extracted, the ARTE composition will be slowly decreased and reached constant (if the steady state is achieved) (Figure 6.16).

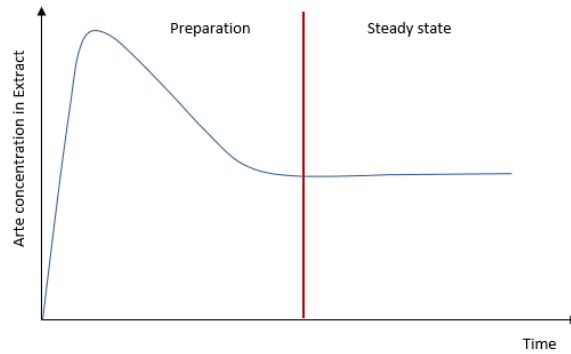


Figure 6.16. The theoretical ARTE concentration development in extract phase. *The composition develops sharply at the beginning and is slowly decreased.*

The red line position is depended on working condition (e.g. when the screw rotates slowly, the steady state requires longer time to be achieved or vice versa).

The complete assembled plant is given in Figure 6.17.

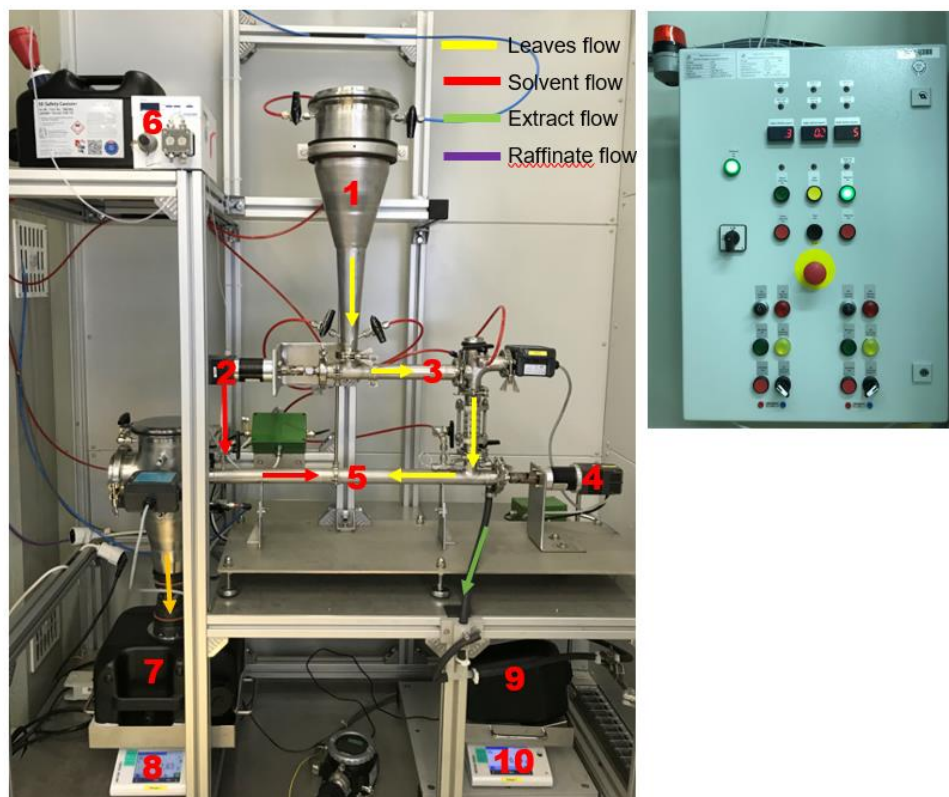


Figure 6.17. The continuous counter-current extraction plant. *Left: Description of flow and relevant instruments, devices; Right: Switch cabinet. 1-Dried leaves storage tank; 2- Motor M2; 3- Screw feeder; 4- Motor M1; 5- Main extractor; 6- Solvent pump; 7- Raffinate container; 8- Weighing scale for raffinate; 9- Extract container; 10- Weighing scale for extract.*

The homogenized dried leaves (section 4.1.2.2) are stored in conical tank **1**, the screw feeder **3** is fully filled by dried leaves. The screw controlled by motor **2** pushes dried leaves forward to the main extractor **5** and the screw of the main extractor transports the leaves to the perforated disk. Pump **6** provides the solvent to the extractor from another side. The scale **8** allows weighing the raffinate masses via container **7**. Extract container **9** is directly put on a scale **10** to control the extract mass/flowrate. The technical drawing can be found in Figure 6.5. For the main extractor, the friction between wet leaves and the perforated disk causes a compressed segment depicted as green block (Figure 6.15), this segment acts as a filter cake which allows the solvent to flow in only one direction. It should be emphasized that the size of the compressed segment should be maintained constant at steady state. Below, the verification that steady state conditions have been established is given.

6.3.1 Overall mass balance to verify steady state conditions

The existence of compressed segment plays a crucial role and it is much related to the solid phase. We searched for appropriate leaves flowrate \dot{m}_S to achieve steady state.

The compressed segment size should be constant at steady state (Figure 6.15). This size is controlled by the leaves flowrate from inlet and raffinate flowrate as:

$$\dot{m}_S + \dot{m}_{L_{int}} = \dot{m}_R \quad (6.13)$$

Furthermore, the internal extract mass $\dot{m}_{L_{int}}$ and raffinate mass \dot{m}_R are connected via a raffinate moisture designated by H . This moisture is assumed constant at every moment and can be calculated:

$$H[\%] = \frac{\dot{m}_{L_{int}}}{\dot{m}_R} * 100 = \frac{\dot{m}_{L_{int}}}{\dot{m}_S + \dot{m}_{L_{int}}} * 100 \quad (6.14)$$

Combining eqs. (6.3) and (6.14) gives:

$$\dot{m}_S = \dot{m}_R * \left(1 - \frac{H}{100}\right) \quad (6.15)$$

Thus, when the moisture of raffinate is determined, then the leaves flowrate can be calculated (eq. (6.15)). The determination of raffinate moisture is described in *Appendix A26*.

The experimental data shows that the raffinate moisture H is about 57% at speed $n = 1.8 \text{ rpm}$. Then, the leaves flowrate is estimated ($\dot{m}_S = 1 \text{ g/min}$) via eq. (6.15). This value should allow the continuous process to achieve steady state and was applied in the experiments described in the next section.

6.3.2 Continuous steady state experiments

The continuous experiments described below were carried out again in Toluene.

In this section, results of the following selected steady state experiments are presented:

- Implementation of first continuous counter-current steady state extraction based on the verified steady state conditions (designated as **Run 1**).
- Implementation of second continuous steady state extraction (optimized conditions: experiment can be implemented at higher leaves flowrate at the input) (designated as **Run 2**).

The verification of steady state conditions above allowed to implement the continuous steady state extraction. The first continuous steady state experiment was carried out with the input parameters (Table 6.5). The experimental procedures are described in *Appendix A27*.

It should be noticed that the dosage should be identical to the optimized conditions ($D = 0.1$) of batch operation. The residence time of leaves was estimated at around 15 minutes by setting the screw speed $n_{\text{Extractor}} = 1.8 \text{ rpm}$ (Table 6.3), the feeder speed $n_{\text{Feeder}} = 0.41 \text{ rpm}$ corresponding to leaves flowrate 1 g/min (Figure A17.1) and the solvent flowrate 0.8 L/h was applied ($D \approx 0.1$). The masses of extract and raffinate were weighed and recorded in a fixed time interval by two scales (Figure 6.17). These data allowed to estimate the flowrates of the extract and raffinate phases (Figure A28.2).

Table 6.5. Run 1: The steady state working condition of continuous ARTE extraction from *Artemisia annua L.* based on verified steady state conditions (section 6.3.1). Given parameters: \dot{m}_S is estimated via eq. (6.15), \dot{m}_L from pump calibration data (Appendix A18), $x_{ARTE,S,0}$ from Table 4.3, n_{Feeder} , $n_{Extractor}$ from calibration data in Appendix A17. Nitrogen pressure is 3.6 bar.

Input parameters	Values	Units
Mass flowrate of leaves, \dot{m}_S	1	g/min
Mass flowrate of solvent, \dot{m}_L	11.7	g/min
Screw speed of feeder (M2), n_{Feeder}	0.41	rpm
Screw speed of extractor (M1), $n_{Extractor}$	1.8	rpm

The experimental procedures showed that the required time to establish the compressed segment was about 40 minutes and it took roughly 60 minutes to reach steady state. The extract samples were collected during the experiments in 15-minute time intervals and stored in fridge at 4°C. The samples were later analyzed by HPLC method (section 4.1.2.1) and the ARTE concentrations in the extract phase are given in Figure 6.18 as **Run 1**.

The given experimental conditions above (Table 6.5) describe only one steady state condition. However, the raffinate flowrate \dot{m}_R can be increased at higher speed of screw $n_{extractor}$ (Figure 6.15), means, the leaves flowrate needs to be higher to hold the steady state condition (6.13). It should be mentioned that when the rotational speed is too high, the leaves will stay too short inside and the process is not efficient. Therefore, a limitation of 10-minute residence time of leaves, corresponding to speed $n_{Extractor} = 2.2 \text{ rpm}$, was fixed. The corresponding speed of screw feeder was set at $n_{Feeder} = 0.48 \text{ rpm}$ leading to leaves mass flowrate 1.2 g/min (Figure A17.1). The experiment with optimized conditions is designated as **Run 2** and the extraction protocol described above was also applied for **Run 2**. The controlled, recorded experimental data are described in Appendix A28. The measured flowrates of the extract and raffinate are fulfilled the total mass balance.

Table 6.6 shows optimized input parameters, at which the leaves flowrate and screw speeds are higher than **Run 1**.

Table 6.6. Run 2: The input parameters for optimized steady state run. *The experiment can be implemented at higher input leaves flowrate \dot{m}_S than previous steady state.*

Input parameters	Values	Units
Mass flowrate of leaves, \dot{m}_S	1.2	g/min
Mass flowrate of solvent, \dot{m}_L	11.7	g/min
Screw speed of feeder (M2), n_{Feeder}	0.48	rpm
Screw speed of extractor (M1), $n_{Extractor}$	2.2	rpm

The extract samples were again analyzed by introduced HPLC (section 4.1.2). The ARTE concentrations at the outlet of **Run 1** and **Run 2** are described in Figure 6.18. The concentration development is similar to theory (Figure 6.16).

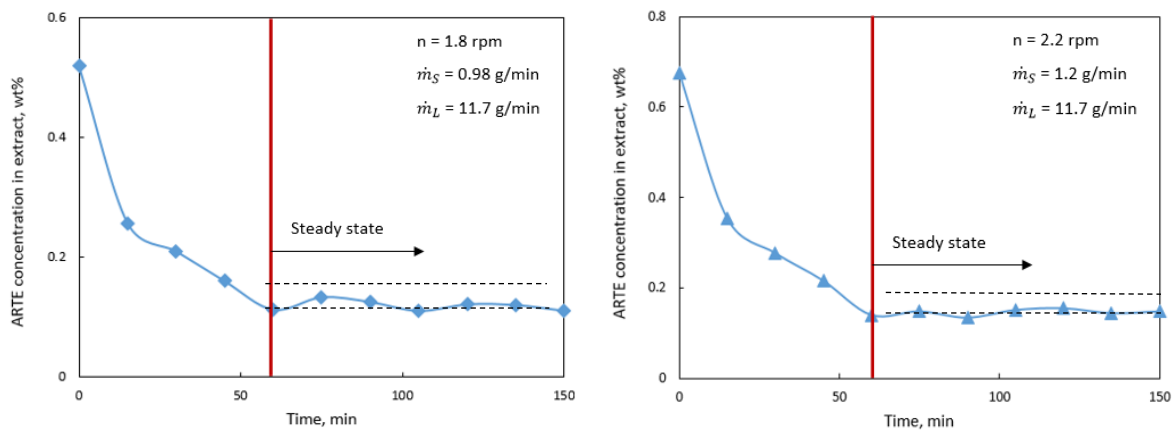


Figure 6.18. The ARTE concentration development of a continuous counter-current steady state extraction. *Left: Run 1 (input parameters: $n = 1.8$ rpm, $\dot{m}_S = 0.98$ g/min, $\dot{m}_L = 11.7$ g/min); Right: Run 2 (input parameters: $n = 2.2$ rpm, $\dot{m}_S = 1.2$ g/min, $\dot{m}_L = 11.7$ g/min) corresponding to higher screw speed and leaves flowrate \dot{m}_S .*

Two dotted lines present the oscillating region of ARTE concentration, the mean ARTE concentrations in the extract phase of **Run 1** and **Run 2** are given in Table 6.7. The improvement of **Run 2** is obvious when more dried leaves can be treated and higher extract concentration is gained. The reducing of extract flowrate \dot{m}_E in **Run 2** is compensated by the enhancing of extract concentration.

Table 6.7. Summary of two steady state continuous extraction combining simulation results. The extract and raffinate flowrates \dot{m}_E, \dot{m}_R are calculated from recorded data (Appendix A28). $x_{ARTE,E}$ is mean value of outlet concentration analyzed by HPLC. $x_{ARTE,E}^{Sim}$ is the simulated results.

	Experiments					Simulated
	Inlet		Outlet			
	\dot{m}_S [g/min]	\dot{m}_L [g/min]	\dot{m}_E [g/min]	\dot{m}_R [g/min]	$x_{ARTE,E}$ [wt.%]	$x_{ARTE,E}^{Sim}$ [wt.%]
Run 1 ($n_{Extractor}=1.8$ rpm)	0.98	11.7	10.3	2.3	0.116	0.162**
Run 2 ($n_{Extractor}=2.2$ rpm)	1.2	11.7	10.1	2.8	0.145*	0.146***

* averaged concentration of optimized steady state conditions (**Run 2** Table 6.6) and data of Figure 6.18; ** the simulated concentration (Code5) (**Run 1**. input parameters based on Table 6.5: $\varepsilon = 0.75$, $q_{in} = 1.3$, $c_{in} = 0$, $k_{i,E} = 0.05$, $\beta_i = 0.17$, $\tau = 10$, $N = 50$ (Figure 3.13)); *** the simulated concentration (Code5) (**Run 2**. input parameters based on Table 6.6: $\varepsilon = 0.7$, $q_{in} = 1.3$, $c_{in} = 0$, $k_{i,E} = 0.05$, $\beta_i = 0.17$, $\tau = 10$, $N = 50$ (Figure 3.13)).

It should be noticed that the input parameters for simulation model of **Run 1** and **Run 2** (determined with Code5, see Appendix) are based on working conditions and exploited experimental data (the phase ratio ε is estimated by wetting factor W (Figure 4.12)).

Comparing to **Run 1**, the raffinate and leaves flowrates in **Run 2** are increased roughly 18% and the ARTE concentration at the outlet gains roughly 20%.

Evaluation of continuous counter-current extraction

The estimated concentration of **Run 2** shows that the agreement of experimental and simulated concentrations is very high. A strong and very satisfying result is good agreement between experiment and theory. The larger value predicted is due to numerous shortcoming of the model. The introduced model in chapter 3 is validated.

The evaluation of the continuous counter-current steady state operation is based on the introduced productivity (eq. (3.86)) and recovery (eq. (3.88)). As a suitable *Scale* factor can be considered the free volume V_{free} of extractor ($V_{free} = 0.4$ L- Figure 6.4).

Thus, the extraction productivity can be estimated based on the value of the outgoing steady state extract concentration $x_{ARTE,E}$ (the bold value in Table 6.7) as:

$$Prod_{ARTE}^{Continuous} = \frac{\dot{m}_{ARTE,E}}{V_{free}} = \frac{\dot{m}_E * x_{ARTE,E}}{V_{free}} = 2.2 \left[\frac{g}{h.L} \right] \quad (6.16)$$

For the corresponding recovery holds:

$$Rec_{Arte}^{Continuous} = \frac{\dot{m}_{ARTE,E}}{\dot{m}_{ARTE,S,0}} * 100 = 93.8 [\%] \quad (6.17)$$

Finally, now a comparison between three extraction modes is possible. The results are given below.

Comparison of three extraction modes

The investigated batch and sequential counter-current equilibrated stage operation were also carried out applying identical dosages D ($D = 0.1$, eqs. (2.8), (2.9)) and allowed evaluating the efficiency separately (Table 5.1, Table 5.5, eqs. (6.16), (6.17)). The summary of input and output parameters is presented below.

Table 6.8. Input and output parameters of three experimental extraction operations for ARTE extraction from *Artemisia annua L.* in Toluene. The dosages of each operation are identical ($D = 0.1$). The parameters in continuous operation are presented in fluxes. The objective functions of batch, sequential multi-stage and continuous operations are taken from Appendix A10 and Table 5.5 respectively. The productivity and recovery of continuous counter-current steady state operation are provided by eqs. (6.16), (6.17).

	Input condition				Results		Objective functions	
	m_S [g]	m_L [g]	V_{free} [L]	Time [h]	m_E [g]	ARTE concentration, [wt. %]	$Prod_{ARTE}$ [g/h/L]	Rec_{ARTE} [%]
Batch	3	30	0.04	0.5	23	0.08	0.86	47.7
Sequential 5-stage counter-current	3	30	0.04	0.5	23	0.14	1.61	82
Continuous counter-current (Run 2)	1.2 g/min	11.7 g/min	0.4	-	10.1 g/min	0.145	2.2	94

The perforated disk of the developed continuous extractor allowed to squeeze the solvent out of raffinate, thus, more extract amount could be achieved at the outlet. The productivity of the sequential 5-stage counter-current operation is much higher than that of the batch. Altogether, the productivity and recovery of continuous steady state extraction clearly provided the best performance (productivity about 2.5-fold

higher than that for batch process and 25 percent higher than that for sequential multi-stage operation). The dead time in the batch and multi-stage causes the reduction of the productivity, while the continuous process delivers extract non-stop. Thus, the advantage of the developed extractor based on continuous counter-current extraction could be demonstrated experimentally.

7 Summary and outlook

Main achievements of this thesis are:

- It was shown that batch extraction processes are applicable for estimating important parameters as mass transfer rate coefficients and equilibrium distribution coefficients.
- The well-established theory of Chemical Reaction Engineering and modeling Solid Liquid Extraction are similar and can be connected. This allows efficiently predicting different extraction variants and operating modes. An essential restriction is hereby the validity of linear distribution equilibria. A model developed was validated experimentally for extracting ARTE from dried *Artemisia annua L.* leaves.
- A continuous counter-current extractor was successfully designed, assembled and operated. The outgoing steady state ARTE extract concentrations were very close to the predicted equilibrium concentrations. The productivity of steady state counter-current operation was about 2.5-fold higher than that for a conventional batch extraction process.

The results are seen as a basis for further scale up and potential application. The high recoveries obtained offer possibilities for direct application of this counter-current extractor close to the farms where the plants are growing.

Outlook

The designed and constructed continuous counter-current extractor provided a very good performance. The results achieved offer potential for future projects. Promising main directions are the improvement of extractor design and the extension of the model to solve other challenging separation tasks. Hereby, treating directly fresh (not dried) plant material is one so far unexplored option. Such approach would help reducing the costs for transportation, storage and energy for drying material. Another promising direction can be testing the functionality of the extractor on a broader range of plant materials. Furthermore, it is known that extraction processes are often more efficient at elevated temperatures because of increased target solubility and accelerated penetration of the solvent into solid matrices. A double-jacketed set

would allow extracting at higher temperatures. Another source for improvement is further optimizing the screw geometry and structure. For example, shorter pitches of the screw cause the smaller angle of screw profiles, this leads to prolong the residence time. Nevertheless, in order to keep the identical inspected residence time, the screw has to be rotated faster, thus, the raffinate outlet flowrates is increased causing the increasing of treatable mass of leaves at the inlet. Last but not least, the applicability of the model developed and applied can be broadened by extending it model to quantify the impact of nonlinear and competitive equilibria.

References

1. Pilz, H.-J.B.u.S., *Industrial scale natural products extraction*. 2009.
2. Nations, U., *World Drugs Report 2021*. 2021. p. 109.
3. *Global Medicines Use in 2020_Outlook and implications*. 2015(IMS Institute for Healthcare informatics): p. 47.
4. Shukar, S., et al., *Drug Shortage: Causes, Impact, and Mitigation Strategies*. Front Pharmacol, 2021. **12**: p. 693426.
5. Organization-Unitaid, W.H., *Global malaria diagnostic and artemisinin treatment commodities demand forecast 2017-2021*. 2018.
6. Miller, L.H. and X. Su, *Artemisinin: discovery from the Chinese herbal garden*. Cell, 2011. **146**(6): p. 855-8.
7. Woerdenbag, H.J., C.B. Lugt, and N. Pras, *Artemisia annua L.: a source of novel antimalarial drugs*. Pharm Weekbl Sci, 1990. **12**(5): p. 169-81.
8. Daddy, N.B., et al., *Artemisia annua dried leaf tablets treated malaria resistant to ACT and i.v. artesunate: Case reports*. Phytomedicine, 2017. **32**: p. 37-40.
9. Guo, Z., *Artemisinin anti-malarial drugs in China*. Acta Pharm Sin B, 2016. **6**(2): p. 115-24.
10. Al-Khayri, J.M., et al., *Biotechnological Approaches for Production of Artemisinin, an Anti-Malarial Drug from Artemisia annua L.* 2022. **27**(9).
11. van der Kooy, F. and S.E. Sullivan, *The complexity of medicinal plants: the traditional Artemisia annua formulation, current status and future perspectives*. J Ethnopharmacol, 2013. **150**(1): p. 1-13.
12. Gilmore, K. and P.H. Seeberger, *Continuous flow photochemistry*. Chem Rec, 2014. **14**(3): p. 410-8.
13. Kopetzki, D., F. Lévesque, and P.H. Seeberger, *A continuous-flow process for the synthesis of artemisinin*. Chemistry, 2013. **19** **17**: p. 5450-6.
14. Lévesque, F. and P.H. Seeberger, *Continuous-flow synthesis of the anti-malaria drug artemisinin*. Angew Chem Int Ed Engl, 2012. **51**(7): p. 1706-9.
15. Triemer, S. and K. Gilmore, *Literally Green Chemical Synthesis of Artemisinin from Plant Extracts*. 2018. **57**(19): p. 5525-5528.
16. Programme, G.M., *World malaria report 2021*. 2021: p. 322.
17. Fidock, D.A., et al., *Mutations in the P. falciparum digestive vacuole transmembrane protein PfCRT and evidence for their role in chloroquine resistance*. Mol Cell, 2000. **6**(4): p. 861-71.
18. Achan, J., et al., *Quinine, an old anti-malarial drug in a modern world: role in the treatment of malaria*. Malaria Journal, 2011. **10**(1): p. 144.
19. Klayman, D.L., *Qinghaosu (artemisinin): an antimalarial drug from China*. Science, 1985. **228**(4703): p. 1049-55.
20. Liao, F., *Discovery of Artemisinin (Qinghaosu)*. Molecules, 2009. **14**(12): p. 5362-5366.

21. Efferth, T. and T. Efferth, *From ancient herb to modern drug: Artemisia annua and artemisinin for cancer therapy*. Seminars in cancer biology, 2017. **46**: p. 65-83.
22. LIU JING-MING, N.M.-Y., FAN JU-FEN, TU YOU-YIU, WU ZHAO-HUA, WU YU-LIN, ZHOU WEI-SHAN, *STRUCTURE AND REACTION OF ARTEANNUIN*. Acta Chimica Sinica, 1979. **37**(2): p. 129-143.
23. de Faveri Favero, F., et al., *Artemisia annua L.: evidence of sesquiterpene lactones' fraction antinociceptive activity*. BMC Complementary and Alternative Medicine, 2014. **14**(1): p. 266.
24. Tu, Y., *The discovery of artemisinin (qinghaosu) and gifts from Chinese medicine*. Nat Med, 2011. **17**(10): p. 1217-20.
25. Tu, Y., *Artemisinin-A Gift from Traditional Chinese Medicine to the World (Nobel Lecture)*. Angew Chem Int Ed Engl, 2016. **55**(35): p. 10210-26.
26. Miller, L.H. and X. Su, *Artemisinin: discovery from the Chinese herbal garden*. Cell, 2011. **146**(6): p. 855-8.
27. Organization, W.H., *Global technical strategy for malaria 2016-2030*. 2015.
28. Gilmore, K., et al., *Continuous synthesis of artemisinin-derived medicines*. Chemical Communications, 2014. **50**(84): p. 12652-12655.
29. Triemer, S., et al., *Kinetic analysis of the partial synthesis of artemisinin: Photooxygenation to the intermediate hydroperoxide*. Journal of Flow Chemistry, 2021. **11**(3): p. 641-659.
30. Ro, D.K., et al., *Production of the antimalarial drug precursor artemisinic acid in engineered yeast*. Nature, 2006. **440**(7086): p. 940-3.
31. Martin, V.J., et al., *Engineering a mevalonate pathway in Escherichia coli for production of terpenoids*. Nat Biotechnol, 2003. **21**(7): p. 796-802.
32. Dietrich, J.A., et al., *A Novel Semi-biosynthetic Route for Artemisinin Production Using Engineered Substrate-Promiscuous P450BM3*. ACS Chemical Biology, 2009. **4**(4): p. 261-267.
33. Brown, G.D., *The Biosynthesis of Artemisinin (Qinghaosu) and the Phytochemistry of Artemisia annua L. (Qinghao)*. Molecules, 2010. **15**(11): p. 7603-7698.
34. Kohler, M., et al., *Extraction of artemisinin and artemisinic acid from Artemisia annua L. using supercritical carbon dioxide*. J Chromatogr A, 1997. **785**(1-2): p. 353-60.
35. Quispe-Condori, S., et al., *Global yield isotherms and kinetic of artemisinin extraction from Artemisia annua L leaves using supercritical carbon dioxide*. Journal of Supercritical Fluids The, 2005: p. 40-48.
36. Lapkin, A.A., P.K. Plucinski, and M. Cutler, *Comparative assessment of technologies for extraction of artemisinin*. J Nat Prod, 2006. **69**(11): p. 1653-64.
37. Martín, L., et al., *Supercritical fluid extraction of wormwood (Artemisia absinthium L.)*. The Journal of Supercritical Fluids, 2011. **56**: p. 64-71.

38. Baldino, L., E. Reverchon, and G. Porta, *An Optimized Process for SC-CO₂ Extraction of Antimalarial Compounds from Artemisia annua L.* Journal of Supercritical Fluids The, 2017. **128**.
39. Vidovic, S., et al., *Extraction of sweet wormwood (Artemisia annua L.) by supercritical carbon dioxide.* Lekovite sirovine, 2020.
40. Ciftci, O.N., et al., *Optimization of artemisinin extraction from Artemisia annua L. with supercritical carbon dioxide + ethanol using response surface methodology.* 2018.
41. del Valle, J.M. and F.A. Urrego, *Free solute content and solute-matrix interactions affect apparent solubility and apparent solute content in supercritical CO₂ extractions. A hypothesis paper.* The Journal of Supercritical Fluids, 2012. **66**: p. 157-175.
42. Lo, T.C. and M.H.I. Baird, *Solvent Extraction*, in *Encyclopedia of Physical Science and Technology (Third Edition)*, R.A. Meyers, Editor. 2003, Academic Press: New York. p. 341-362.
43. Al Khawli, F., et al., *Innovative Green Technologies of Intensification for Valorization of Seafood and Their By-Products.* Marine Drugs, 2019. **17**: p. 689.
44. Khaw, K.Y., et al., *Solvent Supercritical Fluid Technologies to Extract Bioactive Compounds from Natural Sources: A Review.* Molecules, 2017. **22**(7).
45. Petersen, F.a.A., R. , *Natural compounds as drugs.* Vol. Vol.66 Birkhäuser Verlag AG. 860.
46. Demirci, F., *Natural Products Isolation, 2nd Edition (Methods in Biotechnology, Vol. 20) Edited by S. D. Sarker (University of Ulster), Z. Latif (Molecular Nature Limited), and A. I. Gray (University of Strathclyde).* Humana Press Inc., Totowa, NJ. 2006. xii + 515 pp. 15.5 × 23.5 cm. \$135.00. ISBN 1-58829-447-1 (Hardcover). eISBN 1-59259-955-9 (e-book). Journal of Natural Products - J NAT PROD, 2007. **70**: p. 712-712.
47. Rostagno, M.A.a.P., *Natural product extraction: principles and applications.* Vol. No.21. 2013: J.M. RSC Green Chemistry.
48. Petrovska, B.B., *Historical review of medicinal plants' usage.* Pharmacogn Rev, 2012. **6**(11): p. 1-5.
49. Handa, S.S., et al., *Extraction technologies for medicinal and aromatic plants.* International centre for science and high technology, 2008: p. 21-25.
50. *Modern Phytochemical methods.* . Proceeding of 30th meeting of the phytochemical society of North America, Canada, 1990. **25**.
51. Brijesh kumar, T., N. Brunton, and C. Brennan, *Handbook of Plant Food Phytochemicals Sources, Stability and Extraction.* 2013.
52. Chemat, F. and J. Strube, *Green Extraction of Natural Products: Theory and Practice.* 2014. 1-363.
53. Nn, A., *A Review on the Extraction Methods Use in Medicinal Plants, Principle, Strength and Limitation.* Medicinal and Aromatic plants, 2015. **4**: p. 1-6.

-
54. Anandakumar, A.M., et al., *Preliminary phytochemical studies for the quantification of secondary metabolites of medicinal importance in the plant, Acalypha fruticosa Forssk.* Journal of Applied and Natural Science, 2009. **1**: p. 41-43.
 55. Stringham, R.W., et al., *Identification of impurities in artemisinin, their behavior in high performance liquid chromatography and implications for the quality of derived anti-malarial drugs.* J Chromatogr A, 2011. **1218**(38): p. 6838-42.
 56. Schmidt-Traub, H., *Preparative Chromatography of Fine Chemicals and Pharmaceuticals.* 2005.
 57. L., C.E., *Diffusion: Mass transfer in fluid systems* 1984(Cambridge University Press).
 58. Skjold-Jorgensen, S., et al., *Vapor-Liquid Equilibria by UNIFAC Group Contribution. Revision and Extension.* Industrial & Engineering Chemistry Process Design and Development, 1979. **18**.
 59. Lehr, A., et al., *Experimental investigation of the residence time distribution in a screw-type apparatus designated to extract artemisinin.* Chemical Engineering and Processing - Process Intensification, 2023. **187**: p. 109337.
 60. Prausnitz J.M., L.R.N., Gomes de Azevedo E., *Molecular Thermodynamics of Fluid-Phase Equilibria.* 1999(Prentice Hall).
 61. Don, W.G. and H.P. Robert, *Perry's Chemical Engineers' Handbook, Eighth Edition.* 8th ed. / ed. 2008, New York: McGraw-Hill Education.
 62. Castillo-Santos, K., et al., *Analysis of mass transfer equations during solid-liquid extraction and its application for vanilla extraction kinetics modeling.* Journal of Food Engineering, 2016. **192**.
 63. Harouna, H., et al., *Comparison of Kinetic Models for the Aqueous Solid-Liquid Extraction of Tilia Sapwood in a Continuous Stirred Tank Reactor.* Chemical Engineering Communications - CHEM ENG COMMUN, 2007. **194**: p. 537-552.
 64. Simeonov, E. and C. Chilev, *Modeling and kinetics study of solid-liquid extraction from leaves of nicotiana tabacum L.* 2015. **50**: p. 597-600.
 65. Fel, E., et al., *Residence time distribution and efficiency of mixing in high shear extruder.* Society of Plastics Engineers - EUROTECH 2013, 2013: p. 455-459.
 66. Gao, Y., F.J. Muzzio, and M.G. Ierapetritou, *A review of the Residence Time Distribution (RTD) applications in solid unit operations.* Powder Technology, 2012. **228**: p. 416-423.
 67. White, J.L. and E.K. Kim, *Twin Screw Extrusion: Technology and Principles.* 2010: Hanser Publications.
 68. Tzoganakis, C., et al., *Measurements of Residence Time Distributions for the Degradation of Polypropylene in Single-Screw Plasticating Extruder.* Journal of Applied Polymer Science, 1989. **37**: p. 681-693.
 69. Rodrigues, A.E., *Residence time distribution (RTD) revisited.* Chem Eng Sci, 2021. **230**: p. 116188.
 70. Shon, K., D. Chang, and J.L. White, *A Comparative Study of Residence Time Distributions in a Kneader, Continuous Mixer, and Modular Intermeshing Co-*
-

- Rotating and Counter-Rotating Twin Screw Extruders*. International Polymer Processing, 1999. **14**(1): p. 44-50.
71. O., L., *Chemical Reaction Engineering*. 3rd edition ed. 1999: John Wiley & Sons.
72. Seidel-Morgenstern, A., M. Schulte, and A. Epping, *Fundamentals and General Terminology*, in *Preparative Chromatography*. 2012. p. 7-46.
73. Wewers, W., et al., *Selection of Chromatographic Systems*, in *Preparative Chromatography*. 2005. p. 107-172.
74. Liu, Y., H. Lü, and F. Pang, *Solubility of Artemisinin in Seven Different Pure Solvents from (283.15 to 323.15) K*. Journal of Chemical & Engineering Data, 2009. **54**(3): p. 762-764.
75. Bergs, D., et al., *A Standard Procedure for the Selection of Solvents for Natural Plant Extraction in the Early Stages of Process Development*. Chemical Engineering & Technology, 2013. **36**(10): p. 1739-1748.
76. Lapkin, A.A., et al., *Screening of new solvents for artemisinin extraction process using ab initio methodology*. Green Chemistry, 2010. **12**(2): p. 241-251.
77. Xing, et al., *Solubility of Artemisinin in Supercritical Carbon Dioxide*. Journal of Chemical & Engineering Data, 2003. **48**(2): p. 330-332.
78. Wang, L.-H., et al., *Solubility of Artemisinin in Ethanol + Water from (278.2 to 343.2) K*. Journal of Chemical and Engineering Data - J CHEM ENG DATA, 2007. **52**.
79. Nti-Gyabaah, J., K. Gbewonyo, and Y.C. Chiew, *Solubility of Artemisinin in Different Single and Binary Solvent Mixtures Between (284.15 and 323.15) K and NRTL Interaction Parameters*. Journal of Chemical & Engineering Data, 2010. **55**(9): p. 3356-3363.
80. Li, W., et al. *Microwave Multi-Stage Countercurrent Extraction of Dihydromyricetin from *Ampelopsis grossedentata**. 2007.
81. Pan, X., et al., *Microwave-assisted extraction of glycyrrhizic acid from licorice root*. Biochemical Engineering Journal, 2000. **5**(3): p. 173-177.
82. Chanioti, S., G. Liadakis, and C. Tzia, *Solid-Liquid Extraction*. 2014. p. 253-286.
83. Williams, M.A., *14 - Separation technologies in oilseed processing*, in *Separation, Extraction and Concentration Processes in the Food, Beverage and Nutraceutical Industries*, S.S.H. Rizvi, Editor. 2013, Woodhead Publishing. p. 396-429.
84. GEA Niro A/S, P.T.D. *Continuous Extractor*. Available from: www.gea.com/en/products/dryers-particle-processing/extractors/context-extractor.jsp.
85. Plachco, F.P. and M.E. Lago, *Solid-Liquid Extraction in Countercurrent Cascade with Retention of Liquid by the Solid Spherical Geometry Constant Diffusivity*. Industrial & Engineering Chemistry Process Design and Development, 1976. **15**(3): p. 361-365.

-
86. Rittirut, W., C. Thongurai, and C. Siripatana, *Mathematical Simulation of Solid-Liquid Diffusion in Continuous Countercurrent Extraction Process, Part I - Modeling Development*. International Journal of Chemical Reactor Engineering, 2010. **8**(1).
 87. Chilev, C., V. Koleva, and E. Simeonov, *A New Empirical Model for Calculation the Effective Diffusion Coefficient for Solid-Liquid Extraction from Plants*. Industrial & Engineering Chemistry Research, 2014. **53**(15): p. 6288-6296.
 88. Ravenscroft, E.A., *Extraction of Solids with Liquids: Multiple and Countercurrent Extraction*. Industrial & Engineering Chemistry, 1936. **28**(7): p. 851-855.
 89. Simeonov, E., I.K. Tsibranska, and A. Minchev, *Solid-liquid extraction from plants — experimental kinetics and modelling*. Chemical Engineering Journal, 1999. **73**: p. 255-259.
 90. Wright, G. *Mathematical Modeling of the Solid-liquid Extraction of Phenolic-rich Compounds from Pinus contorta Bark*. 2015.
 91. Rakotondramasy-Rabesiaka, L., et al., *Solid-liquid extraction of protopine from Fumaria officinalis L.—Kinetic modelling of influential parameters*. Industrial Crops and Products, 2009. **29**(2): p. 516-523.
 92. Jurinjak Tusek, A., et al., *Kinetics and thermodynamics of the solid-liquid extraction process of total polyphenols, antioxidants and extraction yield from Asteraceae plants*. Industrial Crops and Products, 2016. **91**: p. 205-214.
 93. Ho, Y.-S., et al., *Kinetics and model building of leaching of water-soluble compounds of Tilia sapwood*. Separation and Purification Technology, 2005. **45**(3): p. 169-173.
 94. Wongkittipong, R., et al., *Solid-liquid extraction of andrographolide from plants—experimental study, kinetic reaction and model*. Separation and Purification Technology, 2004. **40**(2): p. 147-154.
 95. Veloso, G.O., V.G. Krioukov, and H.A. Vielmo, *Mathematical modeling of vegetable oil extraction in a counter-current crossed flow horizontal extractor*. Journal of Food Engineering, 2005. **66**: p. 477-486.
 96. Wang, Q.-e., et al., *Development of multi-stage countercurrent extraction technology for the extraction of glycyrrhizic acid (GA) from licorice (Glycyrrhiza uralensis Fisch)*. Biochemical Engineering Journal, 2004. **21**: p. 285–292.
 97. Plachco, F.P. and M.E. Lago, *Counter-current solid liquid extraction in a cascade of batch extractors*. Canadian Journal of Chemical Engineering, 1972. **50**: p. 611-615.
 98. Castillo-Santos, K., et al., *An optimization based algorithm for solving design problems of counter-current multistage batch solid-liquid extractors for complex systems: Application to vanilla extract*. Computers & Chemical Engineering, 2016. **89**.
 99. Dreisewerd, B., J. Merz, and G. Schembecker, *Modeling the Quasi-Equilibrium of Multistage Phytoextractions*. Industrial & Engineering Chemistry Research, 2016. **55**.
-

100. Dreisewerd, B., J. Merz, and G. Schembecker, *Determining the Solute-Solid Interactions in Phytoextraction*. Chemical Engineering Science, 2015. **134**.
101. Münzberg, S., T.G. Vu, and A. Seidel-Morgenstern, *Generalizing Countercurrent Processes: Distillation and Beyond*. Chemie Ingenieur Technik, 2018. **90**(11): p. 1769-1781.
102. Tu, J., G.H. Yeoh, and C. Liu, *Computational Fluid Dynamics: A Practical Approach*. 2007: Butterworth-Heinemann.
103. A., K., *Theoretical analysis of absorption process*. 1930. **22**: p. 43-49.
104. Goring, G.E., *A Modified Kremser Equation for Stagewise Countercurrent Processes*. Separation Science, 1970. **5**(2): p. 113-120.
105. Horosanskaia, E., *Strategien zur kristallisationsbasierten Aufreinigung von pharmazeutisch relevanten Naturstoffen und organischen Mehrkomponentengemischen*. 2019.
106. Widmer, V., D. Handloser, and E. Reich, *Quantitative HPTLC Analysis of Artemisinin in Dried Artemisia annua L.: A Practical Approach*. Journal of Liquid Chromatography & Related Technologies - J LIQ CHROMATOGR RELAT TECHNO, 2007. **30**: p. 2209-2219.
107. Ghafoori, H., et al., *Analysis of artemisinin isolated from Artemisia Annua L. by TLC and HPLC*. Journal of Liquid Chromatography & Related Technologies - J LIQ CHROMATOGR RELAT TECHNO, 2012. **36**.
108. Gabriëls, M. and J.A. Plaizier-Vercammen, *Densitometric thin-layer chromatographic determination of artemisinin and its lipophilic derivatives, artemether and arteether*. J Chromatogr Sci, 2003. **41**(7): p. 359-66.
109. Misra, H., et al., *Extraction of Artemisinin, an Active Antimalarial Phytopharmaceutical from Dried Leaves of Artemisia annua L., Using Microwaves and a Validated HPTLC-Visible Method for Its Quantitative Determination*. Chromatography Research International, 2014. **2014**: p. 361405.
110. Ferreira, J.F. and J.M. Gonzalez, *Analysis of underivatized artemisinin and related sesquiterpene lactones by high-performance liquid chromatography with ultraviolet detection*. Phytochem Anal, 2009. **20**(2): p. 91-7.
111. Lapkin, A.A., et al., *Development of HPLC analytical protocols for quantification of artemisinin in biomass and extracts*. J Pharm Biomed Anal, 2009. **49**(4): p. 908-15.
112. Bhandari, P., et al., *Simultaneous densitometric determination of artemisinin, artemisinic acid and arteannuin-B in Artemisia annua using reversed-phase thin layer chromatography*. J Sep Sci, 2005. **28**(17): p. 2288-92.
113. Avery, B.A., K.K. Venkatesh, and M.A. Avery, *Rapid determination of artemisinin and related analogues using high-performance liquid chromatography and an evaporative light scattering detector*. J Chromatogr B Biomed Sci Appl, 1999. **730**(1): p. 71-80.
114. Peng, C.A., J.F. Ferreira, and A.J. Wood, *Direct analysis of artemisinin from Artemisia annua L. using high-performance liquid chromatography with*

- evaporative light scattering detector, and gas chromatography with flame ionization detector.* J Chromatogr A, 2006. **1133**(1-2): p. 254-8.
115. Stolyhwo, A., H. Colin, and G. Guiochon, *Use of light scattering as a detector principle in liquid chromatography.* Journal of Chromatography A, 1983. **265**: p. 1-18.
116. Stolyhwo, A., et al., *Study of the qualitative and quantitative properties of the light-scattering detector.* Journal of Chromatography A, 1984. **288**: p. 253-275.
117. Ganzera, M. and H. Stuppner, *Evaporative Light Scattering Detection (ELSD) for the Analysis of Natural Products.* Current Pharmaceutical Analysis, 2005. **1**: p. 135-144.
118. Kohler, M., et al., *The evaporative light scattering detector: some applications in pharmaceutical analysis.* TrAC Trends in Analytical Chemistry, 1997. **16**(8): p. 475-484.
119. Cebolla, V.L., et al., *Evaporative Light-Scattering Detection in the Quantitative Analysis of Semivolatile Polycyclic Aromatic Compounds by High-Performance Liquid Chromatography.* Journal of Chromatographic Science, 1997. **35**(4): p. 141-150.
120. Karbwang, J., et al., *Determination of artemether and its major metabolite, dihydroartemisinin, in plasma using high-performance liquid chromatography with electrochemical detection.* J Chromatogr B Biomed Sci Appl, 1997. **690**(1-2): p. 259-65.
121. Na-Bangchang, K., et al., *Simple high-performance liquid chromatographic method with electrochemical detection for the simultaneous determination of artesunate and dihydroartemisinin in biological fluids.* J Chromatogr B Biomed Sci Appl, 1998. **708**(1-2): p. 201-7.
122. Sandrenan, N., et al., *Determination of artemether and its metabolite, dihydroartemisinin, in plasma by high-performance liquid chromatography and electrochemical detection in the reductive mode.* J Chromatogr B Biomed Sci Appl, 1997. **691**(1): p. 145-53.
123. Suberu, J., et al., *A rapid method for the determination of artemisinin and its biosynthetic precursors in Artemisia annua L. crude extracts.* J Pharm Biomed Anal, 2013. **84**: p. 269-77.
124. Wang, M., et al., *Analysis of artemisinin in Artemisia annua L. by LC-MS with selected ion monitoring.* J Agric Food Chem, 2005. **53**(18): p. 7010-3.
125. Carrà, A., et al., *Fast and reliable artemisinin determination from different Artemisia annua leaves based alimentary products by high performance liquid chromatography-tandem mass spectrometry.* Food Chem, 2014. **142**: p. 114-20.
126. Jessing, K.K., R.K. Juhler, and B.W. Strobel, *Monitoring of artemisinin, dihydroartemisinin, and artemether in environmental matrices using high-performance liquid chromatography-tandem mass spectrometry (LC-MS/MS).* Journal of agricultural and food chemistry, 2011. **59** **21**: p. 11735-43.

127. Chen, H.L., et al., *On-line conversion and determination of artemisinin using a flow-injection capillary electrophoresis system*. *Electrophoresis*, 2002. **23**(17): p. 2865-71.
128. Asnin, L., et al., *Calibration of a detector for nonlinear chromatography*. *J Chromatogr A*, 2005. **1076**(1-2): p. 141-7.
129. Asnin, L., *Peak measurement and calibration in chromatographic analysis*. *TrAC Trends in Analytical Chemistry*, 2016. **81**.
130. Charles, D., et al., *Germplasm Variation in Artemisinin Content of Artemisia annua Using an Alternative Method of Artemisinin Analysis from Crude Plant Extracts*. *Journal of Natural Products - J NAT PROD*, 2004. **53**.
131. Gupta, M.M., et al., *Isolation of a high artemisinic acid containing plant of Artemisia annua*. *Planta Med*, 1996. **62**(3): p. 280-1.
132. van Agtmael, M.A., T.A. Eggelte, and C.J. van Boxtel, *Artemisinin drugs in the treatment of malaria: from medicinal herb to registered medication*. *Trends Pharmacol Sci*, 1999. **20**(5): p. 199-205.
133. Duke, M.V., et al., *Localization of Artemisinin and Artemisitene in Foliar Tissues of Glanded and Glandless Biotypes of Artemisia annua L.* *International Journal of Plant Sciences*, 1994. **155**: p. 365 - 372.
134. Wallaart, T.E., et al., *Isolation and identification of dihydroartemisinic acid from artemisia annua and its possible role in the biosynthesis of artemisinin*. *J Nat Prod*, 1999. **62**(3): p. 430-3.
135. Spaninks, J.A.M., *Design procedures for solid-liquid extractors and the effect of hydrodynamic instabilities on extractor performance*. 1979, Pudoc: Wageningen.
136. Lucia, A., *Chemical Engineering Design Principles, Practice, and Economics of Plant and Process Design* By G. Towler and R. Sinnott. *AIChE Journal*, 2008. **54**(11): p. 3034-3035.
137. Walas, S.M. *Chemical Process Equipment : Selection and Design*. 1988.
138. Bates, L. *Guide to the Design, Selection, and Application of Screw Feeders*. 2008.
139. KWS. *Screw conveyor engineering guide*. Available from: <https://www.kwsmfg.com/wp-content/themes/va/pdf/Screw-Conveyor-Engineering-Guide.pdf>.
140. screw, S.a.M. *Conveyor components*.
141. *Screw conveyor corporation- Catalog and engineering manuals*. Available from: https://screwconveyor.com/wp-content/uploads/2018/08/Screw-Conveyor-Catalog-SCC_787F.pdf
142. corporation, S.c., *Catalog and Engineering manual*.
143. Krieger, C., *Experimentelle und Theoretische Untersuchung einer kontinuierlichen Gegenstromextraktion zur Gewinnung von Naturstoffen* 2019.
144. toolbox, T.e. *Explosion and Flammability concentration limits*. Available from: www.engineeringtoolbox.com/explosive-concentration-limits-d_423.html.
145. (DGUV), I.-D.G.U.e.V. *Der Berufsgenossenschaft für Chemie-Gestis Tabelle für Toluol*. Available from: <https://gestis.dguv.de/data?name=010070>.

Appendices

Below 28 following appendices will be given:

Appendix A1- Conversion of distribution coefficients.

Appendix A2- Calculation steps of the Kremser method.

Appendix A3- High performance thin layer chromatography (HPTLC) technique.

Appendix A4- The conversion of signal and concentration and HPLC analytical procedures.

Appendix A5- Calibration data of ARTE in Toluene.

Appendix A6- Procedures of LOD and LOQ determination.

Appendix A7- Relevant solvents, equipment, substances in use for analytical methods.

Appendix A8- Kinetics data of ARTE, DHAA extraction in Toluene, n-Hexane and Ethanol.

Appendix A9- Equilibrium data of ARTE and DHAA extraction in different solvents.

Appendix A10- Productivity and recovery calculation of ARTE extraction in Toluene for batch operation.

Appendix A11- Experimental procedures of sequential counter-current equilibrium stage model (Figure 5.3).

Appendix A12- Technical drawings of the extractor and selection of instruments.

Appendix A13- Instrument selection and specifications.

Appendix A14- Explosion protection.

Appendix A15- Assembling and electrical installation.

Appendix A16- Detail of suppliers and manufacturing companies.

Appendix A17- Flowrate, speed measurements for screws (feeder, extractor).

Appendix A18- Pump calibration.

Appendix 19- Glass beads certificate.

Appendix A20- RTD investigation of leaves- Experimental procedures and results.

Appendix A21- Certificate of sodium chloride analysis.

Appendix A22- Specifications of conductivity meter FiveEasy, Mettler Toledo.

Appendix A23- Calibration procedure of sodium chloride solution by FiveEasy conductivity meter.

Appendix A24- Recorded and calculated data of conductivity measurement for one experimental condition.

Appendix A25- Conductivity measuring data of different solvent flowrates and rotational speeds.

Appendix A26- Measurement of raffinate moisture in continuous extraction.

Appendix A27- Continuous experimental procedures.

Appendix A28- Experimental condition at optimized steady state extraction.

In addition, all Codes (Code1 to Code5) are provided on a CD.

Appendix A1- Conversion of distribution coefficients.

It is mentioned that the difference of thermodynamic and efficient distribution coefficients designated as β_i and β_i^{eff} lies in the denominator, therefore, a conversion between them is feasible and plays an essential role because the efficient distribution coefficient β_i^{eff} is significantly depended on the proportions of extract and raffinate phase, while the thermodynamic distribution coefficient β_i shows the relation of the solid and liquid phase at equilibrium.

A dimensionless factor δ_i called capacity factor is the proportion of component i amount in internal extract and that in the solid phase:

$$\delta_i = \frac{m_{i,Li}}{m_{i,S}} = \frac{m_{Li} * x_{i,Li}}{m_S * x_{i,S}} = W * \beta_i \quad (A1.1)$$

From the relation of thermodynamics and effective distribution coefficients in eq. 2.28 and 2.29, we have:

$$\frac{\beta_i^{eff}}{\beta_i} = \frac{\frac{x_{i,L_e}}{x_{i,R}}}{\frac{x_{i,L_e}}{x_{i,S}}} = \frac{x_{i,S}}{x_{i,R}} = \frac{\frac{m_{i,S}}{m_S}}{\frac{(m_{i,S} + m_{i,Li})}{(m_S + m_{Li})}} = \frac{m_{i,S} \left(1 + \frac{m_{Li}}{m_S}\right)}{m_{i,S} + m_{i,Li}} = \frac{1 + \frac{m_{Li}}{m_S}}{1 + \frac{m_{i,Li}}{m_{i,S}}} = \frac{1+W}{1+W*\beta_i} \quad (A1.2)$$

or:

$$\beta_i^{eff} = \frac{\beta_i * (1+W)}{1+W*\beta_i} = \frac{1+W}{\frac{1}{\beta_i} + W} \quad (A1.3)$$

Eq. A1.3 implies that β_i^{eff} can be defined by thermodynamic characteristic β_i and wetting parameter W .

Appendix A2- Calculation steps of the Kremser method.

The component mass balances illustration of stage j :

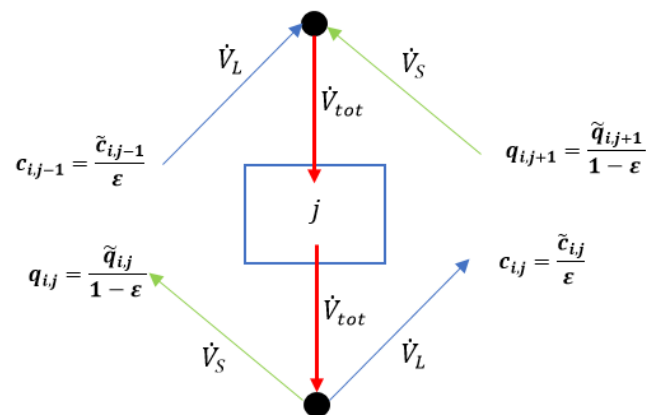


Figure A2.1. Illustration of mass balance of stage j .

As introduced, the relation component mass balance of component i at stage j and two stage $(j - 1)$ and $(j + 1)$ excluding the first and last stages is:

$$\tilde{K}_{i,E}^{eq} \tilde{c}_{i,j-1} - (1 + \tilde{K}_{i,E}^{eq}) \tilde{c}_{i,j} + \tilde{c}_{i,j+1} = 0 \quad i = 1, N_C, j = 2, N_S - 1 \quad (\text{A2.1})$$

The following procedure shows the successive calculation from $1 \rightarrow N_S$

The calculation process is based on mass balances and lumping of stages as follows.

The specific first stage (stage 1) is connected direct to the inlet of the liquid phase, thus, the mass balance holds:

$$\tilde{c}_{i,2} - (1 + \tilde{K}_{i,E}^{eq}) \tilde{c}_{i,1} + \tilde{K}_{i,E}^{eq} \tilde{c}_i^{in} = 0 \quad (\text{A2.2})$$

Since no external streams in the entire cascade, the spatial lumping stage can be carried out very efficient, in which first stage is able to be prolonged by unlimited stages. The first lumping is written for stage $j = 1$ and stage $j^* = 2$ as:

$$\tilde{c}_{i,3} + \tilde{K}_{i,E}^{eq} \tilde{c}_i^{in} - \tilde{c}_{i,1} - \tilde{K}_{i,E}^{eq} \tilde{c}_{i,2} = 0 \quad (\text{A2.3})$$

Substituting of eq. A2.2 into A2.3 gives:

$$\tilde{c}_{i,3} = (\tilde{K}_{i,E}^{eq^2} + \tilde{K}_{i,E}^{eq} + 1) \tilde{c}_{i,1} - (\tilde{K}_{i,E}^{eq^2} + \tilde{K}_{i,E}^{eq}) \tilde{c}_i^{in} \quad (\text{A2.4})$$

Similarly holds for the next extending to stage $j^* = 3$:

$$\tilde{c}_{i,4} + \tilde{K}_{i,E}^{eq} \tilde{c}_i^{in} - \tilde{c}_{i,1} - \tilde{K}_{i,E}^{eq} \tilde{c}_{i,3} = 0 \quad (\text{A2.5})$$

Substitute value of $\tilde{c}_{i,3}$ from eq. A2.4 into eq. A2.5, it holds:

$$\tilde{c}_{i,4} = \left(\tilde{K}_{i,E}^{eq^3} + \tilde{K}_{i,E}^{eq^2} + \tilde{K}_{i,E}^{eq} + 1 \right) \tilde{c}_{i,1} - \left(\tilde{K}_{i,E}^{eq^3} + \tilde{K}_{i,E}^{eq^2} + \tilde{K}_{i,E}^{eq} \right) \tilde{c}_i^{in} \quad (\text{A2.6})$$

Successively implementation of lumping procedure, lumping to stage $j^* = N_S - 1$ with the identical dependence on $\tilde{c}_{i,1}$ and \tilde{c}_i^{in} gives:

$$\tilde{c}_{i,N} = \left(\tilde{K}_{i,E}^{eq^{N-1}} + \dots + \tilde{K}_{i,E}^{eq} + 1 \right) \tilde{c}_{i,1} - \left(\tilde{K}_{i,E}^{eq^{N-1}} + \tilde{K}_{i,E}^{eq^{N-2}} + \dots + \tilde{K}_{i,E}^{eq} \right) \tilde{c}_i^{in} \quad (\text{A2.7})$$

However, the final stage N is direct connected to the material inlet from another end, thus, the mass balance of lumped stage ($j^* = N$) can be expressed for the entire cascade as:

$$\tilde{q}_i^{in} + \tilde{c}_i^{in} - \tilde{q}_{i,1} - \tilde{c}_{i,N} = 0 \quad (\text{A2.8})$$

or multiplying to $\tilde{K}_{i,E}^{eq}$ holds:

$$\tilde{K}_{i,E}^{eq} \tilde{q}_i^{in} + \tilde{K}_{i,E}^{eq} \tilde{c}_i^{in} - \tilde{c}_{i,1} - \tilde{K}_{i,E}^{eq} \tilde{c}_{i,N} = 0 \quad (\text{A2.9})$$

Substituting value of $\tilde{c}_{i,N}$ from eq. A2.7 into A2.9 gives:

$$\tilde{K}_{i,E}^{eq} \tilde{q}_i^{in} = \left(\tilde{K}_{i,E}^{eq^N} + \dots + \tilde{K}_{i,E}^{eq} + 1 \right) \tilde{c}_{i,1} - \left(\tilde{K}_{i,E}^{eq^N} + \tilde{K}_{i,E}^{eq^{N-2}} + \dots + \tilde{K}_{i,E}^{eq^2} + \tilde{K}_{i,E}^{eq} \right) \tilde{c}_i^{in} \quad (\text{A2.10})$$

To simplify the calculation, another dimensionless parameter γ , is introduced as:

$$\gamma_i = \tilde{K}_{i,E}^{eq^N} + \dots + \tilde{K}_{i,E}^{eq} + 1 \quad (\text{A2.11})$$

$$\text{then: } \tilde{K}_{i,E}^{eq} \gamma = \tilde{K}_{i,E}^{eq^{N+1}} + \dots + \tilde{K}_{i,E}^{eq} \quad (\text{A2.12})$$

Now we subtract the eq. A2.12 for A2.11 and notice that almost each term in one equation cancels a term in another one, only two terms left:

$$\tilde{K}_{i,E}^{eq} \gamma_i - \gamma_i = \tilde{K}_{i,E}^{eq^{N+1}} - 1 \quad (\text{A2.13})$$

$$\text{or: } \gamma_i = \frac{\tilde{K}_{i,E}^{eq^{N+1}} - 1}{\tilde{K}_{i,E}^{eq} - 1} \quad (\text{A2.14})$$

As a consequence, the eq. A2.10 is rearranged to gain the $\tilde{c}_{i,1}$ value. The dimensionless parameter γ_i is handled as below:

$$\tilde{K}_{i,E}^{eq} \tilde{q}_i^{in} = \gamma_i \tilde{c}_{i,1} - (\gamma_i - 1) \tilde{c}_i^{in} \quad (\text{A2.15})$$

means:

$$\tilde{c}_{i,1} = \left(\frac{\tilde{K}_{i,E}^{eqN+1} - \tilde{K}_{i,E}^{eq}}{\tilde{K}_{i,E}^{eqN+1} - 1} \right) \tilde{c}_i^{in} + \left(\frac{\tilde{K}_{i,E}^{eq} - 1}{\tilde{K}_{i,E}^{eqN+1} - 1} \right) \tilde{K}_{i,E}^{eq} \tilde{q}_i^{in} \quad (\text{A2.16})$$

Eq. A2.16 shows that the concentration of component i in the liquid phase at the first stage. It relies only on the inlet liquid concentration of component i \tilde{c}_i^{in} and the quality of the solid phase (plant material) \tilde{q}_i^{in} .

Similarly, the calculation of the cascade can be carried in opposite direction as follows. The mass balance for stage j in eq. A2.1 is divided by $\tilde{K}_{i,E}^{eq}$, then, it holds:

$$\frac{1}{\tilde{K}_{i,E}^{eq}} \tilde{c}_{i,j+1} + \tilde{c}_{i,j-1} - \frac{1}{\tilde{K}_{i,E}^{eq}} \tilde{c}_{i,j} - \tilde{c}_{i,j} = 0 \quad i = 1, N_C, j = 2, N_S - 1 \quad (\text{A2.17})$$

Applying for stage N and rearrange the equation:

$$\tilde{c}_{i,N-1} = \left(\frac{1}{\tilde{K}_{i,E}^{eq}} + 1 \right) \tilde{c}_{i,N} - \tilde{q}_i^{in} \quad (\text{A2.18})$$

Analogously manipulated steps as above, writing the lumping mass balance for the both stage $j = N$ and $j^* = N - 1$, we have:

$$\tilde{c}_{i,N-2} - \frac{1}{\tilde{K}_{i,E}^{eq}} \tilde{c}_{i,N-1} - \tilde{c}_{i,N} + \tilde{q}_i^{in} = 0 \quad (\text{A2.19})$$

Substituting the value of $\tilde{c}_{i,N-1}$ in eq. A2.18 into A2.19 results:

$$\tilde{c}_{i,N-2} = \left(\frac{1}{\tilde{K}_{i,E}^{eq^2}} + \frac{1}{\tilde{K}_{i,E}^{eq}} + 1 \right) \tilde{c}_{i,N} - \left(\frac{1}{\tilde{K}_{i,E}^{eq}} + 1 \right) \tilde{q}_i^{in} \quad (\text{A2.20})$$

By lumping repeat for successive steps until $j^* = 2$, the extract composition can be identically expressed as:

$$\tilde{c}_{i,1} = \left(\frac{1}{\tilde{K}_{i,E}^{eqN-1}} + \dots + 1 \right) \tilde{c}_{i,N} - \left(\frac{1}{\tilde{K}_{i,E}^{eqN-2}} + \dots + 1 \right) \tilde{q}_i^{in} \quad (\text{A2.21})$$

The first stage (stage 1) connects to fresh solvent and performs identical form of entire cascade given in eq. A2.8. and it can be manipulated to gain this form:

$$\tilde{q}_i^{in} + \tilde{c}_i^{in} - \frac{1}{\tilde{K}_{i,E}^{eq}} \tilde{c}_{i,1} - \tilde{c}_{i,N} = 0 \quad (\text{A2.22})$$

Substituting the value of $\tilde{c}_{i,1}$ in eq. A2.21 into A2.22 gives:

$$\tilde{c}_i^{in} = \left(\frac{1}{\tilde{K}_{i,E}^{eqN}} + \dots + \frac{1}{\tilde{K}_{i,E}^{eq}} + 1 \right) \tilde{c}_{i,N} - \left(\frac{1}{\tilde{K}_{i,E}^{eqN}} + \dots + \frac{1}{\tilde{K}_{i,E}^{eq}} \right) \tilde{K}_{i,E}^{eq} \tilde{q}_i^{in} \quad (\text{A2.23})$$

To simplify the calculation, a dimensionless factor η_i is introduced as:

$$\eta_i = \tilde{K}_{i,E}^{eq-N} + \tilde{K}_{i,E}^{eq-(N-1)} + \dots + \tilde{K}_{i,E}^{eq-1} + 1 \quad (\text{A2.24})$$

$$\tilde{K}_{i,E}^{eq-1} \eta_i = \tilde{K}_{i,E}^{eq-(N+1)} + \tilde{K}_{i,E}^{eq-N} + \dots + \tilde{K}_{i,E}^{eq-2} + \tilde{K}_{i,E}^{eq-1} \quad (\text{A2.25})$$

thus:

$$\tilde{K}_{i,E}^{eq-1} \eta_i - \eta_i = \tilde{K}_{i,E}^{eq-(N+1)} - 1 \quad (\text{A2.26})$$

$$\text{and: } \eta_i = \frac{\tilde{K}_{i,E}^{eq-(N+1)} - 1}{\tilde{K}_{i,E}^{eq-1} - 1} \quad (\text{A2.27})$$

Substituting the η_i value from eq. A2.27 to A2.23, it holds:

$$\tilde{c}_i^{in} = \eta_i \tilde{c}_{i,N} - (\eta_i - 1) \tilde{K}_{i,E}^{eq} \tilde{q}_i^{in}$$

or:

$$\tilde{c}_i^{in} = \left(\frac{\tilde{K}_{i,E}^{eq-(N+1)} - 1}{\tilde{K}_{i,E}^{eq-1} - 1} \right) \tilde{c}_{i,N} - \left(\frac{\tilde{K}_{i,E}^{eq-N} - 1}{\tilde{K}_{i,E}^{eq-1} - 1} \right) \tilde{K}_{i,E}^{eq} \tilde{q}_i^{in} \quad (\text{A2.28})$$

Then,

$$\tilde{c}_{i,N} = \left(\frac{\tilde{K}_{i,E}^{eq-1} - 1}{\tilde{K}_{i,E}^{eq-(N+1)} - 1} \right) \tilde{c}_i^{in} + \left(\frac{\tilde{K}_{i,E}^{eq-N} - 1}{\tilde{K}_{i,E}^{eq-(N+1)} - 1} \right) \tilde{q}_i^{in} \quad (\text{A2.29})$$

Eq. A2.16 and A2.29 show the compositions of the liquid phase at two ends of the cascade and are summarized as eqs. 3.75 and 3.76 in section 3.2.

The outgoing concentrations of the liquid and solid phases at both ends of the cascade (A2.16 and A2.29) can be easily solved by a Matlab code (*Code4*). This code allows us to calculate the concentrations at every stages inside cascade based on recursive calculation.

Appendix A3- High performance thin layer chromatography (HPTLC) technique.**a) Analytical procedures**

For a specific ARTE analytical case, these following steps are implemented:

- The pre-coated silica gel 60 F254 plate is purchased from Merck, the positions of samples, standards, the baseline are marked and the names of corresponding points are assigned (Figure 4.4).
- The developing chamber is prepared by a mixture of solvent reported in [94] of n-hexane:ethyl acetate (75:25,v/v) and is completely closed in 30 minutes to saturate the air inside by solvent molecules before developing the samples.
- The ARTE in Methanol calibration standard is prepared at 0.2 mg/mL, the concentrations of each standard position are proportional to the applying amount of standard. As a result, a linear calibration curve was achieved in the range 0.4÷2.8 mg/mL (Figure A3.1).
- To derivatize the developed TLC plates, an anisaldehyde-sulfuric acid reagent is prepared by mixing 500 mL acetic acid and 5 mL anisaldehyde, then again mixed with 10 mL sulfuric acid to complete the reagent.

The relevant samples and standards are prepared and controlled by a syringe integrated on Sampler Linomat 5. These samples and standards corresponding to marked spots are applied in a volume of 1 μ L at 6 mm wide-band on silica gel plate at 10 mm from the base (Figure 4.4). The plate is developed in the twin-trough chamber until the solvent front at 95 mm is reached, then, it is taken out of the chamber and dried by air-dryer. The mobile liquid phase is evaporated completely, then, the plate is dipped into prepared anisaldehyde-sulfuric acid prepared derivatization mixture. Afterwards, the plate is heated at 110°C in 10 minutes. The derivatized plate is placed into TLC Scanner 4 and detected at 520 nm using tungsten lamp. It is noticed that each measurement is implemented by analysis of standards and sample in parallel, in which each standard and sample are always duplicated.

b) Calibration data for HPTLC analysis

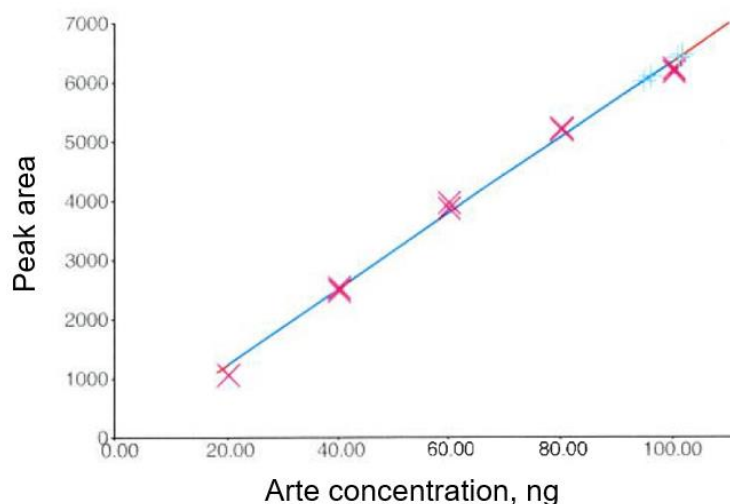
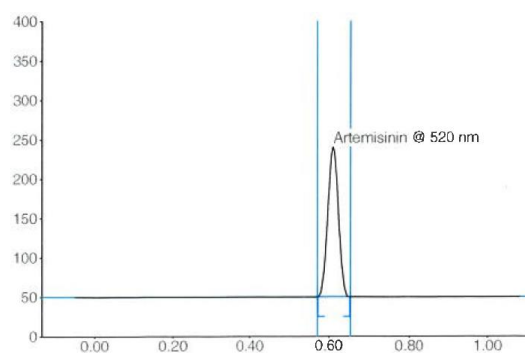
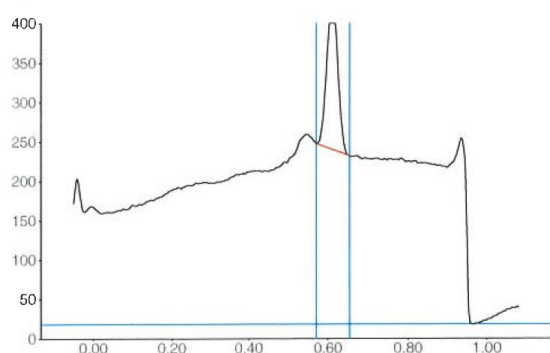


Fig.A3.1. An analytical data with ARTE calibration standards ad samples.

Fig.A3.1 shows the relation of concentration and the area of the peaks detected by Scanner 4, in which the data of standards are pink points and the blue points represent the extract composition. Both standards and samples are always duplicated to ensure the accuracy of analysis.

c) The HPTLC ARTE standard in Ethyl acetate at 520nm

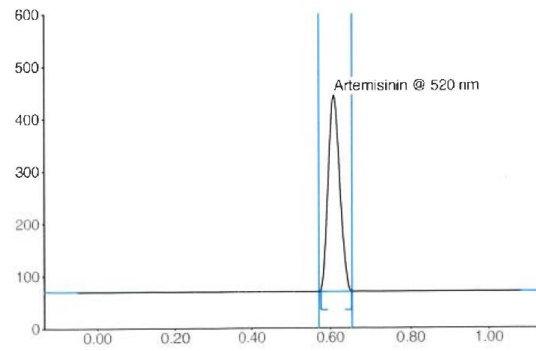
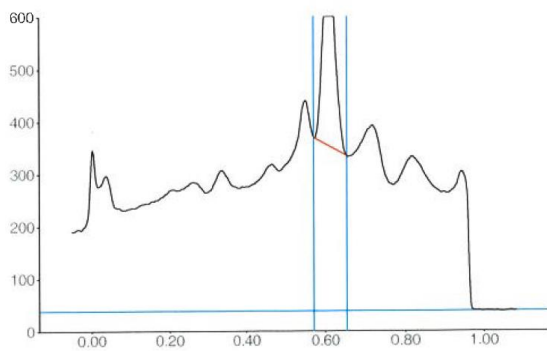
Track 9, ID: Standard3



Peak	Start Rf	Start Height	Max Rf	Max Height	Max %	End Rf	End Height	Area	Area %	Assigned substance
1	0.57	0.1	0.61	190.3	100.00	0.65	0.2	3854.2	100.00	Artemisinin

d) The HPLC extract concentration profile in Ethyl acetate at 520nm

Track 12, ID: V3_3_60mins_2gAA_10gEthAc



Peak	Start Rf	Start Height	Max Rf	Max Height	Max %	End Rf	End Height	Area	Area %	Assigned substance
1	0.58	1.5	0.61	374.7	100.00	0.65	0.9	8220.6	100.00	Artemisinin

Appendix A4- The conversion of signal and concentration and HPLC analytical procedures.

A4.1. The relation of signal and concentration in HPLC analysis

The general solute concentration, C_i^{inj} at the inlet and the detected signal, S at the outlet can be illustrated as follows:

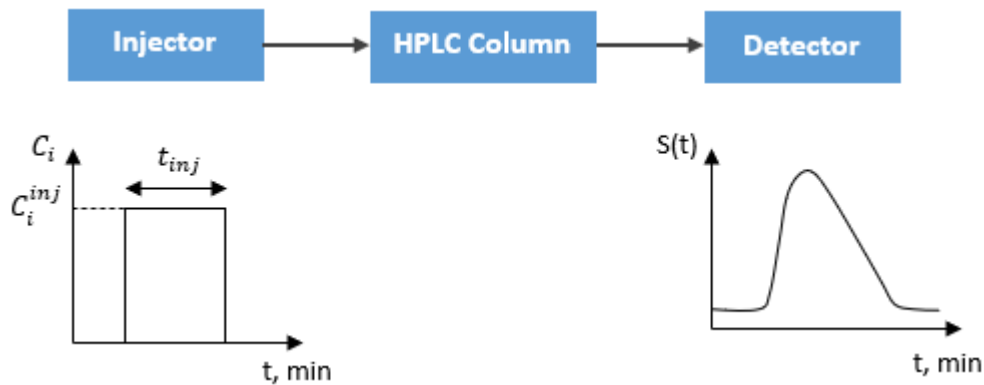


Fig.A4.1. Relation between input and output of an analysis.

At the inlet, the mass of the solute m_i^{inlet} is absolutely known and can be calculated as:

$$m_i^{inlet} = V_{inj} C_i^{inj} = \dot{V} t_{inj} C_i^{inj} \quad (\text{A4.1})$$

within, \dot{V} is flowrate of mobile phase, t_{inj} is injection time and C_i^{inj} represents concentration of solute i in initial sample.

The relative affinity of the solute for mobile and stationary phase results the difference in the retention of solute and gives the response as a function of time. Means,

$$m_i^{outlet} = \dot{V} \int_0^{\infty} C_i^{out}(t) dt \quad (\text{A4.2})$$

In another hand, the detector response relates to the concentration via a factor F :

$$S(t) = F \times C_i^{out}(t) \quad (\text{A4.3})$$

Obviously, the amount of solute at the inlet and that at the outlet remains constant, thus:

$$V_{inj}C_i^{inj} = \frac{\dot{V}}{F} \int_0^{\infty} S(t)dt \quad (A4.4)$$

Manipulating eq. A4.4 with the understanding that the definite integral of response from zero to infinity is the peak area, whence:

$$A_{peak} = \frac{V_{inj}F}{\dot{V}} C_i^{inj} = Ft_{inj}C_i^{inj} \quad (A4.5)$$

Eq. A4.5 performs the relation between the peak area A_{peak} and the concentration of a certain solute i , C_i^{inj} via conversion factor F . While, the injection time of sample t_{inj} implies to injection volume V_{inj} and flowrate of mobile phase \dot{V} and is constant for the whole analysis.

Therefore, the preparation of a series of known concentration samples, called standards, C_i^{std} results the corresponding standard peak areas A_{peak}^{std} which are detected and recorded by system. Then, the calibration curve showing the relation of known concentration and peak areas is plotted (Fig.A4.2), in which factor F is revealed

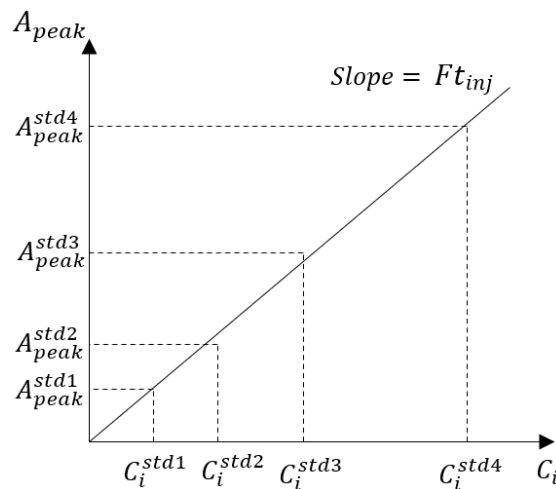


Fig.A4.2. The relation of peak area and concentration (calibration curve).

When any samples with unknown solute concentration is injected, it will give a peak area. As a consequence, the sample concentration is back calculated based on the measured area and calibration curve.

Based on that relation, whenever any parameter, e.g. injection volume, mobile phase flowrate... is changed, calibration process needs to be renewed. It should be noticed that, each solute will have different calibration curve.

Nonetheless, due to the nature of interactions involved, the response of ELSD can not be related to the mass of the solute by a linear equation. This relation is often recommended by an exponential:

$$S(t) = a(C_i(t))^b \quad (\text{A4.6})$$

within, a,b are two constants basically defined by the nature of the mobile phase. But for the large concentration range, this expression is not applicable anymore and it requires more complex models to be used. In the case of ARTE analysis, the calibration curve of HPLD-ELSD is fit by quadratic equation.

A4.2. Typical HPLC analytical procedures

A schedule for ARTE and DHAA analysis of crude extract can be established based on the introduced analytical system as follows:

Calibration

The target concentration of crude extract can be varied in very wide range based on the extraction method and the post treatment processes, thus, the standards of ARTE/DHAA in corresponding solvents are prepared in very wide concentration range from 0,01 to 0,5 wt% corresponding to 15 different standards. The calibration curve can be built up by three different small, middle and large concentration range to assure the accuracy of measurements. The general calibration curves are referred in *Appendix A5*.

Samples

The samples obtained by relevant extraction methods are filtered by 0.2 µm filter from Wicom and preserved in 2 mL glass vials before analysis. Sometimes, these vials can be immediately analyzed or stored in fridge at 4 degree Celsius until HPLC available.

Analysis

The samples are allocated in a sequence of measurement, in which two extra control samples are put in the sequence together. These control samples are fresh prepared with a defined concentration in order to confirm the accuracy of the measurements. The measure starts analyzing first two control samples, then the extract samples are successively detected. The two control samples are again analyzed at the end of measurement. The confirmation of control sample concentration ensures the accuracy and precision of the measurements.

The relevant information of used solvents, equipment, elements and substances are listed in *Appendix A7*.

Appendix A5- Calibration data of ARTE in Toluene.

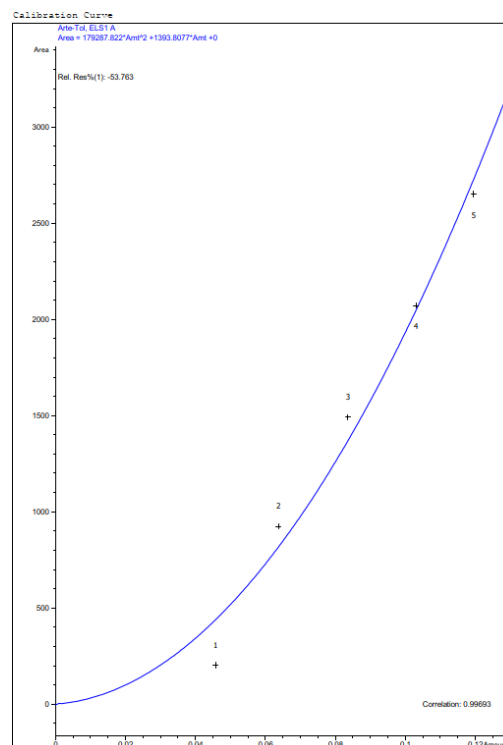
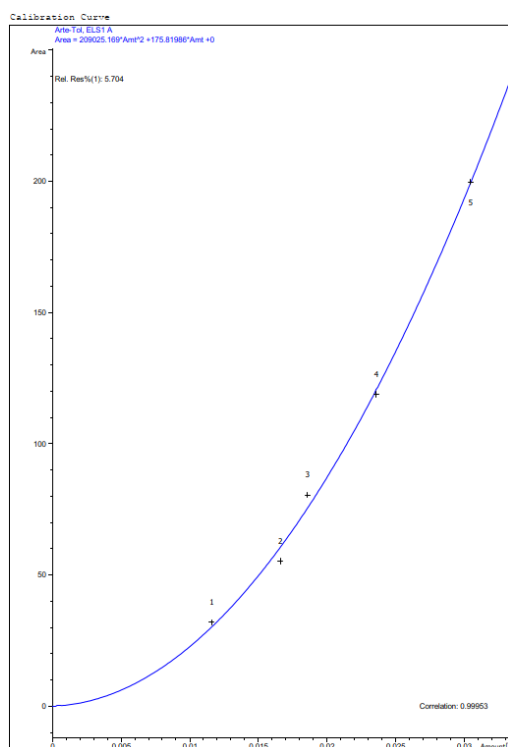


Fig A5.1. Calibration in small concentration range **Fig A5.2.** Calibration in middle concentration range

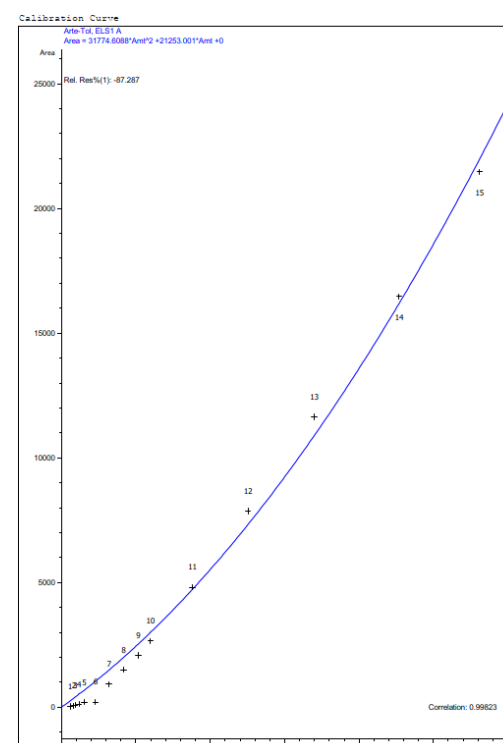
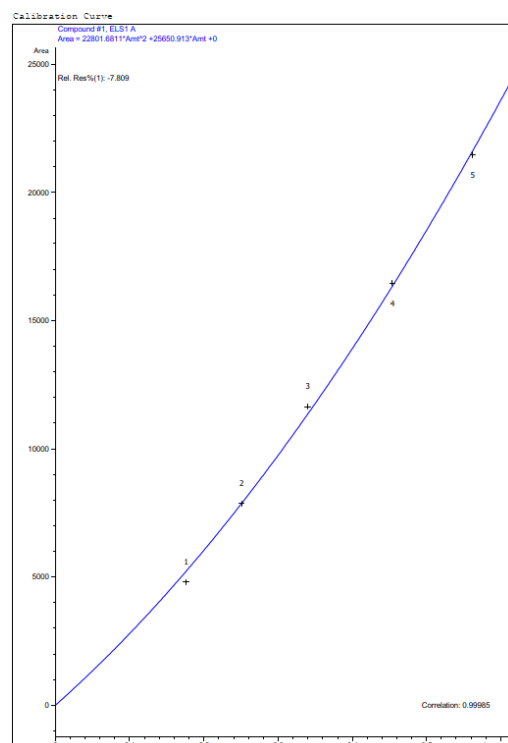


Fig A5.3. Calibration in high concentration range

Fig A5.4. Calibration in the whole range

Appendix A6- Procedures of LOD and LOQ determination.

The measurement is carried out by using the experimental setup in Fig.A6.1. In which, LOD and LOQ are measured isocratic and gradient elution.

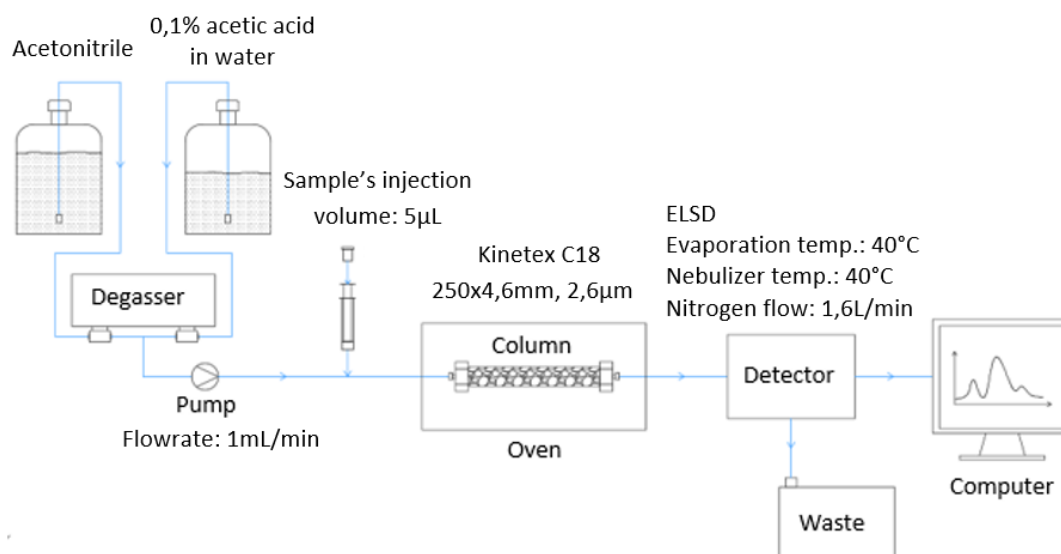


Fig.A6.1. The experimental setup of LOD and LOQ of ARTE and DHAA in Toluene

The samples are prepared in different concentration by mixing the ARTE or DHAA with relevant Toluene amount. 5µL of each sample is injected by automated injector. The mobile phase is supplied by two channel A and B of Acetonitrile and 0,1% acetic acid in water respectively. The isocratic is set at 80% channel A and 20% channel B, while gradient elution is followed by introduced in Table 4.1. The results are reported below.

Isocratic elution

ARTE samples [wt%]	S / N ratio
$1,992 \times 10^{-1}$	2400
$2,344 \times 10^{-2}$	57
$9,917 \times 10^{-3}$	11
$8,01 \times 10^{-3}$	5,8
$3,958 \times 10^{-3}$	2
$1,893 \times 10^{-3}$	1,4
$3,128 \times 10^{-4}$	-

Gradient elution

ARTE samples [wt%]	S / N ratio
$1,992 \times 10^{-1}$	13400
$2,344 \times 10^{-2}$	1060
$1,893 \times 10^{-3}$	14
$3,128 \times 10^{-4}$	3,5
$9,899 \times 10^{-5}$	3,5

Fig.A6.2. The detection results of ARTE in Toluene

Isocratic elution

DHAA samples [wt%]	S / N ratio
$9,946 \times 10^{-2}$	480
$3,063 \times 10^{-2}$	48
$1,998 \times 10^{-2}$	19
$1,21 \times 10^{-2}$	7
$8,987 \times 10^{-3}$	4
$7,797 \times 10^{-3}$	3
$6,997 \times 10^{-3}$	2
$5,003 \times 10^{-3}$	1,5

Gradient elution

DHAA samples [wt%]	S / N ratio
1×10^{-1}	-
$9,946 \times 10^{-2}$	-
$1,213 \times 10^{-2}$	4
$8,987 \times 10^{-3}$	4
$6,997 \times 10^{-3}$	3
5×10^{-3}	3

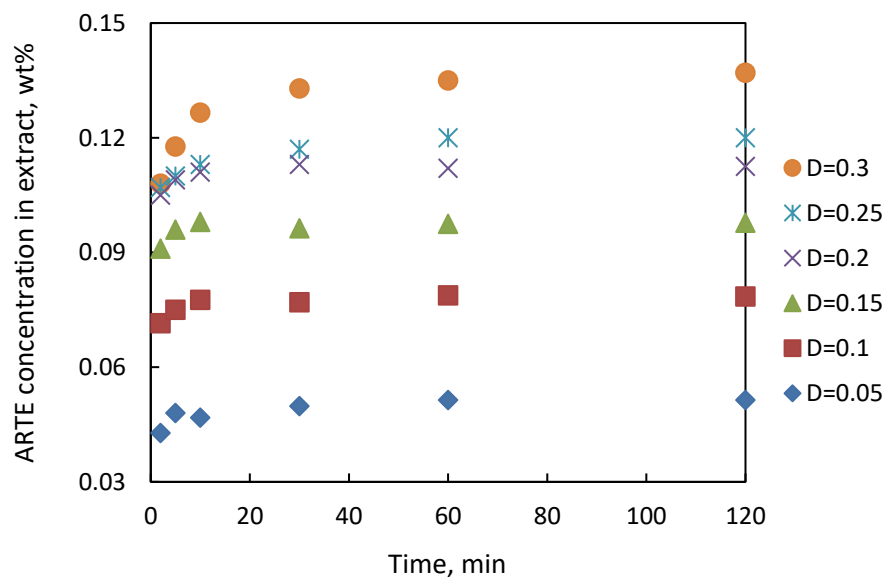
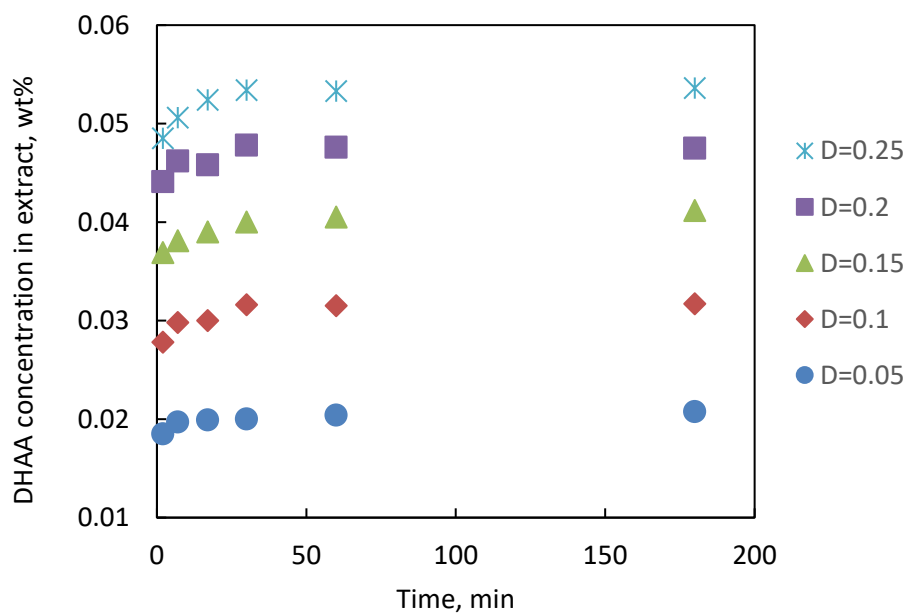
Fig.A6.3. The detection results of DHAA in Toluene

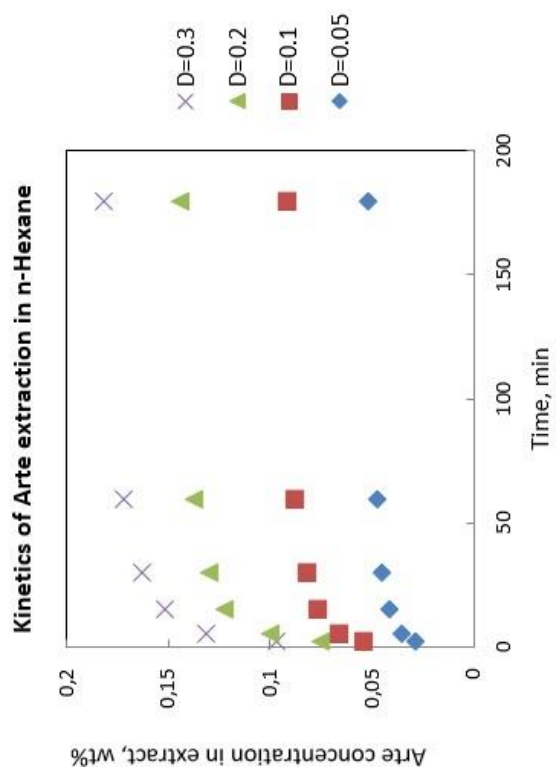
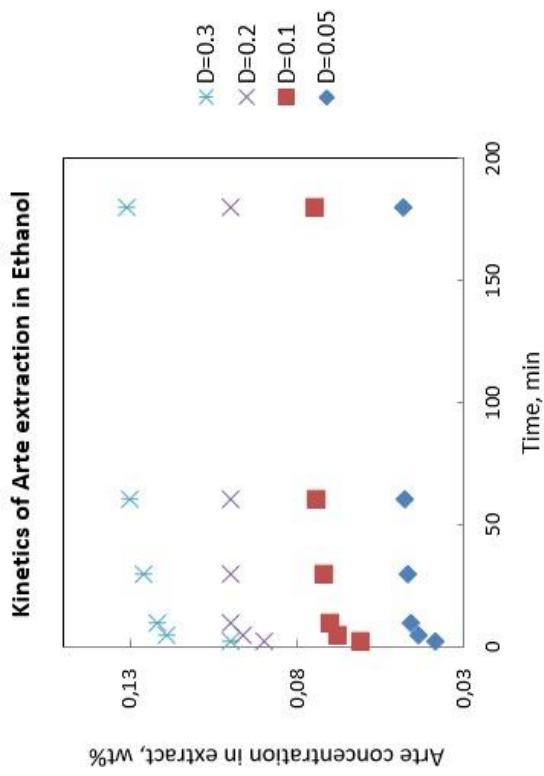
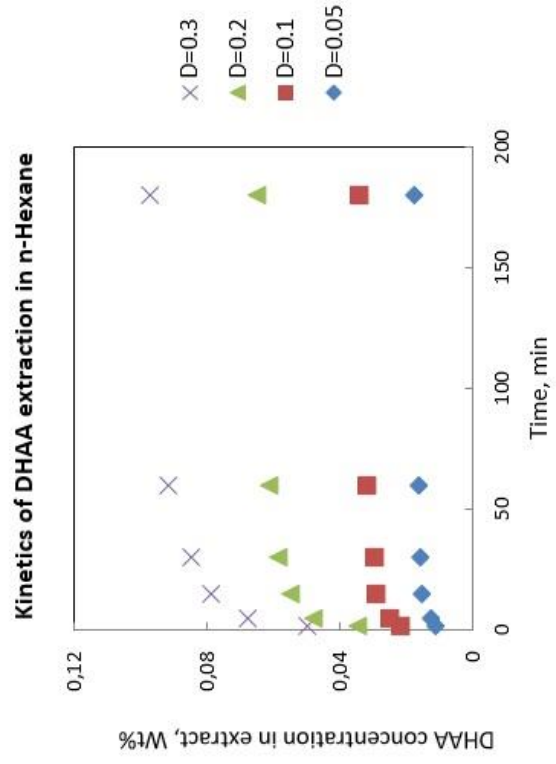
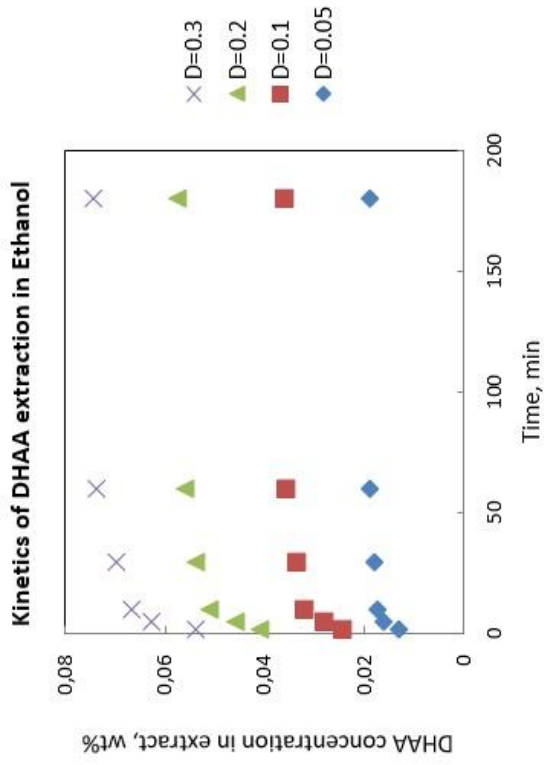
In case of DHAA in Toluene at high concentration, no clear evaluation possible, it might result from impurities.

As a result, the summarized data of LOD and LOQ for ARTE and DHAA in Toluene is performed in Table 4.2 in chapter 4.

Appendix A7- Relevant solvents, equipment, substances in use for analytical methods.

Nr.	Name/Type	Characteristics/ Series	Dimension / Volume	Supplier
1	Artemisinin (ARTE)	Purity: >97%	5g	Tokyo Chemical Industry
2	Dihydroartemisinic acid (DHAA)	Purity > 98%	50g	CFM Tropitzsh
3	HPLC	HP 1100 Open LAB CDS (A.02.14.29)	-	Agilent
4	HPLC Column	C18 Stationary phase, Particle size: 2,6µm	250x4,6 mm	Kinetex
5	Evaporative Light Scattering Detector(ELSD)	1290 Infinity II G7102A	-	Agilent
6	Diode array detector (DAD)	G1315A	-	Agilent
7	HPLC quaternary pump	G1311A	-	Agilent
8	HPLC autosampler	G1313A	-	Agilent
9	Microwave extraction system	MARS 6	-	CEM
10	HPTLC precoated plate	Silica gel 60 F254	20x20cm	Merck
11	TLC scanner	Scanner 4 winCATS software	-	CAMAG
12	TLC semi-auto sampler	Linomat 5	-	CAMAG
13	Toluene	Purity > 99,5%	2,5L	VWR Chemicals
14	Ethanol	Purity: 99,7%	2,5L	VWR Chemicals
15	Acetonitrile	Purity: 99,95%	2,5L	VWR Chemicals
16	n-Hexane	Purity: >97%	2,5L	VWR Chemicals
17	Acetic acid	HPLC grade	0,5L	Fisher Scientific
18	Sulfuric acid			
19	Filter	Cellulose 0,2µm	13mm	WICOM

Appendix A8- Kinetics data of ARTE, DHAA extraction in Toluene, n-Hexane and Ethanol.**Fig A8.1.** ARTE extraction in Toluene**Fig A8.2.** DHAA extraction in Toluene



Appendix A9- Equilibrium data of ARTE and DHAA extraction in different solvents.

Nr.	Experimental condition	m_Leaves	Residence time (mins)	Collected extract (g)	Retained extract (g)	Arte-ELSD	Arte in Extract (mg)	Max. Arte in leaves (mg)	Arte in Raffinate (mg)	Arte in Raffinate (wt%)	Arte in solid (mg)	Conc.Arte in solid (wt%)	DHAA-DAD	DHAA in Extract (mg)	Max. DHAA (mg)	DHAA in Raffinate (mg)	DHAA in Raffinate (wt%)	DHAA in solid (mg)	Conc. DHAA in solid (wt%)
1	1.5g AA in 30g Toluene, 310rpm, room temperature	1,5	180	26.1	4.1	0.053	13.83	16.65	2.82	0.05	0.644	0.043	0.0171	4.4631	5.55	1.0869	0.019	0.3858	0.026
2	3g AA in 30g Toluene, 310rpm, room temperature	3	180	22.5	8.1	0.08	18.00	33.3	15.30	0.14	8.82	0.294	0.0258	5.805	11.1	5.295	0.048	3.2052	0.107
3	4.5g AA in 30g Toluene, 310rpm, room temperature	4,5	180	19.4	10.6	0.0994	19.28	49.95	30.67	0.20	20.13	0.447	0.0321	6.2274	16.65	10.4226	0.069	7.02	0.156
4	6g AA in 30g Toluene, 310rpm, room temperature	6	180	16.1	13.9	0.1136	18.29	66.6	48.31	0.24	32.52	0.542	0.0372	5.9892	22.2	16.2108	0.081	11.04	0.184
5	7.5g AA in 30g Toluene, 310rpm, room temperature	7,5	180	12.8	17.2	0.1276	16.33	83.25	66.92	0.27	44.97	0.600	0.0415	5.312	27.75	22.438	0.091	15.3	0.204
6	9g AA in 30g Toluene, 310rpm, room temperature	9	180	9.8	20.2	0.14	13.72	99.9	86.18	0.30	57.9	0.643	0.0461	4.5178	33.3	28.7822	0.099	19.47	0.216

Table A9.1. Recorded and measured data of *Artemisia annua* L. extraction in Toluene.

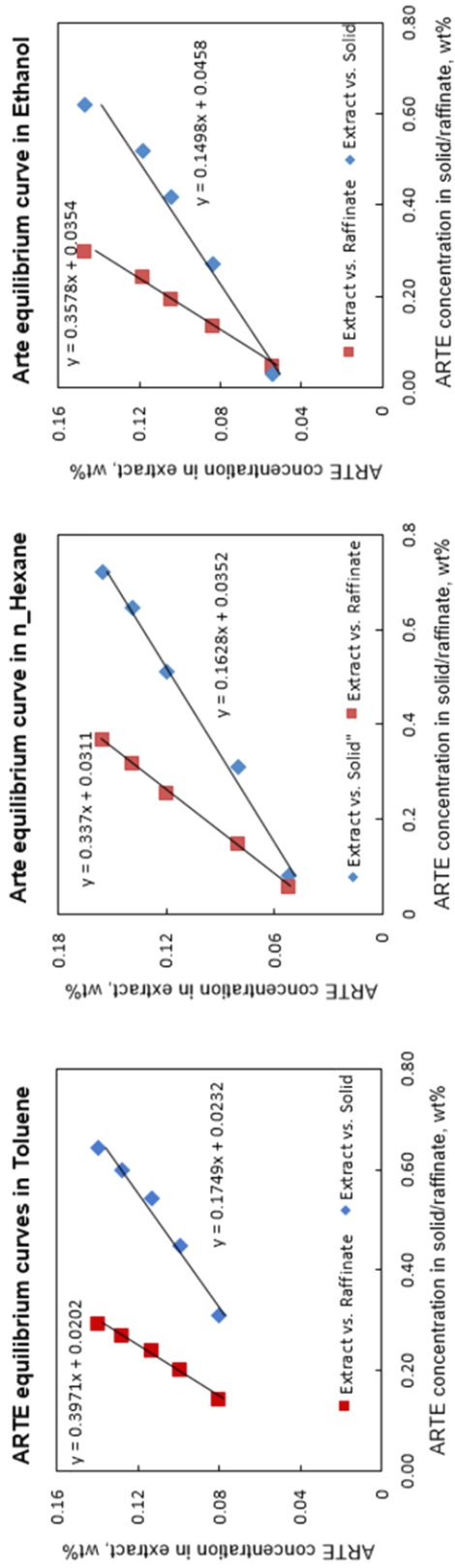


Fig. A11.1. Equilibrium data and distribution coefficients of ARTE extraction in different solvent.

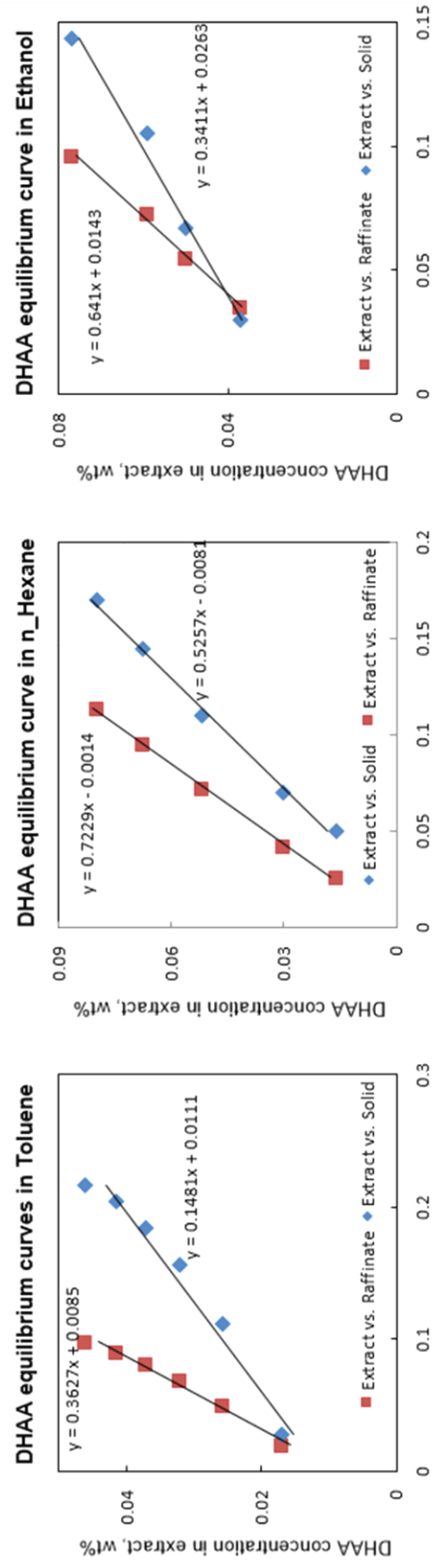


Fig. A9.2. Equilibrium data and distribution coefficients of DHAA extraction in different solvent.

Appendix A10- Productivity and recovery calculation of ARTE extraction in Toluene for batch operation.

Experiment condition	m_S [g]	m_L [g]	Dosage D [-]	Maximal Arte m_ARTE,S,0 [g]	Obtained ARTE, m_ARTE,E [g]	Scale [L]	Cycle time τ_{cycle} [h]	Prod [g/L/h]	Rec [%]
ARTE extraction from <i>Artemisia annua</i> L. at 300rpm, room temperature	1.5	30	0.05	0.0195	0.014	0.041	0.5	0.69	72.4
	3	30	0.10	0.039	0.019	0.043	0.5	0.87	47.7
	4.5	30	0.15	0.0585	0.020	0.045	0.5	0.88	33.8
	6	30	0.20	0.078	0.019	0.046	0.5	0.81	24.0
	7.5	30	0.25	0.0975	0.017	0.047	0.5	0.71	17.2
	9	30	0.30	0.117	0.014	0.048	0.5	0.57	11.7

Table A10.1. Measured and calculated productivity and recovery of ARTE batch extraction in Toluene

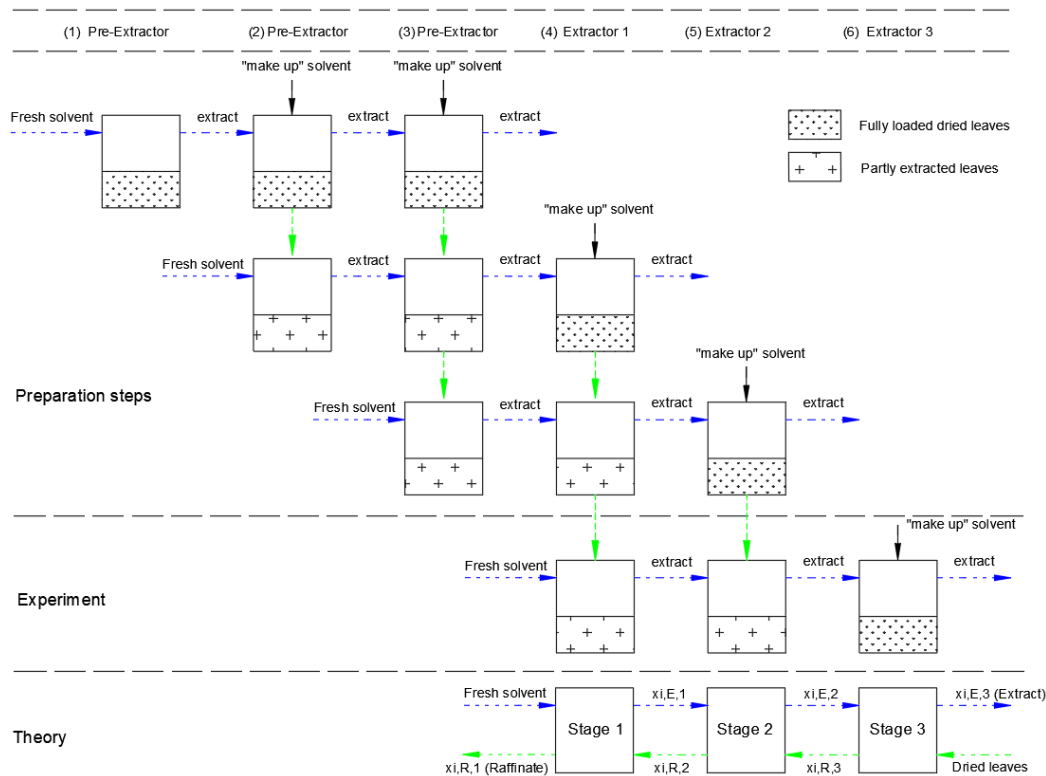
The evaluation is based on two main objective functions (eqs.(5.2)(5.3)):

$$Prod_{ARTE}^{batch} \left(\frac{g}{h \times L} \right) = \frac{m_{ARTE,E}(g)}{\tau_{cycle}(h) \times Scale(L)} = \frac{m_E \times x_{ARTE,E}}{(t_{extraction} + t_{dead}) \times (1 + \theta) V_{suspension}} \quad (A10.1)$$

$$Rec_{ARTE}^{batch} (\%) = \frac{m_{ARTE,E}(g)}{m_{ARTE,S,0}(g)} \times 100 \quad (A10.2)$$

Within, the obtained amount of ARTE, $m_{ARTE,E}$ in corresponding dosages are measured and extracted by measurement data (Table A10.1); the *Scale* factor is based on free volume V_{free} (eq. (2.20)); the cycle time τ_{cycle} consists of extraction time $t_{extraction}$ and the preparing, cleaning, weighing time for the next runs t_{dead} . The maximal ARTE concentration in leaves $m_{ARTE,S,0}$ is 1,3 wt% based on dried weight, thus, the mass of ARTE in the entire leaves portion is depended on the mass of leaves in use.

Appendix A11- Experimental procedures of sequential counter-current equilibrium stage model (Figure 5.3).



In this experimental setup, three preparation extractors (designated as pre-extractors 1 to 3) and three main extractors (numbered from 4 to 6) arranged from left to right are in use. Each phase shift is implemented after a complete batch extraction process. It should be noticed that only extractors with sub-numbered 1 (e.g. 2-1, 3-1, 4-1, ...) are filled by fully loaded dried leaves and an identical amount of retained liquid masses, called “make-up” solvent. This compensation helps to maintain the dosages of all extractors. The sub-numbered indications on the extractors show the number of contacts of the same extractor, e.g. the extractor 2-1 implies to the first contact, 2-2 as second contact and so on, this numbering method is further used for other extractors as well.

The process is started by filling the first three pre-extractors (1,2,3) with dried leaves, the fresh solvent is added to pre-extractor 1-1 to the desired dosage, then, the mixture is agitated to equilibrium, the separated extract without leaves is transported to the next pre-extractor 2-1. Pre-extractor 2-1 is prepared by filling dried leaves and an amount of “make up” solvent, then, this mixture is mixed to the extract portion

from previous pre-extractor 1-1. This mixing ensures the constant dosage to previous one. The entire mixture is again stirred until equilibrium, then it is separated into two phases again: extract and raffinate phase. The transparent extract is taken out and moved to pre-extractor 3-1, while the raffinate is left in the same extractor and contacted again with a certain amount of fresh solvent, this mix establishes extractor 2-2. The implementation, phase transportation and procedures for other extractors are similarly carried out as above steps and followed by the arrow signs.

The analysis of target concentration in extract of extractors 4-3, 5-2 and 6-1 gives the concentration profile of multi-stage counter-current extraction process.

The challenging of preparing the depleted leaves and concentrated extract inside cascade is clearly solved by this setup. The comparison of the simulated and experimental results shows a good agreement of extract concentration at the outlet.

Table A11.1. Experimental and calculated data in sequential counter-current ARTE extraction. *The collected extract amounts $m_{E,j}$ are 23g, the cycle time t_{cycle} including extraction $t_{extraction}$ and dead time t_{dead} is 0.5h and the free volumes equals to 0.04L for all stage.*

Number of stages N	$x_{ARTE,E,N}$ [wt%]	t_{cycle} [h]	Volume [L]	$Prod_{ARTE,real}^{Multi}$ [g/h/L]	Rec_{ARTE}^{Multi} [%]
2-stage	0.115	0.5	0.04	1.32	67
3-stage	0.124	0.5	0.04	1.43	73
5-stage	0.14	0.5	0.04	1.61	82

Appendix A12- Technical drawings of the extractor and selection of instruments.

After estimating the extractor dimension, it is necessary to construct the relevant parts and instruments. The selection and constructing works are briefly described as below.

- *Screw feeder*: the leaves flowrate is precisely controlled by an automated screw conveyor (*Appendix A12.3*).
- *Conical tank*: a container of the dried leaves, which can avoid channeling, bridging phenomenon, is a need. A simple transparent conical shape with adjustable angles is built up and a 5° conical angle is selected and manufactured by Siesing GmbH (*Appendix A12.4*).
- *Perforated disk*: the friction is proportional to the surface area of the disk depended on the diameter of the holes on the disk. The smaller the diameters of the holes are, the higher the surface area is, however, the small holes limit the leaves waste. Thus, the appropriate diameter of the holes is constructed at 5.5mm (*Appendix A12.5*).
- *Raffinate and extract containers*: safety canisters in electrostatic conductive PE-HD purchased from S.C.A.T Europe are used to avoid the ignition risks for flammable liquids. Additional trays are constructed under the canisters and an elastic sector is bound to ensure the accuracy of measurements. (*Appendix A12.6*).
- *Sight glass*: a sight glass is constructed to observe the continuity of input leaves flow (*Appendix A12.7*). Besides, two other sight glass are constructed at the raffinate chamber and above leaves inlet to observe the status of raffinate and leaves flows.
- *Gasket material*: the sealing among flanges should be able to resist the relevant chemical environment, therefore, the EPDM material is chosen to seal the connection between flanges.

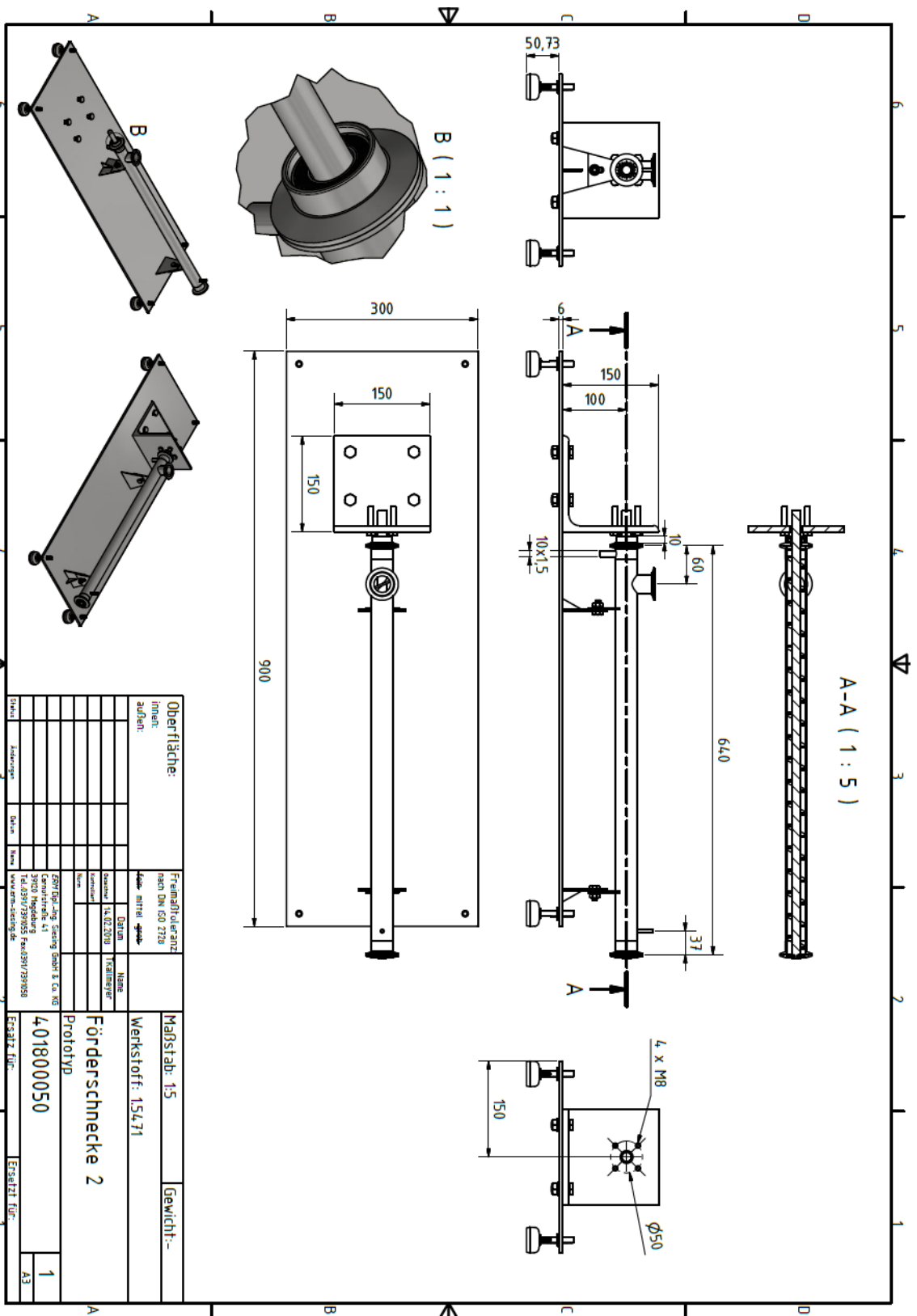


Fig. A12.2. Main extractor technical drawing.

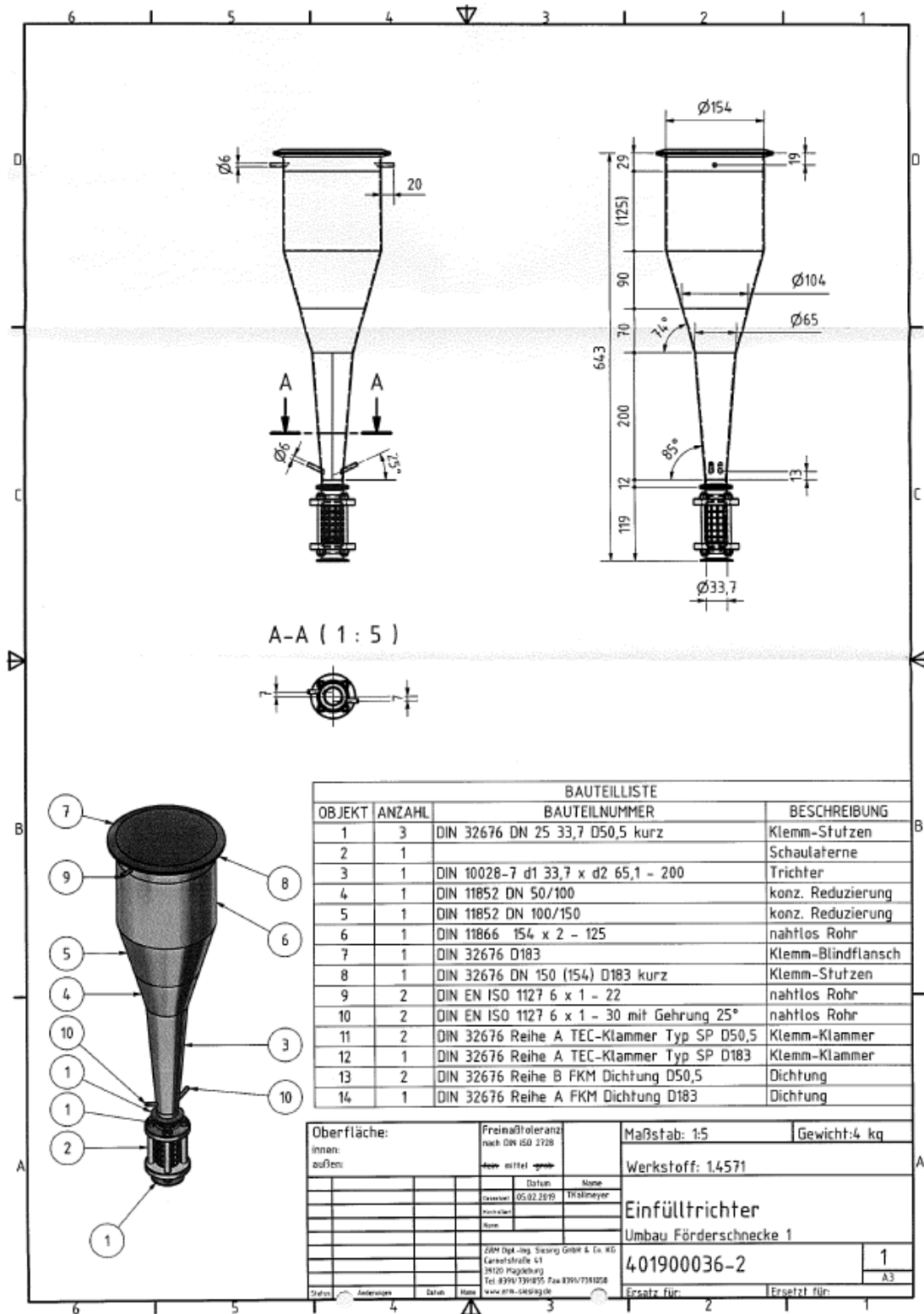
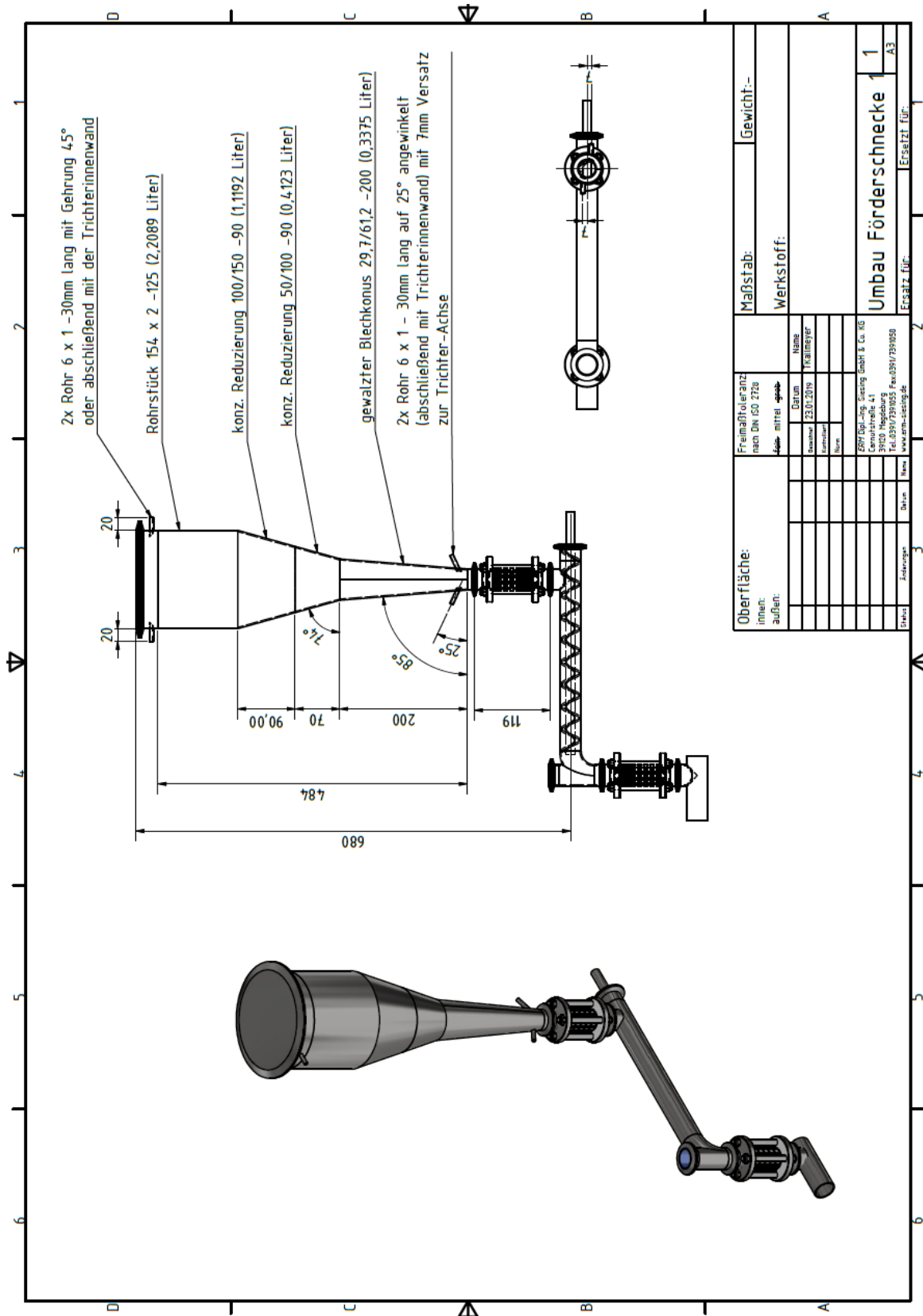


Fig. A12.4. Storage conical tank technical drawing.



Oberfläche:		Freimaßtoleranz nach DIN ISO 2728		Maßstab:	Gewicht-
innen:		Art	mittel	Werkstoff:	
außen:		Datum	23.07.2019		
		Name	Y. B. B. B. B.		
		Durchm.			
		Normen			
		Norm			
		2807 Dipl.-Ing. - Steuerung GmbH & Co. KG 39100 Havelberg Tel.: 0391/7391655 Fax: 0391/7391658 www.erm-steuerg.de			
Status	Zustellungen	Datum	Name	Ersatz für:	
				Umbau Förderschnecke 1	
				A3	

Schaulaternen und Zubehör						
Schaulaterne Schweiß/Schweiß DIN						
DN DIN	D1	D2	L	L1	Gew. [kg]	
10	10	15	88	60	0,25	
15	16	21	88	60	0,30	
20	20	25	88	60	0,73	
25	26	31	98	70	0,75	
32	32	37	104	70	0,76	
40	38	43	112	70	1,08	
50	50	55	112	70	1,34	
65	66	72	127	85	1,90	
80	81	87	135	85	2,35	
100	100	106	189	115	2,80	
125	125	132	202	160	6,35	
150	150	157	216	170	7,11	
Schaulaterne Gewinde/Gewinde DIN						
DN DIN	D1	E	L	L1	Gew. [kg]	
10	10	Rd 28 x 1/8"	122	60	0,32	
15	16	Rd 34 x 1/8"	122	60	0,39	
20	20	Rd 44 x 1/6"	124	60	0,90	
25	26	Rd 52 x 1/6"	142	70	1,00	
32	32	Rd 58 x 1/6"	154	70	1,08	
40	38	Rd 65 x 1/6"	164	70	1,50	
50	50	Rd 78 x 1/6"	168	70	1,94	
65	66	Rd 95 x 1/6"	191	85	2,80	
80	81	Rd 110 x 1/4"	209	85	3,10	
100	100	Rd 130 x 1/4"	257	115	4,38	
125	125	Rd 160 x 1/4"	270	160	8,80	
150	150	Rd 190 x 1/4"	290	170	10,50	
Schaulaterne Gewinde/Kegel DIN						
DN DIN	D1	E	L	L1	Gew. [kg]	
10	10	Rd 28 x 1/8"	122	60	0,38	
15	16	Rd 34 x 1/8"	122	60	0,45	
20	20	Rd 44 x 1/6"	124	60	0,69	
25	26	Rd 52 x 1/6"	142	70	1,02	
32	32	Rd 58 x 1/6"	154	70	1,25	
40	38	Rd 65 x 1/6"	164	70	1,67	
50	50	Rd 78 x 1/6"	168	70	2,17	
65	66	Rd 95 x 1/6"	191	85	3,26	
80	81	Rd 110 x 1/4"	209	85	3,71	
100	100	Rd 130 x 1/4"	257	115	5,10	
125	125	Rd 160 x 1/4"	270	160	9,50	
150	150	Rd 190 x 1/4"	290	170	11,30	
Schaulaterne Kegel/Kegel DIN						
DN DIN	D1	E	L	L1	Gew. [kg]	
10	10	Rd 28 x 1/8"	122	60	0,44	
15	16	Rd 34 x 1/8"	122	60	0,52	
20	20	Rd 44 x 1/6"	124	60	1,08	
25	26	Rd 52 x 1/6"	142	70	1,20	
32	32	Rd 58 x 1/6"	154	70	1,41	
40	38	Rd 65 x 1/6"	164	70	1,89	
50	50	Rd 78 x 1/6"	168	70	2,50	
65	66	Rd 95 x 1/6"	191	85	3,64	
80	81	Rd 110 x 1/4"	209	85	4,27	
100	100	Rd 130 x 1/4"	257	115	5,13	
125	125	Rd 160 x 1/4"	270	160	10,20	
150	150	Rd 190 x 1/4"	290	170	11,79	

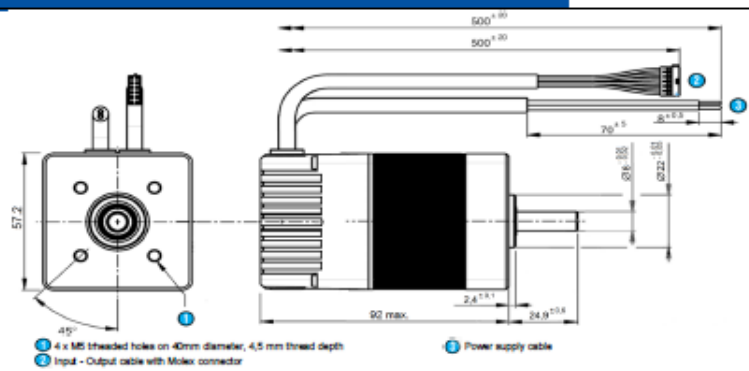
Fig. A12.7. Sight glass selection.

Appendix A13- Instrument selection and specifications.



Fig. A13.1. Motor specifications.

DCmind Brushless motor
Data sheet Series **80 140 TNI21**



General characteristics

Power supply	
Direct current voltage supply	✓
Nominal voltage range	Vdc 12 -> 32
Max. current	A 10

Motor characteristics (1)	12 Vdc			24 Vdc	32 Vdc
	At no load				
Max. output speed	rpm	2 900	4 000	4 000	
Current at the max output speed	A	0,34	0,29	0,27	
Standby current	A	0,08	0,085	0,09	+10%
At nominal					
Speed	rpm	1 900	4 000	4 000	+10%
Torque (2)	mNm	193	184	178	
Output power	W	38	77	75	+10%
Current	A	5,2	4,4	3,2	
Efficiency	%	62	74	73	
At max. output power					
Speed	rpm	1 600	3 050	4 000	
Torque	mNm	250	358	358	
Output power	W	42	114	150	+10%
Current	A	6,5	10	10	
Efficiency	%	53	48	47	
At peak torque					
Speed	rpm	930	3 050	4 000	
Torque	mNm	358	358	358	
Output power	W	35	114	150	
Current	A	10	10	10	+10%
Others					
Life (3)	h		20 000		
Rotor inertia	gcm ²		75		
Thermal Resistance	*W		3		
Thermal time constant	mn		20		
Rotor pole number			4		
Cogging torque	mNm		11		
Weight	kg		0,95		
Noise level	dBA		40		

Connecting	
Input - Output cable	With Molex connector ref: 43026-0800
Output cable, UL style 3464 80°C 300V - 8 wires AWG24	
Input: ON/OFF	1 - Green
Input: Direction	2 - Yellow
Input: Torque limit	3 - Blue
Input: Speed	4 - Orange
DV	5 - Black
Output: Pulse	6 - Brown
Output: Torque limit reached	7 - Purple
Output: Direction	8 - Red
Power supply cable	
Cable UL style 2517 105°C 300V - 2 wires AWG 16 - 500 mm	
+ 12Vdc -> + 32 Vdc	Brown
DV	Blue

Drive	
Type	TNI21
Build-in drive	✓
Internal encoder	12 pulses per turn
Control	
Speed	PWM
Torque	PWM
4 quadrants - low braking	✓
4 quadrants with regenerative energy	✓
Type* Trapezoidal*	✓
Security	
Short-circuit of outputs	✓
Input inverted	✓
Low voltage	Vdc < 10
Short high voltage	Vdc > 36
Stop at max Internal drive temperature (2)	*C 110
Drive temperature allowing to restart	*C 90

Generic parameters	
Output shaft with ball bearings	✓
Max. Radial force (12mm from front face)	N 40
Max. axial force(4)	N 20
Temperature range	*C -30 -> +70
Storage temperature	*C -40 -> +80
Dielectric	1min 2mA 50Hz CEI60335 Vdc
Motor insulation	CEI60085 class E
Salt spray	CEI60088-2-58 severity 48h
Degree of protection (output shaft not included)	CEI60529 IP 65M
EMC	
Electrostatic Discharge	CEI1000-4-2 level 3
Electrical fast transient / burst test	CEI1000-4-4 level 3
Surge test	CEI1000-4-5 level 1
Radiated emission	EN55022 class B
Approvals	
ROHS	2002/95/CE ✓
EC	✓

Notes
 Values without tolerances are average production values.
 Added Informations are in "TNI21 manual and security" on www.crouzet.com
 Motor not protected in case of reversed power voltage
 (1) Cold motor, 20 ° C ambient temperature, full speed
 (2) Max torque for continuous operation at 20 ° C, decrease this value for higher ambient temperature
 (3) Continuously rated torque, zero radial and axial loads
 (4) Pinion or pulley fitting are done at the Crouzet factory, before final assembly.

Crouzet Automatismes
 2 rue du Docteur Abel CS0059
 26902 Valence CEDEX 9 France
 Specifications subject to change without notice. Updated July 6, 2013.
www.crouzet.com

Series 80 140 TNI21

Fig. A13.2. Selected motor.

Appendix A14- Explosion protection.

Explosive limitation

A certain range of the mixture between combustible gases/vapors and oxygen defines lower and upper explosive limit. The mixture below the lower explosive limit (LEL) is too lean to burn and above the upper explosive limit (UEL) is too rich to burn (Figure A). and the explosion happens when these conditions: a combustible gas/vapor; oxygen/air source; an ignition source (spark or flame) are fulfilled at the same time [144].

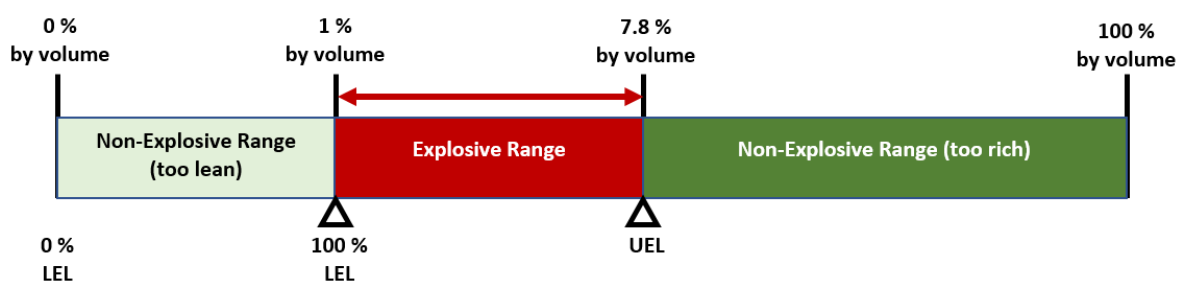


Figure A14.1. An example of LEL and UEL of Toluene at 20°C and atmospheric pressure [145]. *The red-colored zone should be avoided. During the experiment, when the composition of mixture is changed and approached from both end to red zone, a warning should be given.*

Each solvent has different LEL and UEL values which decide the alarm level of sensor to avoid the danger situation.

Solutions for explosion prevention

The working condition, surrounding ambience, assembling area, high-risk positions, danger possibilities are considered and discussed. The solutions and assessments are carried out by experts. Final solutions (Fig.A14.2) can be summarized as: the entire extraction process is carried out in an inert environment (nitrogen), the oxygen sensors are arranged at the high risk oxygen penetration positions, the Toluene detectors is placed to realize the appearance of Toluene vapor during the experiments. The entire plant is put in a fume hood integrated chamber, in which the air is drawn in from front side of the chamber and is expelled to the outside of the building. Finally, the agreement of safety departments and experts allows to start experiments.

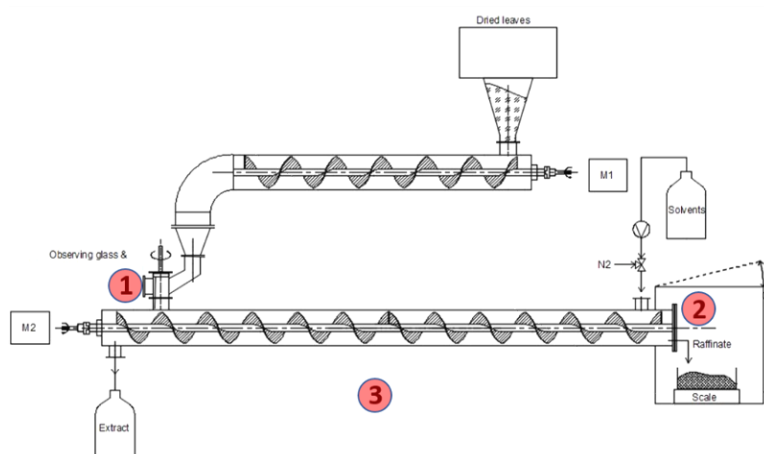


Fig. A14.2. The scheme of supposed high risk positions of the production plant. (1) the inlet area of leaves where contains high concentration of solvent; (2) the raffinate outlet position; (3) ambient outside of the extractor to detect leaking/breaking of the plant.

Appendix A15- Assembling and electrical installation.

The installation and construction work are cooperated with MPI mechanical and electrical workshops. The different scenarios (e.g. the operating conditions, alarm threshold setup, emergency shut down) are discussed. The entire extraction is provided to avoid explosion. The pipeline construction is described below.

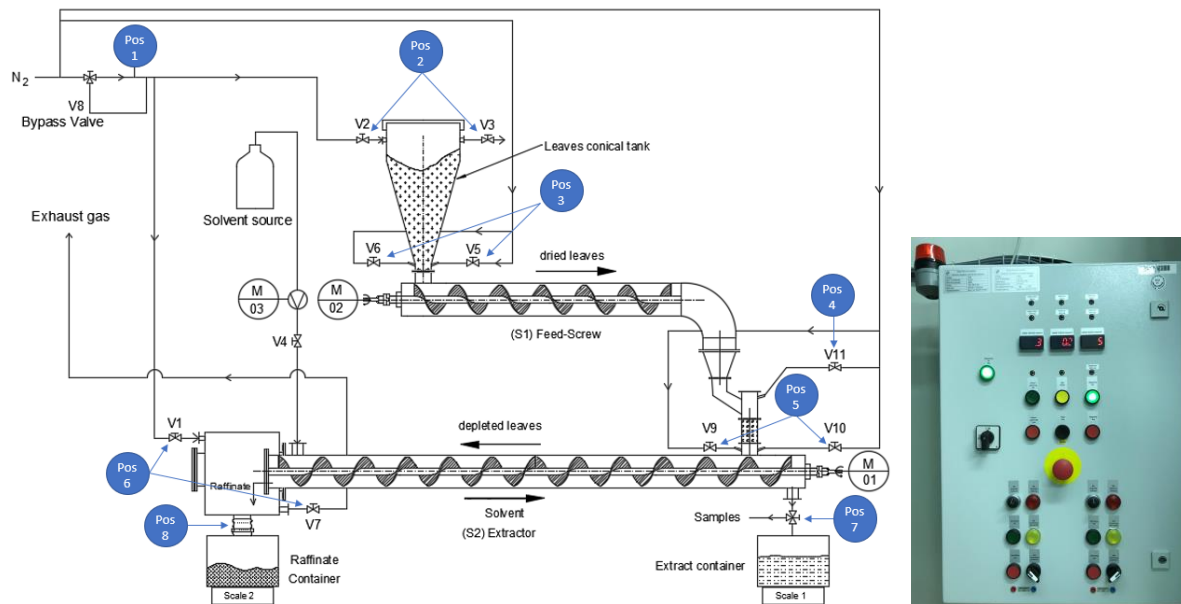


Fig. A15.1. The flowsheet of pipeline construction, specific structure and switch cabinet.

The pipelines are built up to supply nitrogen in crucial positions (Pos.1-6). (Pos.1) a flow controller to ensure the presence of inert gas stream; (Pos.2) valves to force the air out of the system; (Pos.3) valves to break the blockade; (Pos.4) valves to prevent of air penetration; (Pos.5) valves to break the blockade of wet mixture; (Pos.6) valves to ensure the inert gas ambient; (Pos.7) a three-way valve to collect the samples; (Pos.8) a flexible joint.

A 123 page operating manual technical documentation cooperated with engineering office Jürgen Bialek (Halsbrücker Str.34; 09599 Freiberg) is finalized and released.

Appendix A16- Detail of suppliers and manufacturing companies.

No.	Type/Parts	Characteristic/ Series	Quant./ Amount	Supplier
1	Prototype trough	320 x Φ 33,7 x 2mm	1	ERM Siesing GmbH Carnotstr. 41, MD
2	Prototype shaft	380 x Φ 14mm	1	ERM Siesing GmbH Carnotstr. 41, MD
3	Trough	640 x Φ 33,7 x 2mm	1	ERM Siesing GmbH Carnotstr. 41, MD
4	Screw shaft	689 x Φ 14mm	1	ERM Siesing GmbH Carnotstr. 41, MD
5	Screw flight	OD-35mm; ID-14mm	20	Helica- Fördertechnik
6	Conical tank	Capacity: 3,4L	1	ERM Siesing GmbH Carnotstr. 41, MD
7	Perforated disk	OD-36mm; ID-5mm; Hole- 5mm	1	MPI Magdeburg Werkstatt
8	Flange gaskets	Material...	10	ERM Siesing GmbH Carnotstr. 41, MD
9	Tri clamp locking clip	Stainless steel	10	ERM Siesing GmbH Carnotstr. 41, MD
10	Single universal coupling	Stainless steel	2	ERM Siesing GmbH Carnotstr. 41, MD
11	Motors	TNi21_DCmind brussless	2	CROUZET Motors
12	Toluene sensor	PrimaX P, M25 with Relais	1	ACE Instruments
13	Oxygen sensor	MCS electrochemical gas measure for O ₂	2	ACE Instruments
14	Sight glass	Glass	3	AWH
15	Container	10 Liter, PE-HD	5	SCAT

Appendix A17- Flowrate, speed measurements for screws (feeder, extractor).

The feed screw is operated by a motor, and determination of the relation of screw speed and leaves flowrate is an obligation. However, the screw speed is controlled by the given electrical power, thus, the measurements consist of two procedures as follows:

Measurement 1- The relation of electrical power and screw speed (Fig. A17.1).

Setup: Mark a point on the static shelf and another on the moving screw shaft. Use regulating button to set the voltage, the values from multi-meter device are recorded.

Implementation: one round finishing is observed by a stopwatch. Each recorded data is repeated twice. Adjust the voltage and repeat measuring process. The speed is calculated via time as:

$$n = \frac{60}{t_{measured}} \quad (\text{A17.1})$$

Measurement 2- The relation of rotational speed and leaves flowrate.

Setup: use the data from previous measurement to set the screw rotational speed.

Implementation: The leaves masses are recorded in 2-minute time intervals.

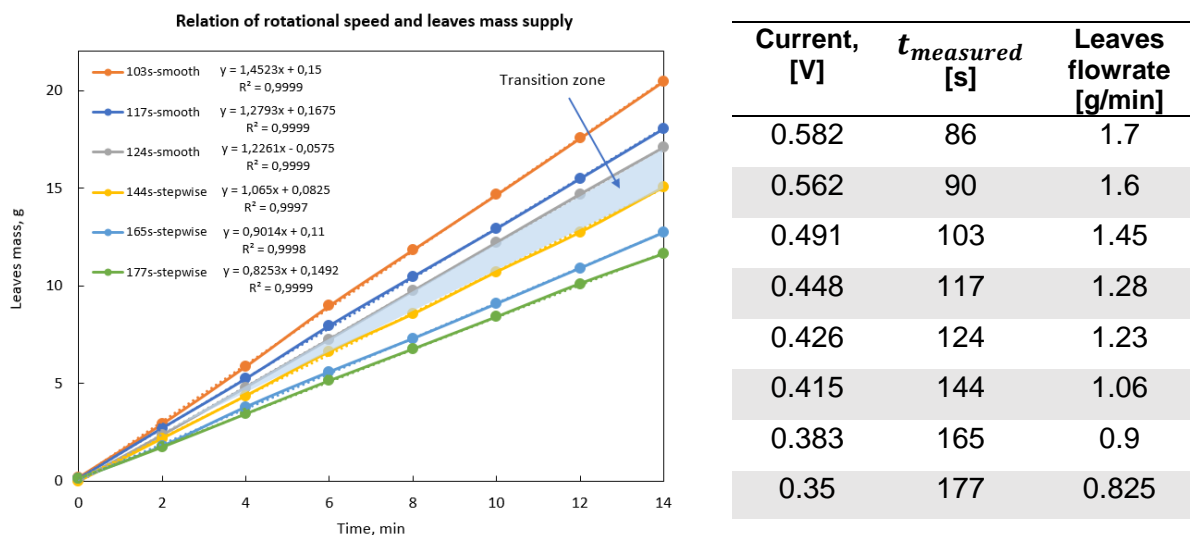


Fig.A17.1. Flowrate of leaves at different rotational speed of screw feeder.

It should be noticed that, the rotational speed is relatively low. Thus, a transition zone shifting from smooth to stepwise rotation is existed and a large variation of flowrate is observed (Fig.A17.1).

Additionally, the main extractor has identical motor and screw pitch to screw feeder, but the main screw is planning to work at higher speed, therefore, it needs to be calibrated at higher range. The similar calibration process is repeated for the main screw extractor and the results are given below.

Current (V)	0.807	1.187	1.42	1.55	1.64	1.8
Rotational speed (<i>rpm</i>)	1	1.5	1.8	2	2.2	2.4

Table A17.1. The relation of electrical power and screw speed of main extractor (M1).

Appendix A18- Pump calibration.



- The pump (P4.1S with pump head 50mL from Knauer) input is directly connected to the solvent canister.
- The pump outlet is put inside a beaker which is weighted by a scale.
- Set the pump value in a certain flowrate mL/min.
- Record the weight at a fixed time interval (30 seconds).
- Adjust the flowrate to another value and repeat the recording data.
- Plot the relation of time and mass, the slope gives the flowrate data measured in gram per minute.

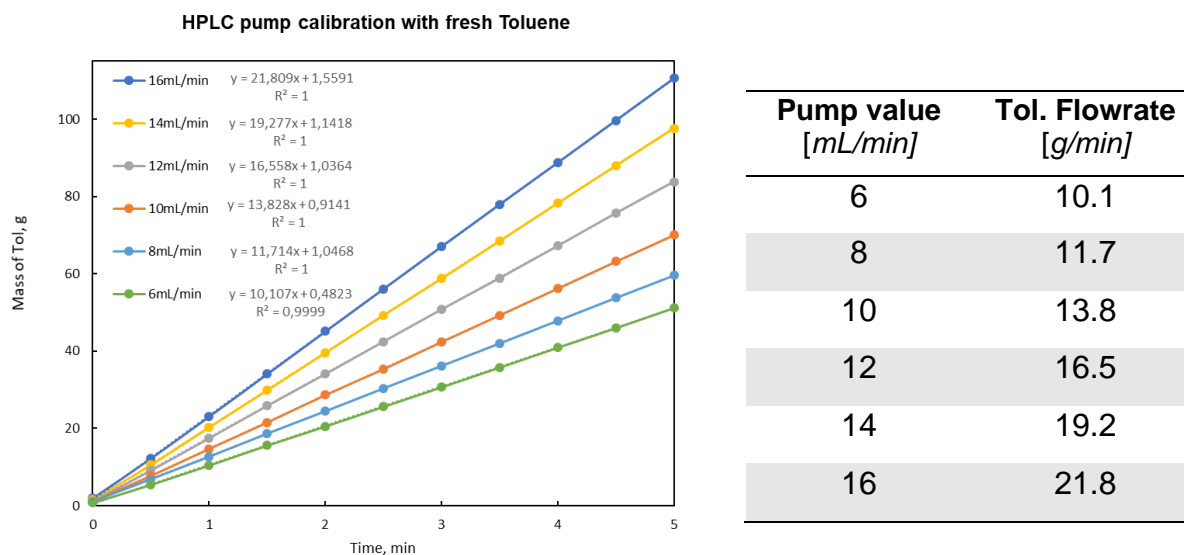


Fig.A18.1. Solvent pump: calibration procedures and results.

Appendix 19- Glass beads certificate.**Analysezertifikat**

Artikelnummer:	A554		
Glasperlen			
Ø 0,75-1,0 mm			
Charge:	312189871		
CAS-Nummer:	Druckdatum:	14.01.2019	
Formel:	Empfohlenes Retest Datum:	30.07.2017	
Dichte:	Freigabedatum:	30.07.2012	
Molekulargewicht:			

Chargenwerte

SiO ₂	72.30 %
Na ₂ O	13.30 %
CaO	8.90 %
MgO	4.00 %
sonstige	1.50 %

Unsere Produkte sind für Laborzwecke geprüft.
Die Angaben beziehen sich auf den aktuellen Stand der Produktqualität.
Wir behalten uns vor, notwendige Änderungen durchzuführen.

S. Lindenfelser
Quality Control

S. Hildebrandt
Quality Management

Dieses Dokument wurde maschinell erstellt und ist ohne Unterschrift gültig.

Carl Roth GmbH + Co. KG
Schoemperlenstraße 3-5
76185 Karlsruhe

Telefon 0721/5606-0
Telefax 0721/5606-149
E-Mail: info@carlroth.de

Die Firma ist eine Kommanditgesellschaft mit Sitz in Karlsruhe, Reg. Gericht Mannheim HRA 100055. Persönlich haftende Gesellschafterin ist die Firma Roth Chemie GmbH mit Sitz in Karlsruhe, Reg. Gericht Mannheim HRB 100428. Vorsitzender des Aufsichtsrats: Eberhard Gaul
Geschäftsführer: Lothar Haidmann



Seite 1 von 1

Appendix A20- RTD investigation of leaves- Experimental procedures and results.

A20.1. Experimental procedures

The experiment is setup as in Fig.A20.1. The dried leaves are automatically conveyed to the extractor by the screw feeder (S1) and further transported to the collecting disk at another end of the second screw (S2). In case of mixing leaves and tracers, the glass beads as tracers are provided into the extractor via a separated inlet.

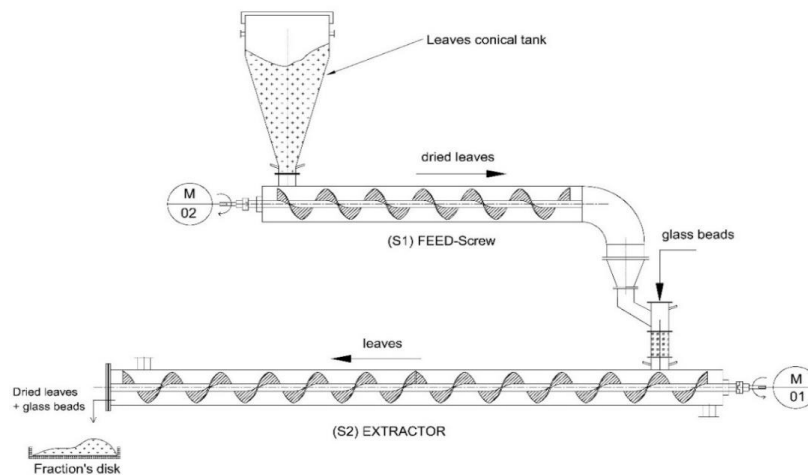


Figure A20.1. Experimental setup of leaves RTD investigation.

The experimental procedures can be outlined as:

- Set the dosing screw speed by setting electrical power (*Appendix A19*).
- Start the stopwatch when the first leaves (or tracers in case of mixture) going into extractor (S2).
- Record the residence time from inlet to outlet when the first leaves/tracers go out extractor.

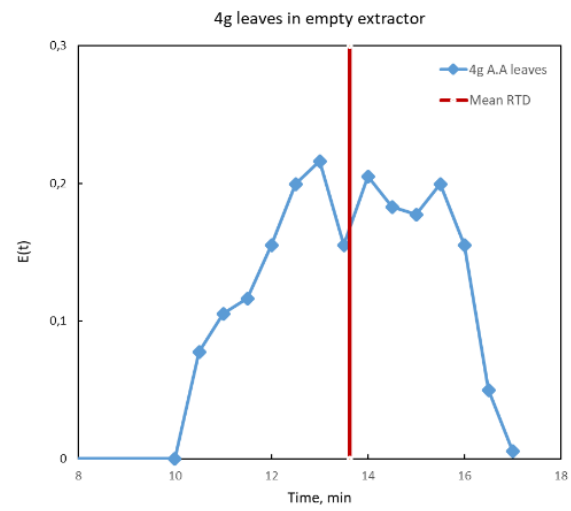
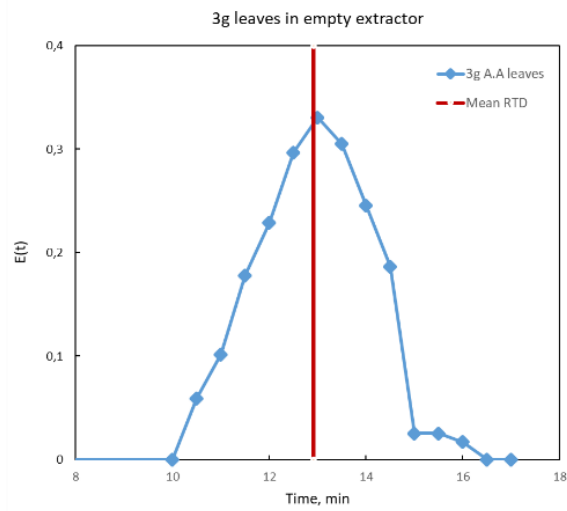
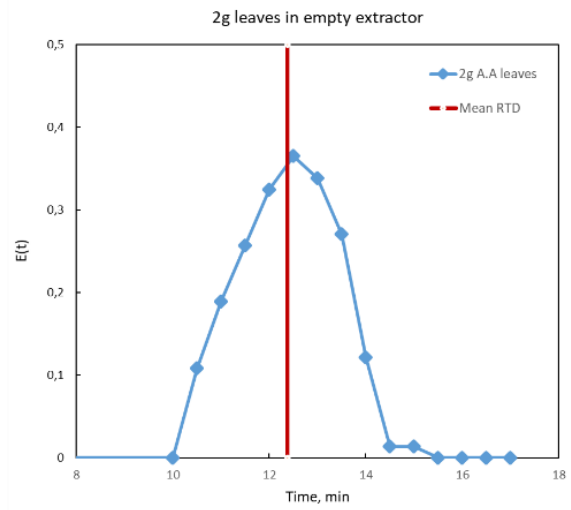
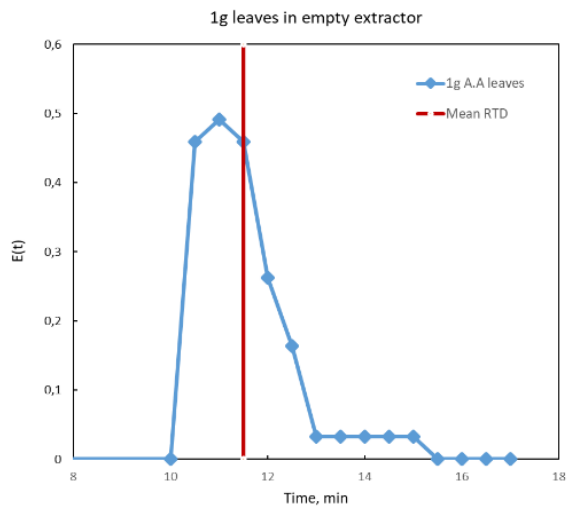
Each fraction is collected in 30-second time interval, the collecting disk is changed after one fraction (every 30 second) (Figure 6.6a). The sampling is finished if no more leaves /tracers are observed at the outlet. In case of mixture of leaves and glass beads, the obtained fractions are further sieved and scaled to define the amount of tracers.

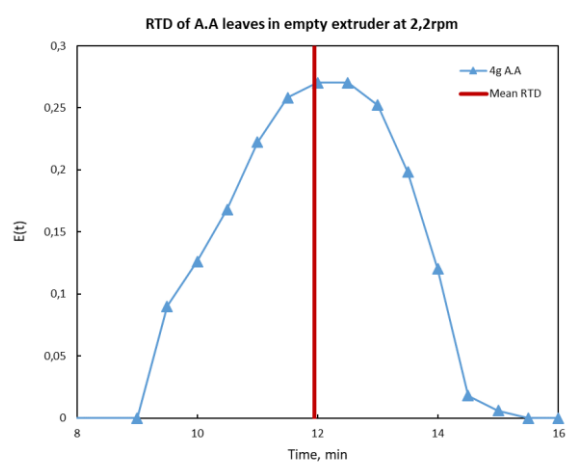
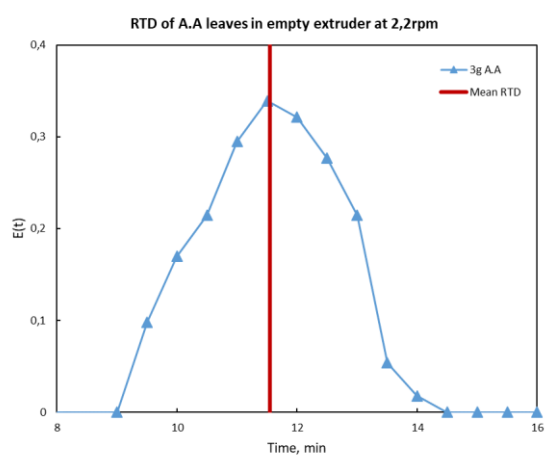
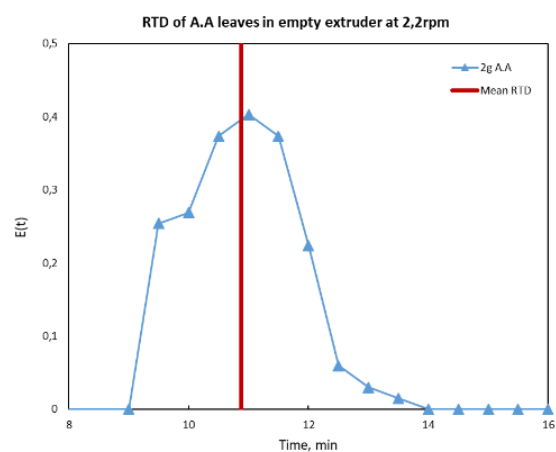
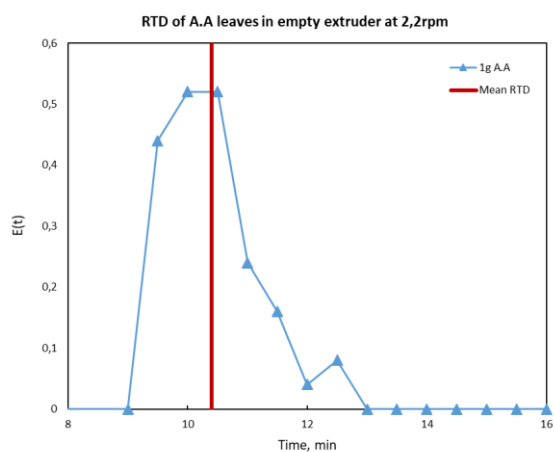
A20.2. An example of measured, recorded data and calculated parameters

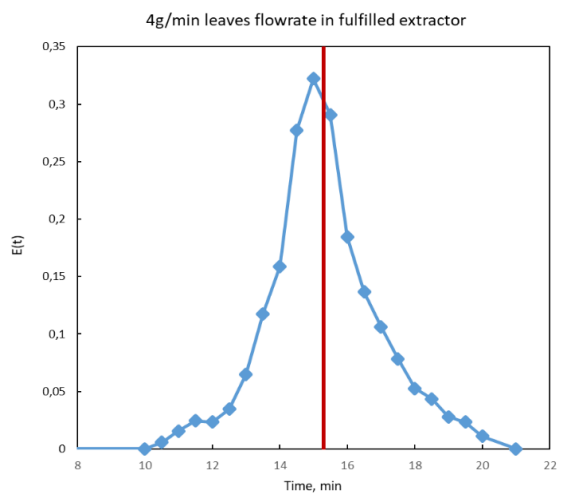
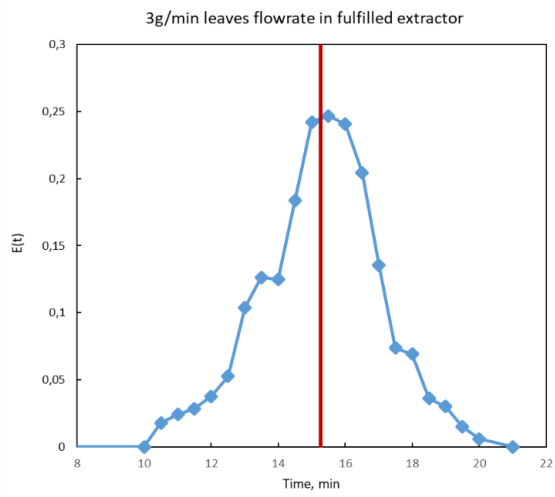
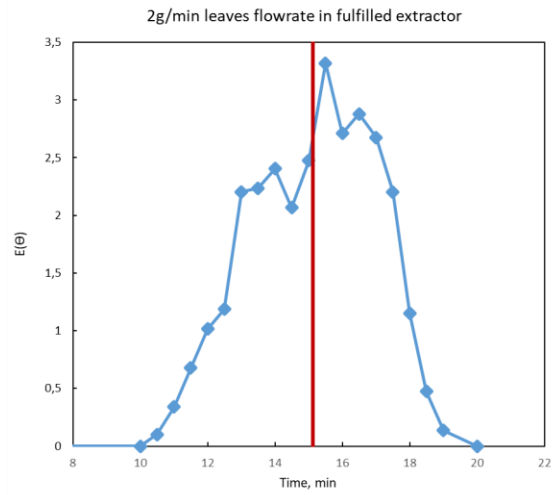
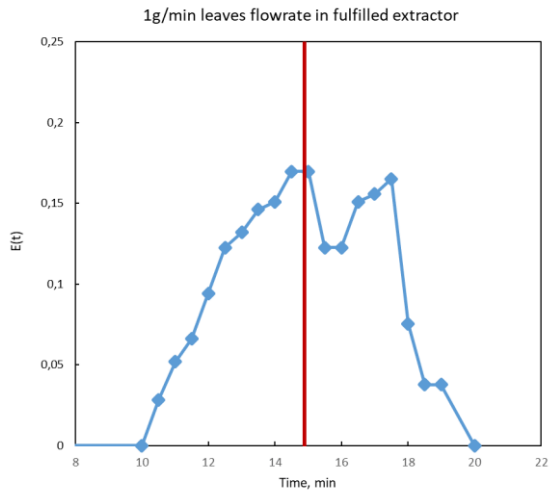
Experimental condition	Time, t_i (min)	Δt_i	Fractions of glass beads (g)	Mass of beads- m_i (g)	$\sum_0^{t_i} m_i$	$F(t_i)$	$t_i m_i$	$\Delta t_i m_i$	$E(t_i)$	$E(t_i) \Delta t_i$	$t_i^2 m_i \Delta t_i$
Extractor M1 speed = 1,8rpm	0	0	0	0	0	0	0	0	0	0	0
	10	10	0	0	0	0	0	0	0	0	0
Feed Screw M2 speed = 0,42rpm(0,46V) Leaves flowrate = 1g/min Mass of glass beads in one chamber = 5,0g	10,5	0,5	0,06	0,06	0,06	0,01415094	0,63	0,03	0,02830189	0,14858491	3,3075
	11	0,5	0,11	0,11	0,17	0,04009434	1,21	0,055	0,05188679	0,28537736	6,655
	11,5	0,5	0,14	0,14	0,31	0,07311321	1,61	0,07	0,06603774	0,37971698	9,2575
	12	0,5	0,2	0,2	0,51	0,12028302	2,4	0,1	0,09433962	0,56603774	14,4
	12,5	0,5	0,26	0,26	0,77	0,18160377	3,25	0,13	0,12264151	0,76650943	20,3125
	13	0,5	0,28	0,28	1,05	0,24764151	3,64	0,14	0,13207547	0,85849057	23,66
	13,5	0,5	0,31	0,31	1,36	0,32075472	4,185	0,155	0,14622642	0,9870283	28,24875
	14	0,5	0,32	0,32	1,68	0,39622642	4,48	0,16	0,1509434	1,05660377	31,36
	14,5	0,5	0,36	0,36	2,04	0,48113208	5,22	0,18	0,16981132	1,23113208	37,845
	15	0,5	0,36	0,36	2,4	0,56603774	5,4	0,18	0,16981132	1,27358491	40,5
	15,5	0,5	0,26	0,26	2,66	0,62735849	4,03	0,13	0,12264151	0,9504717	31,2325
	16	0,5	0,26	0,26	2,92	0,68867925	4,16	0,13	0,12264151	0,98113208	33,28
	16,5	0,5	0,32	0,32	3,24	0,76415094	5,28	0,16	0,1509434	1,24528302	43,56
	17	0,5	0,33	0,33	3,57	0,84198113	5,61	0,165	0,15566038	1,32311321	47,685
	17,5	0,5	0,35	0,35	3,92	0,9245283	6,125	0,175	0,16509434	1,44457547	53,59375
	18	0,5	0,16	0,16	4,08	0,96226415	2,88	0,08	0,0754717	0,67924528	25,92
	18,5	0,5	0,08	0,08	4,16	0,98113208	1,48	0,04	0,03773585	0,3490566	13,69
	19	0,5	0,08	0,08	4,24	1	1,52	0,04	0,03773585	0,35849057	14,44
	Sum				4,24			2,12			14,884434

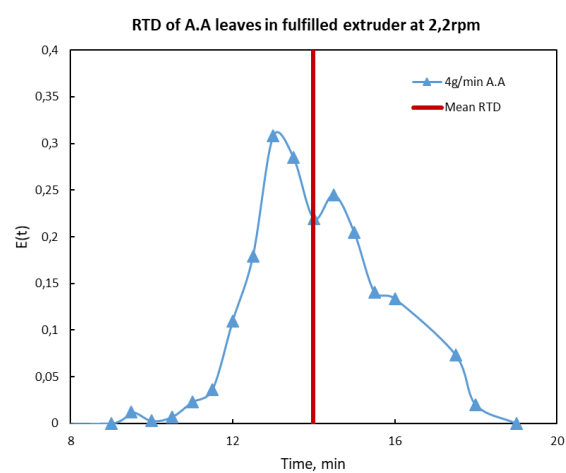
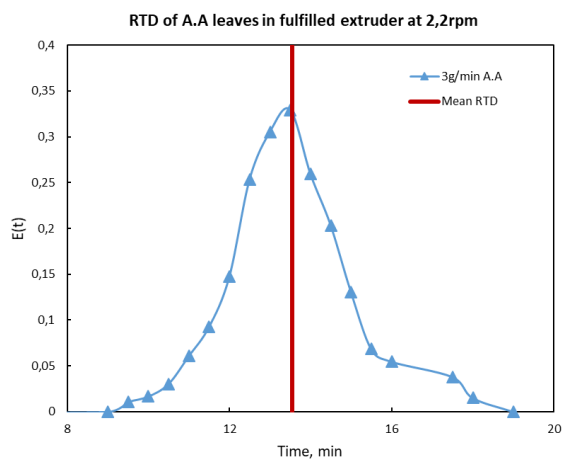
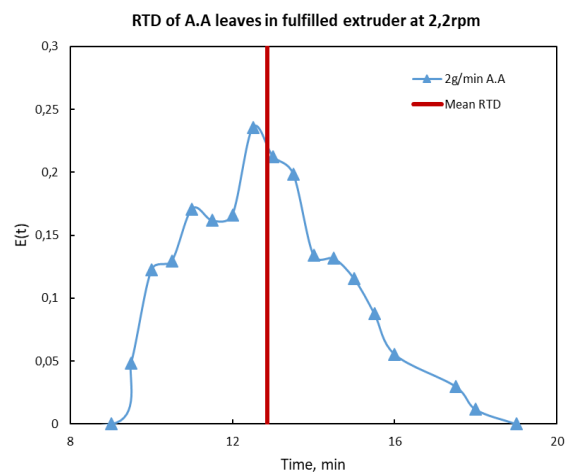
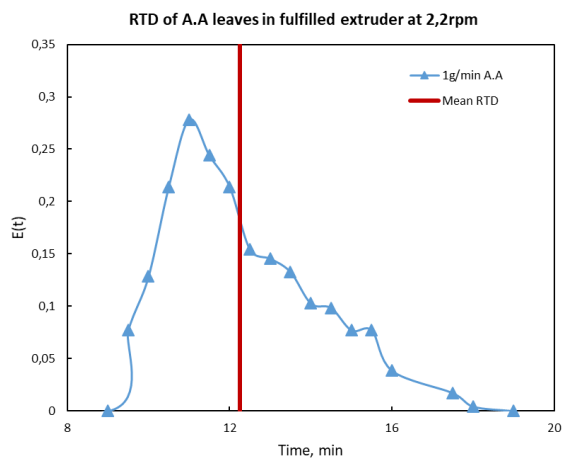
A20.3. Results

Empty extractor at $n = 1,8$ rpm



Empty extractor at $n = 2,2$ rpm

Fulfilled extractor at $n = 1,8$ rpm

Fulfilled extractor at $n = 2,2$ rpm

Appendix A21- Certificate of sodium chloride analysis.

SIGMA-ALDRICH

sigma-aldrich.com

3050 Spruce Street, Saint Louis, MO 63103, USA

Website: www.sigmaaldrich.com

Email USA: techserv@sial.com

Outside USA: eurtechserv@sial.com

Certificate of AnalysisProduct Name:
Sodium chloride - BioXtra, ≥99.5% (AT)**NaCl**Product Number: S7653
Batch Number: SLBV9983
Brand: SIAL
CAS Number: 7647-14-5
MDL Number: MFCD00003477
Formula: NaCl
Formula Weight: 58.44 g/mol
Quality Release Date: 04 OCT 2017
Recommended Retest Date: OCT 2023

Test	Specification	Result
Appearance (Color)	White	White
Appearance (Form)	Powder	Powder
	powder to fine crystals with lumps	
Solubility (Color)	Colorless	Colorless
Solubility (Turbidity)	Clear	Clear
	1M, H ₂ O	
Insoluble Matter	Pass	Pass
	Passes filter test	
Phosphate (PO ₄)	< 0.0005 %	< 0.0005 %
Sulfate (SO ₄)	< 0.05 %	< 0.00 %
Aluminum (Al)	< 0.0005 %	< 0.0005 %
Arsenic (As)	Pass	Pass
	< / = 0.0001%	
Barium (Ba)	< 0.0005 %	< 0.0005 %
Bismuth (Bi)	< 0.0005 %	< 0.0005 %
Bromide (Br)	Pass	Pass
	< / = 0.01%	
Calcium (Ca)	< 0.002 %	< 0.001 %
Cadmium (Cd)	< 0.0005 %	< 0.0005 %
Chromium (Cr)	< 0.0005 %	< 0.0005 %
Cobalt (Co)	< 0.0005 %	< 0.0005 %
Copper (Cu)	< 0.0005 %	< 0.0005 %

Sigma-Aldrich warrants, that at the time of the quality release or subsequent retest date this product conformed to the information contained in this publication. The current Specification sheet may be available at Sigma-Aldrich.com. For further inquiries, please contact Technical Service. Purchaser must determine the suitability of the product for its particular use. See reverse side of invoice or packing slip for additional terms and conditions of sale.

Version Number: 1

Page 1 of 2

Appendix A22- Specifications of conductivity meter FiveEasy, Mettler Toledo.



CO/60022

FiveEasy™ Conductivity meter



Entry-level instrument for measuring conductivity, salinity and TDS.

Is a compact, easy to use bench meter suitable for a wide range of applications in various areas such as food and beverage, agriculture, industry, water and environment

- Outstanding functions such as TDS and salinity modes and meter self-test combined with features such as automatic endpoint, 1 point calibration, linear temperature compensation and selectable reference temperature
- Five self-explanatory buttons for starting and ending a measurement or calibration and for accessing the latest calibration data
- A big, well organised display simultaneously showing readings, temperature, endpoint criteria and various helpful icons
- Useful accessories such as a laminated quick guide enclosed with every FiveEasy. The kit version also includes the robust LE703 conductivity electrode and a handy electrode arm.

This instrument is distinguished by its ergonomic and compact design and excellent value for money. These entry-level instruments naturally come with METTLER TOLEDO quality for reliable measurements and are backed by over 50 years of METTLER TOLEDO sensor know-how.

FE30 Conductivity meter only including meter, operating manual, "quick guide" and power adapter.

FE30-Kit Conductivity meter kit as FE30 meter only plus LE703 conductivity electrode, electrode arm, 2 x 1413 S/cm and 2 x 12.88 mS/cm standard sachets.

Technical Specification

Conductivity range	0.1 S/cm to 199.9 mS/cm
Cond. accuracy	+/- 0.5%
Temperature range °C	0.0 to 100.0
Temperature resolution °C	0.1
Temperature accuracy °C	± 0.3
TDS range	0.1 mg/L ... 199.9 g/L
Salinity range	0.00 ... 19.99 psu
Display	LCD
Power supply	Ext. power supply (standard)
Operating environment	0 ... 40 °C; 5 ... 80 % rel. humidity (not cond.)

Cat. No.	Code	Description
CO/60020	FE30	FiveEasy™ conductivity, instrument only
CO/60022	FE30-Kit	FiveEasy™ conductivity electrode kit incl. LE703*, electrode arm and buffer sachets
CO/60006	LE703	Replacement conductivity electrode

*Please note: the LE703 conductivity electrode has a 1 metre cable

Appendix A23- Calibration procedure of sodium chloride solution by FiveEasy conductivity meter.

Seven samples with different sodium chloride concentration are prepared (the last measuring point reflecting an oversaturated solution). The mass fraction of sodium chloride in a supersaturated solution was determined at 0.265, means, 26.5g of NaCl in 73.5g of water at 20°C.

Nr.	NaCl [g]	Distilled water [g]	x(NaCl)	Conductivity [mS/cm]
1	4.98	99.98	0.047	50.6
2	10.14	100.05	0.092	90.1
3	14.94	99.97	0.13	117.2
4	20.3	99.71	0.169	142.3
5	25.25	99.5	0.202	155.1
6	29.54	98.81	0.23	164.2
7	25.28	50.34	0.265	177.1

Table A23.1. Standard preparation and relevant conductivity

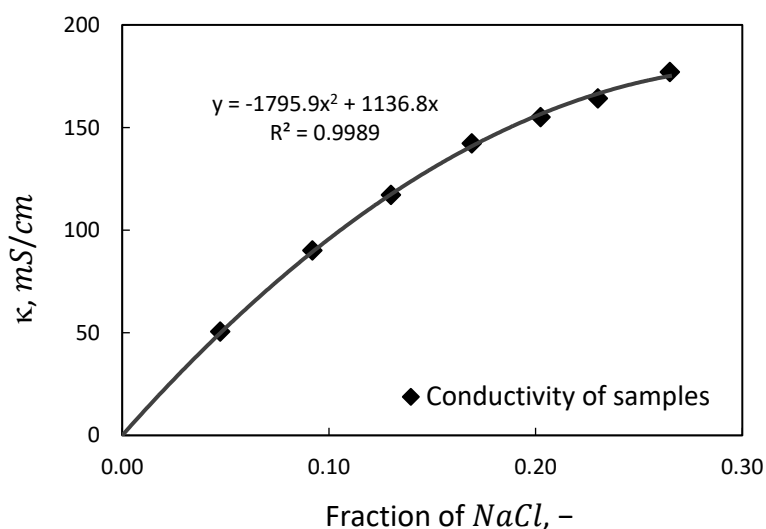


Fig.A23.1. Calibration curve of NaCl and conductivity

The salt solution of 10% which saves the chemical consumption and is in the optimum working range of FiveEasy conductivity meter, is chosen as tracer. It needs to be assured that the conductivity remains constant when the salt solution is in

contact with the leaves. Thus, another test is carried out to examine the stability of the conductivity in real mixture by preparation of five ratios of A.A leaves and the salt solution $x_{NaCl} = 9.7\%$ (Table A23.2.).

Table A23.2. Averaged conductivity and standard deviation of conductivity stability.
* averaged values based on three measurements

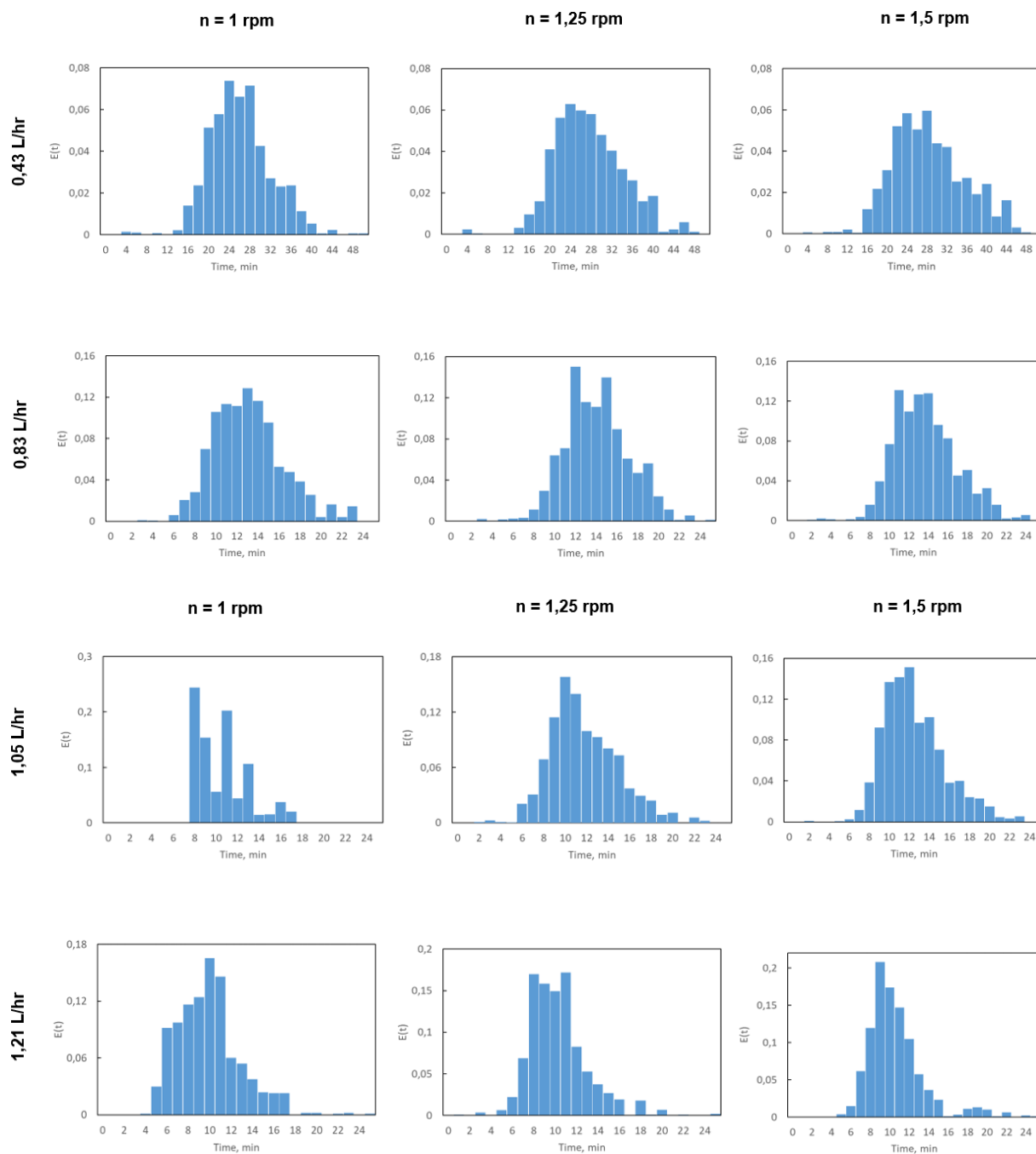
Ratio A.A leaves and NaCl solution	$\bar{\kappa}$ [mS/cm] *	σ [mS/cm]
1.55g / 34g	92.2	0.3
3.02g / 34g	93	0.3
4.52g / 34g	92.2	0.5
6g / 34g	-	-
7.55g / 34g	-	-
0g / 34g	92.3	0.5

The standard deviations are in range of 0.3÷0.5 mS/cm which fits well with the technical specification of conductivity meter indicated an accuracy of $\pm 0.5\%$. The exceptional case of 6.0 and 7.55g leaves was not able to measure since the mass of solvent is insufficient. As a conclusion, the measured data confirm that sodium chloride is absolutely suitable to be used as tracer for investigating residence time of liquid stream.

Appendix A24- Recorded and calculated data of conductivity measurement for one experimental condition.

t_i	Δt_i (min)	Samples	Conductivity k (mS/cm)	K_i	$F(t_i)$	$t_i K_i$	$\Delta t_i K_i$	$E(t_i)$	$E(t_i) \cdot t_i \cdot \Delta t_i$	$t_i^2 \cdot K_i \cdot \Delta t_i$
0	0	-	2,07	0	0	0	0	0	0,000	0
1	1	1	2,1	0,0	0	0	0	0	0,000	0
2	1	2	2,2	0,1	0,00099558	0,18	0,09	0,00101891	0,002	0
3	1	3	2,3	0,2	0,00298673	0,54	0,18	0,00203781	0,006	2
4	1	4	2,5	0,1	0,00431416	0,48	0,12	0,00135854	0,005	2
5	1	5	2,5	0,0	0,00431416	0	0	0	0,000	0
6	1	6	2,6	0,1	0,00575221	0,78	0,13	0,00147175	0,009	5
7	1	7	2,9	0,3	0,00940265	2,31	0,33	0,00373599	0,026	16
8	1	8	4,3	1,4	0,02511062	11,36	1,42	0,01607608	0,129	91
9	1	9	7,8	3,5	0,06360619	31,32	3,48	0,03939771	0,355	282
10	1	10	14,6	6,8	0,13860619	67,8	6,78	0,07675761	0,768	678
11	1	11	26,2	11,6	0,26692478	127,6	11,6	0,13132571	1,445	1404
12	1	12	35,9	9,7	0,37422566	116,4	9,7	0,10981546	1,318	1397
13	1	13	47,1	11,2	0,49811947	145,6	11,2	0,12679724	1,648	1893
14	1	14	58,4	11,3	0,62311947	158,2	11,3	0,12792936	1,791	2215
15	1	15	66,9	8,5	0,71714602	127,5	8,5	0,09623005	1,443	1913
16	1	16	74,2	7,3	0,79789823	116,8	7,3	0,08264463	1,322	1869
17	1	17	78,2	4,0	0,84214602	68	4	0,04528473	0,770	1156
18	1	18	82,7	4,5	0,89192478	81	4,5	0,05094532	0,917	1458
19	1	19	85,1	2,4	0,91847345	45,6	2,4	0,02717084	0,516	866
20	1	20	88,0	2,9	0,9505531	58	2,9	0,03283143	0,657	1160
21	1	21	89,4	1,4	0,96603982	29,4	1,4	0,01584965	0,333	617
22	1	22	89,6	0,2	0,96825221	4,4	0,2	0,00226424	0,050	97
23	1	23	89,9	0,3	0,9715708	6,9	0,3	0,00339635	0,078	159
24	1	24	90,4	0,5	0,97710177	12	0,5	0,00566059	0,136	288
25	1	25	90,4	0,0	0,97710177	0	0	0	0,000	0
Sum	25	25	90,4	88,33	0,97710177	0	0	0	13,723	17566

Table A24.1. Condition of experiment: $\dot{m}_{\text{solvent}} = 13,9 \frac{g}{min}$, $\dot{m}_{\text{leaves}} = 1,01 \frac{g}{min}$, $n = 1,5 \text{ rpm}$, NaCl mass fraction 10%

Appendix A25- Conductivity measuring data of different solvent flowrates and rotational speeds.

Appendix A26- Measurement of raffinate moisture in continuous extraction.

Start the experiment without concerning of steady state or not ($n = 1.8 \text{ rpm}$, $\dot{m}_{leaves} = 1.5 \text{ g/min}$, $\dot{m}_{solvent} = 11.7 \text{ g/min}$). The raffinate samples are collected at outlet (Figure 6.15) and the raffinate masses are recorded to estimate flowrate \dot{m}_R . These samples are dried in vacuum drying oven (VT 6060M–BL) for one day. The raffinate masses before and after drying are recorded. The mass differences allows calculating the moisture (eq. (6.14)), the results are shown below.

Table A26.1. The measured data of raffinate moisture in Toluene.

Drying condition	Sample Name	Before drying		After drying	Calculation		
		m_{plate} [g]	$m_{plate} + m_R$ [g]	$m_{plate} + m_R$ [g]	m_R [g]	m_{Tol} [g]	H [%]
Vacuum drying oven (VT 6060M–BL) integrated with a vacuum pump.	Raff. 1	30.78	32.545	31.542	1.764	1	56.7
	Raff. 2	42.18	43.77	42.841	1.588	0.93	58.5

The raffinate moisture at different periods are almost constant, thus, moisture $H = 57\%$ is chosen. Furthermore, the flowrate of raffinate is estimated by recorded masses in time intervals and resulted at 2.3 g/min . These data allow to estimate the leaves flowrate via eq. (6.15). Thus, the leaves flowrate at 1 g/min is used to gain steady state run. Combining to the recorded flowrate of raffinate, the flowrate of required leaves 1 g/min is found based on eq. (6.15). This result is clearly fulfilled the total mass balance of further applied for steady state run.

Appendix A27- Continuous experimental procedures.

The establishment of compressed segment requires a pre-prepared process which can be carried out as follows: the screw starts at desired speed, the first two compartments of screw are fully filled by dried leaves at very high speed of feeder screw, then, the leaves flowrate is reduced to experimental condition. The dried leaves in the first two full chambers are transported to another end of the screw and are wet by prepared solvent. As a consequence, the friction between the condensed slurry material and perforated disk creates the compressed segment. When this segment is completely established, the continuous run starts. The detail implementing steps are described below and depicted in Fig. A27.1.

- Check the status of solvent source (1) and the leaves material in conical tank (2).
- Provide the nitrogen to the whole cascade until the gauge values under the LOE (3). Start controlling the process: turn on the electrical switch cabinet to active observing the oxygen penetration into the cascade.
- Set the desired speeds of two motors M1 (4) and M2 (5) of the main extractor and the screw feeder respectively. It is noticed that the speed of M1 remains constant for the entire experiment, while that of M2 is manipulated to establish the compressed segment. Start motor M1 and M2. When the first leaves come out of the screw feeder and fall into extractor, start the stopwatch to observe the residence time of leaves.
- Several drops of solvent are provided at solvent input position (7) to wet the dried leaves, then, the wet leaves are further pushed through the perforated disk (6). Afterwards, the solvent is provided in very short time (5 seconds) after each 30 second, then, the leaves is wet but not in slurry state. This wetting process is repeated until all the holes of the perforated disk are completely filled, means, the compress segment is completely built up. Then, we can start the pump and the solvent is continuously supplied to the extractor. Another stopwatch measures the residence time of solvent from start position (7) to the last position (8). (corresponding to the moment of pump start to the first drop observed in another side at sampling point).

- The extract samples are collected from the first drops in 30 seconds, then samples are taken in every 15-minute time intervals. These samples are later analyzed by HPLC.
- The raffinate samples are collected at outside of perforated disk (6) in every 30 minutes. Each raffinate sample is divided into two portions: one for the moisture inspection; another for the rest of ARTE in the raffinate examination based on exhaustive extraction technic (section 4.1.2.2).
- The masses of raffinate and extract are recorded in every 2 minutes via scales 1&2.

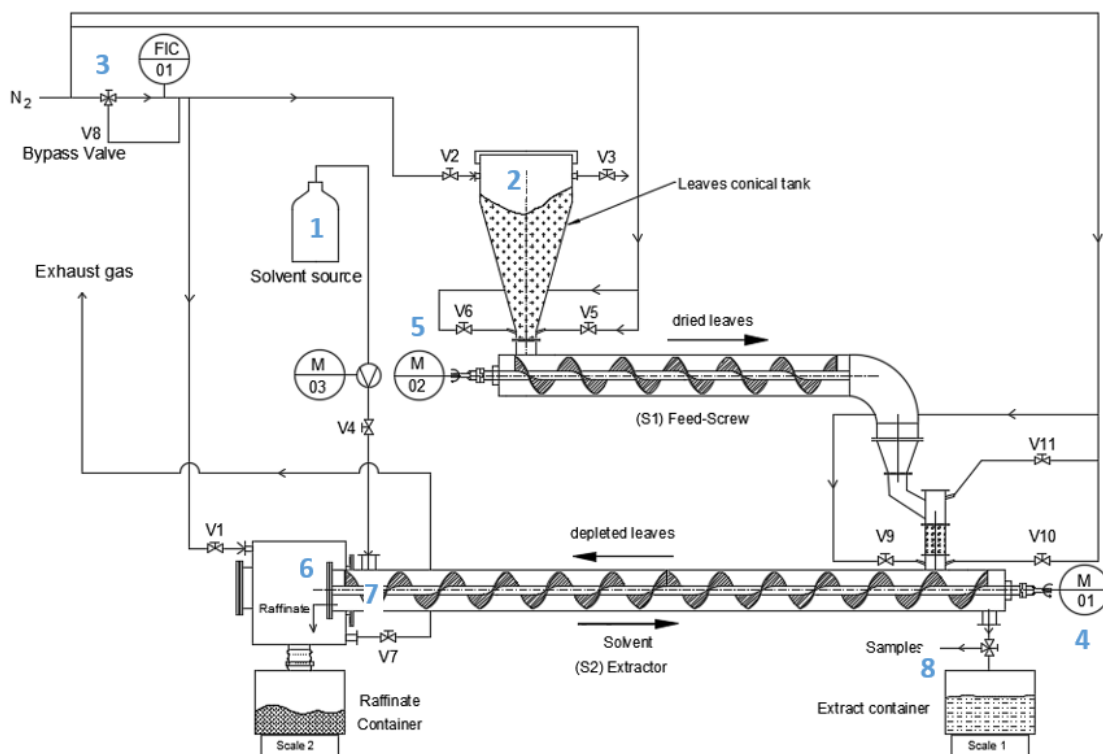


Fig. A27.1. Experimental procedures with relevant positions. 1- solvent source; 2- conical tank; 3- three way valve; 4- motor M1 for screw of the main extractor; 5- motor M2 for screw feeder; 6- perforated disk; 7- solvent inlet; 8- sample collection;

Appendix A28- Experimental condition at optimized steady state extraction.

Steps		Experimental setup		Motor-M1		Motor-M2		Dried LEAVES flowrate		Pump		SOLVENT flowrate		Estimated residence time (min)		EXTRACT flowrate		RAFF. flowrate		Sample Name (Date/Name + HPLC)	
		Nitrogen pressure	Value of sensor	Arte in leaves	Perforated plate	1,3 wt%	5,5mm	Vo(V)	n(rpm)	Vo(V)	n(rpm)	Value	Vo(V)	n(rpm)	Dried leaves	Extract	RAFF. (g/min)	EXTRACT (g/min)	Extract	Raff.	$\dot{m}_{solvent}$ (g/min)
2020.10.15_ 10nd Experiment																					
		3,6 bar		13,7		5,25		2,14		1,7		2,14		5,25		-		-		-	
		13,7		5,5mm		2,14		2,14		1,7		2,14		5,25		-		-		-	
		13,7		5,5mm		2,14		2,14		1,7		2,14		5,25		-		-		-	
		13,7		5,5mm		2,14		2,14		1,7		2,14		5,25		-		-		-	
		13,7		5,5mm		2,14		2,14		1,7		2,14		5,25		-		-		-	
		13,7		5,5mm		2,14		2,14		1,7		2,14		5,25		-		-		-	
		13,7		5,5mm		2,14		2,14		1,7		2,14		5,25		-		-		-	
		13,7		5,5mm		2,14		2,14		1,7		2,14		5,25		-		-		-	
		13,7		5,5mm		2,14		2,14		1,7		2,14		5,25		-		-		-	
		13,7		5,5mm		2,14		2,14		1,7		2,14		5,25		-		-		-	
		13,7		5,5mm		2,14		2,14		1,7		2,14		5,25		-		-		-	
		13,7		5,5mm		2,14		2,14		1,7		2,14		5,25		-		-		-	
		13,7		5,5mm		2,14		2,14		1,7		2,14		5,25		-		-		-	
		13,7		5,5mm		2,14		2,14		1,7		2,14		5,25		-		-		-	
		13,7		5,5mm		2,14		2,14		1,7		2,14		5,25		-		-		-	
		13,7		5,5mm		2,14		2,14		1,7		2,14		5,25		-		-		-	
		13,7		5,5mm		2,14		2,14		1,7		2,14		5,25		-		-		-	
		13,7		5,5mm		2,14		2,14		1,7		2,14		5,25		-		-		-	
		13,7		5,5mm		2,14		2,14		1,7		2,14		5,25		-		-		-	
		13,7		5,5mm		2,14		2,14		1,7		2,14		5,25		-		-		-	
		13,7		5,5mm		2,14		2,14		1,7		2,14		5,25		-		-		-	
		13,7		5,5mm		2,14		2,14		1,7		2,14		5,25		-		-		-	
		13,7		5,5mm		2,14		2,14		1,7		2,14		5,25		-		-		-	
		13,7		5,5mm		2,14		2,14		1,7		2,14		5,25		-		-		-	
		13,7		5,5mm		2,14		2,14		1,7		2,14		5,25		-		-		-	
		13,7		5,5mm		2,14		2,14		1,7		2,14		5,25		-		-		-	
		13,7		5,5mm		2,14		2,14		1,7		2,14		5,25		-		-		-	
		13,7		5,5mm		2,14		2,14		1,7		2,14		5,25		-		-		-	
		13,7		5,5mm		2,14		2,14		1,7		2,14		5,25		-		-		-	
		13,7		5,5mm		2,14		2,14		1,7		2,14		5,25		-		-		-	
		13,7		5,5mm		2,14		2,14		1,7		2,14		5,25		-		-		-	
		13,7		5,5mm		2,14		2,14		1,7		2,14		5,25		-		-		-	
		13,7		5,5mm		2,14		2,14		1,7		2,14		5,25		-		-		-	
		13,7		5,5mm		2,14		2,14		1,7		2,14		5,25		-		-		-	
		13,7		5,5mm		2,14		2,14		1,7		2,14		5,25		-		-		-	
		13,7		5,5mm		2,14		2,14		1,7		2,14		5,25		-		-		-	
		13,7		5,5mm		2,14		2,14		1,7		2,14		5,25		-		-		-	
		13,7		5,5mm		2,14		2,14		1,7		2,14		5,25		-		-		-	
		13,7		5,5mm		2,14		2,14		1,7		2,14		5,25		-		-		-	
		13,7		5,5mm		2,14		2,14		1,7		2,14		5,25		-		-		-	
		13,7		5,5mm		2,14		2,14		1,7		2,14		5,25		-		-		-	
		13,7		5,5mm		2,14		2,14		1,7		2,14		5,25		-		-		-	
		13,7		5,5mm		2,14		2,14		1,7		2,14		5,25		-		-		-	
		13,7		5,5mm		2,14		2,14		1,7		2,14		5,25		-		-		-	
		13,7		5,5mm		2,14		2,14		1,7		2,14		5,25		-		-		-	
		13,7		5,5mm		2,14		2,14		1,7		2,14		5,25		-		-		-	
		13,7		5,5mm		2,14		2,14		1,7		2,14		5,25		-		-		-	
		13,7		5,5mm		2,14		2,14		1,7		2,14		5,25		-		-		-	
		13,7		5,5mm		2,14		2,14		1,7		2,14		5,25		-		-		-	
		13,7		5,5mm		2,14		2,14		1,7		2,14		5,25		-		-		-	
		13,7		5,5mm		2,14		2,14		1,7		2,14		5,25		-		-		-	
		13,7		5,5mm		2,14		2,14		1,7		2,14		5,25		-		-		-	
		13,7		5,5mm		2,14		2,14		1,7		2,14		5,25		-		-		-	
		13,7		5,5mm		2,14		2,14		1,7		2,14		5,25		-		-		-	
		13,7		5,5mm		2,14		2,14		1,7		2,14		5,25		-		-		-	
		13,7		5,5mm		2,14		2,14		1,7		2,14		5,25		-		-		-	
		13,7		5,5mm		2,14		2,14		1,7		2,14		5,25		-		-		-	
		13,7		5,5mm		2,14		2,14		1,7		2,14		5,25		-		-		-	
		13,7		5,5mm		2,14		2,14		1,7		2,14		5,25		-		-		-	
		13,7		5,5mm		2,14		2,14		1,7		2,14		5,25		-		-		-	
		13,7		5,5mm		2,14		2,14		1,7		2,14		5,25		-		-		-	
		13,7		5,5mm		2,14		2,14		1,7		2,14		5,25		-		-		-	
		13,7		5,5mm		2,14		2,14		1,7		2,14		5,25		-		-		-	
		13,7		5,5mm		2,14		2,14		1,7		2,14		5,25		-		-		-	
		13,7		5,5mm		2,14		2,14		1,7		2,14		5,25		-		-		-	
		13,7		5,5mm		2,14		2,14		1,7		2,14		5,25		-		-		-	
		13,7		5,5mm		2,14		2,14		1,7		2,14		5,25		-		-		-	
		13,7		5,5mm		2,14		2,14		1,7		2,14		5,25		-		-		-	
		13,7		5,5mm		2,14		2,14		1,7		2,14		5,25		-		-		-	
		13,7		5,5mm		2,14		2,14		1,7		2,14		5,25		-		-		-	
		13,7		5,5mm		2,14		2,14		1,7		2,14		5,25		-		-		-	
		13,7		5,5mm		2,14		2,14		1,7		2,14		5,25		-		-		-	
		13,7		5,5mm		2,14		2,14		1,7		2,14		5,25		-		-		-	
		13,7		5,5mm		2,14		2,14		1,7		2,14		5,25		-		-		-	
		13,7		5,5mm		2,14		2,14		1,7		2,14		5,25		-		-		-	
		13,7		5,5mm		2,14		2,14		1,7		2,14		5,25		-		-		-	
		13,7		5,5mm		2,14		2,14		1,7		2,14		5,25		-		-		-	
		13,7		5,5mm		2,14		2,14		1,7		2,14		5,25		-		-		-	
		13,7		5,5mm		2,14		2,14		1,7		2,14		5,25		-		-		-	
		13,7		5,5mm		2,14		2,14		1,7		2,14		5,25		-		-		-	
		13,7		5,5mm		2,14		2,14		1,7		2,14		5,25		-		-		-	
		13,7		5,5mm		2,14		2,14		1,7		2,14		5,25		-		-		-	
		13,7		5,5mm		2,14		2,14		1,7		2,14		5,25		-		-		-	
		13,7		5,5mm		2,14		2,14		1,7		2,14		5,25		-		-		-	
		13,7		5,5mm		2,14		2,14		1,7		2,14		5,25		-		-		-	
		13,7		5,5mm		2,14		2,14		1,7		2,14		5,25		-		-		-	
		13,7		5,5mm		2,14		2,14		1,7		2,14		5,25		-		-		-	
		13,7		5,5mm		2,14		2,14		1,7		2,14		5,25		-		-		-	
		13,7		5,5mm		2,14		2,14		1,7		2,14		5,25		-		-		-	
		13,7		5,5mm		2,14		2,14		1,7		2,14		5,25		-		-			

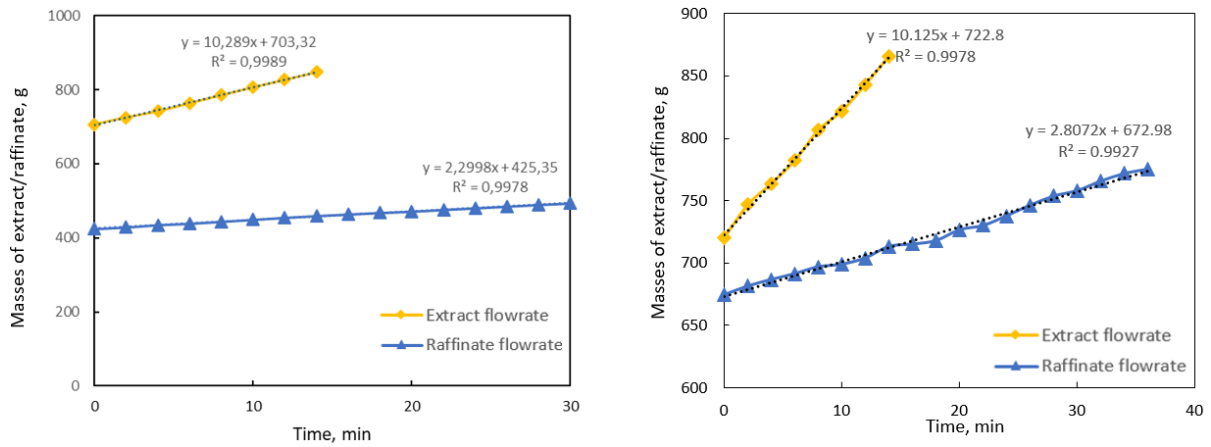


Fig.A28.2. Extract and raffinate flowrates of the first and optimized steady state runs. These data are based on recorded data of extract and raffinate masses in every 2 minutes.